Catalytic Separation of Pure Hydrogen from Synthesis Gas by an Ethanol Dehydrogenation / Acetaldehyde Hydrogenation Loop

by

Petr Chládek

A thesis
presented to the University of Waterloo
in fulfilment of the
thesis requirement for the degree of
Doctor of Philosophy
in
Chemical Engineering

Waterloo, Ontario, Canada, 2007

I hereby declare that I am the sole author of this thesis. This is a true copy of the thesis, including any required final revisions, as accepted by my examiners.

I understand that my thesis may be made electronically available to the public.

Abstract

A novel catalytic process for producing high-purity, elevated-pressure hydrogen from synthesis gas was proposed and investigated. The process combines the advantages of low investment and operating costs with the flexibility to adapt to a small-scale operation. The process consists of a loop containing two complementary reactions: ethanol dehydrogenation and acetaldehyde hydrogenation as depicted in Fig. A. In one part of the loop, hydrogen is produced by dehydrogenation of ethanol to acetaldehyde. Since acetaldehyde is a liquid under standard conditions, it can be easily separated and pure hydrogen is obtained. In the other part of the loop, hydrogen contained in synthesis gas is reacted with acetaldehyde to produce ethanol and purified carbon monoxide. Ethanol, also a liquid under standard conditions, is easily removed and purified carbon monoxide is obtained, which can be further water-gas shifted to produce more hydrogen.
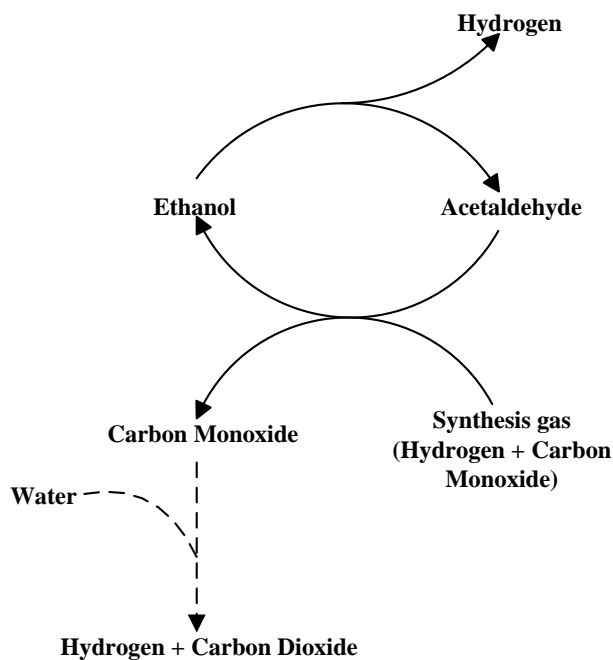
Figure A. Diagram of a novel separation process.

Various dimensionless criteria were evaluated to confirm there was no significant effect of heat and mass transfer limitations and thus the experimental results represent true kinetics. Furthermore, a thermodynamic study was conducted using a Gibbs free energy minimization model to identify the effect of reaction conditions on

ethanol/acetaldehyde conversion and determine the thermodynamically favourable operating conditions.

Various catalysts were synthesized, characterized and screened for each reaction in a down-flow, fixed-bed quartz reactor. A novel gas chromatography analysis method allowing for an on-line detection of all products was also developed.

Unsupported copper in the form of copper foam and copper supported on three different high surface supports were evaluated in ethanol dehydrogenation. Copper foam provided the lowest activity, because of its low surface area. Cu/SiO_2 was the most active catalyst for ethanol dehydrogenation. The effects of temperature, pressure, residence time, and feed composition on ethanol conversion and product composition were determined. While increasing temperature or residence time resulted in increased ethanol conversion, elevated pressure and water content in the feed had no effect on ethanol conversion. On the other hand, acetaldehyde selectivity decreased with increasing temperature, pressure and residence time, as acetaldehyde participated in undesirable transformations to secondary products, out of which the most dominant was ethyl acetate. The maximum operating temperature was limited by the stability of the copper catalyst, which deactivated by sintering at temperatures higher than 300°C. The range of temperatures investigated was from 200°C to 350°C, while pressures ranged from atmospheric to 0.5 MPa. For ethanol:water ratios <1, the addition of water to the ethanol feed improved the catalyst stability and acetaldehyde selectivity, but a detrimental effect was observed at higher ratios. The introduction of acetaldehyde into the feed always lowered the conversion, thus indicating a need for stream purification within the loop. An empirical kinetic model was used to determine the activation energy, the order of reaction and the frequency factor.

Unsupported and SiO_2-supported copper catalysts were compared in acetaldehyde hydrogenation. Pure copper was identified as the best catalyst. Effects of temperature, pressure, residence time, feed composition and catalyst promoter on acetaldehyde conversion and product composition were evaluated. The acetaldehyde hydrogenation was enhanced by increased temperature, pressure and residence time and suppressed in presence of Fe or Zn promoters. Once again, at elevated temperature and residence time, ethanol combined with acetaldehyde to produce undesired ethyl acetate. CO acted as an

inert when testing with the pure copper catalyst, but slightly decreased conversion with the supported catalyst. A decrease in conversion was also observed with the introduction of water and ethanol in the feed, once again indicating a requirement for feed purity within the loop. A temperature range of 150-300°C was investigated with catalysts deactivating at temperatures exceeding 250°C. A pressure range identical to ethanol dehydrogenation was used: 0.1-0.5 MPa. Again, an empirical kinetic model allowed determination of the activation energy, the order of reaction and the frequency factor.

Acknowledgments

I would like to thank my advisors Eric Croiset, Bob Hudgins and Pete Silveston for the trust with which they allowed me to work on this project independently and also for all the invaluable advice and motivation with which they provided me.

Merci mille fois Eric pour la chance d'apprendre votre langue maternelle.

Many thanks to my surrogate-advisor Bill Epling for all the contributions to this work and for teaching me how to enjoy chicken wings without any forethought.

I was very lucky to share my working space (and beyond) with Luke Coleman, without whom this PhD would be half the fun and take twice as long. Thank you, Luke.

My stay in Canada would be less enjoyable, have I not met these unique people: Ellen – my first French teacher, playful Maja, Sarah + Marc (newfie + le chasseur Acadien), Will, who introduced me to the silver screen, Will, who introduced me to Labview, Dom & Joe & Kela & Jeremy– the drinking squad of yesteryears, April - the supergirl, the Tigers (Thai girls) and many others who will have to forgive me for not mentioning their names (if you feel especially upset, send me an email at: petr.chladek@post.cz and we can talk it over). You all made a difference in my life and for that you deserve my thanks.

At last, but not at least, with deepest love I would like to thank you, my dear Janicka, for being such a wonderful person you are.

ᚠᛜᛗᛜᚠ

ᚷᚱ

Table of Contents

List of Figures

List of Tables

Chapter 1: Introduction

The threat of global warming and declining supplies of petroleum drive the search for alternative fuel sources. Hydrogen, although not an energy source, can serve as an ideal energy carrier, because

- it can be produced from a variety of sources including coal, natural gas, organic waste and renewable biomass;

- it serves as a fuel in existing technologies as it can be either combusted in a combustion engine or electrochemically oxidized in fuel cells; and

- it produces only water and heat in electrochemical oxidation or upon combustion. Either reaction is more environmentally friendly than combustion of gasoline or diesel used in current engines.

Most of the recent research has focused on conversion of primary raw materials (natural gas, coal, biomass, and ethanol) to hydrogen. However, in order for the hydrogen produced from these sources to be used in a fuel cell, it must be first purified. Traces of CO, a by-product of steam reforming of any carbonaceous feedstock, is especially harmful to Polymer Electrolyte Membrane Fuel cell (PEM-FC) performance, and PEM-FCs are being considered as a potential replacement for combustion engines in the automotive industry. Therefore, unless hydrogen is produced through a CO-free method such as electrolysis of water, which is very energy intensive, purification of hydrogen is required. As summarized Table 1.1, current purification technologies suffer from serious disadvantages.

Table 1.1 Current H_2 purification technologies and their disadvantages.

Purification Technology	Disadvantage
Partial Condensation	Energy intense
Pressure Swing Adsorption	Pressure loss, Feasible on large scale
Membrane Separation	Membrane cost, Durability, Pressure loss
Selective Oxidation	Inherent impurity (CO_2)
Water Gas Shift Reaction	Inherent impurity (CO_2)

The main objective of this project is the development of a novel separation process which would be free from most if not all of the disadvantages listed in Table 1.1. This novel process, schematically depicted in Fig. 1.1, is based on a catalytic loop, using ethanol and acetaldehyde as reaction intermediates.
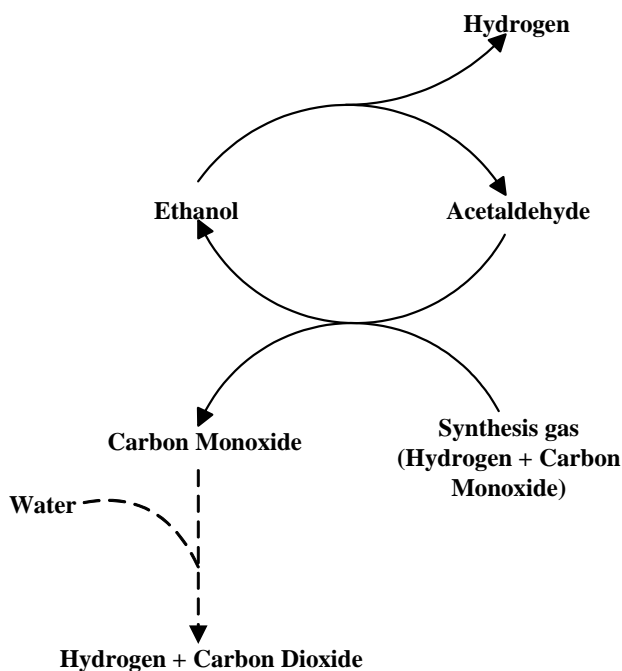
Figure 1.1 Concept of pure hydrogen separation from syngas.

In the loop, hydrogen contained in the synthesis gas is reacted with acetaldehyde producing ethanol, which can be easily separated from the remaining CO by condensation. Purified CO can be further water-shifted in order to produce hydrogen of lesser purity. In the subsequent step, ethanol is dehydrogenated back to acetaldehyde, which once again can be separated by condensation, and pure hydrogen is produced.

Hydrogen, though exhibiting a large mass energy density, unfortunately has a low volumetric energy density and, therefore, is usually stored in high-pressure cylinders. Currently, a pressure of 30-35 MPa is being utilized for storage, but an increase up to 70-75 MPa is proposed for the near future. The compression of hydrogen from atmospheric pressure (0.1 MPa) to its storage pressure represents a major energy loss, therefore causing a significant increase in production costs. Major energy savings can be achieved by pressurizing the liquid ethanol and acetaldehyde and performing the separation cycle

at elevated pressure, thus producing high-pressure hydrogen, compared to a post-reaction pressurization of gaseous hydrogen.

Furthermore, this novel separation process is easily adjustable to different scales of operation, simply by adjusting the amount of catalyst and ethanol/acetaldehyde circulation.

In short, the proposed process represents a completely novel solution that combines the advantages of low investment and operation costs with the flexibility to adapt to small-scale operation. Adaptable also to different sources of syngas, it will provide high-purity pressurized hydrogen to be used as a fuel for fuel cells. It can be easily scaled down or scaled up by adjusting the amount of catalyst and feed rate, and therefore should accommodate a large range of applications.

A major challenge in the implementation of this cycle lies in the development of affordable, highly active and selective catalyst systems for the individual reactions and identification of the optimum reaction conditions with respect to yield, purity, and pressure of hydrogen. Based on a comprehensive literature review and also on economic considerations, copper was identified as an ideal active metal component of the catalyst for both steps. Further steps, necessary to meet the implementation challenges, included the following for each reaction:

1) Support screening was conducted for ethanol dehydrogenation to identify three suitable candidates.

2) Catalysts were characterized by various techniques in order to establish a relation between the catalysts' physical and chemical properties and also to find the required preparation parameters, such as calcination and reduction temperatures.

3) The performance of both supported and unsupported catalysts was compared in a screening study and the best candidates were identified.

4) The effect of reaction parameters, such as temperature, pressure, residence time, and feed composition on the outcome of reaction were evaluated for selected catalysts.

5) Kinetic models were proposed and kinetic parameters were determined for selected catalysts.

This approach results in a collection of data, which will not only determine the applicability of the cycle and identify potential obstacles and limitations, but also provide

a basis for modelling and further implementation of the cycle for pilot and full-scale operation.

In this thesis, a comprehensive literature review pertaining to each reaction is presented in Chapter 2. The general features of catalyst characterization and a detailed description of the experimental apparatus are given in Chapter 3. Chapter 4 contains evaluation of the effects of mass and heat transfer on the outcome of each reaction. The results of thermodynamic modeling are presented in Chapter 5. Experimental results obtained for ethanol dehydrogenation are discussed in Chapters 6 and 7 for unsupported and supported catalysts respectively. Chapter 8 provides the analysis of results obtained in acetaldehyde hydrogenation. The chapters dealing with experimental results are each organized similarly to a journal publication, having their own introduction, experimental, results and discussion, and concluding parts. The most significant results are then highlighted in Chapter 9, together with recommendations for the direction of further research.

Chapter 2: Literature review and background information

This chapter provides background information about the reactions, both desired and undesired, that could possibly occur during the cyclic separation and discusses the factors influencing their significance. Furthermore, a comprehensive literature review is presented for the two reactions essential for the process depicted in Fig. 2.1: dehydrogenation of ethanol to acetaldehyde and hydrogenation of acetaldehyde to ethanol by syngas.
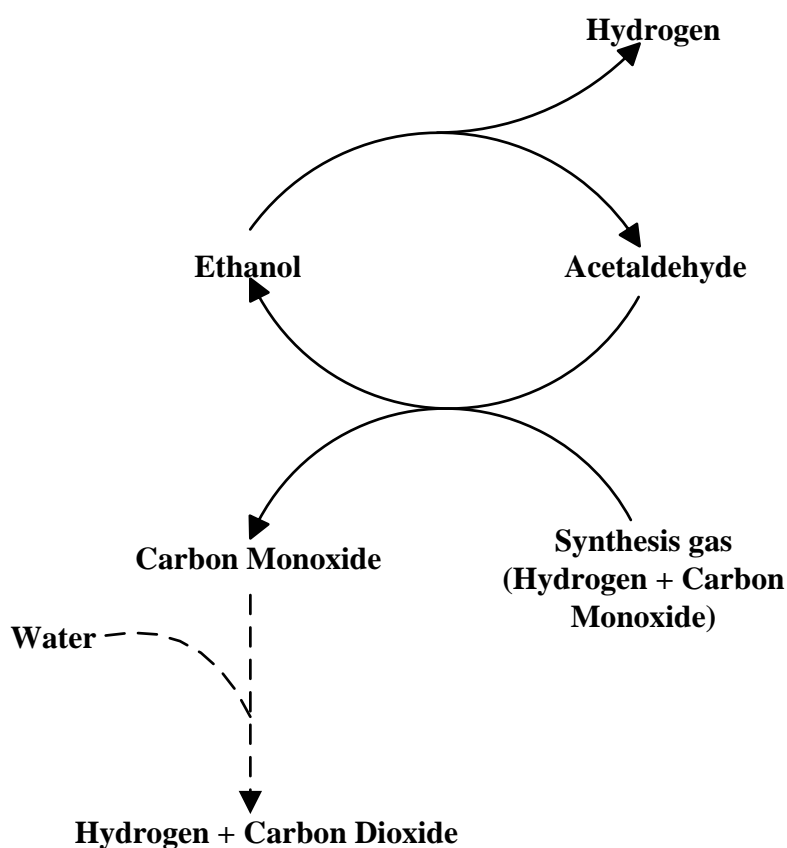
Figure 2.1 Proposed catalytic separation cycle.

2.1 Background information

General information pertaining to the reactions that could possibly occur during the loop operation is presented in this section. Reactions are divided into two groups based on their desirability.

2.1.1 Desirable main reactions

Ethanol dehydrogenation to acetaldehyde

Ethanol dehydrogenation (Reaction 2.1) is a relatively fast endothermic reaction occurring at temperatures higher than 100°C. One mole of hydrogen is released per mole of ethanol reacted. Acetaldehyde is the second main product, which can be separated by condensation (b.p. 21°C at atmospheric pressure) and theoretically 100% pure hydrogen can thus be produced. The reaction can be carried out at higher pressure, thus lowering the cost associated with pressurization of atmospheric pressure hydrogen. However, thermodynamically, the high pressures are expected to favour the reverse reaction.

$$CH_3CH_2OH \text{ (g)} \rightarrow CH_3CHO \text{ (g)} + H_2 \qquad\qquad (2.1)$$

$$\Delta H^\circ_{298K} = 68.45 \frac{kJ}{gmol} \qquad \Delta G^\circ_{298K} = 34.98 \frac{kJ}{gmol}$$

Acetaldehyde hydrogenation by syngas

Acetaldehyde hydrogenation is the reverse reaction of ethanol dehydrogenation. As it is exothermic and consumes 2 moles of reactant per mole of product, it is thermodynamically favoured at lower temperatures and higher pressures. The presence of carbon monoxide is expected to negatively affect thermodynamic equilibrium as it lowers the partial pressures of reactants (see reaction 2.2). However, CO may also have a positive effect on performance by selectively blocking the active sites required for side reactions at the catalyst surface. With regard to energy savings, a source of pressurized syngas, such as outlet streams from biomass converter, coal gasifier or methane steam reformer, is required to execute the reaction at high pressure.

$$CH_3CHO \text{ (g)} + H_2 + CO \rightarrow CH_3CH_2OH \text{ (g)} + CO \qquad\qquad (2.2)$$

$$\Delta H^\circ_{298K} = -68.45 \frac{kJ}{gmol} \qquad \Delta G^\circ_{298K} = -34.98 \frac{kJ}{gmol}$$

Water-gas shift reaction

Although not the focus of this project, the water-gas shift reaction (WGSR, reaction 2.3) can play an important role in the production of lower grade hydrogen from the concentrated CO stream leaving the cycle. This reaction is exothermic and thus thermodynamically favoured by low temperatures. Since there is no change in moles during the conversion, the homogeneous reaction is insensitive to pressure. The WGSR is equilibrium-limited and therefore purification of effluent is required to strip the hydrogen from the remaining CO.

$$CO + H_2O \text{ (g)} \rightarrow CO_2 + H_2 \hspace{4cm} (2.3)$$
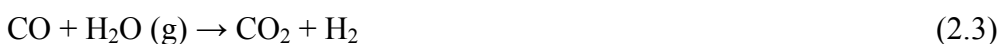
$$\Delta H^{\circ}_{298K} = -41.16 \frac{kJ}{gmol} \hspace{1cm} \Delta G^{\circ}_{298K} = -28.51 \frac{kJ}{gmol}$$

2.1.2 Undesirable side reactions

The undesirable reactions can be divided into four main groups:

- Acetaldehyde condensation reactions – main products of these reactions are generally higher C_3 and C_4 species, such as alcohols, aldehydes, ketones, acids and their esters.
- Ethanol dehydration – main products are ethylene, ethane, diethyl ether and water.
- Ethanol and acetaldehyde decomposition reactions – main products are simple C_1 species such as CO, CO_2 and CH_4.
- Fischer-Tropsch synthesis – syngas mixture in the second step of the cycle is commonly used for production of various hydrocarbons.

Out of these three groups, ethanol and acetaldehyde decompositions are the most detrimental, because these contaminate the hydrogen stream with CO, which prevents its direct utilization in certain applications such as PEM-FC. Ethanol dehydration is also highly undesirable since the dehydration products can serve as precursors to coke formation, thus deactivating the catalyst. Fortunately each group is favoured under different experimental conditions and can therefore be successfully suppressed by the right choice of catalyst system and reaction conditions.

Acetaldehyde condensation reactions

A simplified scheme from Inui et al. (2004) of acetaldehyde secondary reactions is depicted in Fig. 2.2. The scheme represents a network of homogeneous reactions and does not take into account any surface-intermediate interactions. Within this scheme, further subdivision of products is still possible: for example an ethyl acetate route and aldol condensation route.
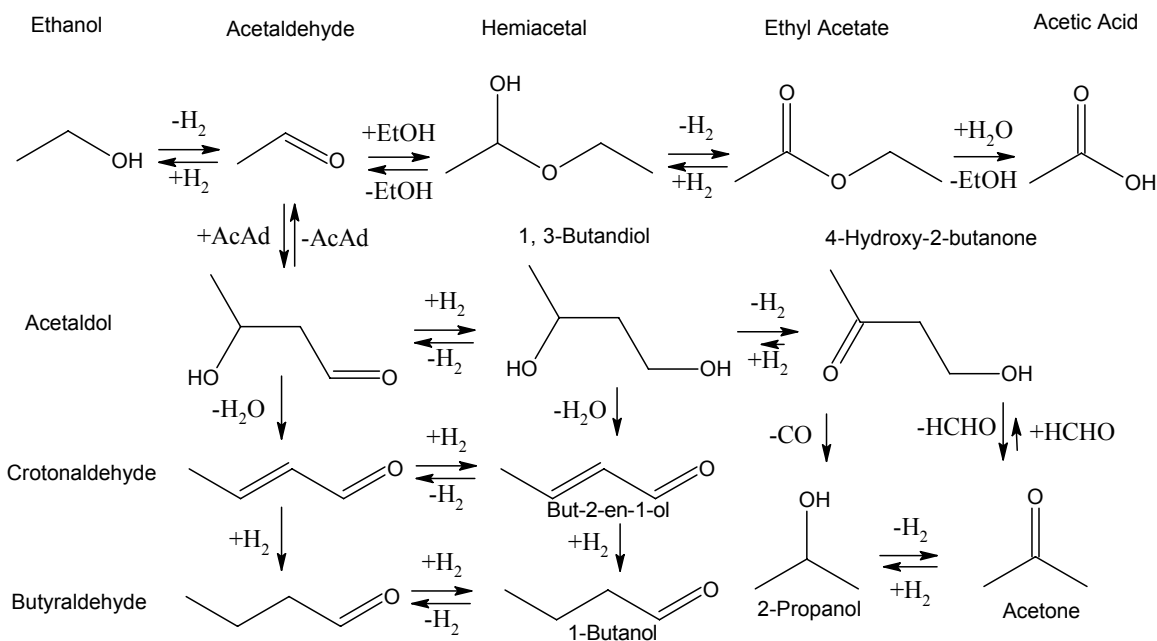
Figure 2.2 Simplified scheme of acetaldehyde related secondary reactions. Adapted from Inui et al. (2004).

Formation of ethyl acetate

Formation of acetaldehyde can be expected in both portions of the cycle and even though this reaction does not affect the purity of the hydrogen stream exiting the cycle in the first step, it is undesirable as it fouls the liquid product stream and extra separation of ethyl acetate, acetaldehyde and unconverted ethanol may be required. Ethyl acetate can be formed through different reaction pathways, with overall pathways listed in reactions 2.4 to 2.6. Most authors (Franckaerts and Froment, 1964; Fujita et al., 2001; Iwasa and Takezawa, 1991; Raich and Foley, 1998) agree that its formation is enhanced by increased residence times and ethanol conversions and by decreased temperatures, because ethyl acetate is thermodynamically favoured over acetaldehyde up to 200°C. In

addition, ethyl acetate formation can be enhanced by increasing the size of the active metal particles on the catalyst surface (Kenvin and White, 1991). The presence of water in the ethanol stream suppresses the formation of ester (Iwasa and Takezawa, 1991), but can lead to the formation of acetic acid as seen from Fig. 2.2.

$$2 \text{ CH}_3\text{CHO (g)} \rightarrow \text{CH}_3\text{COOCH}_2\text{CH}_3 \text{ (g)} \qquad\qquad (2.4)$$
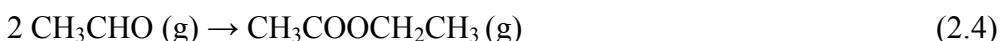
$$\Delta H^\circ_{298K} = -110.02 \frac{kJ}{gmol} \qquad \Delta G^\circ_{298K} = -60.80 \frac{kJ}{gmol}$$

$$\text{CH}_3\text{CH}_2\text{OH (g)} + \text{CH}_3\text{CHO (g)} \rightarrow \text{CH}_3\text{COOCH}_2\text{CH}_3 \text{ (g)} + \text{H}_2 \qquad\qquad (2.5)$$

$$\Delta H^\circ_{298K} = -41.75 \frac{kJ}{gmol} \qquad \Delta G^\circ_{298K} = -25.82 \frac{kJ}{gmol}$$

$$2 \text{ CH}_3\text{CH}_2\text{OH (g)} \rightarrow \text{CH}_3\text{COOCH}_2\text{CH}_3 \text{ (g)} + 2 \text{ H}_2 \qquad\qquad (2.6)$$
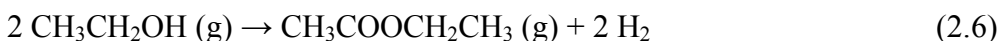
$$\Delta H^\circ_{298K} = 26.70 \frac{kJ}{gmol} \qquad \Delta G^\circ_{298K} = 9.16 \frac{kJ}{gmol}$$

Both Iwasa and Takezawa (1991) and Kenvin and White (1991) stated that ethyl acetate is a product of coupling of an acetyl fragment with an ethoxy fragment, therefore indicating pathway (2.5) as the most probable.

Aldol condensation and subsequent reactions

Aldol condensation (reaction 2.7) is a reaction between two aldehyde molecules resulting in a compound containing alcohol and aldehyde functional groups. It occurs readily in solution at low temperatures (4-5°C) provided some base is supplied as a catalyst. Several authors, studying ethanol dehydrogenation (Armstrong and Hilditch, 1920; Raich and Foley, 1998; Iwasa and Takezawa, 1991; Chung et al., 1993; Davidson et al., 2001b), reported trace amounts of crotonaldehyde – product of subsequent aldol

dehydration – and C_4 species such as 1-butanol, butanal and methylethylketone to pollute the outlet acetaldehyde stream. Contrary to the reaction mechanism in solution, Raich and Foley (1998) and Iwasa and Takezawa (1991), who conducted their dehydrogenation experiments in gas-solid system, ascribed the formation of higher oxygenates to weakly acidic sites present on the support. Davidson et al. (2001a) confirmed that the support played an essential role in aldol condensation, as no higher species were detected with high active metal loadings.

$$2\ CH_3CHO \rightarrow CH_3CHOHCH_2CHO \rightarrow C_4, \text{ aldehydes and alcohols} \qquad (2.7)$$
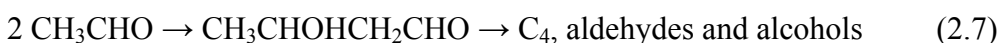
$$\Delta H^{\circ}_{298K} = -46.21\frac{kJ}{gmol} \qquad \Delta G^{\circ}_{298K} = -11.38\frac{kJ}{gmol} \quad \text{(for crotonaldehyde)}$$

Ethanol dehydration

Ethanol can undergo dehydration to diethyl ether (DEE) (reaction 2.8) or ethylene (reaction 2.9) which can polymerize on the catalyst surface and form carbon deposits. Dehydration has usually high activation energy and, therefore, is favoured by high temperatures. For example, Freni et al. (2000) reported that, under his conditions, ethylene formation occurred on copper catalysts only at temperatures exceeding 500°C. Both ethylene and DEE formation are catalyzed by acidic sites present on the support, e.g., Al_2O_3. Thus Iwasa and Takezawa (1991) detected DEE formation on supports with strong acidic sites.

$$2CH_3CH_2OH\ (g) \rightarrow CH_3CH_2OCH_2CH_3\ (g) + H_2O\ (g)$$

$$(2.8)$$
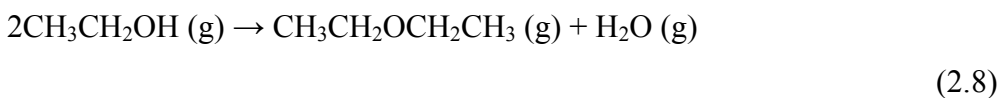
$$\Delta H^{\circ}_{298K} = -24.01\frac{kJ}{gmol} \qquad \Delta G^{\circ}_{298K} = -14.99\frac{kJ}{gmol}$$

$$CH_3CH_2OH\ (g) \rightarrow CH_2CH_2 + H_2O\ (g) \qquad\qquad (2.9)$$
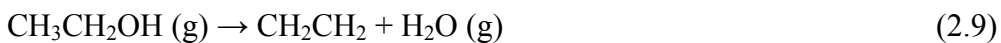
$$\Delta H^{\circ}_{298K} = 45.30\frac{kJ}{gmol} \qquad \Delta G^{\circ}_{298K} = 7.81\frac{kJ}{gmol}$$

Acetaldehyde and ethanol decomposition

The decomposition reaction can be viewed as simple decomposition or as water assisted (steam reforming). In both cases the exiting stream is fouled by traces of CO_2, CO and CH_4. Acetaldehyde decomposition (reaction 2.10) is exothermic and irreversible producing CO and CH_4. Different amounts have been detected during ethanol dehydrogenation depending on reaction conditions and catalyst systems, but usually not exceeding 1 or 2 mol. % (Freni et al., 2000; Franckaerts and Froment, 1964). Raich and Foley (1998) reported that the importance of the decomposition reaction increases when increasing temperature, becoming eventually dominant at high temperatures. The rate of ethanol decomposition (2.11), which consists of two steps, ethanol dehydrogenation and acetaldehyde decomposition, is severely suppressed at higher pressures, at which conditions, dehydrogenation to acetaldehyde is favoured (Davidson et al., 2001a).

$$CH_3CHO \ (g) \rightarrow CO + CH_4 \hspace{4cm} (2.10)$$

$$\Delta H^{\circ}_{298K} = -19.03 \frac{kJ}{gmol} \hspace{1cm} \Delta G^{\circ}_{298K} = -54.82 \frac{kJ}{gmol}$$

$$CH_3CH_2OH \ (g) \rightarrow CO + CH_4 + H_2 \hspace{3cm} (2.11)$$
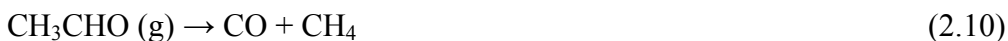
$$\Delta H^{\circ}_{298K} = 49.42 \frac{kJ}{gmol} \hspace{1cm} \Delta G^{\circ}_{298K} = -19.84 \frac{kJ}{gmol}$$

Steam reforming of ethanol (reaction 2.12) is a highly endothermic reaction resulting in conversion of ethanol to hydrogen and a mixture of CO_2 and CO. Fortunately, the reaction is not thermodynamically favourable below 327°C. However, Iwasa and Takezawa (1991) reported steam reforming resulting in acetic acid and hydrogen (reaction 2.13) occurring at lower temperatures (250°C). They also mentioned that the selectivity to acetic acid increased with increasing ethanol conversion and residence time.

The same authors reported that steam reforming of acetaldehyde (reaction 2.14) also resulted in a mixture of acetic acid and hydrogen.

$$CH_3CH_2OH \text{ (g)} + H_2O \text{ (g)} \rightarrow 2\ CO + 4\ H_2 \quad\quad\quad\quad (2.12)$$
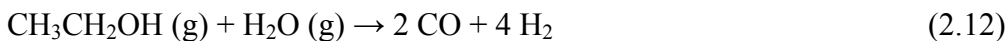
$$\Delta H^{\circ}_{298K} = 255.54\frac{kJ}{gmol} \quad\quad \Delta G^{\circ}_{298K} = 122.31\frac{kJ}{gmol}$$

$$CH_3CH_2OH \text{ (g)} + H_2O \rightarrow CH_3COOH \text{ (g)} + 2\ H_2 \quad\quad\quad\quad (2.13)$$
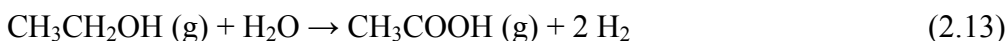
$$\Delta H^{\circ}_{298K} = 41.78\frac{kJ}{gmol} \quad\quad \Delta G^{\circ}_{298K} = 20.18\frac{kJ}{gmol}$$

$$CH_3CHO \text{ (g)} + H_2O \text{ (g)} \rightarrow CH_3COOH \text{ (g)} + H_2 \quad\quad\quad\quad (2.14)$$
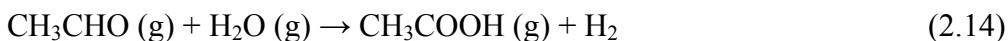
$$\Delta H^{\circ}_{298K} = -26.67\frac{kJ}{gmol} \quad\quad \Delta G^{\circ}_{298K} = -14.8\frac{kJ}{gmol}$$

Nevertheless, the extent of the decomposition side-reactions can be significantly reduced by the choice of catalyst. For example, as early as 1920, Armstrong and Hilditch (1920) compared two common active metals, Ni and Cu, in both ethanol dehydrogenation and acetaldehyde hydrogenation, and found Cu incapable of splitting the C-C bond. Therefore, by using copper catalyst supported on appropriate support and running the reaction at mild temperatures in order to avoid thermal decomposition, the extent of decomposing and reforming reactions should be minimized, preferably to virtually 0%.

Fischer-Tropsch synthesis

Mixtures of carbon monoxide and hydrogen can be used for the production of a large variety of organic compounds (reaction 2.15). The product distribution is affected mainly by reaction conditions and type of catalyst. Copper catalysts, especially when mixed with ZnO, are commonly used for methanol synthesis. Even though much harsher pressures (7.5 MPa) would have to be applied to produce significant amounts, traces of

methanol and lower hydrocarbons can still appear in the outlet stream (Ehwald et al., 1991).

x CO + y H$_2$ $\rightarrow$ various hydrocarbons   (2.15)

It is therefore apparent that the system of reactions, which may occur during the proposed two-step hydrogen separation from syngas, is rather complex. However, each undesirable reaction can be suppressed by the selection of a suitable catalyst system and optimization of reaction conditions. The following section will, therefore, focus solely on the review of literature pertaining to the two major reactions involved in the cycle: ethanol dehydrogenation and acetaldehyde hydrogenation.

2.2 Ethanol dehydrogenation

2.2.1 Introduction

Ethanol, as a renewable fuel, is playing an increasingly important role in both chemical and energy industries. Its mixture with water can be easily produced via fermentation of renewable sources such as corn, cane, fast-growing plants, or biomass waste. This product, containing up to 20% of ethanol, is then refined and can be used either as alternative fuel or a precursor in the synthesis of many important industrial chemicals.

An extensive amount of literature concerning acetaldehyde production via dehydrogenation is available. Acetaldehyde was first synthesized by ethanol oxidation in 1817 (Davy, 1817) and later was produced by hydration of acetylene. Armstrong and Hilditch (1920) reported that the dehydrogenation process was developed and applied during the First World War, but more thorough investigation (Church and Joshi, 1951; Franckaerts and Froment, 1964; Shiau and Chen, 1961) was spurred by an increasing significance of acetaldehyde as one of the most important aliphatic intermediates in the production of acetic acid, acetone, ethyl acetate, C_4-aldehydes, 1-butanol, pentaerythritol and many other chemicals. More recently, the importance of ethanol dehydrogenation as a source of hydrogen for fuel applications was recognized (Freni et al., 2000).

In order to successfully incorporate ethanol dehydrogenation into the proposed novel catalytic separation cycle, it is necessary to identify an active, selective and stable catalyst system and also to find optimum conditions at which the production of hydrogen and acetaldehyde will be maximized and secondary reactions suppressed. The following factors play important roles and will be considered further in the text: catalyst composition (nature of active metal phase, effect of promoters and supports, and effect of deposition techniques), reaction temperature and pressure, residence time, and feed composition. Furthermore, the available kinetic data will be summarized and the mechanism of the surface reaction listed in the literature will be replicated.

2.2.2 Catalyst composition
Active phase

The most popular metal used for selective dehydrogenation of alcohols to aldehydes or ketones is copper, mainly because of its ability to dehydrogenate ethanol without splitting the C-C bond, which would lead to the undesirable decomposition of acetaldehyde to CH_4 and CO. Various studies (Tu et al., 1994a,b; Kanoun et al., 1993; Chang et al., 2006) have shown that it is metallic Cu^0 formed by reduction of CuO, which acts as an active phase in dehydrogenation. Other alternatives to Cu, including Pt, Pd, Cr, Cd, Ni, Fe, Mn, Co, Zn and Ru, were proposed, but none of them matched the selectivity obtained with copper catalysts. However, Cu suffers from poor stability at high temperatures, where dehydrogenation is thermodynamically favourable. The reaction only approaches 100% equilibrium conversion at temperatures higher than 500°C, while Cu is reported to deactivate at temperatures as low as 190°C (Kanoun et al., 1991a). The most probable mechanism of thermal deactivation of copper is sintering, which is expected to become significant in the temperature range of 177–400°C (Hüttig temperature - Tamman temperature – empirically determined temperatures, when metal particles become mobile on the catalyst surface, $T_H = 0.33 \cdot$m.p., $T_T = 0.5 \cdot$m.p.). Sintering as a deactivation mechanism was experimentally confirmed by the Tu group (Tu and Chen, 2001; Tu and Chen, 1998; Tu et al., 1994a,b). On the other hand, other experimenters (Church et al., 1951; Franckaerts and Froment, 1964) reported deactivation by carbon formation, which may originate from ethanol dehydration or from polymerization of higher hydrocarbons formed in subsequent acetaldehyde reactions. In either case, the selection of catalyst preparation technique, suitable support and promoter can eliminate or significantly inhibit deactivation.

Support

Unsupported copper is a very active and selective catalyst which has been successfully used in ethanol dehydrogenation in the form of a copper screen (Church and Joshi, 1951), as a powder prepared by decomposition of $Cu(NO_3)_2$ (Iwasa and Takezawa, 1991) or precipitated as $Cu(OH)_2$ (Chung et al., 1993; Kanoun et al., 1991a,b, 1993) or $CuCO_3$ (Tu et al., 1994a,b) which was then calcined and reduced *in-situ.* In all studies,

where the performance of unsupported metallic copper was compared to a supported copper catalyst, unsupported copper provided superior acetaldehyde selectivity under identical reaction conditions. However, unsupported copper suffers from lower thermal stability and, more importantly, from low metallic surface area, resulting in less acetaldehyde produced per g of copper than in any of the supported or promoted copper catalysts (Kanoun et al., 1991a,b, 1993). Therefore copper has been deposited on a variety of high surface area materials.

In the middle of the 20th century, various naturally occurring materials were commonly used as supports. Church et al. (1951) demonstrated the superior properties of asbestos and pumice for ethanol dehydrogenation. Nowadays, modified natural or synthetic materials with better-defined, more homogeneous structures and properties are employed. Iwasa and Takezawa (1991) compared unsupported copper catalyst performance to copper supported on SiO_2, ZrO_2, Al_2O_3, MgO and ZnO. ZrO_2- and ZnO-supported catalysts were selective for ethyl acetate formation, while the use of Al_2O_3 support promoted undesired secondary reactions that resulted in higher amounts of diethyl ether and C_4 species. It was concluded that these by-products were formed on the acidic sites of Al_2O_3, because selectivity to these by-products rapidly dropped after the support was doped with basic KOH. On the other hand, Church et al. (1951) observed increased formation of undesired higher hydrocarbons not only with basic oxides promoters (ZnO, MgO) but also with Al_2O_3 and ascribed this formation to base-catalyzed aldol condensation. This observation was further confirmed by Inui et al. (2002) who reported that both Al_2O_3 and ZrO_2 additions to pure Cu completely switched selectivity from acetaldehyde to ethyl acetate, and diethyl ether and ethyl acetate, respectively. In contrast, the addition of ZnO had no effect on product distribution. Repeatedly and independently, SiO_2 was proven to be a superior support by Iwasa and Takezawa (1991), Chang et al. (2006), Nischiguchi at al. (2005) and Gole and White (2001), in all cases exhibiting high activity and selectivity to acetaldehyde formation. These superior properties were related to its high surface area, allowing for a high dispersion of Cu and also to its inertness, resulting in the absence of active sites required for undesired parallel or secondary reactions. Furthermore, SiO_2 adsorbs oxygenated hydrocarbons (Carlos-Cuellar et al., 2003), thus serving as a pool of surface ethanol for active copper sites. The

only aspect in which SiO_2 may be lacking is thermal stability. SiO_2-supported catalysts are commonly prepared by impregnation, a technique in which active metal is merely deposited in the pores and on the surface of the support, but not anchored in the support oxide lattice. From this perspective, hydrotalcites, i.e., a class of layered materials consisting of positively charged brucite $Mg(OH)_2$-like sheets where several Mg^{2+} ions are replaced by trivalent Al^{3+} ions and the excess of positive charge is counterbalanced by anions, such as CO_3^{2-} or NO_3^-, in the interlayer plus water molecules, may provide a stable, high surface alternative to SiO_2. Thus, Di Cosimo et al. (1998) reported that small addition of Al to MgO (Mg/Al molar ratio > 5) leads to a creation of hydrotalcite material, which by itself was capable of producing significant amounts of acetaldehyde. When impregnated with Cu solution, Al^{3+} ions are exchanged for Cu^{2+} and copper is therefore incorporated in the support lattice as shown by Alejandre et al. (1999).

Promoters

Since the activity of copper catalyst quickly decreases with time on stream at temperatures higher than 300°C, most likely because of copper sintering, many researchers focused on improving the stability by adding a textural promoter to the catalyst formula, which would act mainly as a mechanical barrier decreasing copper particle mobility. The common feature of the promoters studied was their irreducibility at the dehydrogenation reaction conditions, i.e., promoters were present on the catalyst surface in the form of metal oxides.

Church et al. (1951) evaluated the effect of 5-7 % addition of Cr_2O_3, CoO, ZnO and MgO on Cu/asbestos catalyst performance. It was found that Zn and Mg alkaline oxides had a detrimental effect on the selectivity of reaction, promoting aldol condensation and thus forming undesirable higher hydrocarbons. Amphoteric Cr_2O_3 favoured the creation of ethylene via dehydration of ethanol. Although deposition of 5% CoO slightly decreased the selectivity of dehydrogenation to acetaldehyde, its addition resulted in increased conversion of ethanol. To further improve the stability of Cu-CoO catalyst, 2% Cr_2O_3 was added to the catalyst formula. Indeed, Cr_2O_3 is the most popular of all additives considered in the literature as a potential stabilizer.

Tu et al. (1994a,b) published two papers addressing the effect of Cr_2O_3 on the dehydrogenation activity of unsupported copper catalysts. Even trace amounts increased the metallic copper surface area and also increased the stability, though sintering was never completely suppressed at temperatures higher than 300°C. Below this temperature, the catalyst did not show any signs of deactivation, but the reaction did not achieve 100% conversion. At 310°C, a Cr/Cu ratio of 4/40 resulted in the smallest decrease in Cu surface area and consequently in activity after 8 h on stream. Overloading the catalyst with chromium, for example at a Cr/Cu ratio of 20/40, had a significantly negative effect on the catalyst activity, since a new catalytically inactive $CuCr_2O_4$ phase was formed.

Kanoun et al. (1993) tested the influence of Cr and Al oxides addition on the catalyst properties and found that Al_2O_3 increased the total catalyst surface area while Cr_2O_3 increased specific copper surface area. Cr addition also increased the activity of catalyst per copper weight. However, if activity was defined per weight of catalyst, then any addition of Al or Cr led to a decrease. The authors then concluded that Cr is a better structural promoter. Unfortunately, the low reaction temperature of 190°C and deliberately low ethanol conversion (<1%) made it impossible to determine the effect of promoters on either acetaldehyde selectivity (always 100%) or catalyst stability.

The same mild experimental conditions served for testing of other promoters, namely Zr, V, and Zn oxides, by the same research group (Kanoun et al. 1991a,b). The highest amounts of acetaldehyde produced per g of Cu were always obtained with the highest Cu dispersion, which was attained at the lowest Cu loading. A Cu-Zr catalyst exhibited the highest activity (but only 80% selectivity) of all three binary mixtures tested, while a ternary mixture of Cu-V-Zr was inferior in performance to a Cu-V-Zn catalyst. The highest amount of acetaldehyde produced per g of copper was achieved with a Cu-V-Zn catalyst with minimum Cu loading. But once again, pure Cu proved to be most active in terms of acetaldehyde produced per g of catalyst. Even at such mild temperature (190°C), the authors reported a steady decline in activity over 16 h on stream.

From all three papers published by Kanoun et al. (1993, 1991a,b) it can be concluded that the total surface area decreases with the addition of promoters in this order: Al>Cr>Zr>V>Zn, while metallic copper surface area, which is responsible for the

18

activity of the catalyst decreases with the additives in the following order: Cr>V=Zr>Al>Zn. Cr is thus the best structural promoter and also a good stabilizer. However, Cr_2O_3 is not very environmental friendly and thus attempts have been made to replace it with less harmful, comparably active promoters.

Tu and Chen carried out series of tests on the effect of alkali metals (Na, K, Rb) (Tu and Chen, 2001) and alkaline earth metals (Mg, Ca, Sr, Ba) (Tu and Chen, 1998) as promoters on the performance of Cu/SiO_2 catalyst. The metal oxides of alkaline metals and alkaline earth metals did not undergo reduction at a reaction temperature of 300°C, neither did they contribute significantly to the dehydrogenation activity. While alkali metals created only slightly basic sites on the catalyst surface, all alkaline-earth-metals-containing catalysts, with the exception of Mg addition, possessed both strong and weak basic sites. The presence of strong basic sites resulted in an extreme drop in activity after a short time on stream, thus deeming especially Ba and Sr as poor promoters. MgO proved to be most stable of alkaline earth oxides, but even this additive did not prevent the catalyst from losing 20% of its initial activity after just 4 h on stream. Among the alkali metals, a K-doped catalyst displayed the highest resistance to sintering, losing only 8% of its activity after 4 h on stream. Thus K was identified as the best promoter out of all metals tested, even though the initial ethanol conversion was 2% lower (68%) than the highest conversion obtained with a MgO promoter (70%). Similar to the detrimental effect of Cr overloading reported by Tu et al. (1994a,b), K also has a negative effect on catalyst performance if used in excess. Juan-Juan et al. (2006) and Snoeck and Froment (2002) relate this loss of activity to blockage of active sites by K.

Though it is rather difficult to compare the effects of various promoters, because of different conditions used by researchers, there seems to be a general agreement throughout the literature that the best promoter is Cr_2O_3 (Church et al., 1951; Franckaerts and Froment, 1964; Shiau and Chen, 1991; Kanoun et al., 1993; Tu et al., 1994a,b) with K_2O providing an environmentally friendlier alternative (Tu and Chen, 2001). Nevertheless, both promoters did not eliminate sintering but merely decreased the rate of deactivation. It may therefore be impossible to achieve stable operation with complete conversion and selectivity to acetaldehyde, in which case the reaction will have to be

operated at lower non-deactivating temperatures and then the use of a promoter would be superfluous.

Preparation techniques

While precipitation and impregnation are the most common preparation techniques reported in ethanol dehydrogenation literature, there is some evidence suggesting that an ion exchange method may provide better activity and stability by providing a better dispersion of Cu and also its incorporation into the support matrix.

Sodesawa (1984) published a paper comparing the effect of different preparation techniques of unsupported Cu catalyst (precipitation) and Cu/SiO$_2$ catalyst (impregnation and ion-exchange) of various Cu-loadings on the dehydrogenation of methanol. Metallic copper surface area increased with decreasing metal loading and also the ion-exchange prepared catalyst exhibited the highest metal surface area compared to other catalysts with the same loading. Surprisingly, all catalysts, except for the ion-exchanged one, completely lost their activity after 3 h on stream at 250°C. The ion-exchanged catalyst retained its initial activity for 5 h on stream. Minimum loss of active metal surface area was observed for this catalyst.

Better performance attained with ion-exchange (IE) preparation is also supported by Raich and Foley (1998) who compared catalysts for ethanol dehydrogenation prepared by an incipient wetness technique and ion-exchange method. The IE catalyst exhibited higher activity than the impregnated catalyst, which on the other hand had higher acetaldehyde selectivity. Contrary to Sodesawa (1984), Reich's ion-exchange catalyst displayed a steady loss of activity at temperatures higher than 225°C. Surprisingly, faster deactivation was observed at 250°C than at 275°C.

Furthermore, Chang et al. carried out ethanol dehydrogenation on Cu deposited on rice husk ash (90-97% SiO$_2$) by incipient wetness impregnation (Chang et al., 2003) and ion-exchange (Chang et al., 2006) to show that the ion-exchanged catalyst provided better copper dispersion. The higher dispersion was linked to a higher activity and also to a higher stability: while the IE catalyst provided steady operation at 275°C for 2 h, the impregnated catalyst quickly lost some of its initial activity because of sintering.

Despite these positive results, impregnation/co-impregnation and precipitation/co-precipitation are more favoured among researchers and remain the technique of choice in the majority of articles. The reason for this preference lies probably in the different ion exchange capacity of different supports, which makes it impossible to deposit identical copper loadings. Furthermore, in all three pro-IE studies the copper loading was < 5% suggesting that IE is inappropriate for the preparation of highly loaded catalysts, once again because of a limited number of sites where copper or other metals can be ion-exchanged. Also, in all three cases, the catalyst prepared by IE was unpromoted and difficulties in preparation of promoted catalysts resulting from promoter – active metal competition for ion-exchange sites can be expected.

2.2.3 Reaction conditions

Temperature

80% of journal articles dealing with ethanol dehydrogenation catalyzed by some sort of copper catalyst reported the reaction temperature at which all the experiments were carried out to be in the range of 200 – 310°C. This choice is governed by the effort to find an optimum between

- Thermodynamics limitations: dehydrogenation, being endothermic, is favoured at high temperatures;
- Kinetics: the rate of reaction is always positively influenced by higher temperatures; and
- Catalyst stability: copper catalyst is subject to rapid deactivation most likely because of sintering at elevated temperatures.

Pressure

Le Chatelier's principle suggests that higher pressure will have a negative impact on ethanol dehydrogenation as 2 moles of products are produced from 1 mole of reactant. For this reason dehydrogenation was generally carried out at atmospheric pressure with most researchers decreasing the partial pressure of ethanol even further by using highly diluted feedstocks. Saturated ethanol vapours were supplied by bubbling an inert gas, such as N_2 or He, through a saturator maintained at steady temperature. Resulting partial pressures of ethanol were as low as 4.5 kPa (Kanoun et al., 1993, 1991a,b) but usually

around 20 kPa. In other cases water was used as a diluent, and its mixture with ethanol was delivered to the reactor by a pump through a vaporizer stage. However, evidence exists in the literature indicating that ethanol dehydrogenation may not be limited by pressure as much as thermodynamics predict, or possibly not at all.

- Church at al. (1951) mentioned in the theoretical part of their article, that the rate of alcohol dehydrogenation was pressure insensitive.

- Davidson et al. (2001a) studied the decomposition of ethanol catalyzed by Pd catalyst. Again, the reaction was found to be rather insensitive to the ethanol partial pressure. Ethanol, as the strongest binding species in the system, covered quickly the catalyst surface and saturated it; the reaction was then insensitive to gas phase ethanol pressure. For a temperature of 206°C the strength of species adsorption decreased in the following order: ethanol = acetaldehyde > CO > H_2 > CH_4. Furthermore, acetaldehyde was found to be favourably produced at higher partial pressures of ethanol, while a $CH_4/CO/H_2$ mixture was the preferred product at low partial pressures, which could be explained by scarcity of available active sites required for decomposition of ethanol under high ethanol partial pressure conditions.

- According to Franckaerts and Froment (1964), who conducted a kinetic study on ethanol dehydrogenation and ran the reaction in a pressure range of 0.1-1 MPa, the rate of reaction initially increased with increasing partial pressure, went through a maximum at 0.2-0.3 MPa and then slightly decreased.

- Shiau and Chen (1991) also studied the kinetics of ethanol dehydrogenation. The calculated equilibrium conversions suggested a negative response to higher partial pressures of ethanol; however, when experiments were conducted in the ethanol partial pressure range of 25 – 71 kPa, the conversion was found to increase with increasing pressure and to reach a maximum at the upper boundary level.

- Lin and Chang (2004) showed that an increase in pressure from 0.1 to 1 MPa did not affect ethanol conversion in dehydrogenation, despite the shift in reaction selectivity from acetaldehyde to DEE and ethyl acetate.

Residence time

Residence time affects both the conversion of ethanol and the composition of the outlet stream. Several authors (Peloso et al., 1979; Shiau and Chen, 1991; Lin and Chang, 2004) reported an increase in conversion with increasing residence time. However, the higher the contact time, the lower the selectivity towards acetaldehyde, which is subject to subsequent reactions (Marino et al., 2004; Iwasa and Takezawa, 1991).

Generally, it is rather difficult to extract information on residence time from different articles, because of a non-uniform nomenclature as well as the omission of the values for catalyst loadings and/or feed flow rates. It is also questionable whether the W/F (mass of catalyst/active phase to gas feed rate) ratio should be based on the amount of catalyst or active phase. The majority of the authors, who provided sufficient information, conducted their experiments at W/F range 1-4 kg_{Cu} h L^{-1}. Copper loading varied from 1-5% and 1-15% for catalysts prepared by IE and impregnation respectively to 0-100% for catalysts prepared by precipitation. The actual total amount of catalyst used in the experiments was in the range 0.02 – 1 g.

Ethanol feed flow rate and composition

The gas flow rate directly affects the residence time and is also responsible for external diffusion limitations. The significance of external diffusion can be determined by conducting experiments at different gas flow rates and different catalyst loadings while maintaining the same W/F ratio. Thus, Marino et al. (2004) found their dehydrogenation experiments to be mass transfer limited. Total gas flow rates cited in literature varied from 40 – 216 mL min^{-1}, but flow rates no lower than 120 mL min^{-1} were employed by researchers who were using concentrated ethanol streams (Freni et al., 2000; Church et al., 1951; Shiau and Chen, 1991; Marino et al., 2004).

Papers can be divided into three main categories based on the feed composition:

- Ethanol vapours in the inert carrier gas (He, N_2) or hydrogen.
- Liquid ethanol/water mixture vaporized and either fed directly to the reactor or mixed with additional inert serving as a tracer and then fed into the reactor.
- Kinetic studies concentrating on the effect of co-feeding products: acetaldehyde or hydrogen together with ethanol fed into the reactor.

The most interesting are the results obtained from the last two points. Water, in certain amounts, is an inevitable component of the ethanol feed, because it is rather difficult to obtain 100% pure ethanol and also should a bio-ethanol be used as a feedstock, large amounts of energy would have to be employed for the separation. For these reasons, it is important to know what side-effects the presence of water can have. Armstrong and Hilditch (1920) as well as Iwasa and Takezawa (1991) reported that formation of undesirable ethyl acetate and C_4 hydrocarbons was suppressed in the presence of water. Unfortunately, the formation of acetic acid − another undesirable product − was enhanced, especially at higher residence times. Similarly, Marino et al. (2004) observed that the presence of water improved acetaldehyde and hydrogen selectivities. Water, as well as hydrogen, improved the stability of the catalyst (Davidson et al., 2001a,b; Shiau and Chen, 1991; Marino et al., 2004) but decreased the conversion of ethanol by 2-3% (Armstong and Hilditch, 1920; Davidson et al., 2001a,b; Shiau and Chen, 1991). On the other hand, the presence of even a small amount of acetaldehyde (acetaldehyde/ethanol = 0.1) in an inlet stream had a more detrimental effect, lowering the conversion by 4-6% depending on reaction temperature and feed composition (Shiau and Chen, 1991).

2.2.4 Ethanol dehydrogenation kinetics and mechanism

From a kinetic standpoint, each surface reaction consists of three basic steps:

1) Adsorption of reactants
2) Conversion of reactants to products
3) Desorption of products.

Any one of these steps can be rate-controlling. In the ethanol dehydrogenation literature different models of various complexities, ranging from simple semi-empirical models to Langmuir-Hinshelwood-Hougen-Watson semi-mechanistic models, are discussed.

The dehydrogenation order of reaction is disputed. While Bond (1962) and Davidson et al. (2001a) claimed that ethanol dehydrogenation is a zero order reaction, because of the strong adsorption of the ethanol to the catalyst surface, which thus becomes saturated, other authors (Tu et al., 1994b; Morgenstern and Fornango, 2005) showed that ethanol dehydrogenation is a first order reaction with respect to ethanol. The values of activation energies, reaction conditions and types of models are summarized in Table 2.1.

Table 2.1 Activation energies of ethanol dehydrogenation.

Year	Author	Catalyst	T (°C)	Model	Order of Reaction	Ea (kJ/mol)
2005	Morgenstern and Fornago	Cu/Ni	220-280	Integral	1	149.0
1994	Tu et al.	Cu	250-310	Integral	1	50.6
		Cu/Cr				48.2
1993	Kanoun et al.	Cu	140-200	Differential	1	83.7
		Cu/Cr				
		Cu/Cr/Al				92.0
1991a	Kanoun et al.	Cu/V/Zn	140-200	Differential	1	83.7
		Cu/V				108.8
1962	Bond	Cu/Si-Al	200-280	Not	0	77.8-96.2
		Cu/Al	230	Reported		59.0

There is, however, a strong agreement among the authors that ethanol dehydrogenation is occurring on the copper sites. This was confirmed by Kanoun et al. (1993) who deduced from the virtually identical values of apparent activation energies (83.68 kJ mol^{-1}) obtained on various Cu/Cr and Cu/V/Zn mixed catalysts that zero valent Cu atoms are the active centers of all catalyst notwithstanding differences in the promoter or its amount. A similar conclusion was reached by Kazanskii (1970) who proposed that the dehydrogenation occurs by interaction of an ethanol molecule with an unfilled d-orbital of a Cu^{2+} ion. According to Peloso at al. (1979), a simplified mechanism can be then written as:

$$CH_3CH_2OH \text{ (g)} + S_{Cu} \rightarrow CH_3CH_2OH–S_{Cu} \qquad (2.16)$$

$$CH_3CH_2OH–S_{Cu} + S_{Cu} \rightarrow S_{Cu}–CH_3CH_2OH–S_{Cu} \qquad (2.17)$$

$$S_{Cu}–CH_3CH_2OH–S_{Cu} \rightarrow H_2–S_{Cu} + CH_3CHO–S_{Cu} \qquad (2.18)$$

$$H_2–S_{Cu} \rightarrow H_2 + S_{Cu} \qquad (2.19)$$

$$CH_3CHO–S_{Cu} \rightarrow CH_3CHO + S_{Cu} \qquad (2.20)$$
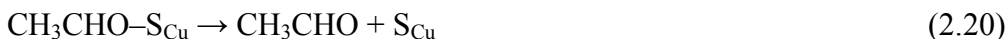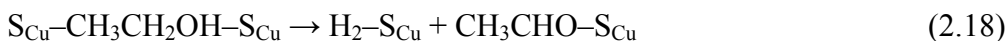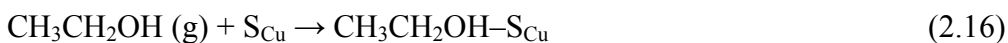
where S_{Cu} is an active copper site.

The nature of the rate-limiting step is disputed. Franckaerts and Froment (1964) as well as Peloso at al. (1979) showed that the rate-controlling step in ethanol dehydrogenation is the dual-site reaction without splitting of the C-C bond (reaction 2.18). On the other hand Shiau and Chen (1991) dismissed this mechanism as incorrect and claimed that, under their conditions, dehydrogenation takes place at a single site, where product hydrogen gets adsorbed on the catalyst surface and the rate-limiting step is the adsorption of ethanol. Davidson et al. (2001a) tested a large number of different ethanol dehydrogenation models and showed that both ethanol adsorption and its

dehydrogenation can be rate-limiting as these models provided good fit to experimental data. Another possible candidate for the rate-limiting step was a decomposition of surface-bound ethoxide. The existence of different adsorption routes was confirmed by Alcala et al. (2005) who studied conversion of ethanol on PtSn catalysts. It was found that on a Pt catalyst ethanol adsorbed through 1-hydroxyethyl species while on a PtSn catalyst ethoxide was preferentially formed. The different reaction intermediates may explain identification of different rate-limiting steps. Another explanation may be linked to the disagreement in the order of reaction. If the surface of the catalyst is saturated and the observed order of reaction is 0, then the rate-limiting step would be ethanol dehydrogenation. On the other hand, if the surface is not saturated and the order of reaction is 1, then it is foreseeable that ethanol adsorption is rate-limiting.

Surface saturation is a function of surface area, which can be significantly enhanced by the use of a support, which, according to Sheng et al. (2004), should be capable of dissociating ethanol to ethoxide and surface bound hydrogen. Ethoxide is then supplied to the active copper sites, where the second hydrogen is abstracted from oxygen-containing carbon (Chung et al., 1993). The resulting surface-bound acetaldehyde can desorb or migrate back to the support. Furthermore, despite evidence of dehydrogenation occurring predominantly on copper sites, the support can also play an active part. Thus, Di Cosimo et al. (1998) proposed a mechanism of ethanol dehydrogenation over the acid-base hydrotalcite support as:
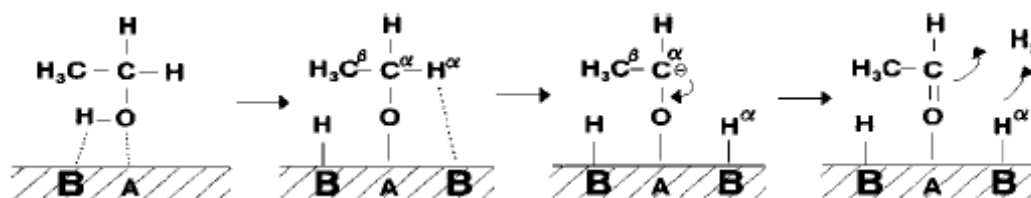
where ethanol is adsorbed on an acid-strong base pair site and the O-H bond is broken to form an ethoxide intermediate. The α-hydrogen is then abstracted by another strong base site and acetaldehyde is formed. Thus it was shown that, despite dehydrogenation itself occurring predominantly on copper sites, the reaction can be affected by the choice of support.

Another factor affecting the reaction mechanism is the presence of water. Marino et al. (2004) proposed the following mechanism occurring on copper sites in the absence of water:

$$CH_3CH_2OH \text{ (g)} + S_{Cu} \rightarrow CH_3CH_2OH–S_{Cu} \qquad (2.21)$$

$$CH_3CH_2OH–S_{Cu} \rightarrow CH_3CHO + H_2 + S_{Cu} \qquad (2.22)$$

However, when water was present, a different mechanism was postulated:

$$CH_3CH_2OH \text{ (g)} + S_{Cu} \rightarrow CH_3CH_2OH–S_{Cu} \qquad (2.23)$$

$$H_2O + S_{Cu} \rightarrow H_2O–S_{Cu} \qquad (2.24)$$

$$H_2O–S_{Cu} + S_{Cu} \rightarrow H–S_{Cu} + HO–S_{Cu} \qquad (2.25)$$

$$HO–S_{Cu} \rightarrow H–S_{Cu} + O–S_{Cu} \qquad (2.26)$$

$$H–S_{Cu} + H–S_{Cu} \rightarrow H_2 + 2 S_{Cu} \qquad (2.27)$$

$$CH_3CH_2OH–S_{Cu} + O\text{-}S_{Cu} \rightarrow CH_3CHO + H_2O + 2 S_{Cu} \qquad (2.28)$$
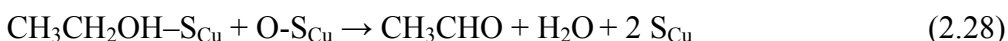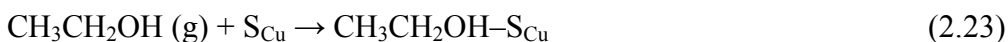
Therefore it can be concluded that dehydrogenation of ethanol can occur through different mechanisms. Despite dehydrogenation itself occurring predominantly on copper sites, it can be affected by the support or a promoter by influencing ethanol adsorption and dehydrogenation or by addition of water which may change the dominant mechanism.

An overview of the publications related to dehydrogenation of lower alcohols is presented in Table 2.2. It is apparent that ethanol dehydrogenation has been, for the past century, and still remains a centre of attention of many researchers.

Table 2.2 Overview of ethanol dehydrogenation literature.

Year	Author	Catalyst system	Temperature Pressure/ EtOH Pressure W/F [kgCu h/l] Feed Composition	EtOH conversion	Acetaldehyde selectivity	By - products	Hours on stream Deactivation	Objectives
2006	Chang	2-7wt.%Cu/SiO2 (rice husk ash)	275 °C atmospheric 40 mg 40 ml/min EtOH / N2	up to 77%	100%	none	2 none	Ethanol dehydrogenation over Cu/ Rice Ash husk prepared by ion exchange
2005	Morgenstern	28%Cu 69%Ni 3%Al	165-345 °C atmospheric 10-130 gcat h / mole EtOH 70wt% EtOH/H2O	up to 80%	up to 20%	CO, CH4, CO2	450 sintering	Low temperature steam reforming of ethanol
2004	Inui	Cu Cu/ZnO/ZrO2/Al2O3 posttreatment with Li, Na, K, Cs, Ca, B	200-250°C atmospheric W/F = 1.6 gcat h g EtOH 99.5% EtOH:H2O	up to 68%	up to 22%	Ethyl acetate, methyl ethyl ketone, butyraldehyde, acetic acid, diethyl ether, 1-butanol, methyl acetate, propanol, others	not reported	Mechanism of ethanol-acetaldehyde reaction system with regards to ethyl acetate formation
2004	Lin	Cu-Zn/Al2O3	350-450°C 200-1100 kPa WHSV = 3-5 h-1 6:1 and 4:1 N2:EtOH	up to 91%	up to 60%	diethyl ether, ethyl acetate	not reported	Ethanol dehydrogenation in Pd membrane reactor
2004	Marino	6wt.%Cu/Al2O3 6wt.%Cu4wt.% Ni/Al2O3 6wt% Ni/Al2O3	300 °C atmospheric 1-2 g min/ml 0.125-0.250 ml/min 0-9 mol ratio H2O:EtOH	70% up to 82% 7%	95% app. 80-90% 91%	Acetic Acid CH4, CO, Acetic Acid CH4, CO	not reported	Mechanism of ethanol gasification
2004	Nishiguchi	20 mol% CuO/CeO2 20 mol% CuO/K-Al2O3 20 mol% CuO/SiO2 20 mol% CuO/CeO2 + MgO	150-400 °C atmospheric constant CuO loading of 0.05g H2O:EtOH (6:1.2)e-4 mol/min + Ar	up ro 96%	up to 28%	CO2, acetone, C2H4, butyraldehyde, ethyl acetate, methyl ethyl ketone, acetal, others	not reported	Steam reforming of ethanol to acetone
2003	Chang	1-15wt.% Cu/SiO2 (rice husk ash)	250 °C atmospheric 50 mg EtOH/N2 15ml/min to saturator	up to 75%	100%	none	3 sintering	Ethanol dehydrogenation over Cu/ Rice Ash husk prepared by incipient wetness impregnation
2002	Inui	Cu Cu/ZnO Cu/ZrO2 Cu/Al2O3 Cu/ZnO/ZrO2/Al2O3	200-250°C atmospheric LHSV = 0.2-50 h-1 EtOH	32% 36% 81% 80% up to 75%	84% 84% 9% 10% up to 12%	Ethyl acetate, methyl ethyl ketone, butyraldehyde, acetic acid, diethyl ether, 1-butanol, others	not reported	Direct synthesis of ethyl acetate from ethol
2002	Zhang	10 wt% Cu/SiO2	230, 300 °C atmospheric/ less than atmosperic not reported 0.1% MeOH/Ar	not reported	not reported	CO, methyl formate	0 - 2	FTIR study of methanol adsorption and decomposition
2001	Abu-Zied	Cd-Cr Cd Cr	150 - 400 °C atmospheric/ less than atmosperic various EtOH/ carrier gas	80% 2% 19%	70% 95% 19%	C2H6, C2H4 ethyl acetate	12 mainly stable	Characterization of Cd-Cr catalysts calcined at different temperature for ethanol decomposition, XRD, electrical conductivity, FTIR, TPR
2001a	Davidson	0.5 % Pd/Al2O3	196-231 °C atmospheric/ up to 78 kPa various Ar/EtOH (0.22-0.74 % mol.), EtOH/H2O, CH4-CO-H2-CH3CH0/EtOH, CH3CH0	<3%, 25%	yield up to 45%	CH4, CO, Propane, Propene, 2-butenal	not reported Fast coking	Kinetics of Pd-catalyzed ethanol decomposition, LHHW
2001b	Davidson	0.5 % Pd/Al2O3	100 - 230 °C atmospheric/ less than atmosperic Pulse CH3CH0/EtOHl/H2O-He/CO/H2/	not reported	not reported	CH4, CO, Propane, Propene, 2-butenal, diethyl ether, C2H6	not reported	Comparison of kinetic and surface science studies, mechanism of Pd catalyzed ethanol decomposition
2001	Fujita	Cu/ZnO (10/90 - 70/30)	160-220 °C atmospheric / 20.2 kPa 2.67 EtOH / carrier	3.5 - 82%	6 - 100%	ethyl acetate methyl ethyl ketone acetone	not reported	Effect of catalyst precursor on ethanol dehydrogenation

Year	Author	Catalyst system	Temperature Pressure/ EtOH Pressure W/F [kgCu h/l] Feed Composition	EtOH conversion	Acetaldehyde selectivity	By - products	Hours on stream Deactivation	Objectives
2001	Gole	3wt%Cu/SiO2 nanoparticles	330°C atmospheric pulse 10 uL EtOH in He	45%	100%	none	not reported	Selective production of acetaldehyde on new type of support.
2001	Tu	Na,K,Rb/Cu/SiO2 M/Cu -1/10 molar Cu/SiO2 14/86 weight	300 °C atmospheric/ less than atmosperic 1.56 N2/95% EtOH/ 5% H2O	max. 68 %	>99%	none	4 sintering	Effect of alkali metal oxides promoters on ethanol dehydrogenation, XRD, TPR, TPD, Surface measurements
2000	Freni	15 wt% Cu/SiO2	300 - 650 °C atmospheric/ less than atmosperic 1.38 9.4 vol% EtOH / 76.8 vol% H2O/ 13.8 vol% N2	100% at 370- 450 °C	100 % at 320 - 500 °C	CO trace, CH4 trace, C2H4 above 500 °C	2 none	Hydrogen production by two step ethanol steam reforming
1998	Di Cosimo	MgO-Al2O3 mixed oxides	300 °C atmospheric 46 (gcat h/mol EtOH) w=0.2g 1:10 EtOH:N2	0.05%	55%	n-butanol, diethyl ether, C2H4	10 50%	Structure, surface and catalytic properties of Mg-Al Basic Oxides
1998	Raich	Pt-Sn/SiO2 Cu/SiO2	175 - 275 °C atmospheric/ 7.8 kPa 11 - 37 Ar/EtOH	50% 28%	up to 96-98%	CH4,CO ethyl acetate, CH4, butanal, CH3COOH, trace of 1,1 diethoxy ethane	6 Fast deactivation above 225 °C	Ethanol dehydrogenation with 3 different reactors: conventional, 2xmembrane and 3 different catalysts. Thermodynamics, XRD
1998	Tu	Mg,Ca,Sr,Ba/Cu/SiO2 M/Cu -1/10 molar Cu/SiO2 14/86 weight	300 °C atmospheric/ less than atmosperic 1.56 N2/95% EtOH/ 5% H2O	max. 70 %	>99%	none	4 significant sintering	Effect of alkaline earth oxides promoters on ethanol dehydrogenation, XRD, TPR, TPD, SEM, Surface measurements
1997	Liu	2% Cu-P/Al2O3 Cu:P 5:1	260 - 310 °C atmospheric/ less than atmosperic various Ar/EtOH	up to 90 %	100%	none	not reported	Catalytic dehydrogenation of ethanol in Ru/Al2O3 membrane reactor
1995	Deng	2% Cu-P/Al2O3 Cu:P 5:1	250 - 310 °C 110-120 kPa/ less than atmosperic various Ar/EtOH	not reported	yield up to 65%	not reported	not reported	Catalytic dehydrogenation of ethanol in metal (Pd,Pt,Cu, Ni) membrane reactor - SEM,STEM,XRD,BET,BJH, pore size distribution, gas permeation
1994	Deng	Cu-P/Al2O3	350 - 500 °C not reported/ less than atmosperic various Ar/ MeOH	up to 100%	up to 90% to formaldehyde	CO, Dimethyl ether, CH4 traces: CO2, methyl formate	not reported	Comparison of 3 membrane reactors to conventional based on methanol dehydrogenation, SEM, pore size, gas permeation
1994a	Tu	Cu-Cr 0-0.5 molar	310 °C atmospheric/ less than atmosperic 16-30 N2/95% EtOH/ 5% H2O	not reported	100%	none	8 slow sintering	Characterization of unsupported Cu-Cr catalyst for ethanol dehydrogenation, SEM, XRD, surface measurements, TPR
1994b	Tu	Cu-Cr 0-0.5 molar	250 - 310 °C atmospheric/ less than atmosperic 16-30 N2/95% EtOH/ 5% H2O	up to 80%	>99%	none	8 slow sintering	Effect of Cr promoter on ethanol dehydrogenation, XRD, surface measurements, kinetics
1993	Chung	Cu ZnO	200 - 320 °C atmospheric/ less than atmosperic not reported He/2%D2 or He/D2O + EtOH/CH3CH0	> 80% less than 50%	> 95 % lower than 10 %	traces of propanone, butanone, butanal, ethyl acetate C2H4, ethyl acetate	not reported	Deuterium exchange study to identify different mechanisms of ethanol dehydrogenation
1993	Kanoun	Cu-Cr Cu-Al Cu-Cr-Al (various)	190 °C atmospheric/4.5 kPa 2.77 EtOH / H2 (97.32 kPa)	below 1 %	100%	none	not reported	Characterization of Cu-Cr-Al catalyst for ethanol dehydrogenation and CO2-H2 conversion. BET, Cu surface, Cu dispersion, XRD
1993	Szymanski	Carbon Carbon-Ni	50-360 °C atmospheric 0.5 g 91 kPa EtOH in N2	up to 100%	up to 72%	C2H4, diethyl ether, 1,1-diethoxy ethane	not reported	Converion of EtOH on carbon supports

Year	Author	Catalyst system	Temperature Pressure/ EtOH Pressure W/F [kgCu h/l] Feed Composition	EtOH conversion	Acetaldehyde selectivity	By - products
1992	Kenvin	2.4 wt. %Cu/SiO2 3.8 wt. %Cu/SiO2 8.6 wt. %Cu/SiO2	275 °C 448 kPA 1-2 ul EtOH pulse over 0.11-0.32 g cat	15% 19% 57%	93% 100% 27%	ethyl acetate, light gases
1991	Iwasa	Cu 0.5-90 wt% Cu/SiO2 0.5-30 wt% Cu/ZrO2 6.3 & 30 wt% Cu/Al2O3 30 wt% Cu/ZnO	150 - 250 °C atmospheric/ 20.5 or 10.1 kPa various EtOH (20.5 kPa), CH3CH0, EtOH (10.1kPa)/H2O (20.2kPa)	up to 80%	88% 53.90% 56.20% 55.10% 36.40%	Acetone, CH3COOH, Ethyl acetate Acetone, CH3COOH, Ethyl acetate, C4-species Acetone, C4-species, Ethyl acetate Acetone, CH3COOH, Ethyl acetate, C4-species, diethyl ether Acetone, CH3COOH, Ethyl acetate
1991a	Kanoun	V-Cu V-Zn V-Cu-Zn (various)	190 °C atmospheric/4.5 kPa 2.77 - 0 EtOH / H2 (97.32 kPa)	below 1 %	100%	none
1991b	Kanoun	V-Cu-Zr (various) V-Cu V-Zr	190 °C atmospheric/4.5 kPa 2.77 - 0 EtOH / H2 (97.32 kPa)	below 1 %	80-100 %	none
1991	Shiau	3% Cr-10% Cu/SiO2	210-290 °C atmospheric/ 20-71kPa not reported EtOH/inert or EtOH/CH3CH0 or EtOH/H2	low	>99%	none
1984	Sodesawa	Cu 1.47 - 60 wt% Cu/SiO2	250 °C atmospheric/less than atmospheric 3.22 - 131 MeOH/He	up to 70 %	not reported	not reported
1979	Peloso	CuO-Cr2O3-SiO2-Na2O-binder -commercial catalyst	255 - 285 °C atmospheric 8 - 45 95% EtOH	low	high	traces CO, CH4, CH3COOH, ethyl acetate
1964	Franckaerts	Cu-5% CoO - 1% Cr2O3/asbestos	225-285 °C atmospheric - 1013 kPa various EtOH/ H2O 13.5% molar various EtOH/CH3CH0/H2O	100%	high	traces CH4, CO ethylacetate
1951	Church	Cu - pellet/gauze Cu-5% Cr2O3 Cu-5% CoO Cu-7% ZnO Cu-5% MgO Cu/asbestos Cu-1.62% Cr2O3/pumice Cu/Al2O3 Cu-5% CoO/pumice Cu-5% MgO/pumice Cu-5.2% CoO/asbestos Cu-5.2% CoO/alundum Cu-5.2% CoO-1.8% Cr2O3/asbestos Cu-5.2% CoO-4.4% Cr2O3/asbestos	275-340 °C atmospheric 1 gcat h/l 40 ml/h (l) 95% EtOH	up to 94%	up to 90%	ethyl acetate, CH3COOH traces: CH4,CO, C2H4
1920	Armstrong	Cu - powder Ni - powder	240-335 °C atmospheric not reported 50% - 100% EtOH:H2O	up to 30%	up to 95%	CH4, CO, C2H4, CO2, butyraldehyde, crotonaldehyde, ethyl acetate

2.3 Acetaldehyde hydrogenation

2.3.1 Introduction

Acetaldehyde obtained by dehydrogenation of ethanol in the first part of the cycle is used in the second part as a reactant to remove hydrogen from its mixture with carbon monoxide, commonly known as syngas. Syngas can originate from various processes such as gasification of coal or biomass, stream reforming of methane or ethanol or even from the reforming of landfill gas. Through acetaldehyde hydrogenation, the loop is closed by recreating ethanol and a purified CO stream is produced which can be utilized in the production of lesser purity hydrogen by water-gas shift reaction or as a valuable chemical (reducing agent or reactant) in the chemical industry. In this section, a literature review pertaining to the subject of acetaldehyde hydrogenation is presented.

Early in the 20th century, ethanol was commercially produced in Switzerland by hydrogenation of acetaldehyde by hydrogen over a Ni catalyst (Armstrong and Hilditch, 1920). This process was rendered economically obsolete by the availability of cheap petroleum leading to a widespread use of ethylene pyrolysis and ethylene's sequential hydration to ethanol.

The interest in acetaldehyde hydrogenation was renewed in 1970s with the investigation of syngas as an alternative resource base for the production of various hydrocarbons. By changing reaction conditions and the type of catalyst, a wide variety of products ranging from methane and various hydrocarbons to methanol, ethanol and higher oxygenates can be produced from syngas mixtures containing various compositions of CO and H_2. Even though several attempts were made to propose one universal mechanism of formation for species of interest, data collected suggested the existence of many different routes of formation. For ethanol, two pathways were proposed in the literature:

- Ethanol formed by hydrogenation of an acetaldehydic precursor.
- Ethanol formed independently of acetaldehyde.

To prove the validity of the former mechanism, reactions of acetaldehyde were studied (Burch and Petch, 1992a).

Recently, acetaldehyde has been identified as a pollutant in the exhaust from vehicles operating on pure ethanol and therefore its interaction with surfaces has been studied in order to find the best way for its breakdown to harmless substances (Rasko and Kiss, 2005a,b; Zhao et al., 2003).

Compared to ethanol dehydrogenation, acetaldehyde conversion is a reaction of much lesser industrial importance and as such, scientific publications are much scarcer. Nonetheless, in the following section, the effect of catalyst composition together with several results obtained at different reaction conditions will be discussed together with the proposed adsorption and reaction mechanisms.

2.3.2 Catalyst composition
Active phase

Armstrong and Hilditch (1920) showed the superiority of unsupported Cu powder over Ni in acetaldehyde hydrogenation; the latter decomposing acetaldehyde to CH_4 and CO to the same extent as hydrogenating it to ethanol.

Fischer-Tropsch synthesis shifted attention from common transition metals such as Cu or Ni to more active noble metals. From indications that acetaldehyde hydrogenation is in itself one step in ethanol synthesis from syngas, catalysts active for oxygenate synthesis were studied as a first choice. The common aspect shared by these catalysts is their ability to non-dissociatively adsorb CO. This feature is essential for successful hydrogenation of acetaldehyde and minimization of its decomposition, because it is the carbonyl group in the acetaldehyde that is hydrogenated to form ethanol. In the case of dissociative adsorption, decomposition products, CO and CH_4, would be formed.

Perhaps surprisingly, methanol synthesis catalysts were found to be superior to ethanol synthesis catalysts for acetaldehyde hydrogenation. The explanation lies in the different mechanism of synthesis of these two alcohols. While for ethanol synthesis from syngas two types of sites are required: sites that dissociate CO, so that methyl group can be created and sites that adsorb non-dissociated CO and attach it to the methyl group, methanol is formed solely by hydrogenation of non-dissociated CO molecule. In acetaldehyde hydrogenation to ethanol, the situation is very similar to methanol synthesis, as the desired reaction involves hydrogenation of adsorbed acetaldehyde

species and therefore methanol synthesis catalysts work better. Ethanol synthesis catalysts with their dissociating sites, on the other hand, contribute to undesired decomposition of acetaldehyde to CH_4 and CO.

The most promising results for acetaldehyde hydrogenation or methanol synthesis from syngas were obtained using Pd- (Ponec, 1992a; Lee at al., 1987), Rh- (Burch and Petch, 1992a; Trunschke et al., 1991; Yin et al., 2003) and Cu- (Armstrong and Hilditch, 1920; Agarwal et al., 1988; Ehwald et al., 1991; Arimitu et al., 1989; Inui at al., 2004) based catalysts.

Supports

Although no support is required for successful hydrogenation of acetaldehyde on Cu (Armstrong and Hilditch, 1920), use of a high-surface-area material allows better dispersion of the active phase, thus producing catalysts that can have higher activity than their pure metal components can provide. Large cost savings can therefore be achieved, especially with noble metals. SiO_2 is the most commonly used support material in ethanol and methanol synthesis from syngas and consequently in acetaldehyde hydrogenation, even though, as Ojeda at al. (2004) argued, Al_2O_3 offers as high or even higher activity. Although CeO_2 provides significantly lower surface area than SiO_2 or Al_2O_3, it has the ability to strongly adsorb and hydrogenate acetaldehyde making it an interesting alternative to the above-mentioned commonly-used supports.

Promoters

Once again, based on the results of Armstrong and Hilditch (1920) and Kenvin and White (1992), who studied acetaldehyde hydrogenation on pure Cu and Cu/SiO_2 respectively, it can be stated that pure copper is sufficient for acetaldehyde hydrogenation and the presence of promoter is therefore not necessary. However, promoters may play a beneficial role in improving both activity and selectivity of the reaction. For example, in oxygenate synthesis from syngas, promoters can play a very important role in product distribution. Thus Rh, a common active catalyst component in hydrocarbon synthesis from syngas, produces mainly CH_4 when deposited on Al_2O_3 or SiO_2. However, an addition of even small amounts of Fe (0.1 wt.%) results in a complete inversion of the

product distribution: hydrocarbon formation is largely suppressed, while significant amounts of oxygenates are produced. Multiple mechanisms of promoter effects on catalyst performance have been proposed in various reviews (Ponec 1992b; Lee et al., 1987; Hindermann et al., 1993). These include:

- stabilization of a positive charge on the active metal component, which consequently stabilizes reactive intermediates on the surface (Herman et al., 1979; Ponec, 1992b; Hindermann et al., 1993)

- selective blocking of larger active metal clusters required for methanation (Burch and Hayes, 1997)

- formation of a new active phase on the interface of the active metal and the promoter (Burch and Hayes, 1997)

- creation of a hydrogen pool providing extra hydrogen for the hydrogenation (Burch and Petch, 1992a)

- and stabilization of reactive intermediates (Burch and Petch, 1992a).

Existence of blocking mechanisms and new phase formation is supported by several studies that report an optimum loading of metal promoter at which the highest activity and selectivity to the desired product was achieved (Burch and Petch, 1992a; Burch and Hayes, 1997; Guglielminotti et al., 1995, 1994). This phenomenon can be explained by the progressive formation of new active sites up to a point where then too many promoter atoms start to block active metal clusters and ruin the catalyst activity. Further evidence for the hydrogen pool hypothesis was provided by Takenaka et al. (2002) who studied the redox properties of Fe oxides for storage of hydrogen.

According to Guglielminotti et al. (1994), it is possible to categorize promoters into two main groups depending on their effect on the Rh catalyst system in oxygenate synthesis:

1)   oxophilic oxides (MoO_3, MnO_2, Ti_2O_3, ZrO_2) that enhance both activity and selectivity towards oxygenates

2)   and basic oxides (Fe_2O_3, ZnO) whose addition results only in selectivity improvement.

A slightly different classification is proposed by Burch and Petch (1992b) who divide promoters into a group which boosts either the activity (Sc, Ti, V, Cr, Mn, Mo, La) or the selectivity (Fe, Co, Ir, Ti, K, Li) of the catalyst.

2.3.3 Results obtained for acetaldehyde hydrogenation

In this section, results obtained solely for acetaldehyde hydrogenation will be discussed. Due to the scarcity of literature sources, the effects of individual reaction conditions will not be treated separately, but rather these conditions will be explicitly stated together with the results obtained.

Armstrong and Hilditch (1920) obtained 68% conversion of acetaldehyde (AcAd) with 83% selectivity to ethanol when using pure powder Cu. The reaction was operated at $T = 200\text{-}210°C$, $P = 0.1$ MPa and 1:2 molar ratio of $AcAd:H_2$.

Burch and Petch (1992a) achieved 100% conversion of acetaldehyde to ethanol with $Rh\text{-}Fe/SiO_2$ in a hydrogen atmosphere and reaction conditions of $T = 100\text{-}150°C$ and $P = 2$ MPa. When syngas was used as a hydrogenating agent, the catalyst retained its activity even though ethanol selectivity dropped to 90%. However, this might have been caused by the elevated reaction temperature of 270°C, because, also in the article, 100% activity and selectivity were reported for Rh catalyst containing 1 wt.% of Fe in syngas atmosphere at 200°C. These authors also tested Mn and Ce oxide promoters, the former exhibiting comparable properties to Fe and the latter being slightly less active. In addition to promoter and temperature effects, different CO/H_2 mixtures were used to demonstrate the influence of the composition of the hydrogenating agent. It was found, that unpromoted Rh/SiO_2 lost its activity with increasing amounts of CO in the mixture, presumably as a result of ethyl acetate formation on the surface. On the other hand, an Fe-promoted catalyst retained its initial activity and only a slight 4% increase in hydrocarbon yield at the expense of ethanol was observed.

Similar results were obtained by Trunchke et al. (1991) who studied acetaldehyde hydrogenation over various $Rh\text{-}Mo/Al_2O_3$ catalysts. Hydrogenation was investigated at atmospheric pressure in the temperature range of 142-220°C. At first, in pure hydrogen and at a temperature of 163°C, the selectivity to ethanol reached 95%. After switching to syngas and further increasing the temperature to 200°C, the selectivity increased to 99%. Superior hydrogenation selectivity in the syngas atmosphere was explained by the

selective blocking of large Rh clusters, required for acetaldehyde decarbonylation, by CO molecules.

As part of a C1 research program in Japan, an investigation on ethanol synthesis from syngas was conducted. A large variety of promoters for Rh/SiO_2 catalysts was tested. Particularly of interest with regard to acetaldehyde hydrogenation, was a short note mentioning the utilization of a physical mixture of two different catalysts: an oxygenate synthesis catalyst to produce ethanol with unavoidable amounts of undesired oxygenates, such as acetic acid and acetaldehyde, and a hydrogenation catalyst, which would hydrogenate these undesired by-products to ethanol (Arimitu et al., 1989). Rh-Fe/SiO$_2$, Ir-Fe/SiO$_2$, Pd-Fe/SiO$_2$ and Pd-Mo/SiO$_2$ were found to selectively hydrogenate acetaldehyde to ethanol under ethanol-from-syngas reaction conditions (4.9 MPa, 300°C). However, the Japanese goal was to find a catalyst which would hydrogenate not only acetaldehyde but also acetic acid to ethanol. Industrial methanol synthesis catalysts exhibited excellent hydrogenation activity, thus providing a solution to the problem. Cu-Zn/SiO$_2$ and Zn-Cr/SiO$_2$ were prepared by impregnation and their performances compared. Copper-based catalysts were found to be superior and a further investigation of promoters identified ZnO to be the best promoter. It was further mentioned that the hydrogenation activity was affected by copper particle size, which was adjustable by changing the air flow rate during calcination treatments.

According to Kenvin and White (1992) particle size distribution affects not only the activity but also the selectivity. SiO$_2$-supported catalysts with various Cu loadings were used in acetaldehyde hydrogenation and provided up to 60% conversion at atmospheric pressure and 275°C. Acetaldehyde was delivered in the form of 1-2 μL pulses injected in the gas flow of 15.5 mL min^{-1} of 25 mol% H$_2$/He. Catalysts with Cu loadings < 3.8 wt.% proved to be 100% selective to ethanol, while higher Cu loadings shifted selectivity to ethyl acetate.

Ehwald et al. (1991) used a similar approach as Arimitu et al. (1989): by mixing two catalysts with different functions it was expected that a higher conversion and selectivity in ethanol synthesis would be obtained. Different promoters such as Ir, Mn and Li were used to prepare a Rh-M/SiO$_2$ oxygenate synthesis catalyst. Once

acetaldehyde or ethyl acetate was formed, a Cu-ZnO/SiO$_2$ catalyst was expected to hydrogenate them to ethanol. Three different methods of preparation were used:

- a physical mixture of two catalysts,
- co-precipitation of all components forming only one catalyst phase and
- grinding the two catalysts together, pressing the powder and crushing it to form a homogeneous mixture.

Out of these three, the anticipated results were achieved only with the physical mixture: though the overall activity was decreased, the addition of Cu-ZnO/SiO$_2$ resulted in a large increase in ethanol yield, indicating that acetaldehyde, the formation of which was earlier observed in runs with Rh-based catalysts only, was successfully converted to ethanol. The two other catalyst systems, i.e., grinded mixture and co-precipitated catalyst, exhibited only negligible activity. When the effect of temperature was evaluated, it was found that the selectivity to ethanol started to decrease above 300°C and methane then became the predominant product. The yield of ethanol also increased by increasing the pressure from 1 to 3 MPa, but unfortunately so did the yield of undesired methanol.

The behaviour of Cu/SiO$_2$ in acetaldehyde hydrogenation was studied by Agarwal et al. (1988). Two samples containing 4.4 and 6.8% of Cu deposited on SiO$_2$ were prepared by ion-exchange. The experiments were carried out at temperatures of 92, 125 and 145°C, under atmospheric pressure and with pure hydrogen as a reducing agent. In a differential mode, at conversions under 10%, ethanol was the only product detected except at high residence times and low H$_2$/AcAd ratios, when traces of ethyl acetate were also formed. Significant deactivation was observed, with the catalyst losing half of its activity after just 3.5 h on stream, which was ascribed to the polymerization of acetaldehyde on the catalyst surface. The activity was restored by passing a stream of pure hydrogen over the catalyst sample.

Inui et al. (2004), in an attempt to elucidate the reaction pathway from ethanol to ethyl acetate, conducted an acetaldehyde hydrogenation experiment over Cu-Zn-Zr-Al-O catalyst at 200°C to gain 90% conversion but only 17% selectivity to EtOH. This low selectivity can be explained by high residence times, which favour formation of ethyl acetate via secondary reactions.

These literature results indicate that Cu-based catalysts are active and selective in acetaldehyde hydrogenation. The reaction proceeds readily in a temperature range of 200-300°C and is not negatively influenced by pressure. The selectivity can be affected by Cu loading, residence time, feed composition and selection of promoters.

2.3.4 Acetaldehyde hydrogenation kinetics and mechanism

The first step in acetaldehyde hydrogenation – adsorption of acetaldehyde – differs depending on the nature of the surface. Rasko and Kiss (2005a,b) reported that acetaldehyde adsorbs on oxygen containing surfaces, e.g., catalyst supports, in two forms: 1) a less stable H-bridge bonded form or 2) a more stable form adsorbed on Lewis sites through one of the oxygen lone pairs. Both forms were found to be reactive and were converted to several different products, one of them being an ethoxy surface species – precursors of ethanol.

On metal surfaces, acetaldehyde is reported (Zhao et al., 2003) to adsorb also in two forms: 1) a weak surface-adsorbate bond through an oxygen lone electron pair or 2) a stronger bond where both the carbonyl carbon and oxygen atoms interact with surface metal atoms. While the former interaction usually leads to desorption of acetaldehyde, the latter results in acetaldehyde conversion.

Once the acetaldehyde is adsorbed it can be converted to ethanol. Kenvin and White (1992) proposed that for hydrogenation to occur on a Cu site, it must contain both acetaldehyde and hydrogen. Furthermore, Agarwal et al. (1988) conducted deuterium exchange study on acetaldehyde hydrogenation on Cu/SiO_2 in temperature range of 92-145°C to propose a mechanism of the reaction and elucidate kinetics. Hydrogenation was found to have an activation energy of 69 kJ mol^{-1} and to be 0.63 and 0.04 order with regard to hydrogen and acetaldehyde, respectively. Near-zero dependence of the reaction on acetaldehyde concentration was explained by complete saturation of the surface. Combining these kinetic results with deuterium exchange data, two reaction mechanisms were proposed. Acetaldehyde was found to bind to the surface through its oxygen contained in carbonyl group. Adsorbate is then involved in 1) enol transformation, which does not lead to dehydrogenation:
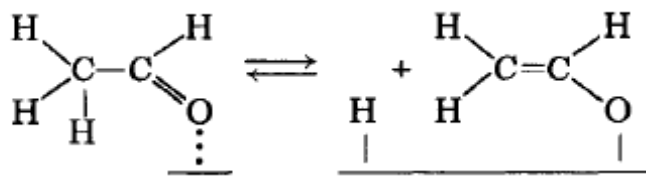
and 2) in hydrogenation of a carbonyl group, for which two mechanisms were proposed:
2a) formation of ethoxy group, where hydrogen attacks the carbon in carbonyl group:
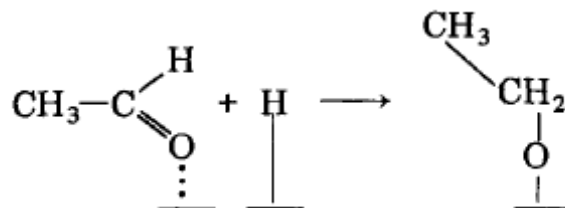
and 2b) mechanism involving hydrogen attack on oxygen:
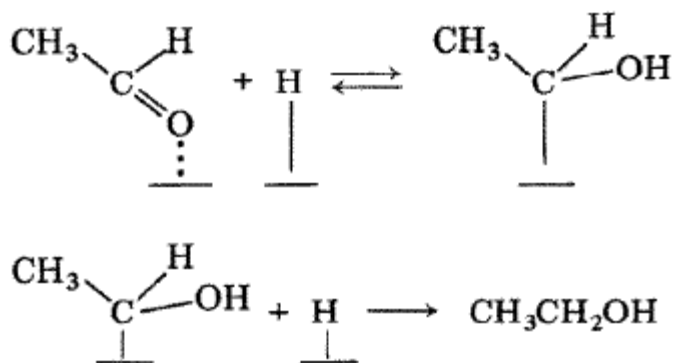
The second mechanism was found to be in a better agreement with Agarwal's kinetic results. The resulting ethanol or ethoxide can then migrate to the support or desorb to the gas phase.

The overall evaluation of literature sources including catalyst systems, reaction conditions applied, and results obtained by various research groups is summarized in Table 2.3.

Table 2.3 Overview of acetaldehyde hydrogenation literature.

Year	Author	Catalyst system [wt. %]	Temperature Pressure Feed Composition Flow rate Sample weight/volume	Reaction	Conversion / Activity	Selectivity to main product	By-products	Hours on stream Deactivation	Objectives
2005a	Rasko	TiO2, CeO2, Al2O3	27-400 °C subatmospheric AcAd	AcAd adsorption	N/A	N/A	Crotonaldehyde, Benzene, H2, C2H2, C2H6, CH4	N/A	Adsorption and surface reactions of AcAd on oxides, FTIR, MS
2005b	Rasko	1 Rh/Al2O3 1 Pt/Al2O3 Au/Al2O3	27-400 °C subatmospheric AcAd	AcAd adsorption	N/A	N/A	Crotonaldehyde, Benzene, H2, C2H2, C2H6, CH4	N/A	Adsorption and surface reactions of AcAd on alumina supported noble metals, FTIR, MS
2004	Inui	Cu:ZnO:ZrO2:Al2O3 12:1:2:2	220°C atmospheric AcAd/H2 W/F = 1.6 h-1 not reported	AcAd hydrogenation	90%	EtOH 17% EtAc 47%	Methyl ethyl ketone, 2-butanol, methyl acetate, butyraldehyde, 1-butanol, 2-pentanone, butyl acetate, ethyl butyrate	Not reported	Elucidation of reaction pathway from ethanol to ethyl acetate, Co-feed, alkaline pre + post treatment
2004	Ojeda	1.6 Mn/Al2O3 3 Rh/Al2O3 3 Rh - 0.8 Mn/Al2O3 3 Rh - 1.6 Mn/Al2O3 3 Rh - 3.2 Mn/Al2O3	240-260°C 2.03 MPa CO/H2=1:2 50 ml/min 0.5 g	CO hydrogenation	none 4.90% 5.20% 5.90% 6.30%	none CH4 26.7% EtOH 27% EtOH 30 % Alkanes 35 %	none EtOH, EtAc, Alkanes, AcAd, AA CH4, EtAc, Alkanes, AcAd, AA CH4, EtAc, Alkanes, AcAd, AA EtOH, CH4, EtAc, AcAd, AA	Not reported	Effect of Mn loading on performance of Rh-Mn/Al2O3 catalysts in CO hydrogenation, TEM, TPR, XPS, Chemisorption, FTIR, TPSR.
2003	Yin	1 Rh/SiO2 1Rh-1Mn/SiO2 1 Rh-1 Mn- 0.075 Li -(0.05-1)Fe/SiO2 1 Rh-1 Mn- 0.075 Li/SiO2 1 Rh -0.05 Fe/SiO2 1Rh-1Mn-0.05Fe/SiO2	320°C 3 Mpa CO/H2=1:2 GHSV = 12000 h-1 0.4g	CO hydrogenation	2.61% 8.66% 8.44-4.12% 6.69% 2.94% 8.96%	EtOH 12.3% EtOH 23% EtOH 27% EtOH 35% EtOH 13% EtOH 23%	C1 hydrocarbonsMeOH, AcAd, propanol, butanol, AA	Not reported	Effect of Fe promoter on catalytic properties of Rh-Mn-Li/SiO2 for CO hydrogenation, TPR, CO TPD, CO upatke
2003	Zhao	Pt (111), Sn/Pt(111)	-183-927 °C atmospheric AcAD	AcAd adsorption	N/A	N/A	CH4, CO, H2	N/A	Adsorption of AcAd, HREELS, TPD
2002	Wang	1.65 Rh/SiO2 1.89 Rh/CeO2	180°C atmospheric CO/H2=2:1, probes: EtOH, MeOH, AcAd 30ml/min 200 mg	CO hydrogenation	2.94 0.235 (umolC.g-1.min-1)	AcAd - 21.7 % EtOH - 31.2	Alkanes, EtOH, MeOH Alkanes, MeOH, AcAd, EtAc	no deactivation 70 min, deactivation	Probing study of Rh catalysts on two different supports in CO hydrogenation, BET, pore volume, chemisorption.
1997	Burch	2 Rh-0-14 -Fe/Al2O3	270°C 1 MPa CO/H2=1:1 20 ml/min 150 mg	CO hydrogenation	max. 4%	EtOH 50%	CH4, MeOH, alkanes	continuous, loss of 1/4 activity in 2 hrs.	Effect of Fe loading in Rh-Fe/Al2O3 on EtOH synthesis from syngas, SEM, AEM, chemisorption, TPR.
1995	Guglielminotti	0.75-1.39 Rh- 0.26-2.5 -Fe/ZrO2 Rh/ZrO2 Fe/ZrO2	220°C atmospheric CO/H2=1:3 20 ml/min 0.2g	CO hydrogenation	max. 9.2 % max. 6 % <1%	CH4 50% CH4 50% none	Alkanes, EtOH, CO2, MeOH EtOH, alkanes, CO2, MeOH none	Not reported	Effect of Fe loading in Rh-Fe/ZrO2 on EtOH synthesis from syngas, FTIR, chemisorption, TPR.
1995	Idriss	CeO2 3 Pd/CeO2 3 Co/CeO2 3Pd-3 Co/CeO2	r.t. --> 570°C atmospheric He/AcAd 30 ml/min not reported	AcAd TPR+D	47% 76% 66% 84%	Crotonaldehyde 28% EtOH 27% Propane 20% CH4 32%	Crotyl alcohol, acetone CO, CO2 EtOH, Acetone CO2, CO	Not reported	Analysis of acetaldehyde reactions on CeO2 supported catalysts by TPD and FTIR, chemisorption, XRD, XPS.
1994	Guglielminotti	1 Rh-Mo/ZrO2	220°C atmospheric CO/H2=1:3 20 ml/min 1.2g	CO hydrogenation	max. 13 %	CH4 55%	EtOH, alkanes, MeOH	Not reported	Elementary steps in CO hydrogenation on Rh-Mo/ZrO2. TEM, EPR, FTIR, TPR, chemisorption.
1994	Benitez	1 Rh- 10 Lu2O3/Al2O3	180-300°C atmospheric CO/H2/N2 = 1:3:8.5 20 ml/min 300 mg	CO hydrogenation	low	CH4	EtOH, alkanes, MeOH	Not reported	DRIFTS in CO hydrogenation. BET.

Year	Author	Catalyst system [wt. %]	Temperature Pressure Feed Composition Flow rate Sample weight/volume	Reaction	Conversion / Activity	Selectivity to main product	By-products	Hours on stream Deactivation	Objectives
1993	Idriss	3 Pd/CeO2 3 Co/CeO2 3Pd-3 Co/CeO2	215°C atmospheric CO/H2 + CH2Cl2 not reported not reported	CO hydrogenation	0.21% not reported 1.97%	MeOH 55% hydrocarbons hydrocarbons	Hydrocarbons, EtOH none MeOH, EtOH	Not reported	CO hydrogenation on CeO2 supported Pd and Co catalysts, TPR, TPD, probe.
1992a	Burch	2 Rh/SiO2 2 Rh- 0.034 Li/SiO2 2 Rh- 0.1-1 Fe/SiO2 2 Rh- 1 Mn/SiO2 2 Rh- 1 Ce/SiO2 Rh/SiO2 + Fe/SiO2	50-270°C 2 MPa CO/H2=0:1, 1:3, 1:1, 3:1 + AcAD 20-40 ml/min 20-150 mg	AcAd hydrogenation	10.10% 26.20% 92.6-99% 87.50% 72% 10.70%	EtOH 45.7% EtOH 81.9% EtOH 99.6% EtOH 94.8% EtOH 93.4 % EtOH 37.7%	EtAc, CH4, DEE EtAc, CH4, DEE CH4, DEE CH4, EtAc, DEE CH4, DEE, EtAc EtAc, CH4, DEE	Deactivation w/ large CO/H2 stable stable stable stable	Reaction of acetaldehyde on various promoted Rh catalysts, FTIR.
1992b	Burch	2 Rh/SiO2 2 Rh- 0.1-1 Fe/SiO2 2 Rh- 1 Mn/SiO2 2 Rh- 1 Ce/SiO2 2 Rh- 0.034 Li/SiO2 2 Rh- 0.37 Ir/SiO2	210-300°C 2 MPa CO/H2 = 1:1 20 ml/min 150 mg	CO hydrogenation	1.52% 2.28-4.45% 1.68% 1.15% 0.46% 1.22%	CH4 48% EtOH 39% CH4 36% CH4 37% CH4 23% CH4 47%	Alkanes, AcAd, AA, EtAc CH4, MeOH, alkanes EtOH, alkanes, AcAd, AA, EtAc EtOH, alkanes, AA, EtAc, MeOH AA, AcAd, EtOH, EtAc, MeOH Alkanes, AcAd, AA, EtOH, EtAc	Not reported	Oxygenates from syngas on various promoted Rh catalysts, FTIR.
1992	Kenvin	2.4 wt.% Cu/SiO2 3.8 wt.% Cu/SiO2 8.6 wt.% Cu/SiO2	275°C atmospheric AcAd pulse in 25:75 H2:He 1-2 uL pulse in 15 ml/min carrier gas 100-350 mg	AcAd hydrogenation	53% 59% 56%	EtOH 96% EtOH 98% EtOH 45%	light gases light gases Ethyl Acetate	Not reported	Effect of copper particles size in acetaldehyde hydrogenation and ethanol dehydrogenation
1991	Trunschke	2 Rh/Al2O3 2 Rh- Mo/Al2O3	142-220°C atmospheric CO/H2=1:1 + AcAd (15%) 30 ml/min not reported	AcAd hydrogenation Hydroformylation	high	EtOH 99%	CH4	Not reported	Effect of different Rh precursor on olefin hydroformylation and acealdehyde hydrogenation.
1991	Chuang	15 Ni/SiO2 5 Ni-Mn/SiO2 5 Ni-Mn-Na/SiO2 Ni-Mn-Na coprec.	200-300°C 1 Mpa CO/H2=1:1 GHSV: 2100 - 11000 h-1	CO hydrogenation	high low low low	Methane 96% Methane 35 % Methane 50 % Methane 20-30 %	Alkanes Alkanes, AcAd, PrAd Alkanes, AcAd, PrAd AcAd, Alkanes, EtOh, PrAd, MeOH	fast deactivation fast deactivation fast deactivation stable for 70 hours	Effect of preparation technique on Ni catalyst performance in CO hydrogenation, BET, XRD, TPD.
1991	Ehwald	4.8 Rh/SiO2 5 Rh- 0.06 Mn -0.02 Li/SiO2 5 Rh-1.2 Ir- 0.06 Mn -0.02 Li/SiO2 5 Rh- 0.06 Mn -0.02 Li-15 Cu -4 Zn/SiO2 15 Cu - 4Zn/SiO2 Mixture of 2+5 1:1 Mixture of 3+5 1:1 Grinding Mixture of 3+5 Rh-Ir-Ti-Fe	215-300°C 1.1-5.0 MPa CO/H2/N2 = 3:6:1 GHSV: 2000 - 8000 h-1 1.5 ml	CO hydrogenation	very low high medium none insignificant medium medium insignificant low	hydrocarbons hydrocarbons hydrocarbons none MeOH hydrocarbons EtOH = hydrocarbons EtOH = hydrocarbons hydrocarbons	none AcAd, EtOH AcAd, EtOH none hydrocarbons EtOH none none EtOH, MeOH	Not reported	Development of bicomponent catalyst for selective production of EtOH, TEM, TPR.
1988	Agarwal	4.4 Cu/SiO2 6.8 Cu/SiO2	92, 125, 145°C atmospheric H2 + AcAD 1000 ml/min 0.05-0.3 g	AcAd hydrogenation	max. 30 %	EtOH 100%	EtAc at low H2:Ad ratios	continuous, loss of 1/3 activity in 3 hrs.	Acetaldehyde hydrogenation over Cu/SiO2 catalysts. Deuterium tests.
1979	Herman	ZnO 2-67 Cu0- 98-33 ZnO CuO 60 CuO- 30 ZnO- 10 Cr2O3 60 CuO- 30 ZnO- 10 Al2O3	250-300°C 7.6 MPa H2/CO/CO2 = 70:24:6 GHSV 5000 hr-1 3 ml	MeOH from syngas	none max. 51.1 % none 40% 47%	none MeOH 99% none MeOH 99% MeOH 99%	none none none Hydrocarbons EtOH	Fast without CO2	MeOH synthesis from syngas on Cu-Zn based catalysts. XRD, APS, XPS, UV, VIS, IR, surface properties.
1920	Armstrong	Cu-powder Ni-powder	120-300°C atmospheric AcAd:H2 = 1:2 1070 ml/min not reported	AcAd hydrogenation	68.50% 63.70%	EtOH 83% EtOH 52%	CO2, CO, CH4, olefines CO,CH4	2-5 hours no deactivation reported	Hydrogenation of acetaldehyde and dehydrogenation of ethanol in the presence of Cu and Ni.

Chapter 3: Catalyst preparation/characterization and experimental setup

This chapter introduces general concepts of catalyst preparation and characterization. The detailed procedures for the preparation of the catalysts used either in the ethanol dehydrogenation or acetaldehyde hydrogenation experiments are listed in the following chapters that pertain to the specific experiments.

3.1 Catalyst preparation

Occasionally, catalytic material can be used in its original form such as metal wire, mesh, screen, powder or, as in the part of this work, as metal foam. More often, however, a catalyst must be prepared by transformation of its precursor, usually a metal salt, to the active component. Transformation may involve conversion of a soluble precursor into an insoluble compound as in precipitation, or deposition of the precursor in solution on a high-surface support as in impregnation. Impregnation can be further classified as:

- Wet impregnation, where support in a powder form is immersed in a solution of metal salt and the resulting slurry is then stirred to dryness at a desired temperature.

- Incipient wetness impregnation, which is suitable for supports which lose their structure upon contact with a large amount of liquid, such as SiO_2. The precursor salt is then dissolved in the amount of liquid, which is equal to the pore volume of the support. Solution is then added drop wise to the support. After each addition, the powder is vigorously shaken to ensure proper distribution of the liquid over the pores of the support. Ensuing material is dried in an oven.

Regardless of the preparation technique, dry material is treated at a high temperature to decompose the metal compounds, such as carbonates, nitrates, acetates or hydroxides into metal oxides; this step is commonly called calcination. Prior to actual use, the catalyst may require activation by reduction of the metal oxides to metal form.

In the present work, aside from the copper foam, catalysts were prepared by precipitation, and wet and incipient wetness impregnation with details given in the Ethanol Dehydrogenation and Acetaldehyde Hydrogenation chapters.

3.2 Catalyst characterization

Physical and chemical properties of catalysts and their precursors were determined by various instrumental techniques. The following list contains all techniques utilized in this work, the details of the experimental parameters can be found in the following chapters.

Thermogravimetric Analysis (TGA)

Thermogravimetric analysis was conducted utilizing a TA Instruments SDT 2960. The results allowed determination of the calcination temperature of the catalyst precursors and also for estimation of the degree of oxidation of copper foam.

Temperature Programmed Reduction (TPR)

An in-house built unit depicted in Fig. 3.1 was utilized for TPR. A catalyst sample was placed into a quartz fixed-bed down-flow microreactor (i.d. 4 mm, length 40 cm) and pretreated in air at temperature ensuring complete oxidation to CuO (450°C). The sample was then cooled and TPR was carried out by passing a 5% v/v H_2/N_2 mixture over the sample. The difference between inlet and outlet hydrogen concentration was detected by a thermal conductivity detector (TCD). Collected data allowed determination of the catalyst reduction temperature and also for the calculation of copper content of the catalyst by numeric integration of the hydrogen consumption peak and assumption of the following reduction stoichiometry: $CuO + H_2 \rightarrow Cu + H_2O$
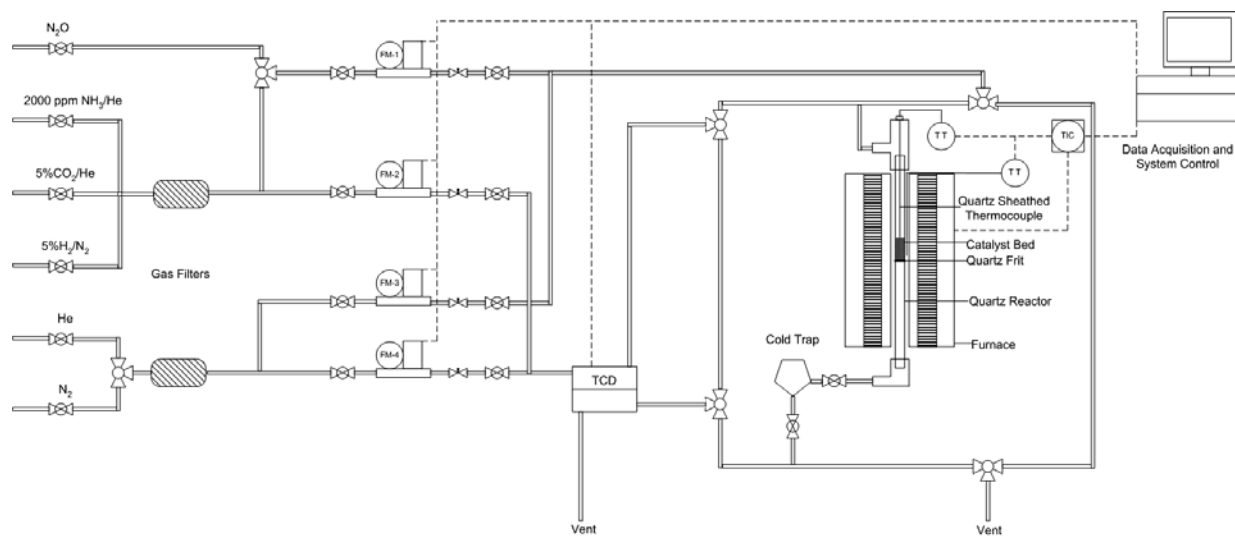
Figure 3.1 Schematic of TPR and TPD unit.

TPR-N$_2$O

The TPR unit was also used for determination of copper surface area and copper dispersion of supported catalysts according to the method of Bond and Namijo (1989). After completing TPR, the sample was cooled to 60°C and the top layer of copper particles, present on the support, was selectively oxidized by N$_2$O according to the reaction: $N_2O + 2Cu \rightarrow Cu_2O + N_2$. The sample was then cooled to room temperature and a second TPR was conducted. The change in hydrogen concentration can be related to reduction of Cu$_2$O to Cu. Once again, the peak was numerically integrated and the number of copper surface atoms determined. Copper dispersion was calculated as a ratio between the moles of surface copper and total moles of copper. Assuming an equal presence of (100), (110), and (111) Miller index planes, the surface-atom density was 1.47×10^{19} atoms/m^2 (Bond and Namijo, 1989) and copper surface area could then be estimated. Once the copper surface area and copper content in the catalyst were determined, it was possible, knowing the copper density [8920 kg/m^3 (Baram, 1988)] and assuming the spherical size of copper aggregates, to calculate the average diameter of copper particles on the catalyst surface.

Temperature Programmed Desorption (TPD)

Acid and base properties of catalysts or supports can be evaluated by using probe molecules, such as NH_3 or CO_2 respectively. Using the unit depicted in Fig. 3.1, the sample was pre-treated in He at its calcination temperature to remove any chemisorbed water and CO_2. After cooling to room temperature, 5% CO_2 in He or 2000 ppm NH_3 in He was passed over the sample. The reactor was then purged with He to remove physisorbed probe molecules. Finally, by ramping the temperature, adsorbed molecules were removed from the surface and detected by TCD. The temperature of desorption and amount desorbed can be directly related to the strength and number of acid or base sites on the catalyst surface.

Brunauer-Emmett-Teller Surface Analysis (BET)

BET surface area, pore size distribution and pore volume were determined using a Micromeritics Gemini^{TM} V-Series surface analyzer. Prior to analysis, samples were pre-treated in N_2 at elevated temperature to remove any physisorbed moisture. Eleven points were typically collected in the pressure range $(P/P_0) \in (0-0.3)$, where P and P_0 are the equilibrium and the saturation pressure of N_2 at the temperature of adsorption, in order to determine the BET surface area, while the whole adsorption span of $(P/P_0) \in (0-1)$ as well as desorption data in the range $(P/P_0) \in (1-0.5)$ were used for pore size distribution and pore volume determination. For low surface area materials, such as copper foam, special vials were used, which allowed for insertion of large amounts of specimen.

X-Ray Diffraction (XRD)

A Bruker AXS D8 Advance diffractometer was used to obtain X-ray diffraction patterns of copper foam samples. The crystal phases on the sample surface were recorded after various treatments prior to the reaction together with their state after reaction.

Scanning Electron Microscopy (SEM)

Scanning electron microscopy was utilized for surface morphology characterization of copper foam samples using a LEO 1530 SEM (5-kV electron beam)

equipped with a secondary electrons detector. Because copper foam inherently conducts electric current, no gold plating pretreatment was required.

Catalytic activity

A fully automated experimental apparatus built in-house, depicted in Fig. 3.2, was used for the evaluation of catalyst activity in both ethanol dehydrogenation and acetaldehyde hydrogenation. The apparatus consisted of separate gas and liquid delivery sections. In ethanol dehydrogenation, an Eldex A-60-S stainless steel HP metering pump was used to deliver a desired water-ethanol mixture at a constant flow rate to the evaporator where it was vaporized and combined with a N_2 stream. N_2 served as an internal reference, i.e., its corresponding constant GC signal served as an indication of proper operation of the whole system. In the case of acetaldehyde hydrogenation, CO and H_2 gas streams were mixed in a desired ratio and delivered to a dual stage acetaldehyde saturator, which was located in a temperature controlled liquid bath. The saturated stream then proceeded to the evaporator section, where an additional liquid component, such as ethanol, could be added to the inlet flow. The resulting gaseous mixture was, after passing through a pre-heater zone, directed to a standard fixed-bed down-flow quartz reactor depicted in Fig. 3.3 with the following dimensions:

- Atmospheric pressure fixed bed: length = 45 cm, i.d. = 10 mm, o.d. = 12 mm
- Elevated pressure fixed bed: length = 45 cm, i.d. = 6 mm, o.d. = 12 mm.

The catalyst sample was placed on a quartz frit, located 18 cm from the top rim of the quartz tube – this set the catalyst in the isothermal zone of the tubular furnace. The temperature of the reaction was controlled by a quartz-sheathed thermocouple, which was immersed in the catalyst sample. The product stream was then passed through three heated zones to a gas chromatograph sampling loop and further to a high-pressure liquid separator. Here, the condensable species were removed from the gas stream which was then directed through a back pressure regulator, allowing for the maximum pressure of 0.79 MPa, to a vent line.

The separation and detection of the individual species, both condensable and gaseous, in a product stream using one gas chromatograph was made possible by the development of a novel separation method, which is described in detail in Appendix A.

The method is universal and can be used for a broad range of reactions. Steam reforming of ethanol, which yields identical products as encountered in ethanol dehydrogenation and acetaldehyde hydrogenation, was selected to prove the viability of the method.

Nitrogen/Air/Carbon Monoxide

Hydrogen

Filters

Helium

Zero Gas Air Generator

Varian 3800 GC

Gas Chromatograph

Heated Valve Oven

Post-Heater

Liquid Drain

To Vent

PI

Temperature Adjustable Fluid Bath with Dual Stage Saturator

Liquid Feed Reservoir

Liquid Feed Metering Pump

Furnace

Quartz Reactor

Quartz Frit

Catalyst Bed

Quartz Sheathed Thermocouple

Vaporizer

MFC Unit

MFC-1

MFC-2

PI

PT

TIC

TIC

TT

Data Acquisition and System Control

*Enclosed components are located in a walk-in fumehood

Figure 3.2 Experimental apparatus**.**

48
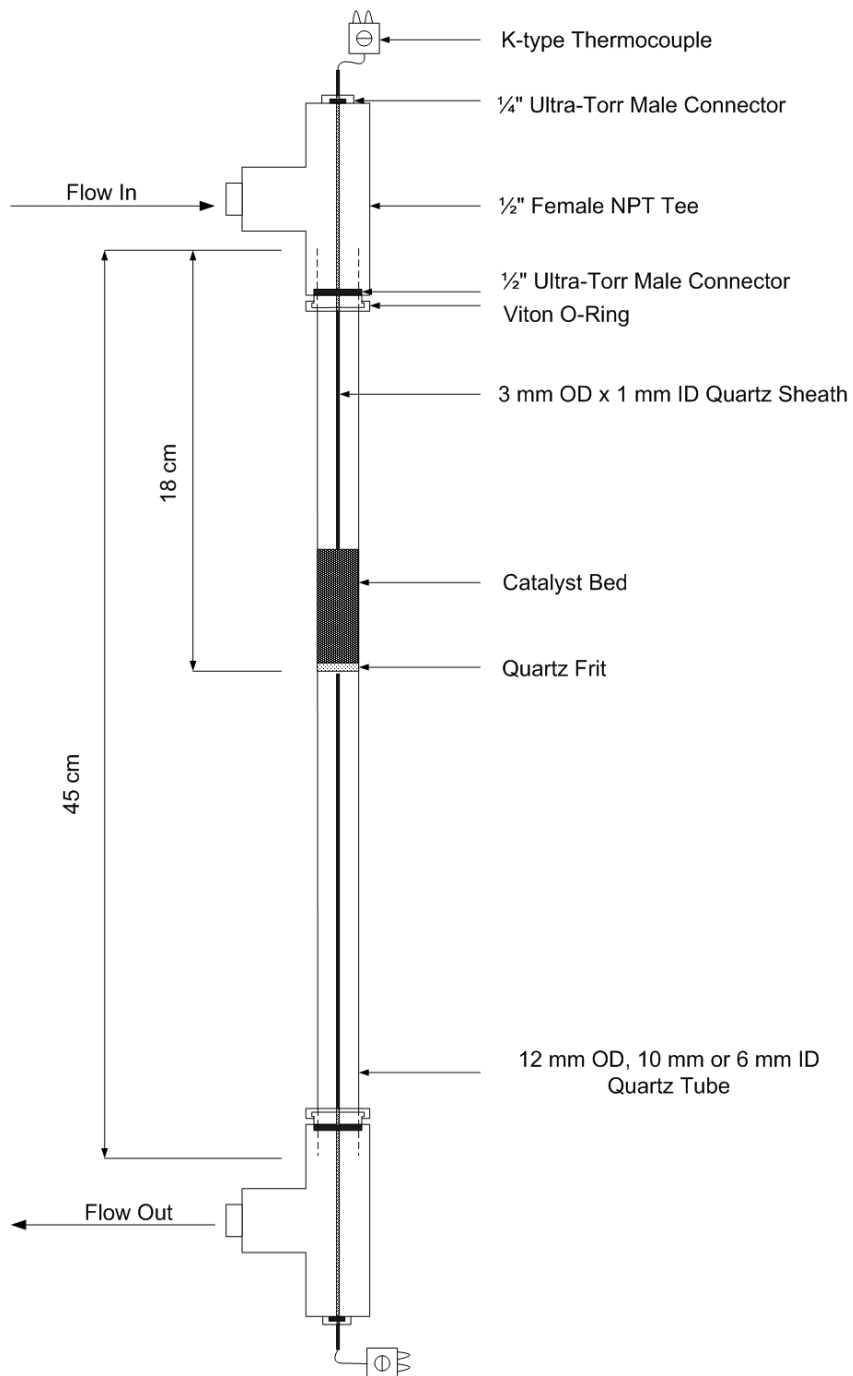
Figure 3.3 Down-flow, fixed-bed, quartz reactor.

Chapter 4: Mass and heat transfer effects

As will be seen in detail in Ethanol Dehydrogenation and Acetaldehyde Hydrogenation chapters, both parts of the separation cycle were evaluated in as close to industrial conditions as possible, i.e., with concentrated reactant streams and at temperature and residence time conditions which maximized the activity and selectivity of the catalyst. An attempt has also been made to obtain the basic kinetic parameters of ethanol dehydrogenation and acetaldehyde hydrogenation using an integral reactor model.

A heterogeneous catalytic reaction can usually be described by the following 7 steps:

1) Diffusion of the reactants from the bulk fluid to the external surface of the catalyst.

2) Diffusion of the reactants into the pores of the catalyst.

3) Adsorption of the reactant molecules onto an active site of catalyst.

4) Conversion of reactants to products.

5) Desorption of products.

6) Diffusion of products through the pores to the catalyst surface.

7) Diffusion of products from the catalyst surface into the fluid bulk.

Only steps 3-5 are considered true chemical kinetics, and it is therefore necessary to determine, and if possible eliminate, any external – steps 1 and 7 – and internal – steps 2 and 6 – mass transfer effects which may obfuscate true kinetics and thus render the kinetic parameters inaccurate or useless. Similarly, external and internal heat transfer effects must also be considered. Useful criteria in determining the effect of the mass and heat transfer effects on the outcome of the reactions have been proposed in standard kinetics texts and will be utilized in the following paragraphs.

4.1 External mass and heat transfer

The existence of external mass or heat transfer will result in a concentration or temperature difference between the catalyst surface and bulk fluid. External resistance can be eliminated by increasing the velocity of the reaction mixture through the catalyst

bed or reducing the size of catalyst particles. However, in both cases, pressure drop over the catalyst bed will increase.

4.1.1 External mass transfer

Hudgins (1972) developed a criterion which may be used to determine the presence or absence of mass transfer resistance:

$$\frac{r d_p r'(c_0)}{k_c r(c_0)} < 0.3$$

where r is measured reaction rate, d_p is a particle diameter, $r(c_0)$ is a known form of rate expression evaluated at c_0, which is an inlet concentration of reactant in the bulk phase, $r'(c_0)$ is its first derivative with respect to c and k_c is a mass transfer coefficient calculated from the definition of the mass transfer factor j_D defined by Froment and Bishoff (1979) for Re< 190 and a bed porosity of 0.37 as:

$$j_D = 1.66 \, \mathrm{Re}^{-0.51} = St Sc^{\frac{2}{3}}$$

where 1) Reynolds number is calculated as:

$$\mathrm{Re} = \frac{v d_p}{\upsilon} = \frac{\dot{V} d_p}{A_x \upsilon}$$

where v is the gas velocity, $\dot{V}$ the volumetric flow rate, A_x the reactor cross sectional area and υ the kinematic viscosity of the gas mixture defined as:

$$\upsilon = \frac{\mu}{\rho} = \frac{\sum y_i \mu_i \sqrt{M_i}}{\rho \sum y_i \sqrt{M_i}}$$

where y_i is the molar fraction, M_i is the molecular weight of each component, μ_i is the dynamic viscosity of each component and ρ is the density of the gaseous mixture defined as

$$\rho = \frac{P \sum y_i M_i}{RT}$$

where P is the reaction pressure, T the reaction temperature and R the ideal gas law constant.

2) The Schmidt number is calculated as:

$$Sc = \frac{\upsilon}{D_{AB}}$$

where D_{AB} is the bulk diffusivity defined as:

$$D_{AB} = \frac{10^{-4} T^{\frac{3}{2}} \sqrt{\frac{1}{M_A} - \frac{1}{M_B}} (1.084 - 0.249 \sqrt{\frac{1}{M_A} - \frac{1}{M_B}})}{r_{AB}^2 f(\frac{K_B T}{\varepsilon_{AB}})P}$$

where r_{AB} is the molecular separation at collision, calculated from individual molecular radii (Treybal, 1980) as $r_{AB} = \frac{r_A + r_B}{2}$, K_B is the Boltzmann's constant, ε_{AB} is the energy of molecular attraction calculated from individual molecular force constants (Treybal, 1980) as: $\varepsilon_{AB} = \sqrt{\varepsilon_A \varepsilon_B}$ and $f(\frac{KT}{\varepsilon_{AB}})$ is a collision function, which can also be obtained from Treybal (1980).

3) The Stanton number is defined as:

$$St = \frac{k_c y_A P \overline{M}}{RTG}$$

where $\overline{M}$ is the average molecular weight of reactant mixture and G is the mass velocity.

The values of Hudgins criteria are listed in Table 4.1 for three catalysts used in ethanol dehydrogenation and two catalysts for acetaldehyde hydrogenation at most extreme conditions, i.e., conditions of highest conversion of primary reactant (ethanol or acetaldehyde) in mixture with H_2O or H_2 in ratio of 1:1 molar. It is clear that all values are much lower than 0.3 and therefore it can be concluded that neither ethanol dehydrogenation nor acetaldehyde hydrogenation is external mass transfer limited.

Table 4.1 Test for external mass transfer.

Reaction	Catalyst	T (°C)	Hudgins Criterion
Ethanol Dehydrogenation	Cu/SiO$_2$	300	1.0E-02
	Cu/K-Al$_2$O$_3$		7.4E-03
	Cu/MO*		7.8E-03
Acetaldehyde Hydrogenation	Cu	258	6.5E-03
	Cu/SiO$_2$		5.1E-03

*Mixed Oxide consisting of MgO and Al$_2$O$_3$

4.1.2 External heat transfer

The Mears criterion (Mears, 1971) was used to determine the presence of external heat transfer:

$$\frac{\Delta H d_p r E_a}{h T_b^2 R} < 0.3$$

where ΔH is the absolute value of heat of reaction, E_a is the activation energy of the reaction, T_b is the bulk temperature and h is heat transfer coefficient, which was calculated assuming:

$$j_D = j_H = \frac{h \Pr^{\frac{2}{3}}}{Cp\ G}$$

where j_H is a heat transfer factor and Cp is a heat capacity of the gas mixture calculated as:

$$Cp = \sum y_i Cp_i$$

and Pr is the Prandtl number defined as:

$$\Pr = \frac{Cp\ \mu}{\lambda}$$

with λ representing the heat conductivity of gas mixture:

$$\lambda = \frac{\sum y_i \lambda_i \sqrt{M_i}}{\rho \sum y_i \sqrt{M_i}}$$

where λ_i is a heat conductivity of each component.

The values of Mears criteria listed in Table 4.2 show that some caution may be required when analyzing results at the extreme reaction conditions boundaries for ethanol dehydrogenation catalyzed by Cu/SiO$_2$, where the limitation of heat transfer is approached. However, the limitation should not be severe as the boundary is not overstepped and furthermore the catalyst bed was diluted by SiC in the ratio 5:1 SiC:catalyst which served as a heat pool/sink. Ethanol dehydrogenation catalyzed by the remaining two catalysts as well as acetaldehyde hydrogenation are not external heat transfer limited in the whole range of conditions investigated.

Table 4.2 Test for external heat transfer

Reaction	Catalyst	T (°C)	Mears Criterion
Ethanol Dehydrogenation	Cu/SiO$_2$		0.28
	Cu/K-Al$_2$O$_3$	300	0.23
	Cu/MO		0.25
Acetaldehyde Hydrogenation	Cu	258	0.22
	Cu/SiO$_2$		0.16

4.2 Internal mass and heat transfer

Internal mass and heat transfer resistance can become a problem for highly porous materials, where most of the active surface area is located within the particle. The internal mass transfer then limits the reaction rate. Furthermore the pore structure can affect the product selectivity. Internal heat transfer usually becomes an issue with highly exothermic reactions, where temperature profiles across catalyst particle can develop, thus affecting the overall reaction rate.

The internal transfer limitations can be reduced by using smaller catalyst particles, thus reducing the length of pores or by increasing the internal surface area.

4.2.1 Internal mass transfer

The Hudgins criterion (Hudgins, 1968) predicts absence of internal mass transfer limitation if

$$\frac{r d_p^2 r'(c_0)}{D_e r(c_0)} < 3$$

where D_e is effective diffusivity and can be approximated by

$$D_e = \frac{D\Phi_P\sigma}{\tilde{\tau}} = \frac{D}{20}$$

where Φ_P represents pellet porosity, σ is a constriction factor, $\tilde{\tau}$ is a tortuosity. The term consisting of these three factors can range from 0.32 to 0.032 (Fogler, 1999). The value of 0.05 was used as an approximation, because of the unavailability of experimentally determined values. D is global diffusivity, which can be calculated as

$$D = \frac{1}{\dfrac{1}{D_{AB}} + \dfrac{1}{D_K}}$$

where D_K is Knudsen diffusivity defined as

$$D_K = \frac{d}{3}\sqrt{\frac{8g_c RT}{\pi M_A}}$$

where d is average pore diameter calculated by BET and g_c is a conversion factor.

From the values contained in Table 4.3, it can be concluded that ethanol dehydrogenation on Cu/MO catalyst, which has the smallest average pore diameter, can become internal mass transfer limited at the extreme conditions (i.e., 300°C, 0.5 g of catalyst). On the other catalysts, neither reaction should suffer from internal mass transfer limitations. Furthermore, since most of the experiments were carried out at 275°C or lower, and since the value is very close to recommend value, even internal mass transfer limitation for Cu/MO should not be critical.

Table 4.3 Test for internal mass transfer.

Reaction	Catalyst	T (°C)	Hudgins Criterion
Ethanol Dehydrogenation	Cu/SiO$_2$	300	2.43
	Cu/K-Al$_2$O$_3$		1.55
	Cu/MO		3.00
Acetaldehyde Hydrogenation	Cu	258	2.71
	Cu/SiO$_2$		2.09

4.2.2 Internal heat transfer

The Anderson criterion for the absence of internal heat transfer requires that:

$$\frac{\Delta H d_p^2 r E_a}{h T_s^2 R} < 3$$

where T_s is the surface temperature, which was assumed to be identical to the bulk temperature T_b (no external heat transfer limitation).

The results presented in Table 4.4 clearly indicate that neither ethanol dehydrogenation nor acetaldehyde hydrogenation are hindered by internal heat transfer.

Table 4.4 Test for internal heat transfer.

Reaction	Catalyst	T (°C)	Anderson Criterion
Ethanol Dehydrogenation	Cu/SiO$_2$	300	1.7E-02
	Cu/K-Al$_2$O$_3$		1.4E-02
	Cu/MO		1.5E-02
Acetaldehyde Hydrogenation	Cu	258	1.3E-02
	Cu/SiO$_2$		1.0E-02

It can be, therefore, tentatively concluded that the kinetic studies presented in the Ethanol Dehydrogenation and Acetaldehyde Hydrogenation chapters provide true kinetic parameters unaffected or virtually unaffected by any transfer effects.

Chapter 5: Thermodynamics

In this chapter, the feasibility of the cyclic separation process from a thermodynamic point of view will be addressed using a Gibbs free energy minimization method and the results will be discussed in relation to experimental data found in the literature.

5.1 Ethanol dehydrogenation

An extensive amount of literature concerning acetaldehyde production via dehydrogenation is available. Acetaldehyde was first synthesized by ethanol oxidation in 1817 (Davy, 1817) and later it was produced by hydration of acetylene. Armstrong and Hilditch (1920) reported that the dehydrogenation process was developed and applied during the First World War, but deeper dehydrogenation investigation (Church and Joshi, 1951; Franckaerts and Froment, 1964; Shiau and Chen, 1991) was spurred by an increasing significance of acetaldehyde as one of the most important aliphatic intermediates in the production of acetic acid, acetone, ethyl acetate, C_4-aldehydes, 1-butanol, pentaerythritol and many other chemicals. Lastly, the importance of ethanol dehydrogenation as a source of hydrogen for fuel applications was recognized (Freni at al., 2000).

Copper has been identified as an excellent catalyst for its ability to dehydrogenate ethanol without splitting the C-C bond, which would lead to undesirable decomposition of acetaldehyde to CH_4 and CO. However, besides the major reaction:

$$C_2H_5OH(g) \rightarrow CH_3CHO(g) + H_2 \quad \Delta H^0_{298K} = 68.75\,kJ/mol \quad \Delta G^0_{298K} = 34.75\,kJ/mol$$
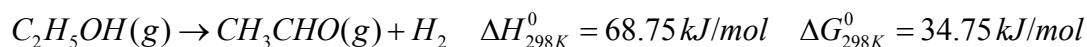
a parallel undesirable dehydration to ethylene or diethylether (DEE), either thermal or catalyzed by acid sites on the catalyst can occur:

$$C_2H_5OH(g) \rightarrow C_2H_4 + H_2O(g) \quad \Delta H^0_{298K} = 45.65\,kJ/mol \quad \Delta G^0_{298K} = 7.7\,kJ/mol$$

and
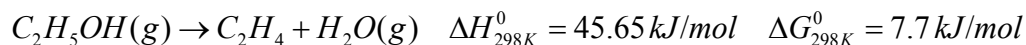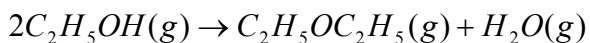
$$2C_2H_5OH(g) \rightarrow C_2H_5OC_2H_5(g) + H_2O(g)$$
$$\Delta H^0_{298K} = -24.01kJ/mol \quad \Delta G^0_{298K} = -14.99kJ/mol$$

Furthermore, Inui et al. (2004) outlined the complex network (Fig. 5.1) of subsequent acetaldehyde reactions.
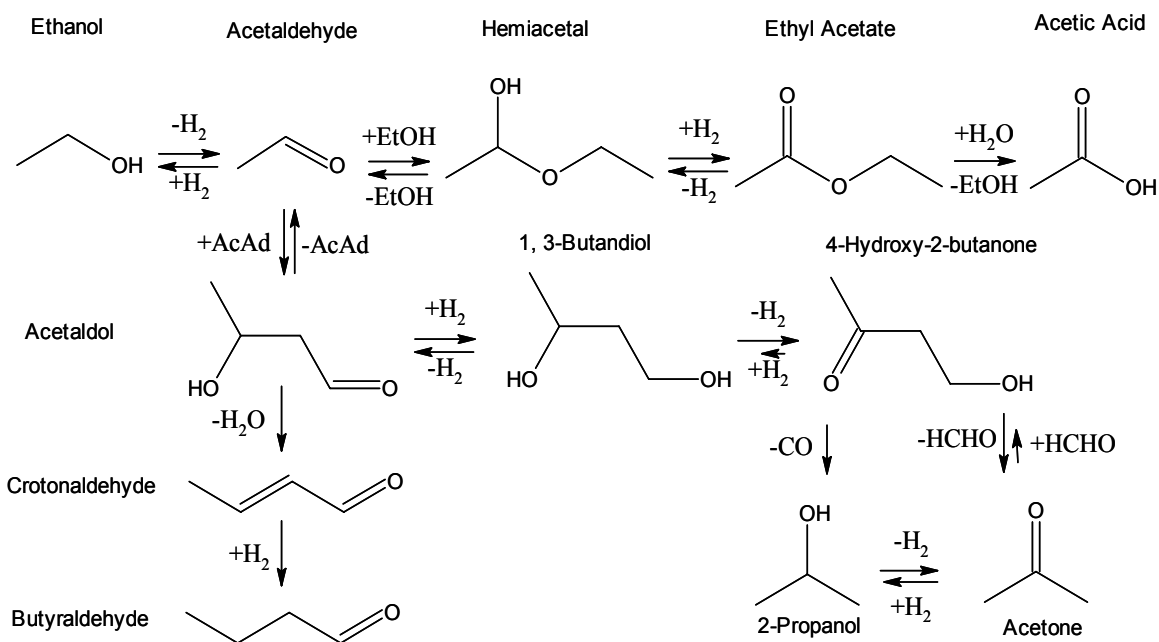
Figure 5.1 Network of probable subsequent reactions resulting from acetaldehyde. Modified from Inui et al. (2004).

The dominance of different reaction pathways is affected by the catalyst, reaction conditions and residence time. The most significant by-product, identified in our previous work focused on ethanol dehydrogenation catalyzed by copper foam under atmospheric pressure and in the temperature range of 200-400°C (Chladek et al., 2007b, see Chapter 6), was ethyl acetate, which is formed by reaction of ethanol and acetaldehyde:
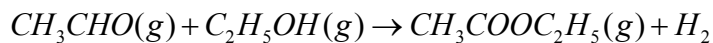
$$CH_3CHO(g) + C_2H_5OH(g) \rightarrow CH_3COOC_2H_5(g) + H_2$$
$$\Delta H^0_{298K} = -43.35 \, kJ/mol \quad \Delta G^0_{298K} = -27.05 \, kJ/mol$$

When these secondary reactions are included in the thermodynamic model, it becomes apparent that dehydration products are thermodynamically favourable at all

temperatures investigated. Fig. 5.2 presents the effect of temperature on ethanol conversion, defined as: $X_{EtOH} = \dfrac{\dot{n}^0_{EtOH} - \dot{n}_{EtOH}}{\dot{n}^0_{EtOH}}$, where $\dot{n}^0_{EtOH}$ is the inlet molar flow of ethanol and $\dot{n}_{EtOH}$ is the outlet molar flow of ethanol, and on the product selectivities defined as: $S_i = \dfrac{\dot{n}_i}{\sum\limits_{Products} \dot{n}_i}$, where $\dot{n}_i$ is an outlet product molar flow. These results are in direct contradiction not only to the experimental results discussed in the following chapters but also to the data contained in the literature (see Chapter 2: Literature review). It can be therefore concluded that dehydration is not kinetically favoured under these conditions: finite residence time and dehydrogenation catalyst. Therefore, the dehydration products can be omitted from the model.
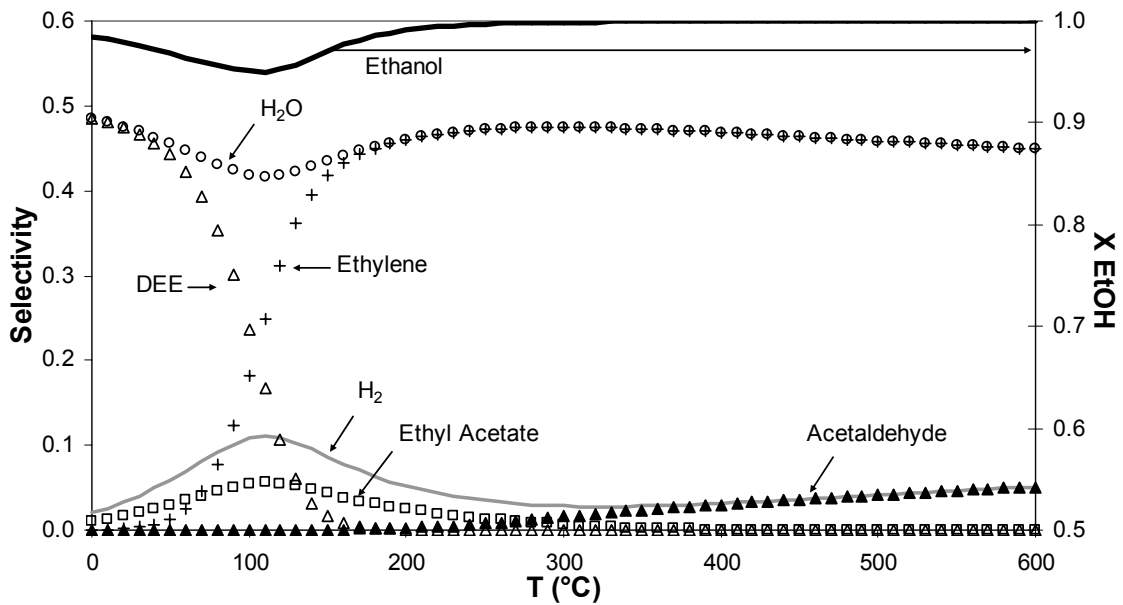
Figure 5.2 Ethanol conversion and product selectivities as functions of temperature in ethanol dehydrogenation and dehydration, P = 0.1 MPa.

The similar contradiction is obtained for competition of dehydrogenation to acetaldehyde and to ethyl acetate depicted in Fig. 5.3. Thermodynamically, ethyl acetate is a more favourable species up to 340°C. Once again this result can be explained by the infinite residence time assumption used in Gibbs free energy minimization. In reality, residence time is finite and therefore only part of the acetaldehyde formed by

dehydrogenation reaction, which is the first and fastest reaction to occur, gets converted to ethyl acetate. Selectivity to ethyl acetate can be affected not only by residence time but also by the size of copper particles (Kenvin and White, 1992).
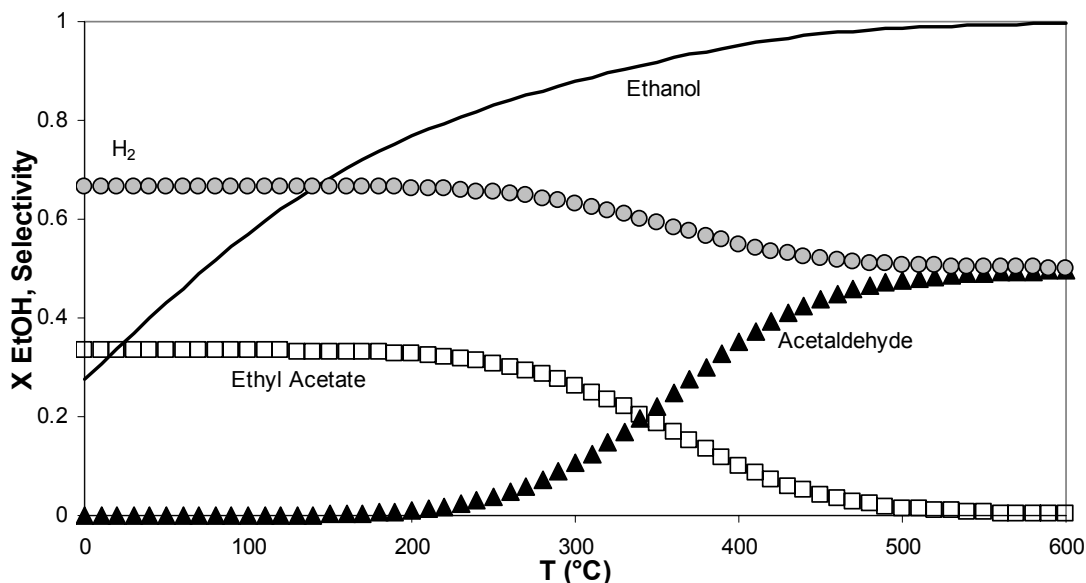
Figure 5.3 Ethanol conversion and product selectivities as a function of temperature in ethanol dehydrogenation to acetaldehyde and ethyl acetate, P = 0.1 MPa.

Therefore, in the following section, only the dehydrogenation reaction will be considered for modeling purposes. Since the product composition is thereby limited only to acetaldehyde and hydrogen, the effect of temperature, pressure and acetaldehyde concentration in the feed will be evaluated solely on the basis of ethanol conversion.

Temperature

Ethanol dehydrogenation is an endothermic reaction and therefore, as can be seen from Fig. 5.4, its conversion is expected to rise with increasing temperature. Virtually complete conversion is achieved at T>500°C. However, this temperature is high above Tamman temperature for copper (405°C), the temperature at which metal particles become mobile on the catalyst surface and catalyst loses activity because of sintering. Indeed this temperature limitation was experimentally observed (Tu and Chen, 1998, 2001). Therefore, complete conversion cannot be expected and it will be necessary to

examine the effect of unconverted ethanol on acetaldehyde hydrogenation. For the following discussion, 300°C was selected as a safe model reaction temperature.
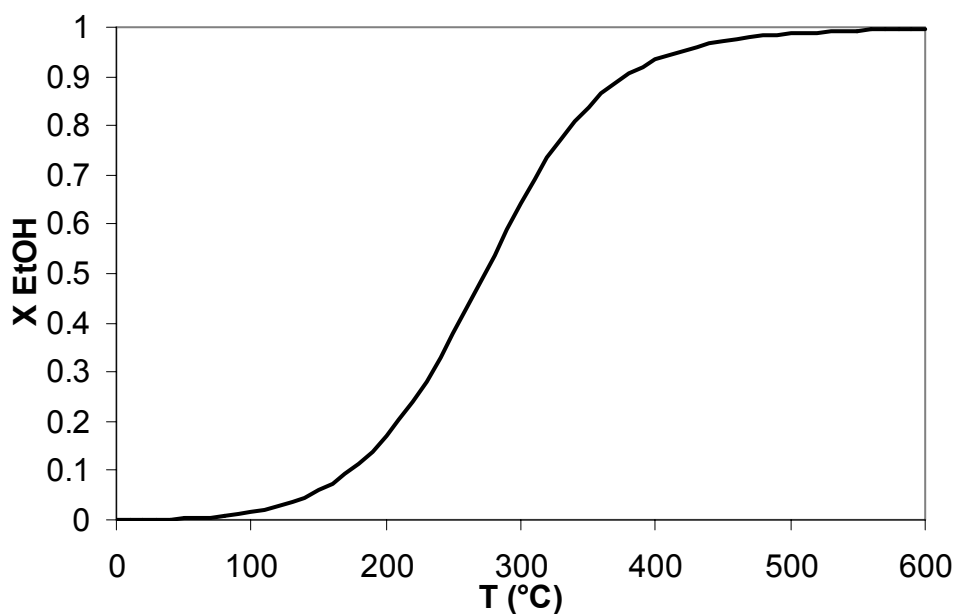
Figure 5.4 Ethanol conversion as a function of temperature, P = 0.1 MPa.

Pressure

Le Chatelier's principle predicts that the dehydrogenation will be favoured at low pressures, which is confirmed in Fig. 5.5 where increasing pressure has negative effect on thermodynamic equilibrium ethanol conversion. This obviously influences the prospect of high-pressure hydrogen production.
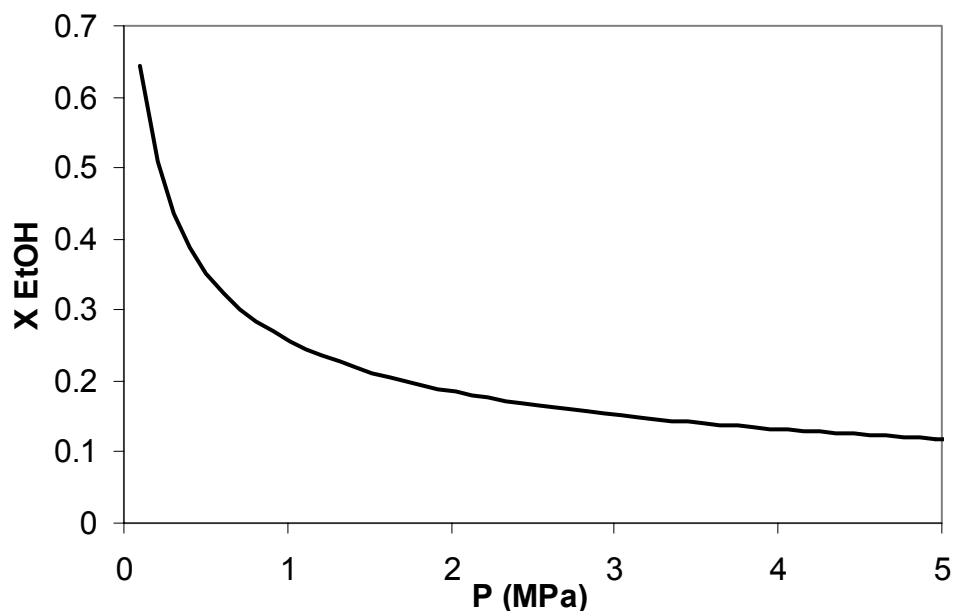
Figure 5.5 Ethanol conversion as a function of pressure, T = 300°C.

However, Shiau and Chen (1991) reported an increase in the ethanol conversion with increasing ethanol partial pressure. Furthermore, Franckaerts and Froment (1964) showed that the rate of dehydrogenation increases with increasing pressure, passes through a maximum and then reaches a steady value. This contradiction to thermodynamic expectations can be explained by saturation of the catalyst surface by ethanol at which point the reaction rate becomes independent of the gas phase pressure of ethanol. These experimental results therefore demonstrate the possibility of producing high-pressure hydrogen despite thermodynamic limitations.

Feed composition

The incoming ethanol feed may contain some unconverted acetaldehyde from the acetaldehyde hydrogenation step. Since acetaldehyde is a main product in the ethanol dehydrogenation, it can be expected to negatively influence the thermodynamic equilibrium. The results in Fig. 5.6 show that at 300°C, the acetaldehyde presence indeed lowers the equilibrium ethanol conversion. To obtain the highest conversions it is therefore desirable to separate as much unconverted acetaldehyde from ethanol as possible. However, the decrease in conversion is not severe and small amounts of

acetaldehyde impurity will not stop the production of hydrogen, just decrease the maximum attainable.
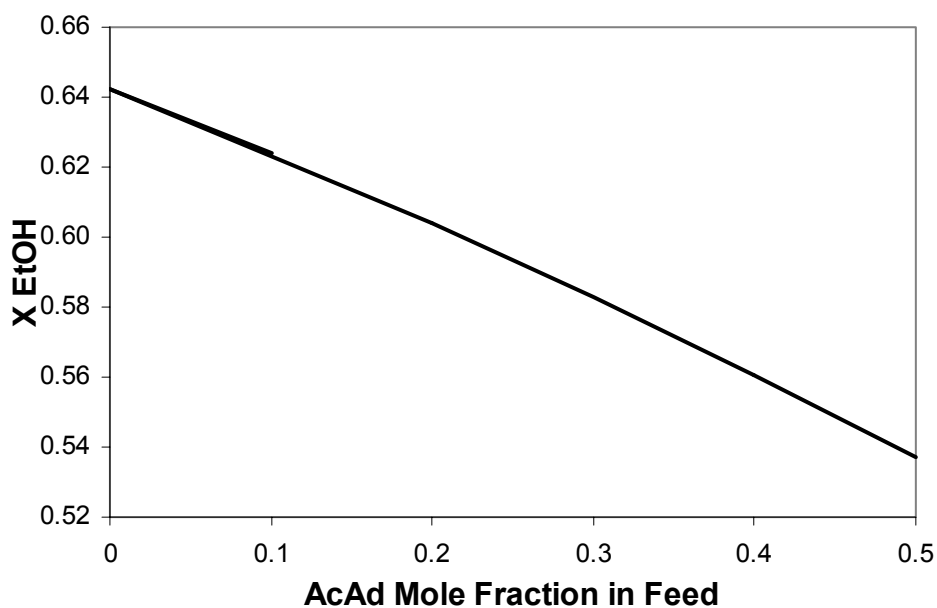
Figure 5.6 Ethanol conversion as a function of acetaldehyde content in the feed, T= 300°C, P= 0.1 MPa.

The thermodynamic expectations are in a good agreement with literature data reported by Shiau and Chen (1991), who diluted the ethanol feed with acetaldehyde (90:10) and observed a 7-12% drop in conversion depending on reaction conditions.

Summary

Ethanol dehydrogenation is a thermodynamically feasible way to produce high purity hydrogen. Copper has been identified as an active metal component for the reaction. The sintering of copper limits the maximum reaction temperature to <325°C, which consequently results in incomplete conversion and therefore requirement of product-stream refinement. Similar purification step is expected to be required for the ethanol/acetaldehyde stream coming from the other portion of the cycle. However, small amounts of acetaldehyde are not likely to have overly detrimental effect on conversion. Experimental results regarding the effect of pressure on ethanol conversion reported in

literature contradict the thermodynamic expectations, therefore suggesting that the pressurized hydrogen can be produced from this step.

5.2 Acetaldehyde Hydrogenation

Early in the 20th century, ethanol was commercially produced in Switzerland by hydrogenation of acetaldehyde by hydrogen over a Ni catalyst (Armstrong and Hilditch, 1920). This process was rendered economically obsolete by availability of cheap petroleum, a widespread use of ethylene pyrolysis and ethylene's sequential hydration to ethanol. The interest in acetaldehyde hydrogenation was renewed with the investigation of syngas as an alternative resource base for production of various hydrocarbons. Acetaldehyde was considered an intermediate in the production of ethanol from syngas (Burch and Petch, 1992a; Trunschke et al., 1991, Arimitu et al., 1989). Promising results were obtained with Rh-(Burch and Petch, 1992a; Trunschke et al., 1991) and Cu-(Arimitu et al., 1989; Agarwal et al., 1988) based catalysts, which are commonly used in methanol synthesis from syngas. Copper once again is of special interest because of its low cost and ability to preserve the C-C bond.

Aside from the main reaction:

$$CH_3CHO(g) + H_2 + CO \rightarrow C_2H_5OH(g) + CO \quad \Delta H^0_{298K} = -68.75\,kJ/mol \quad \Delta G^0_{298K} = -34.75\,kJ/mol$$

the same undesirable parallel and subsequent reactions proposed for ethanol dehydrogenation might be encountered. In addition, the presence of syngas might lead to formation of additional hydrocarbons through CO reaction with hydrogen. However, once again these reactions will be omitted from modeling, because experimentally the rate of acetaldehyde hydrogenation is much higher than rates of these secondary reactions. Acetaldehyde conversion defined as: $X_{AD} = \dfrac{\dot{n}^0_{AD} - \dot{n}_{AD}}{\dot{n}^0_{AD}}$, where $\dot{n}^0_{AD}$ is the entering molar flow of acetaldehyde and $\dot{n}_{AD}$ is the exiting molar flow of acetaldehyde, will be used to evaluate of the effects of temperature, pressure and feed composition on the outcome of reaction. A syngas composition of 3:1 H_2:CO, typical for methane steam

reforming, will be used and a 1:1:0.33 AcAd:H$_2$:CO stoichiometric ratio will be assumed unless stated otherwise.

Temperature

Acetaldehyde hydrogenation is an exothermic reaction and therefore favoured at low temperatures. As can be seen from Fig. 5.7, complete conversion can be achieved at T<100°C. While such a low temperature range may still be kinetically feasible for Rh-based catalysts (Burch and Petch, 1992a; Trunschke et al., 1991), temperatures higher than 200°C are required for the hydrogenation to proceed on Cu-based catalysts (Arimitu et al., 1989). A temperature range of 150-300°C will be considered in the ensuing discussion.
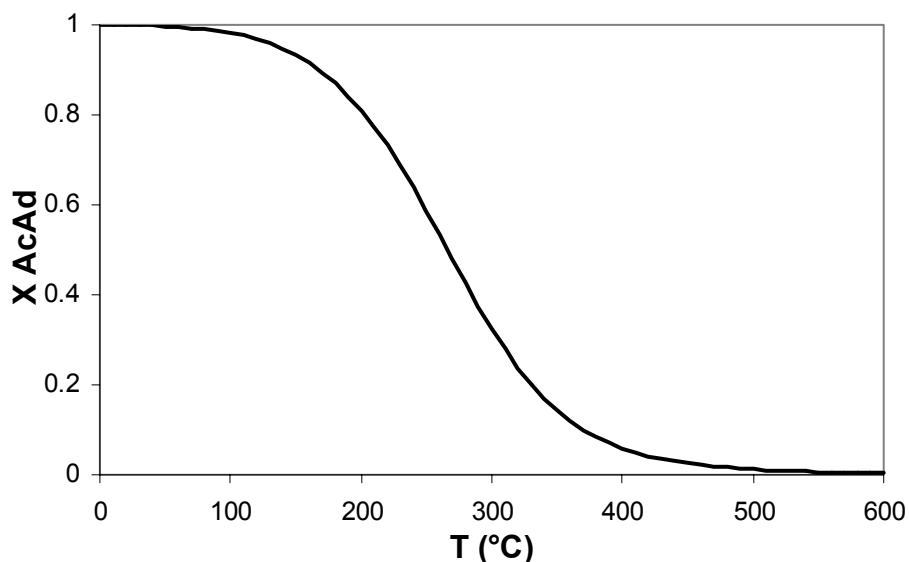
Figure 5.7 Acetaldehyde conversion as a function of temperature, P=0.1 MPa.

Pressure

Acetaldehyde hydrogenation is favoured at high pressure because of its negative entropy change. As seen from Fig. 5.8 this positive pressure effect is most pronounced in the range 0.1-1 MPa. At higher pressures the conversion slowly approaches 100%.

65
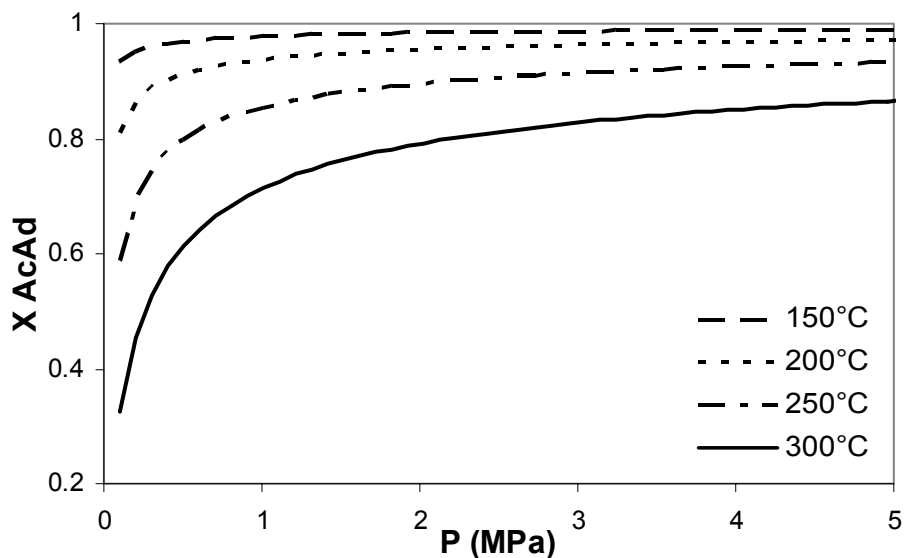
Figure 5.8 Acetaldehyde conversion as a function of pressure.

To the best of our knowledge, there are no experimental data available confirming or contradicting these thermodynamic observations. While it is tempting to assume that a similar catalyst surface saturation phenomenon may occur as in the case of ethanol dehydrogenation, it is important to realize the higher complexity of the hydrogenation system, where acetaldehyde competes for active sites with both hydrogen and CO molecules. Furthermore, carrying out the hydrogenation at elevated pressures requires a pressurized inlet syngas stream and unless the process of making the upstream syngas is conducted under high pressure, this will result in significant energy requirements. Nevertheless, the hydrogenation step is not essential for production of high pressure hydrogen and it would suffice to complete a cycle by successfully carrying out hydrogenation at atmospheric pressure. For the following discussion, atmospheric pressure and a pressure of 1 MPa will be considered.

Feed composition

Due to thermodynamics and catalyst limitations, as discussed previously, the acetaldehyde stream originating from the ethanol dehydrogenation step will contain unconverted ethanol. When considering the effect of ethanol content in the feed on hydrogenation thermodynamics, two scenarios arise. 1) The flow rate of syngas is

decreased proportionally to the decreased acetaldehyde content in order to maintain the target 1:1 H_2:AcAd stoichiometric ratio or 2) the syngas flow is maintained constant regardless of change in feed composition. The first case is applicable for ideal, long-term stable operation, where the composition of acetaldehyde feed coming out from ethanol dehydrogenation is constant. In that case, as expected and seen from Fig. 5.9, the addition of ethanol has a detrimental effect on acetaldehyde conversion, but the hydrogen removal from the gas stream remains constant. This negative effect is magnified by increased temperature and alleviated by increased pressure.
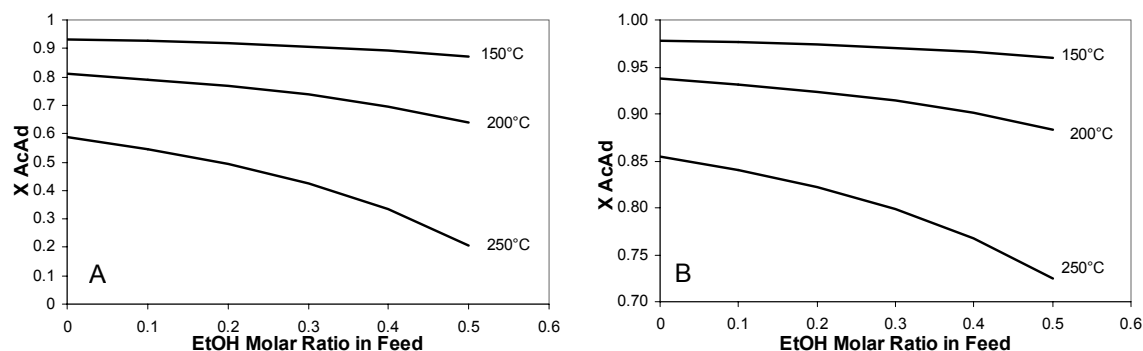
Figure 5.9 Acetaldehyde conversion as a function of ethanol content in the feed at P=0.1 MPa (A) and P=1 MPa (B) and constant AcAd:H_2:CO molar ratio: 1:1:0.33.

The second case is more applicable to dynamic operation, where the composition of the incoming acetaldehyde stream can change because of variations in operating conditions, while the syngas stream flow rate remains constant. The acetaldehyde conversion is affected by two contradictory forces:

- the presence of ethanol, the product of hydrogenation, decreases equilibrium conversion,
- on the other hand, ethanol dilutes the acetaldehyde feed affecting the stoichiometry of the hydrogenation. Excess hydrogen then increases acetaldehyde conversion.

As a result, with the exception of atmospheric pressure at 250°C scenario, acetaldehyde conversion with increasing ethanol content increases or passes through maximum, as can be seen in Fig. 5.10. In contrast to the previous scenario, hydrogen removal from the

syngas did not remain constant but continually decreased with increasing ethanol content as seen in Fig. 5.11.
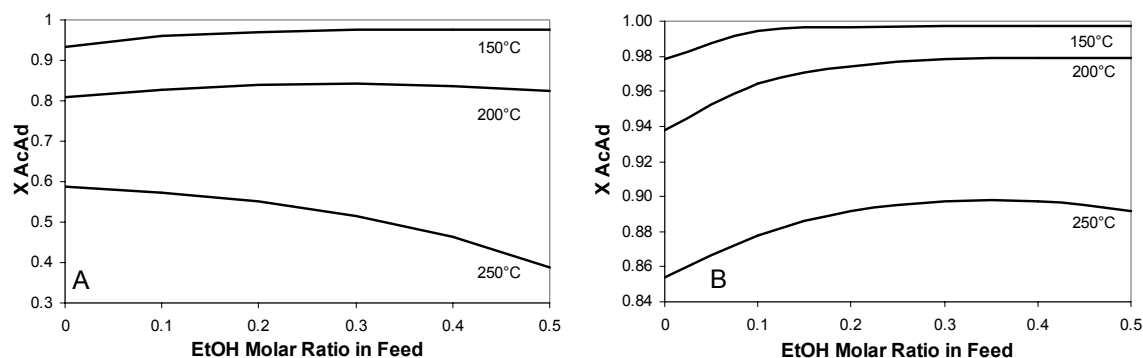
Figure 5.10 Acetaldehyde conversion as a function of ethanol content in the feed at P=0.1 MPa (A) and P=1 MPa (B) and constant syngas flow rate.
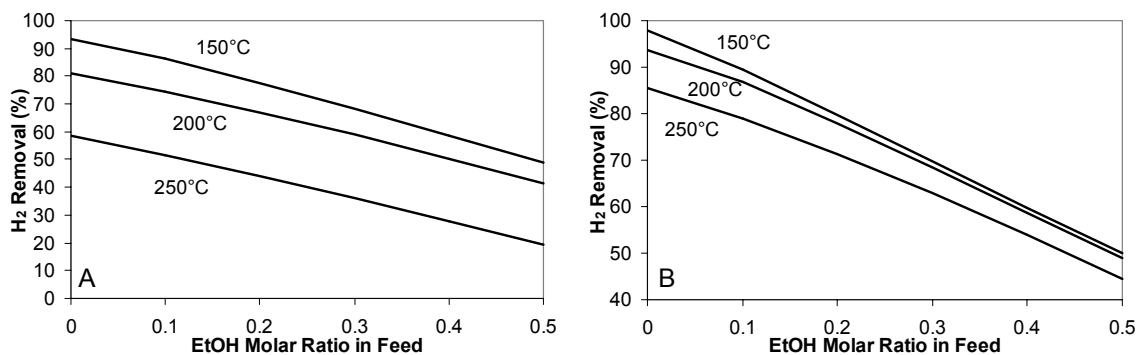
Figure 5.11 Hydrogen removal from syngas as a function of ethanol content in the feed at P=0.1 MPa (A) and P=1 MPa (B) and constant syngas flow rate.

These results imply that, depending on the process requirements, it may be beneficial to perform the acetaldehyde hydrogenation in an excess of syngas, in order to achieve higher conversion and under certain conditions decrease the separation costs. Furthermore, it can be concluded from both scenarios that small amounts of ethanol can be acceptable, because they would not have a severe detrimental effect on the outcome of the reaction.

Summary

Acetaldehyde hydrogenation completes the cycle for the production of high pressure hydrogen. Hydrogenation is thermodynamically favoured at low temperatures,

which is in conflict with the kinetic requirements on the rate of reaction. However, the negative thermodynamic impact of higher temperature on acetaldehyde conversion can be easily offset by increasing the pressure or using hydrogen in excess.

5.3 Conclusions

A thermodynamic analysis was utilized to examine the feasibility of a cycle and identify the limitations in operating conditions. The limitations were the high-temperature requirements for complete conversion in ethanol dehydrogenation and also the detrimental effect of pressure on the dehydrogenation outcome. However, these limitations were found to be modest, merely indicating a need for process optimization rather than hindering the overall proposed process.

Chapter 6: Ethanol dehydrogenation – copper foam

Due to the unique nature of copper foam, this chapter is fully dedicated to the evaluation of its performance in ethanol dehydrogenation. Chapter 7 then deals exclusively with the performance of supported copper catalysts.

6.1 Introduction

Copper-based catalysts were found to be excellent catalysts for ethanol dehydrogenation because of their ability to maintain the C-C bond intact while dehydrogenating the C-O bond. While the majority of work has been conducted on supported copper catalysts, several studies evaluating catalytic activity of metallic copper have also been published. Metallic copper was used either in the form of a copper screen (Church and Joshi, 1951), or as a powder prepared by decomposition of $Cu(NO_3)_2$ (Iwasa and Takezawa, 1991) or precipitated as $Cu(OH)_2$ (Chung et al., 1993; Kanoun et al., 1991a,b, 1993) or $CuCO_3$ (Tu et al., 1994a,b) which was then calcined and reduced *in-situ*. In all studies, where the performance of unsupported metallic copper was compared to a supported copper catalyst, unsupported copper provided superior acetaldehyde selectivity under identical reaction conditions.

Metal foams are a highly permeable cellular form of metals having properties comparable to ceramic monoliths commonly used in automotive exhaust gas clean-up. Unlike monoliths, foams contain tortuous channels through which the reactants must travel, thus promoting better mixing and achieving better temperature control. High bulk heat conductivity assures homogenous temperature profiles and, together with the possibility of welding foam directly to reactor walls, prevents formation of hot or cold spots. Metal foams generally have low density, high mechanical strength and high surface area per unit volume, which makes them attractive as a support for noble metal catalysts. For example, various FeCr-based foams have been used as a support for Pd (Giani et al., 2006), Pt (Sirijarupan et al., 2005a) or Pt-Fe (Sirijarupan et al., 2005b; Chin et al., 2006) deposited on γ-Al_2O_3 in CO oxidation and in CH_4 oxidation carried over Ni-MgO (Shamsi and Spivey, 2005). Various metal (Cu, Ni, Ag) or metal alloy foams (Cu-Ni, Fe-Ni, Ni-Cr, Fe-Cr-Ni) have been used as catalytic supports or active metal catalysts for

alcohol partial oxidation to aldehydes (Pestryakov et al., 2002, 2003), alkane deep oxidation (Pestryakov et al., 1994, 1995) and for purification of automotive exhausts (Pestryakov et al., 1994). With few exceptions (Pestryakov et al., 1994, 2002, 2003), metal foams, having relatively low surface area per unit of weight (0.01-0.1 m^2 g^{-1}), have not been used in pure metal form but rather as a carrier for a material with higher surface area, such as γ-Al_2O_3, serving as a support for active noble metal. Deposition and mechanical stability of this layer represent a technological challenge and if avoidable would result in time and capital savings. The focus of this study is on metallic copper foam which is characterized and evaluated as a catalyst for ethanol dehydrogenation to acetaldehyde and hydrogen.

6.2 Experimental Section

6.2.1 Catalyst preparation

Copper foam (Circuit Foil Luxembourg, thickness 1.5 mm, porosity 90 ppi, specific surface area 0.033 m^2 g^{-1}) was cut from the original sheet in the form of circular pads (10 mm diameter). Ethanol dehydrogenation was studied on untreated virgin copper foam and copper foam pretreated by oxidation, reduction or a combination of both.

6.2.2 Catalyst characterization
Thermogravimetric analysis (TGA)

Thermogravimetric analysis was conducted utilizing a TA Instruments SDT 2960. The weight change of copper foam sample during oxidation in air was recorded as a function of time on stream and temperature. In separate tests, each sample was ramped to a desired temperature in He and then treated in air for 65 min and 1089 min respectively.

X-ray diffraction (XRD)

X-ray diffraction patterns were obtained using a Bruker AXS D8 Advance diffractometer employing Cu Kα radiation with 2θ interval defined from 20 to 95° with a step size of 0.05°.

Scanning electron microscopy (SEM)

Scanning electron microscopy was utilized for surface morphology characterization using a LEO 1530 SEM (5-kV electron beam) equipped with a secondary electrons detector. Samples of interest consisted of copper foam before any pretreatment, oxidized copper foam, oxidized and reduced copper foam and copper foam sampled during and after the reaction.

BET surface area

BET surface area was determined by a Micromeritics Gemini[TM] V-Series surface analyzer. The samples were pretreated in N_2 at 120°C for 1 h in order to remove any moisture adsorbed on the catalyst surface. Surface areas of virgin, oxidized, oxidized and reduced, and spent copper foam samples were measured.

Catalytic activity

A standard down-flow, fixed-bed reactor consisting of a quartz tube (i.d. 10 mm, length 48 cm) with a quartz frit located at 19 cm from the rim of the tube (furnace's isothermal zone), was used for all experiments. Copper foam pads were evenly interlayered with SiC (Kramer Industries, 36 Grit), serving as a flow and temperature distributor, and loaded onto the frit. The reactor was placed into the tubular convection furnace and the thermocouple, used for the control of the reaction temperature, was inserted into the layer of SiC above the first copper foam pad. An Eldex A-60-S stainless steel HP metering pump was used to deliver a desired water-ethanol (Commercial Alcohols, anhydrous) mixture at a constant flow rate of 0.2 mL min^{-1} to the evaporator where it was gasified and combined with a N_2 stream (15 mL min^{-1}) utilized as an internal reference. The combined gaseous feed was then passed over the catalyst bed. The resulting product stream was directed into the online-attached Varian GC 3800 gas chromatograph. A novel gas chromatograph separation method (Chladek et al., 2007a, see Appendix A) developed previously allowed for simultaneous analysis of both gaseous and condensable components once every 32 min. The reaction was studied at atmospheric pressure and for temperatures ranging from 200 to 400°C.

6.3 Results and discussion

6.3.1 Catalyst characterization

TGA

   Complete oxidation of a copper foam sample (M_{CuO}/M_{Cu} = 1.25) was achieved by ramping the temperature at 5°C /min from room temperature to 1000°C and was used as a reference for other oxidation experiments. Fig 6.1 shows the oxidized percentage of bulk copper foam after passing air for 65 min, and it can be concluded that oxidation of copper foam is negligible at temperatures below 100°C but increases rapidly with increasing temperature. As seen in Fig. 6.2, at 500°C, the highest rate of oxidation is achieved in the first 4 h after which the weight increase becomes significantly slower indicating that the oxidation of easily accessible copper is complete.
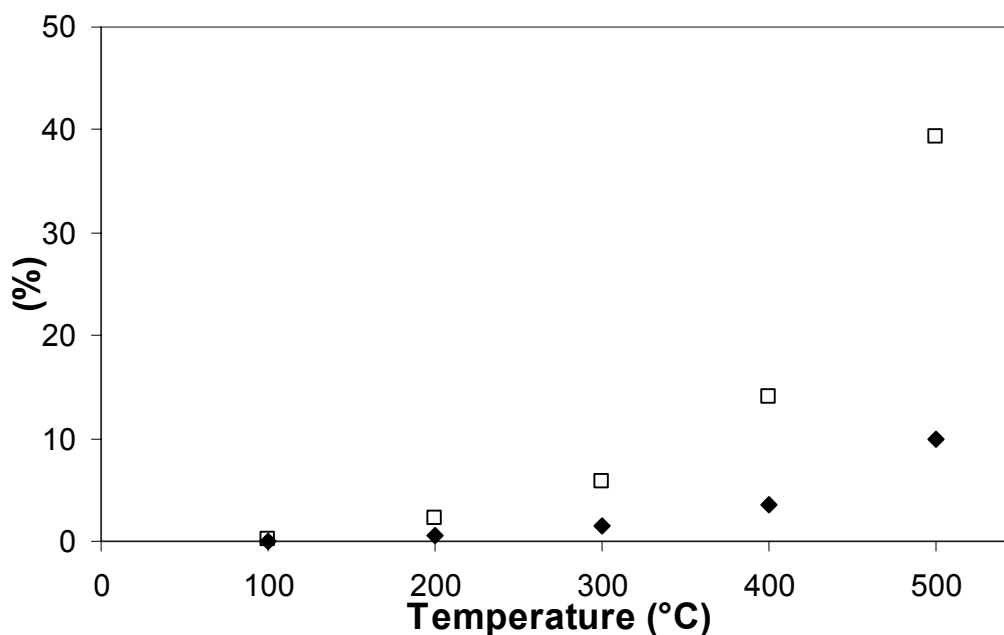
Figure 6.1 TGA - oxidized percentage of bulk copper foam (□) and percentage weight gain (♦) upon oxidative pretreatment for 65 min as a function of temperature.
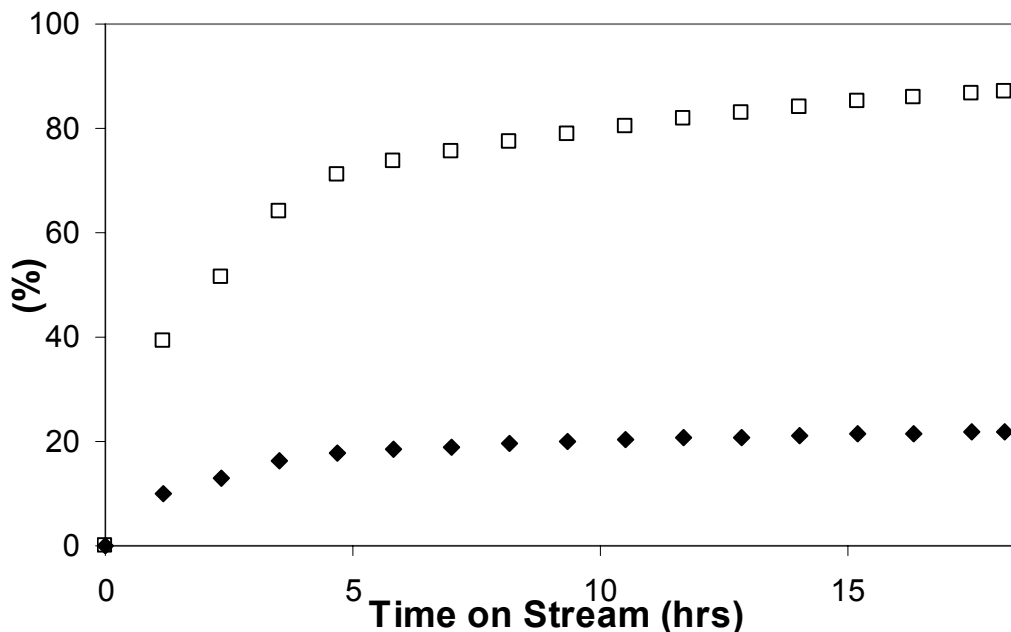
Figure 6.2 TGA - oxidized percentage of bulk copper foam (□) and percentage weight gain (♦) upon oxidative pretreatment at 500°C as a function of time.

XRD

The XRD patterns of virgin, oxidized, oxidized and reduced, after-2-h-on-stream and after-20-h-on-stream copper foam samples are depicted in Fig. 6.3. As expected, only the metallic copper crystal phase (Δ) is present on virgin copper foam. After oxidation, copper foam contains crystal phases of both Cu_2O (●) and CuO (□) but metallic copper still remains present. In the subsequent reduction, or during reaction, the oxides are quickly reduced back to the original pure metallic copper. One should note, that during the reaction, both (111) and (200) crystal surfaces become more dominant most probably at the expense of less stable surfaces. The reconstruction of the copper surface, i.e., the reordering of atoms to minimize the surface free energy, was reported before and found to be enhanced by the presence of H_2 (Rieder and Stocker, 1986), N_2 (Spitzl et al., 1991) or surface adsorbates (Chen and Voter, 1991) and linked to negative changes in copper chemical activity (Alexander and Pritchard, 1972) – i.e., certain active sites can be found only on rough surfaces, which virtually do not exist on well-sintered copper surfaces.
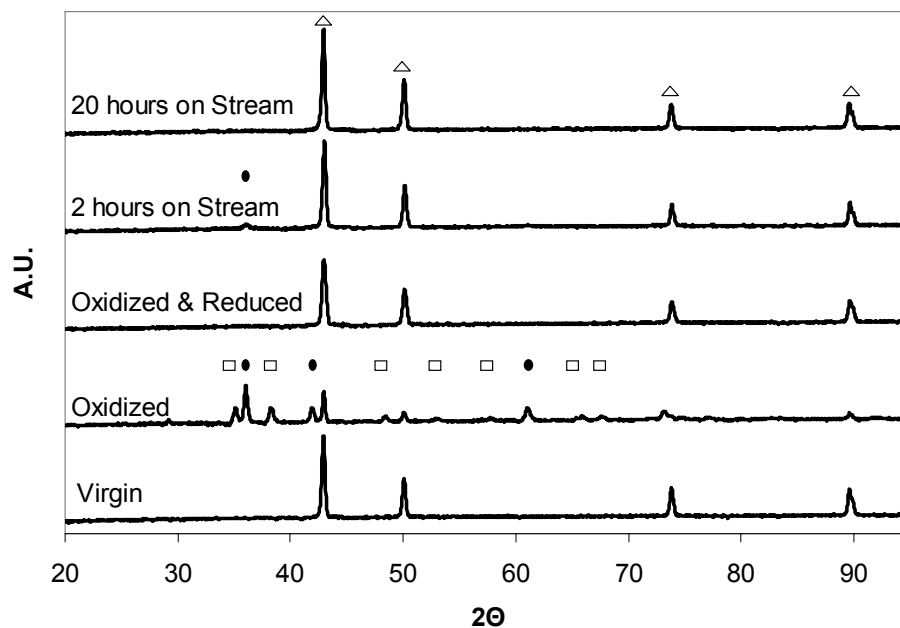
Figure 6.3 XRD patterns of virgin, oxidized, oxidized and reduced, copper foam and copper foam after 2 and 20 h on stream. The presence of copper ($\triangle$), Cu_2O ($\bullet$) and CuO ($\square$) crystal phases is indicated.

SEM

Scanning electron microscope images of virgin (a), oxidized (b), oxidized and reduced (c), after-2-h-on-stream (d) and after-20-h-on-stream (e) copper foam samples are presented in Fig. 6.4. SEM reveals significant changes in copper foam surface morphology upon oxidation. The smooth surface of virgin copper foam (Fig. 6.4-a) becomes covered by needle-like crystals (Fig. 6.4-b), presumably of CuO, as detected by XRD (Fig. 6.3). After the reduction, the needles retract as the copper is reduced to its metallic form but the surface retains a high level of roughness, which translates into a high number of active sites (Fig. 6.4-c). As the reaction proceeds, the surface gradually becomes smoother but still contains some sharp edges (Fig. 6.4-d). After 20 h on stream, the surface becomes covered by spherical aggregates, suggesting the minimization of surface area free energy and a decrease in the availability of active sites (Fig. 6.4-e).

75
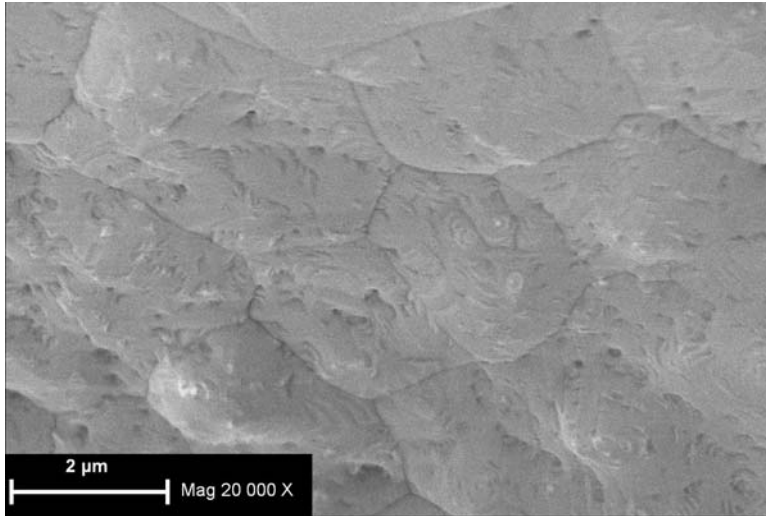
(a)
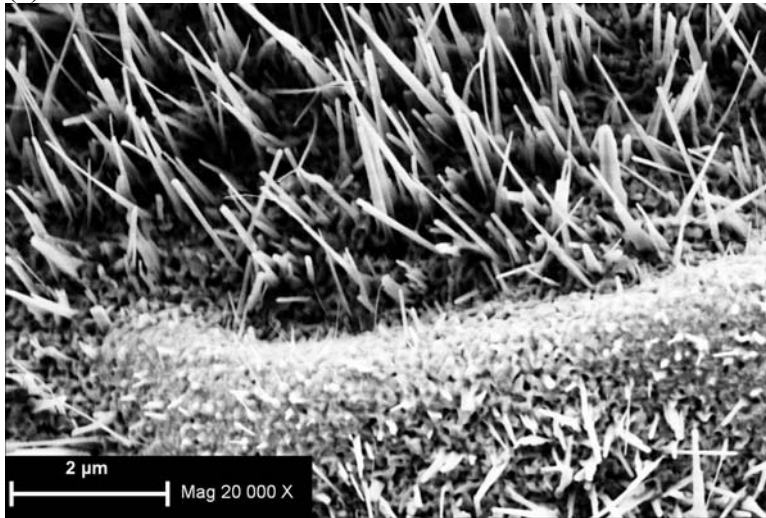
(b)
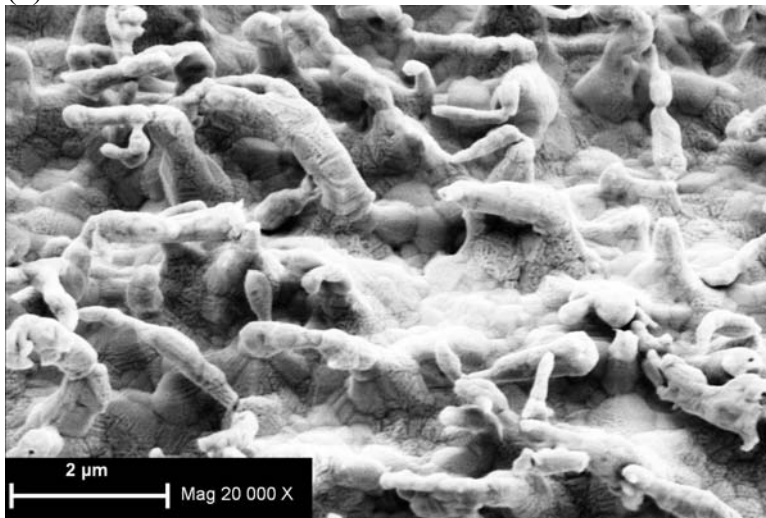
(c)
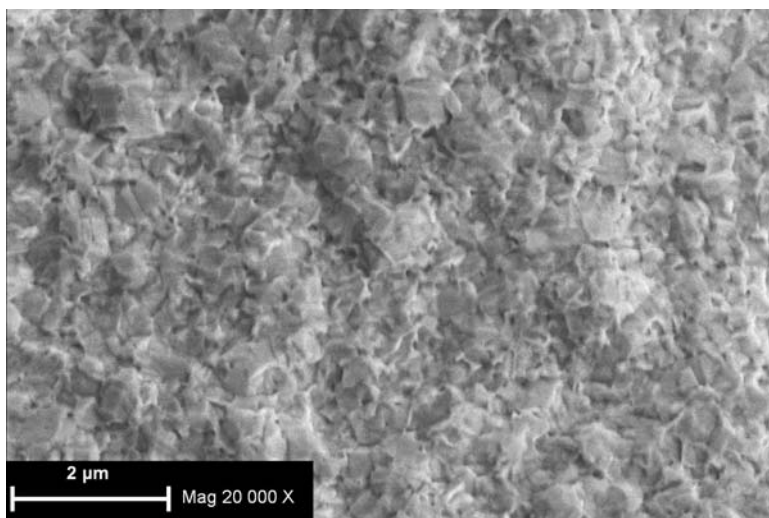
(d)
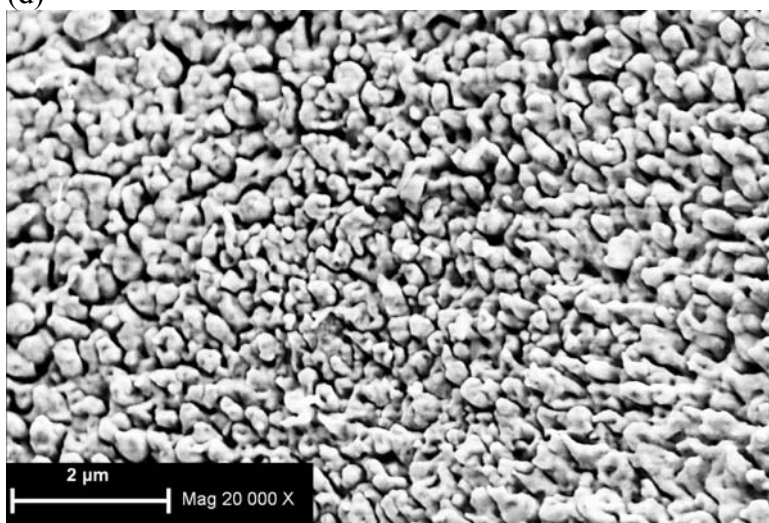
(e)

Figure 6.4 SEM images (5-kV electron beam, secondary electrons detector) of untreated virgin (a), oxidized (b), oxidized and reduced (c), after-2-h on stream (d) and after-20-h-on-stream (e) copper foam samples.

BET surface area

Total surface areas of the copper foam samples measured by BET are presented in Table 6.1. Upon oxidation, the virgin foam surface area increased by an order of magnitude and decreased only slightly when reduced at 300°C in a 30:150 mL min^{-1} H_2:N_2 stream. During reaction, the surface area decreased, but remained significantly higher than that of the virgin copper foam.

It should be noted that the surface areas of oxidized, oxidized and reduced and after-20-h-on-stream copper foam samples are qualitative rather than quantitative values. An inconsistency in copper surface area measurements was encountered and could be

explained by possible reconstruction of copper surface during N_2 pretreatment. Spitzl et al. (1991) reported that a N_2 coverage determination on copper surfaces is difficult and questionable because of implantation of N_2 into surface layers. Furthermore, the same authors reported absorption of N_2 within the surface layers of copper. This would be and indeed was an issue for the pretreated copper foam with larger surface area, where more N_2 could absorb compared to virgin untreated copper foam.

Table 6.1 Copper content, BET and Copper surface areas and Copper dispersion of untreated and pretreated copper foam samples and supported copper catalysts.

	Pretreatment	BET Surface Area (m^2/g)
	Virgin	0.03
Copper Foam	Oxidized	0.50
	Oxidized + Reduced	0.44
	Oxidized + Reaction 20 hrs	0.22

6.3.2 Ethanol dehydrogenation

Prior to the dehydrogenation experiments, a blank run was performed to verify the inertness of the quartz reactor and SiC packing. In all experiments, with a few exceptions to be mentioned later, the major products were acetaldehyde and hydrogen. The hydrogen selectivity was higher than 99% and the carbon balance always added up to 98-100%. The performance of copper foam in ethanol dehydrogenation to acetaldehyde was therefore evaluated solely based on the overall ethanol conversion, which was defined as:

$$X_{EtOH} = \frac{\dot{n}^0_{EtOH} - \dot{n}_{EtOH}}{\dot{n}^0_{EtOH}} = \frac{\sum\limits_{carbonaceous\ products}^{i} a_i \dot{n}_i}{\sum\limits_{carbonaceous\ products}^{i} a_i \dot{n}_i + \dot{n}_{EtOH}}$$

where $\dot{n}^0_{EtOH}$ is the entering molar flow of ethanol; $\dot{n}_{EtOH}$ is the exiting molar flow of ethanol; a_i is the number of carbon atoms in any product species divided by the number of carbons contained in an ethanol molecule; and $\dot{n}_i$ is the exiting molar flow of any carbonaceous product.

Minor by-products accounting in total for less than 1% of product stream included ethyl acetate and crotonaldehyde. These are products of subsequent acetaldehyde reactions and were detected exclusively at higher ethanol conversions.

Pretreatment

In addition to unmodified virgin copper foam (VCF), the effect of four different pretreatments - copper foam oxidized in air flow at 500°C for 3 h and 40 min (CFOX), copper foam reduced in 30:150 $H_2:N_2$ stream at 300°C for 1 h (CFRED), and combinations of both preceding treatments (CFOXRED and CFREDOX) - on ethanol conversion was studied. Ethanol dehydrogenation was carried out at 300°C with an average weight of 0.1370 g of copper foam (5 pads) used as a catalyst. The copper foam pads were separated by layers of SiC (total weight of 2.4 g). A 1:1 molar mixture of ethanol and water at a liquid flow rate of 0.2 mL min^{-1} together with N_2 tracer (15 mL min^{-1}) were supplied as a feed.

Both VCF and CFRED did not show any catalytic activity over 20 h on stream (not shown). Ethanol conversion as a function of time on stream for the remaining three pretreatments is depicted in Fig. 6.5. In all cases, ethanol conversions followed a similar hyperbolic decline. CFREDOX and CFOX had very similar initial conversions with a slightly higher conversion achieved by CFREDOX. Initial ethanol conversion in CFOXRED experiment was lower because of the loss of surface area associated with the reduction of the oxide-covered foam surface. As the dehydrogenation proceeded, oxidized catalysts were reduced by *in-situ* generated hydrogen and the catalyst was gradually deactivated by copper sintering/reconstruction into larger aggregates as shown in SEM images (Fig. 6.4). The catalytic activity can therefore be correlated with an increase in copper foam surface area which consequently affects the number of active sites. Therefore the oxidative pretreatment was identified as an essential step in catalyst activation and oxidized copper foam was used as a catalyst in the following experiments.
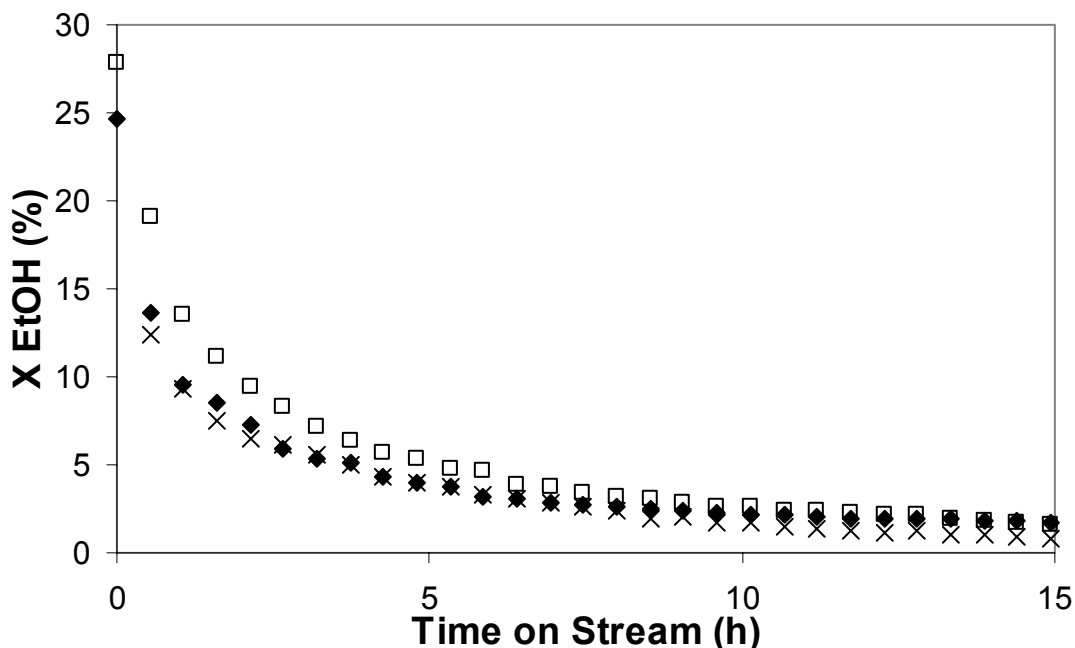
Figure 6.5 Ethanol conversion (%) as a function of time-on-stream (h) for oxidation (♦), oxidation and reduction (X), and reduction and oxidation pretreatments (□) at 300°C, 0.1370 g of copper foam and 1:1 molar EtOH:H_2O feed.

Temperature

Ethanol dehydrogenation was studied at three different temperatures; 200, 300 and 400°C, with 0.1370 g of copper foam (5 pads), pretreated for 3 h and 40 min at 500°C in 200 mL min^{-1} of air, used as the catalyst. The feed composition, flow rate and pressure were identical to the conditions described in the previous section. From Fig. 6.6, it can be observed that the experiment at 300°C yielded the highest ethanol conversion, followed by the experiments at 400°C and 200°C. In all cases the copper foam deactivated. However, at 200°C the copper foam showed two distinguishable periods: 1) an activation period, when high-surface-area but catalytically-inactive copper oxides were converted by the hydrogen generated *in-situ* on remaining metal copper active sites (as seen from XRD in Fig. 6.3) to high-surface-area catalytically-active metallic copper, and 2) deactivation period in which the surface area of metallic copper decreased because of loss of surface area. The same activation phase exhibiting a maximum in copper catalyst activity is expected to occur at higher temperatures only faster, which made it impossible to observe because of limitations of our analytical system. The copper foam deactivated faster as the temperature increased, as can be seen when comparing

80

experiments at 300 and 400°C. While in both 200 and 300°C experiments the main product was acetaldehyde with selectivity >99%, the favored products at 400°C were diethyl ether and ethylene with selectivities steadily increasing with decreasing catalyst activity and reaching 57% and 20%, respectively, at the end of the experiment. This indicates that at temperatures above 300°C, ethanol dehydration plays a significantly more important role in ethanol conversion than does dehydrogenation. A temperature of 300°C was therefore identified as an optimum temperature for subsequent experiments, yielding a satisfactory initial concentration, while maintaining high acetaldehyde selectivity.
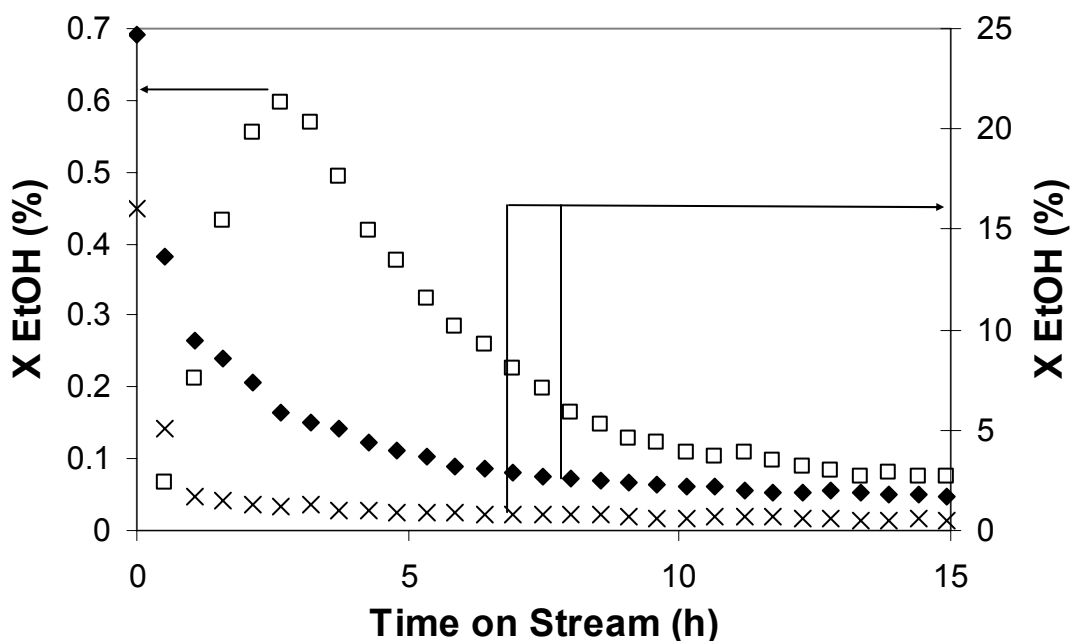
Figure 6.6 Ethanol conversion (%) as a function of time-on-stream (h) and reaction temperature: 200°C (□), 300°C (♦) and 400°C (X) at 0.1370 g of oxidation treated catalyst and 1:1 molar EtOH:H$_2$O feed.

Feed composition

0.1370 g of copper foam (5 pads) pretreated in air were used as a catalyst for ethanol dehydrogenation at 300°C and at three different fractions of ethanol in the liquid feed: pure ethanol, 1:1 EtOH:H$_2$O molar mixture, and 1:50 EtOH:H$_2$O molar mixture. The total liquid feed flow rate was maintained at 0.2 mL min^{-1} and nitrogen was added as a tracer at 15 mL min^{-1}. The results presented in Fig. 6.7 show an activation period for low ethanol content feed accompanied by ethanol conversion reaching 54%. The

observation of both an activation phase and high ethanol conversion can be explained by the low concentration of ethanol in the feed; a concentration which provides insufficient hydrogen production to reduce the copper oxides to active metallic copper. However, once these metal sites are created, they yield higher ethanol conversion, because, in the presence of low ethanol concentration, the surface does not become saturated with ethanol. On the other hand, the increase from the 1:1 EtOH:H₂O solution to pure ethanol did not bring about any significant change in ethanol conversion, suggesting that the surface is fully saturated and the conversion is independent of ethanol concentration in the gas phase and can only be increased by the addition of more catalyst or creation of more active sites.
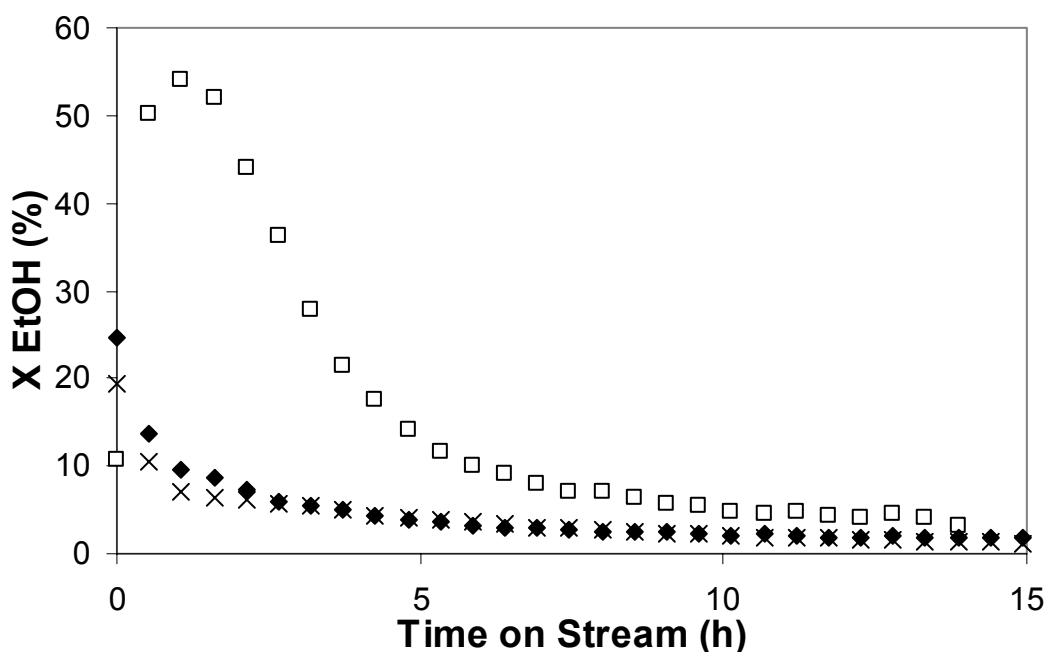
Figure 6.7 Ethanol conversion (%) as a function of time-on-stream (h) and ethanol feed composition: 1:50 molar EtOH:H₂O (□), 1:1 molar EtOH:H₂O (♦) and pure EtOH (X) at 300°C and 0.1370 g of oxidation treated catalyst.

Catalyst weight

Using 0.2 mL min^{-1} of 1:1 molar EtOH:H$_2$O + 15 mL min^{-1} N$_2$ as a feed, setting the reaction temperature to 300°C and using an oxidative pretreatment, the effect of catalyst weight on ethanol conversion was evaluated at three different levels: 0.027 g (1 pad), 0.1370 g (5 pads) and 0.5537 g (20 pads). The layers of copper foam were separated by 2.5, 2.4 and 2 g of SiC, respectively, to maintain the total catalyst bed weight at 2.5 g. As seen in Fig. 6.8, the ethanol conversion was directly proportional to the amount of catalyst used. In the case of high catalyst loading, the first data point suggests the presence of an activation phase, which would last longer than in the other two cases, because a larger amount of copper oxides is available for *in-situ* reduction. In all three cases copper foam is subject to deactivation by loss of surface area, with the highest catalyst loading maintaining the highest residual activity after 20 h on stream.
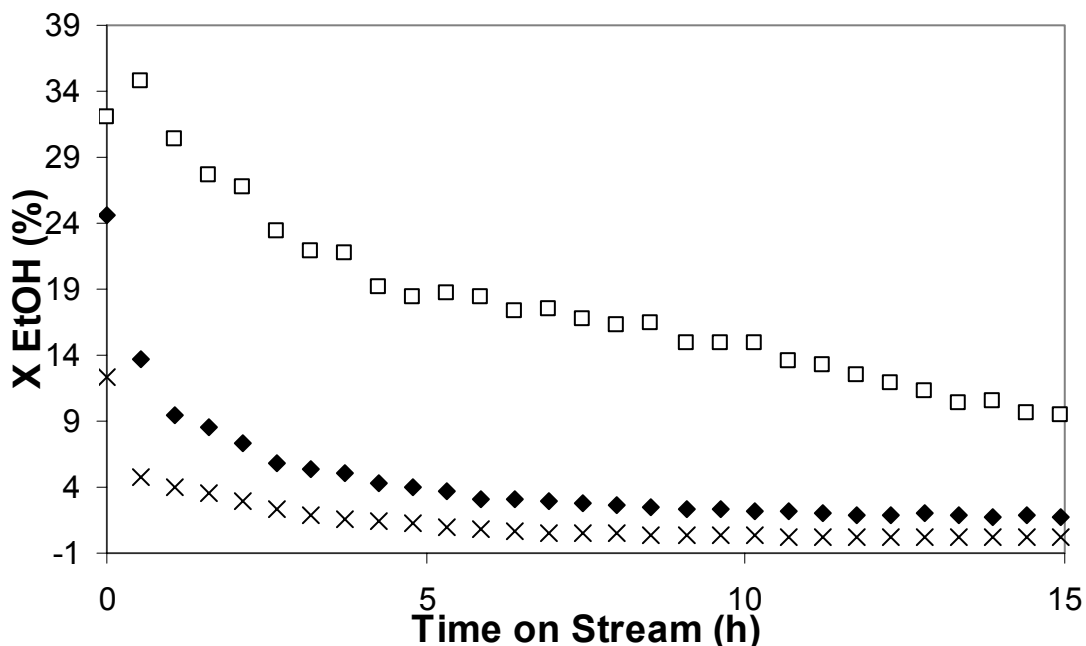
Figure 6.8 Ethanol conversion (%) as a function of time-on-stream (h) and catalyst weight: 0.5537 g (□), 0.1370 g (♦) and 0.0270 g (X) at oxidation treated catalyst, 300°C and 1:1 molar EtOH:H$_2$O feed.

Periodic operation – dehydrogenation + oxidation

The preceding experiments indicated the existence of activation and deactivation periods which can be linked to the presence of active metal copper sites, the formation of which is greatly increased upon oxidative pretreatment of copper foam. The experiment described in this section was designed to establish whether the deactivation of copper foam caused by the loss of active sites can be reversed by a short oxidation period. Prior to the experiment, 0.1370 g (5 pads) of copper foam was pretreated in air (200 mL min^{-1}) at 500°C for 3 h and 40 min. The reactor was then cooled to 300°C and a 1:1 molar EtOH:H$_2$O feed (0.2 mL min^{-1}) together with tracer N$_2$ (15 mL min^{-1}) was introduced into the reactor. After 3 h on stream, the feed mixture was replaced with an air stream (200 mL min^{-1}) for 25 min (time required to complete a GC analysis of the previous injection). The dehydrogenation and oxidative cycle was repeated for a total duration of 37 h. The reaction was then allowed to proceed for an additional 6 h, after which the copper foam catalyst was again reactivated in air and three additional cycles were conducted. The results, displayed in Fig. 6.9, prove that copper foam can be effectively re-activated by re-oxidation of the surface. The smoothed exterior is periodically disrupted by generation of CuO needles, which are then reduced by *in-situ* generated H$_2$ leading to the surface reconstruction into a less active, smooth form. However, the periodic increase in ethanol conversion thus achieved decreased with the number of reactivation cycles until reaching and maintaining a steady value of approximately 15% after the 6th cycle. It is important to note that after each reactivation cycle, the first product sample was taken after 7-8 min had elapsed since the introduction of the liquid feed. Therefore, neither a fast activation cycle, when copper oxides are reduced and conversion is below the maximum, nor the maximum conversion are detected. It can be assumed that the maximum achievable conversion after six cycles is between 15-17%. As can be seen from the Fig. 6.9, the copper foam catalyst can be successfully reactivated by oxidation at any time during the reaction, however for practical purposes it would be beneficial to alternate the reaction and activation cycles in a fast sequence thereby maintaining copper foam in its peak performance. Besides, short activation periods will ensure sole oxidation of top layers of copper foam without compromising mechanical integrity of bulk copper foam.
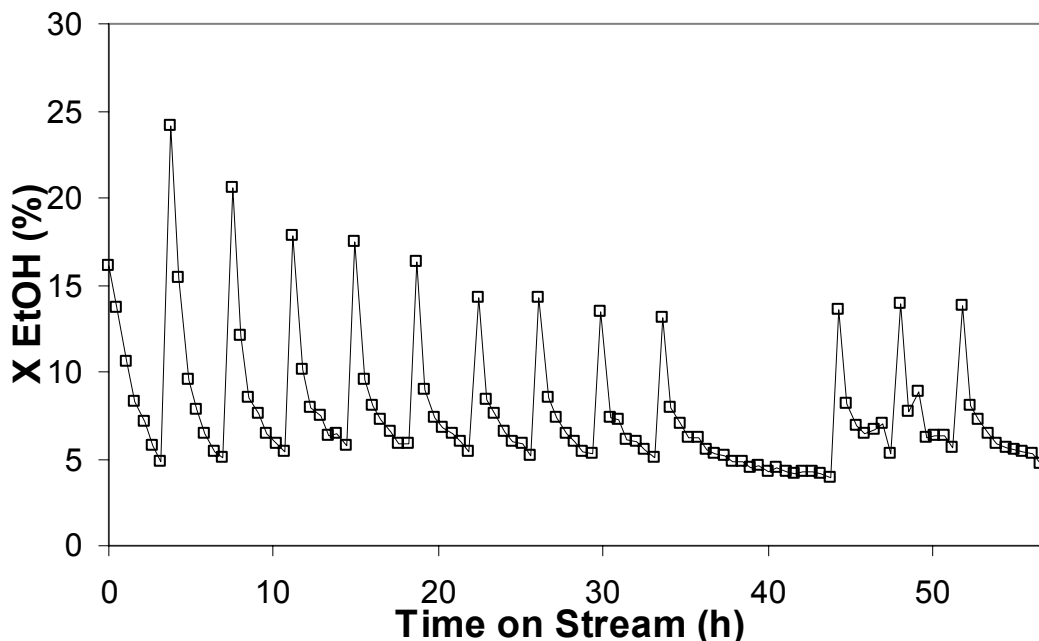
Figure 6.9 Ethanol conversion (%) as a function of time-on-stream (h) in re-activation experiment at 300°C, 0.1370 g of catalyst and 1:1 molar EtOH:H_2O feed alternated with 25-min periods of 200 mL min^{-1} of air.

6.4 Conclusions

Pure untreated copper foam is inactive in ethanol dehydrogenation to acetaldehyde as a result of a smooth surface with an extremely low surface area; a combination which results in virtually no active sites. However, simple oxidation in air at reaction conditions transforms copper foam into a highly selective, moderately active catalyst. The surface becomes covered by CuO needles and remains rugged even after reduction by H_2. During reaction, the oxidized form of copper foam is subject to an activation period, when Cu_2O and CuO are reduced *in-situ* by generated H_2. The activation period is then followed by a deactivation period, during which the rugged surface containing a relatively large number of active sites reconstructs to create a surface with minimum free energy. The sintered copper catalyst can be regenerated by pulses of air.

The ethanol conversion is affected by reaction temperature, catalyst loading and, to a certain degree, by ethanol feed composition. Ethanol conversion increases with increasing temperature but so does the rate of deactivation. At temperatures higher than 300°C ethanol becomes subject to thermal dehydration to ethylene and diethyl ether.

85

Increased copper foam catalyst loading ensures both higher conversion and a lower rate of deactivation. High ethanol conversions can be achieved with water diluted ethanol feeds. With increasing the ratio of ethanol in the feed, the conversion decreases until reaching a steady value, when the surface is saturated with adsorbed ethanol and conversion becomes independent of ethanol concentration in the gas phase.

Despite its superior physical properties (high thermal conductivity, low pressure drop and high mechanical strength) and its low manufacturing costs, copper foam, yielding a low conversion and being subject to deactivation, was deemed inadequate catalyst for ethanol dehydrogenation. Therefore, the following chapter will focus on the evaluation of supported Cu-based catalyst in ethanol dehydrogenation.

Chapter 7: Ethanol dehydrogenation – supported catalysts

In this chapter, various supported copper-based catalysts are characterized and their performance evaluated in ethanol dehydrogenation.

7.1 Introduction

An extensive amount of literature concerning acetaldehyde production via dehydrogenation is available. As stated in Chapter 2: Literature Review, copper has been identified as an excellent catalyst for its ability to dehydrogenate ethanol without splitting the C-C bond, which would lead to undesirable decomposition of acetaldehyde to CH_4 and CO. However, copper suffers from poor stability at high temperatures, where dehydrogenation is thermodynamically favourable. From Chapter 5: Thermodynamics, it can be seen that the conversion only approaches 100% at temperatures higher than 500°C, while copper is reported to deactivate because of sintering at temperatures as low as 190°C (Kanoun et al., 1991a). Furthermore, depending on reaction conditions and the nature of the catalyst, various side-products including ethyl acetate, acetone, C_4-aldehydes, diethyl ether, ethylene, CO, CO_2, and CH_4 have been reported (e.g., Armstrong and Hilditch, 1920; Church and Joshi, 1951; Franckaerts and Froment, 1964; Peloso at al., 1979; Iwasa and Takewaza, 1991; Kenvin and White, 1991; Chung et al., 1993; Raich and Foley, 1998; Fujita et al., 2001; Inui et al., 2004; Colley at al., 2005). The challenge then lies in the identification of an active, selective and stable catalyst and optimization of reaction conditions. It was shown in Chapter 6, that unsupported copper in the form of copper foam did not provide sufficient activity or stability and therefore our attention in this chapter will be shifted to supported catalysts.

While some studies focused on improving only one factor at a time, such as stability (Tu et al., 1994a,b; Tu and Chen 1998, 2001), deliberately maintained conversions below 1% (Kanoun et al., 1993, 1991a, 1991b) or studied dehydrogenation with dilute ethanol feeds (Fujita et al., 2001; Iwasa and Takewaza, 1991), the objective of this thesis was to evaluate the catalysts and the effect of reaction conditions with all three factors (activity, selectivity and stability) in mind and to optimize the reaction outcome under feed conditions similar to what would be encountered in an industrial application.

Six suitable supports were tested. The best candidates were impregnated with copper and the resulting catalysts were characterized. The effect of temperature, pressure, residence time, and water and acetaldehyde content in the ethanol feed were evaluated with regard to catalysts' activities, selectivities and stabilities. The order of reaction, frequency factors, activation energies and deactivation rate constants were also determined for all catalysts by employing empirical models.

7.2 Experimental section

7.2.1 Support preparation

Prior to copper deposition, several commercially available catalyst supports, including γ-Al_2O_3 (Alfa Aesar, #39812, 99.97% purity, 3 micron), SiO_2 (Aldrich, grade 646, 35-45 mesh), TiO_2 (Degussa, P25) and MgO (Aldrich, #24,338-8, 98% purity) were tested for their catalytic activity in order to determine the ideal candidates. The best support would either be completely inert for ethanol dehydrogenation or convert ethanol selectively to acetaldehyde and hydrogen. In addition to these commercial supports, two other materials were considered: γ-Al_2O_3 was doped with K in order to create a less acidic support, and an Al/Mg mixed oxide support was precipitated for similar reasons.

In order to prepare K-γ-Al_2O_3, the acidity of the Al_2O_3 was estimated based on literature data. Aberuagba et al. (2002) calculated the acidity of γ-Al_2O_3 to be 336 μmol g^{-1} and, according to Shen et al. (1994), approximately 500 μmol of K per g of γ-Al_2O_3 are required to neutralize strong acid sites without creating any additional strong basic sites. Therefore, 350-400 μmol K (i.e., 0.028-0.032 g of KOH) per g of support were used. The required amount of KOH (Aldrich, #30,656-8, 99.99% purity) was dissolved in an arbitrary volume of D.I. water (approx. 400 mL) and γ-Al_2O_3 powder was then added. The suspension was stirred for 20 h and then heated to 70°C to evaporate most of the water. The residue was dried overnight at 80°C. This material was then calcined for 6 h at 450°C in a 200 mL min^{-1} stream of air.

According to Di Cosimo et al. (1998), the incorporation of small amounts of Al^{3+} ions into the MgO matrix significantly increases the rate of acetaldehyde formation. Furthermore, the density of basic sites as a function of Al content reaches a minimum at an Al/(Al+Mg) molar ratio of 0.14 and, therefore, the subsequent conversion of

acetaldehyde to C_4 aldehydes, catalyzed by basic sites, should be diminished. For this reason, the mixed oxide support was prepared based on a Al:Mg molar composition of 14:86. The required amounts of $Mg(NO_3)_2.6H_2O$ and $Al(NO_3)_3.9H_2O$ were dissolved in approximately 700 mL of distilled water to achieve a 1-M solution. The solution was fed dropwise into a 2-L 3-neck round-bottom flask filled with 750 mL of 0.5-M solution of Na_2CO_3 (EMD, #SX0395-1, ACS). The contents of the flask were vigorously stirred and the pH continuously monitored with a pH meter. The pH was allowed to drop from an initial value of ~11.8 to 10 and then held constant at 10 by dropwise addition of 6-M NaOH (Bioshop, #SHY 700, ACS). The resulting white precipitate was heated to 65°C and left to age overnight. The suspension was then filtered and the precipitate re-suspended three times in distilled water in order to remove Na^+ and NO_3^- ions. The residue was dried overnight at 80°C, crushed to powder and calcined for 12 h at 500°C in 200 mL min^{-1} air.

Support activity tests were carried out on the powder form of the support (<60 mesh) with the exception of SiO_2, where 35-45 mesh size particles were used. In order to simulate typical catalyst pretreatment, all supports were reduced *in-situ* prior to the activity test for 1 h at the reaction temperature (300°C or 400°C) in 30:150 mL min^{-1} H_2 (Praxair, 4.5 PP):N_2 (Praxair, 4.8 PP).

7.2.2 Catalyst preparation

From the results obtained from support screening (see 7.3.1 Support Screening), SiO_2, K- γ-Al_2O_3 and Mg/Al mixed oxide (MO) were selected as satisfactory supports for copper deposition.

The Cu/SiO_2 catalyst was prepared by depositing 15 wt. % Cu on SiO_2 by incipient wetness impregnation. The accessible pore volume of SiO_2 was experimentally determined to be 0.9 mL g^{-1}. $Cu(NO_3)_2 \cdot 2.5H_2O$ (Aldrich, #31288, 99.99% purity) was dissolved in a proper volume of D.I. water and the resulting solution was added dropwise to dry SiO_2. After each drop, the vial, containing SiO_2, was vigorously shaken. After impregnation, this material was dried overnight at 80°C and calcined for 3 h at 450°C in a 200 mL min^{-1} stream of air (Parker Balston 75-83 Zero Air Generator).

15 wt. % Cu was deposited on both K-doped γ-Al_2O_3 and Mg/Al mixed oxide support by wet impregnation. Again $Cu(NO_3)_2 \cdot 2.5H_2O$ was dissolved in 250 mL of D.I.

water to which the required amount of support was added. While being stirred, the suspension was heated to 70°C and water evaporated to form a thick slurry. The slurry was dried overnight at 80°C, crushed and sieved to obtain 35-45 mesh fraction. This material was calcined for 3 h in 200 mL min^{-1} stream of air at 450°C.

Prior to reaction, all SiO$_2$-, Al$_2$O$_3$- and MO- supported catalysts were reduced *in-situ* in 30:150 mL min^{-1} H$_2$:N$_2$ at the reaction temperature for 1 h.

7.2.3 Catalyst characterization

TGA

Thermogravimetric analysis was conducted utilizing a TA Instruments SDT 2960. The weight change of catalyst sample during oxidation in air was recorded as a function of temperature which was ramped at 10°C min^{-1} from room temperature to 900°C. The results were used to determine the calcination temperature necessary for complete decomposition of Cu(NO$_3$)$_2$ to CuO.

BET surface area, Pore volume and Pore size distribution

BET surface areas were measured by means of N$_2$ adsorption isotherms at 77 K using a Micromeritics Gemini^{TM} V-Series surface analyzer, which also estimated the pore volume and pore size distribution from the adsorption branch of the isotherms. The samples were pretreated in N$_2$ at 300°C for 1 h prior to the measurements in order to remove any moisture adsorbed on the catalyst surface.

Copper content and Copper surface area

Copper contents, copper surface areas and copper dispersions of supported catalysts were determined by H$_2$-N$_2$O titration following the method of Bond and Namijo (1989). 0.2 g of catalyst were placed into a quartz fixed-bed down-flow microreactor (i.d. 4 mm, length 40 cm) and pretreated in air (approx. 470 mL min^{-1}) at 450°C for 3 h to ensure that all copper was oxidized to CuO. The reactor was then cooled to 30°C and temperature programmed reduction (TPR) was carried out. While the temperature was being ramped from 30°C to 300°C at 5°C/min, the catalyst was gradually reduced in a stream of 4.97% H$_2$/N$_2$ stream flowing at 30 mL min^{-1}. The amount of hydrogen consumed was detected by a thermal conductivity detector (TCD) and used to estimate

the wt.% of copper contained in each catalyst (Cu_{tot}). The reactor was then cooled in O_2-free N_2 to 60°C and purged for an additional 30 min. The surface copper atoms were then selectively oxidized to Cu_2O by passing 80 mL min^{-1} of N_2O (Praxair, 5.5) over the catalyst for 1 h. Following the N_2O treatment, the reactor was cooled to 30°C and purged with O_2-free N_2 to remove all traces of N_2O. A second TPR was carried out from 30 to 300°C at a rate 5°C/min with 30 mL min^{-1} of a 4.97% H_2/N_2 stream being passed over the catalyst. After the second TPR, the number of surface atoms (Cu_s) was calculated assuming $O/Cu_s = 0.5$. The dispersion, defined as Cu_s/Cu_{tot}, was computed using the Cu content determined from the first TPR. Assuming an equal presence of (100), (110) and (111) Miller index planes, the surface-atom density was 1.47×10^{19} atoms/m^2 and the copper surface area could then be calculated. Once the copper surface area and copper content in the catalyst were determined, it was possible, knowing the copper density [8920 kg/m^3 (Baram, 1988)] and assuming a spherical shape of copper aggregates, to calculate the average diameter of copper particles on the catalyst surface.

Acid-base properties

The acidity and basicity of the three supports of choice were compared by carrying out temperature programmed desorption (TPD) of NH_3 and CO_2, respectively. In all experiments, 1 g of material was loaded into a dual-volume, fixed-bed, down-flow quartz reactor (upper half i.d. 10 mm, lower half i.d. 4 mm, length 40 cm), and pre-treated in 50 mL min^{-1} He (Praxair, 5.0) at 450°C (SiO_2, K-γ-Al_2O_3) or 500°C (MO) for 90 min. The reactor was then cooled to 25°C and purged with He for 30 min. The He stream was then replaced by 50 mL min^{-1} of either 2000 ppm NH_3/He (Praxair) or 5% CO_2/He (Praxair) After 2 h, the reactor was purged with 50 mL min^{-1} of He for an additional 1 h in order to remove physisorbed adsorbents. The He flow rate was then decreased to 15 mL min^{-1} and the temperature was ramped to 450 or 500°C at a rate of 15°C/min. The desorption of either NH_3 or CO_2 was detected by TCD.

Catalytic activity

A standard down-flow, fixed-bed reactor consisting of a quartz tube (i.d. 10 mm, length 45 cm) with a quartz frit located 19 cm from the inlet of the tube (the furnace's

isothermal zone), was used for all atmospheric pressure experiments. The desired amount of catalyst was mixed with SiC (Kramer Industries, 36 Grit) which served as a flow and temperature distributor. The mixture, which always had a combined weight (w_{cat} + w_{SiC}) of 2.5 g, was then loaded onto the frit. For the higher pressure experiments, a thick-wall quartz reactor (i.d. 6 mm, length 45 cm) was utilized, which permitted limited loading of 0.1 g of catalyst mixed with 1 g of SiC. The reactor was placed into the tubular convection furnace and the thermocouple, controlling the reaction temperature, was inserted into the catalyst bed. An Eldex A-60-S stainless steel HP metering pump was used to deliver a desired water-ethanol (Commercial Alcohols, anhydrous) mixture at a constant flow rate of 0.2 mL min^{-1} to the evaporator where it was gasified and combined with a N$_2$ stream (15 mL min^{-1}) utilized as an internal reference. The combined gaseous feed was then passed over the catalyst bed. The resulting product stream was directed into the online-attached Varian GC 3800 gas chromatograph. A novel gas chromatograph separation method previously developed (Chladek et al., 2007a, see Appendix A) allowed for simultaneous analysis of both gaseous and condensable components once every 32 min. The reaction was studied for temperatures ranging from 250 to 350°C and a pressure range of 0.1-0.5 MPa.

7.3 Results and discussion

7.3.1 Support screening

Prior to the screening a blank run was performed to verify the inertness of the quartz reactor. Catalytic performance of six selected supports was evaluated based on ethanol conversion defined as:

$$X_{EtOH} = \frac{\dot{n}_{EtOH}^0 - \dot{n}_{EtOH}}{\dot{n}_{EtOH}^0} = \frac{\sum\limits_{carbonaceous\ products}^{i} a_i \dot{n}_i}{\sum\limits_{carbonaceous\ products}^{i} a_i \dot{n}_i + \dot{n}_{EtOH}}$$

where $\dot{n}_{EtOH}^0$ is the entering molar flow of ethanol; $\dot{n}_{EtOH}$ is the exiting molar flow of ethanol; a_i is the number of carbon atoms in any product species divided by the number

of carbons contained in an ethanol molecule; and $\dot{n}_i$ is the exiting molar flow of any carbonaceous product.

Main products selectivities are defined as:

$$S_i = \frac{b_i \dot{n}_i}{\underset{carbonaceous\ species}{\sum^i b_i \dot{n}_i}}$$

where b_i is the number of carbon atoms in that particular product and $\dot{n}_i$ is the molar flow of this product.

Ethanol dehydrogenation was studied with sample loading of 0.5 g, an EtOH:H$_2$O molar ratio of 1:1, a liquid feed flow rate of 0.2 mL min^{-1}, at atmospheric pressure and at two different temperature levels: 300 and 400°C. The main products selected for comparison were products of ethanol dehydrogenation [acetaldehyde (AcAd)], dehydration (ethylene, diethyl ether (DEE) and ethane) and secondary condensation reactions (higher C species, such as ethyl acetate (EtAc), crotonaldehyde, butyraldehyde and 1-butanol). Results of the screening study carried out at 300°C are displayed in Table 7.1.

Table 7.1 Catalytic performance results of various supports in ethanol dehydrogenation at 300°C.

	SiO$_2$	Al$_2$O$_3$	K-Al$_2$O$_3$	TiO$_2$	MgO	Mg/Al
X EtOH %	0.4	19.0	0.5	0.3	0.5	0.5
Selectivity to AcAd %	97.2	0.5	97.5	36.4	84.3	87.0
Selectivity to Ethylene %	2.2	8.0	2.0	6.2	2.4	2.6
Selectivity to Ethane %	0.6	0.1	0.6	13.0	0.5	0.4
Selectivity to DEE %	0.0	91.5	0.0	44.3	12.8	8.8
Selectivity to higher C species %	0.0	0.0	0.0	0.0	0.0	1.1

With the exception of Al$_2$O$_3$, which showed activity for ethanol dehydration to diethyl ether, all other supports yielded conversions lower than 0.5% and differed only slightly in product stream composition. In order to narrow down the selection of suitable supports, the dehydrogenation was studied at 400°C with results reported in Table 7.2.

Table 7.2 Catalytic performance results of various supports in ethanol dehydrogenation at 400°C.

	SiO_2	Al_2O_3	$K-Al_2O_3$	TiO_2	MgO	Mg/Al
X EtOH %	1.2	90.3	1.5	41.5	7.4	6.7
Selectivity to AcAd %	42.6	1.1	46.6	25.9	6.3	31.3
Selectivity to Ethylene %	15.1	96.3	20.0	9.6	28.1	15.5
Selectivity to Ethane %	0.4	0.5	0.6	10.7	0.3	0.3
Selectivity to DEE %	41.8	2.0	32.8	18.1	65.3	37.9
Selectivity to other C species %	0.1	0.0	0.0	35.7	0.0	15.0

SiO_2 and K-γ-Al_2O_3 proved to be the most inert of all supports, both materials yielding conversions slightly above 1% with the major product being acetaldehyde followed by diethyl ether. On the other hand, the test of pure Al_2O_3 and TiO_2 resulted in high ethanol conversion to ethylene and higher C_4 species respectively, indicating that these supports were unsuitable for further investigation. The remaining two supports, MgO and mixed Mg/Al oxide, both yielded conversions of about 7%. However, the Mg/Al sample resulted in five times higher selectivity to acetaldehyde than MgO and, therefore, the Mg/Al mixed oxide (MO) was selected, together with SiO_2 and K-γ-Al_2O_3, as potentially appropriate carriers for copper in subsequent ethanol dehydrogenation studies.

7.3.2 Support characterization

BET surface area, Pore volume and Pore size distribution

The BET surface areas together with pore volumes of all three supports are reported in Table 7.3. The total surface area is proportional to pore volume with SiO_2 being the most porous followed by MO and K-γ-Al_2O_3.

Table 7.3 BET surface area and Pore volume of supports.

Support	BET Surface Area (m^2/g)	Pore Volume (ml/g)
SiO$_2$	287	0.9
K-γ-Al$_2$O$_3$	96	0.3
MO	184	0.5

Pore size distributions with regard to pore volume and pore area are depicted in Figs. 7.1 and 7.2, respectively. The supports differ in their pore volume distribution, but all have a large percentage of surface area contained in the pores smaller than 10 nm, especially MO and K-γ-Al$_2$O$_3$. In the case of SiO$_2$, the highest percentage of surface area is for pores in the range 11-33 nm.
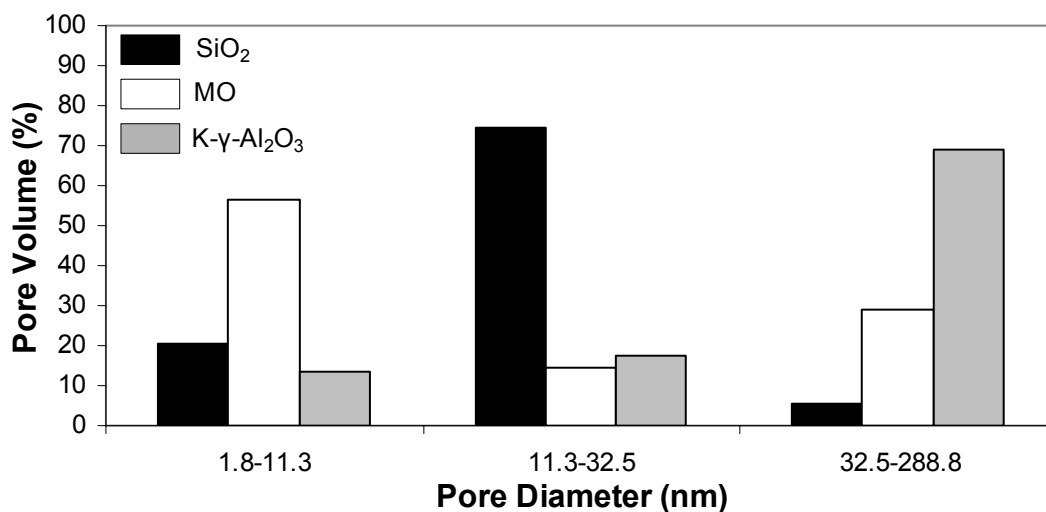
Figure 7.1 Pore volume distribution of various supports calculated from the N$_2$ adsorption branch of BET isotherm.
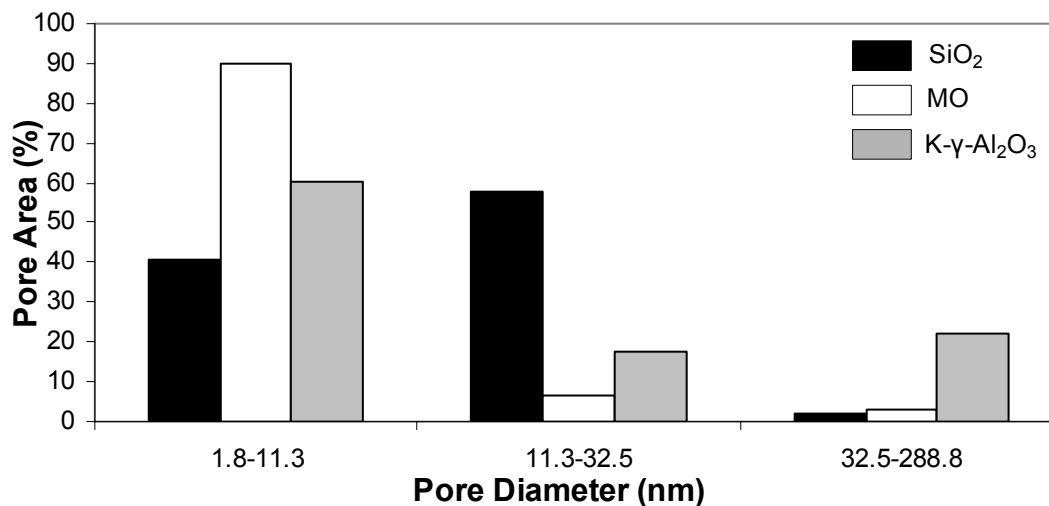
Figure 7.2 Pore surface area distribution various supports calculated from the N_2 adsorption branch of BET isotherm.

Acid-base properties

A qualitative measure of acid and base site strength was obtained for all supports by NH_3 and CO_2 TPD, respectively. The rate of adsorbate evolution as a function of sample temperature is shown in Figs. 7.3 and 7.4. It can be concluded that SiO_2 is an extremely inert support being more than 100 times less acidic than the remaining two supports and more than 30 times less basic. In general all three supports show predominantly basic character with acid sites being 3-10 times less abundant. Regarding the strength of the sites, it can be observed that, with the exception of SiO_2, the supports contain a broad variety of different strength types as shown by the long tailing of the peaks. However, the maximum is obtained at temperatures lower than 200°C, a fact suggesting that most of both acid and basic sites are weak.
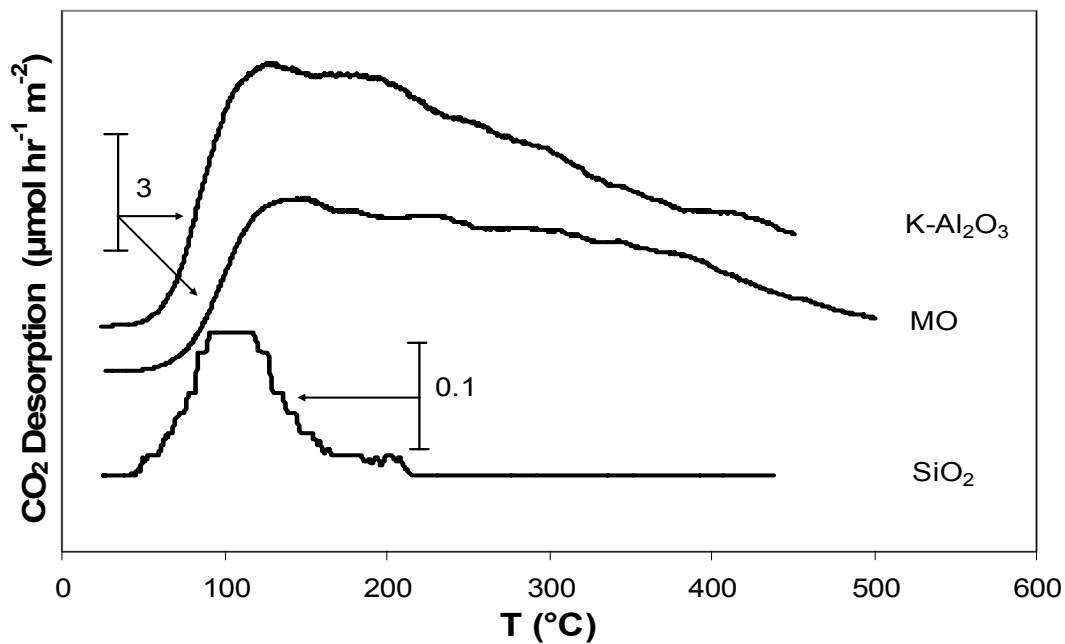
Figure 7.3 Basicity of supports measured by CO_2-TPD.
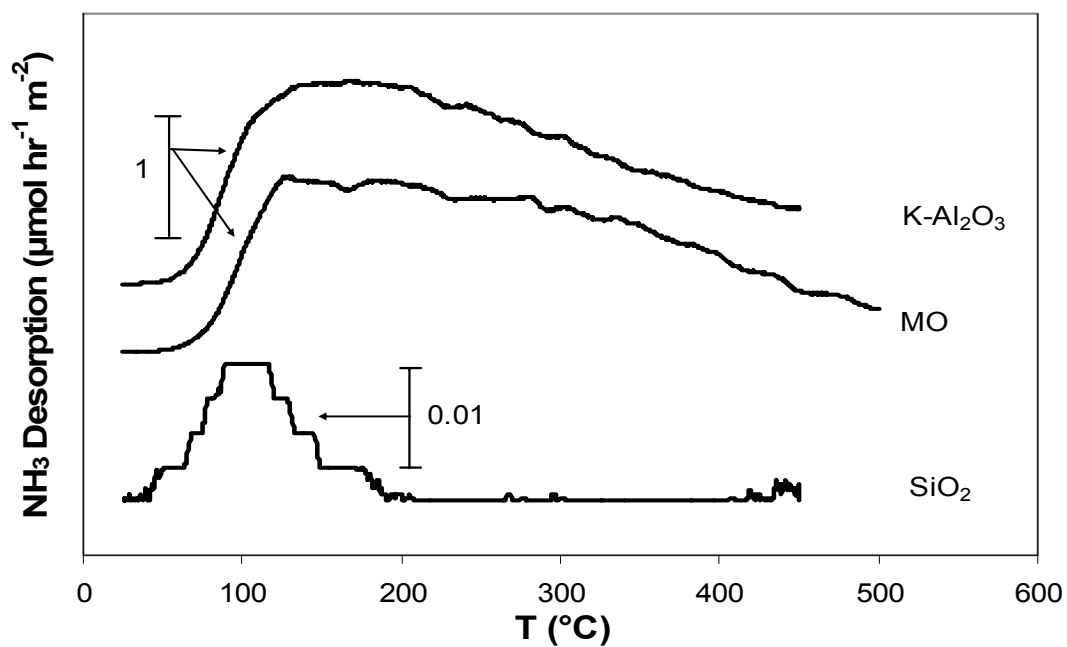
Figure 7.4 Acidity of supports measured by NH_3-TPD.

7.3.3 Catalyst characterization

The three supports of choice were impregnated with copper and resulting materials characterized by various techniques.

TGA

Both SiO$_2$- and K-γ-Al$_2$O$_3$-supported catalysts yielded similar TGA profiles, displayed in Fig. 7.5, with one major peak occurring around 225-250°C and tailing up to approximately 400°C. The peak represents a weight loss of approximately 17% which correlates well with the expected weight loss of 20% for the decomposition of copper nitrate: $Cu(NO_3)_2 \rightarrow CuO + 2NO_2 + 1/2O_2$. The location of peak is in good agreement with literature data for decomposition of copper nitrate: 247-260°C (L'vov and Novichikin, 1995).

The TGA profile for the SiO$_2$-supported catalyst shows a sharper and narrower peak compared to the one supported on K-γ-Al$_2$O$_3$, because of larger pores, as seen in Fig. 7.1, from which evolving nitrogen oxides can easily escape.
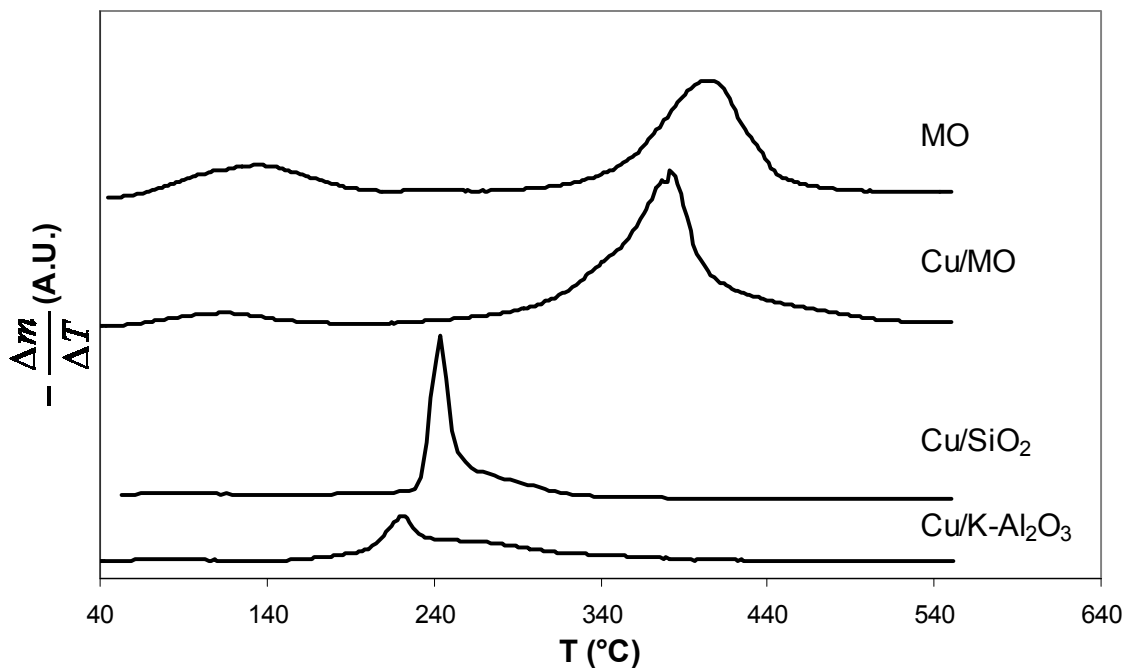
Figure 7.5 TGA profiles of MO support, Cu/MO, Cu/SiO$_2$ and Cu/K-Al$_2$O$_3$ in air.

The MO-supported catalyst yielded a pattern with a small peak occurring at 115°C and a large and broad peak with 2 maxima at 379 and 384°C with a total corresponding weight loss of 40%. This pattern is very similar to the TGA decomposition profile of pure MO (weight loss of 20%), also depicted in Fig. 7.5. Furthermore, Alejandre et al. (1999) reported a weight loss of 50% and similar twin peak shape for

thermal decomposition of a copper-aluminum (Cu/Al atomic ratio 0.5) hydrotalcite sample. It can therefore be concluded that despite the temperature treatment of 500°C, the original MO support is, upon impregnation, transformed back to a hydrotalcite form, i.e., a class of layered material consisting of positively charged brucite $Mg(OH)_2$-like sheets where several Mg^{2+} ions are replaced by trivalent Al^{3+} ions and the excess of positive charge is counterbalanced by anions, such as CO_3^{2-} or NO_3^-, in the interlayer, plus water molecules. As a result of impregnation, Cu^{2+} ions are incorporated in the hydrotalcite structure. During a TGA run, the first peak can be attributed to the removal of weakly bound water, located in the interlayer space of copper hydrotalcite phase (Alejandre et al., 1999). The second major peak can be ascribed to the further removal of water caused by condensation of hydroxyl groups in the brucite-like layer, but also to decomposition of CO_3^{2-} and NO_3^- anions (Alejandre et al., 1999). The total weight loss (40%) is, therefore, a combination of original hydrotalcite support weight loss (20%) and weight loss associated with decomposition of nitrates (20%). The result of calcination is, as in case of the other two supports, conversion of Cu^{2+} ions to CuO.

Based on these results, a temperature of 450°C was chosen as a safe temperature for catalyst calcination.

BET, Copper surface area and Copper content

The copper content, copper dispersion and copper surface areas of supported catalysts and catalysts deactivated during the ethanol dehydrogenation reaction at 350°C as measured by TPR and N_2O titration, together with the total surface areas of the supported copper catalysts measured by BET are presented in Tables 7.4 and 7.5. In all cases, the initial total surface area of the support (see Table 7.3) decreased upon introduction of copper. This drop was less significant for the MO-support which can be explained by the fact that it possesses the smallest percentage of copper deposited. The low copper loading coupled with the second highest total surface area also resulted in the highest copper surface area and copper dispersion and the smallest diameter of copper particles on the surface. The low copper loading was possibly caused by the entrapment of copper particles in pores, which were then rendered inaccessible either because of the

restoration of hydrotalcite material or the pressing required to produce the correct size distribution.

Table 7.4 BET, copper surface area and dispersion of fresh catalysts.

Catalyst	Cu Content	BET Surface Area	Cu Surface Area		Fresh Dispersion	Cu Particle Diameter
	(wt%)	(m^2/g)	(m^2/g$_{cu}$)	(m^2/g$_{cat}$)	(%)	(nm)
Cu/SiO$_2$	12	238	136	17	21	5
Cu/K-Al$_2$O$_3$	11	68	132	14	20	5
Cu/MO	9	163	168	15	26	4

If ethanol dehydrogenation was conducted at 350°C or higher, all catalysts lost activity (as shown in Temperature section). The loss of activity was caused by sintering as can be seen from the comparison of copper surface area values between fresh and spent catalyst samples listed in Tables 7.4 and 7.5.

Table 7.5 Copper surface area and dispersion of spent catalysts.

Catalyst	Cu Surface Area		Sintered (350°C) Dispersion	Cu Particle Diameter
	(m^2/g$_{cu}$)	(m^2/g$_{cat}$)	(%)	(nm)
Cu/SiO$_2$	109	13	17	6
Cu/K-Al$_2$O$_3$	108	12	17	6
Cu/MO	88	7	14	8

7.3.4 Ethanol dehydrogenation

Prior to the dehydrogenation experiments, a blank run was performed to verify the inertness of the quartz reactor and SiC packing. In all of the experiments the carbon balance added up to 100±2%. The catalysts performances were evaluated based on ethanol conversion, acetaldehyde and major by-product selectivities (all defined in the support screening section), hydrogen yield defined as: $Y_{H_2} = \dfrac{\dot{n}_{H_2}}{X\dot{n}^0_{EtOH}}$ and hydrogen productivity defined as: $P_{H_2} = \dfrac{\dot{n}_{H_2}}{w_{Cat}}$ where $\dot{n}_{H_2}$ is the exiting hydrogen molar flow and w_{Cat} is the weight of catalyst. Furthermore, the turnover frequency (TOF), defined as $TOF = \dfrac{\dot{n}_{AcAd}}{n_{Cu_S}}$, where n_{Cu_S} is the number of moles of exposed copper atoms determined

100

from copper surface area measurements, was used for comparison of catalytic activities. In cases of a linear loss of activity, deactivation was evaluated on the basis of loss of ethanol conversion (%) per h-on-stream. In the majority of the cases, with the exceptions stated, the catalysts showed no or negligible signs of deactivation over the specified period of time and evaluation parameters are thus taken as averages over the duration of experiments with standard deviation being in the range of 0.5-1.5%.

Temperature

Ethanol dehydrogenation was studied at four temperatures (250, 275, 300 and 350°C), at atmospheric pressure, with 0.522 g of catalyst, and with a 1:1 EtOH:H_2O molar liquid feed delivered at a constant liquid flow rate of 0.2 mL min^{-1} together with 15 mL min^{-1} of N_2 tracer (GHSV (STP) = 16 436 mL h^{-1} g$_{cat}^{-1}$). All experiments were carried out for a minimum of 20 h. The results for the first three temperatures at which all three catalysts showed negligible signs of deactivation are listed in Table 7.6.

Table 7.6 Effect of temperature on ethanol dehydrogenation.

Catalyst	T (°C)	X EtOH (%)	S AcAD (%)	S EtAc (%)	P_{H2} (ml min^{-1} g$_{cat}^{-1}$)	TOF (s^{-1})	Deactivation (%X hr^{-1})
	250	45	92	6	50	0.12	-0.2
Cu/SiO$_2$	275	64	91	7	78	0.17	-0.1
	300	77	91	7	94	0.20	-0.2
	250	19	97	2	20	0.04	-0.1
Cu/K-γ-Al$_2$O$_3$	275	33	95	2	39	0.08	-0.1
	300	56	93	3	71	0.13	-0.5
	250	24	96	4	29	0.04	0.1
Cu/MO	275	42	94	6	53	0.07	-0.3
	300	59	92	7	77	0.10	-0.5

The Cu/SiO$_2$ catalyst yielded the highest ethanol conversion, hydrogen productivity and TOF. In fact, the conversion of this catalyst was higher than the thermodynamic equilibrium values for ethanol dehydrogenation (38% at 250°C, 52% at 275°C, 64% at 300°C). The higher-than-equilibrium-conversion can be explained by secondary reactions which consumed acetaldehyde, thus shifting the equilibrium (see Fig. 5.3). The acetaldehyde involvement in subsequent reactions is observable for all three

catalysts: as ethanol conversion increases, the acetaldehyde selectivity decreases. In Fig. 7.6, a scheme of a reaction pathway describing potential subsequent reactions as proposed by Inui et al. (2004) is depicted. The species detected in this work are framed by black rectangles. Out of these, the most dominant by-product on all catalysts is ethyl acetate, followed by butyraldehyde and crotonaldehyde. Aside from subsequent reactions, ethanol can also be consumed in parallel dehydration reactions leading to ethylene, ethane and diethylether. The same amount of H_2 is produced when ethanol is converted to acetaldehyde or to ethyl acetate, as is evident from Fig. 7.6. The increase in hydrogen yield observed at elevated temperatures must be therefore attributed to minor secondary reactions. It is obvious that combined acetaldehyde and ethyl acetate selectivities account in all cases for 97% of the product stream. It can therefore be concluded that differences in support properties play a negligible role in product selectivity.
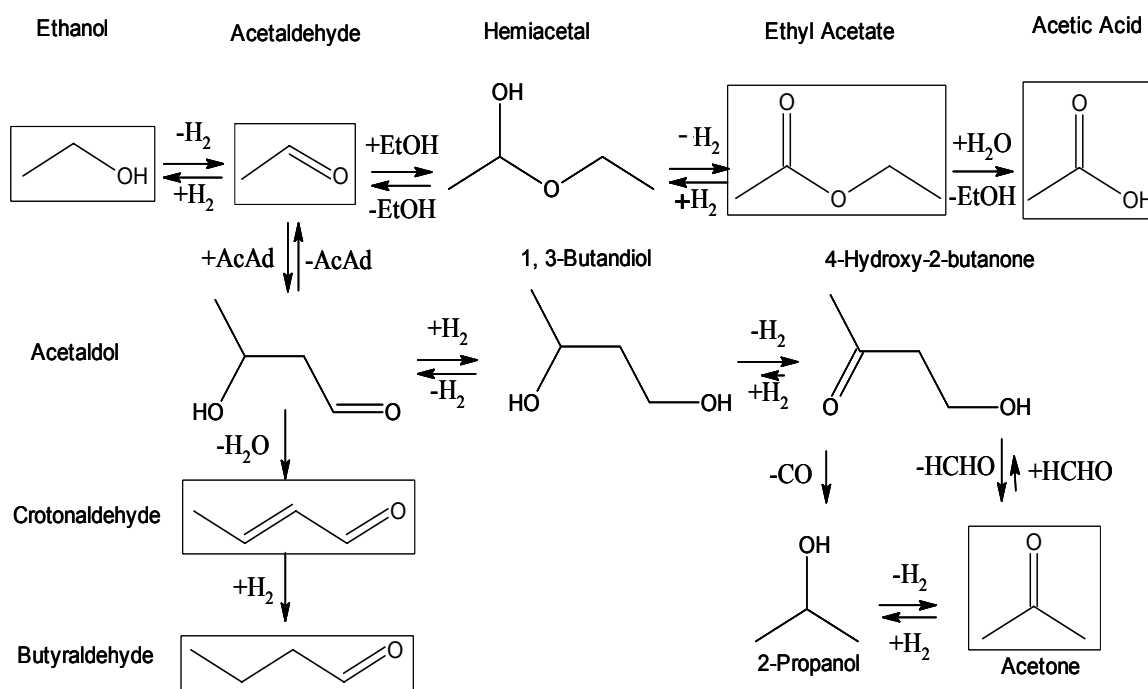
Figure 7.6 Network of possible subsequent reactions. Products detected in this study are framed black. Modified from Inui et al. (2004).

However, support type certainly affects the conversion of the reaction. It can be concluded from TOF values that the SiO_2-supported catalyst is a superior

dehydrogenation catalyst than the other two supported catalysts at all three temperatures. Its superiority can be explained by

- its higher total surface area, which may act as a reservoir for adsorbed ethanol, supplying it instantly to vacant active copper sites;

- its apparent inertness (see Acid Base properties) allowing for easier desorption of products; and

- a higher volumetric residence time. Even though the weight of catalyst is the same in all experiments, the volumes of the supports are different. The density of Cu/SiO_2 (441 g L^{-1}) is only a half of those of Cu/MO (854 g L^{-1}) and Cu/ K-γ-Al_2O_3 (840 g L^{-1}); a physical property resulting in the catalyst bed consisting of Cu/SiO_2 being two times longer than the beds of other two supports.

Increasing the reaction temperature to 350°C resulted in rapid loss of catalytic activity of all three catalysts as depicted in Fig. 7.7.
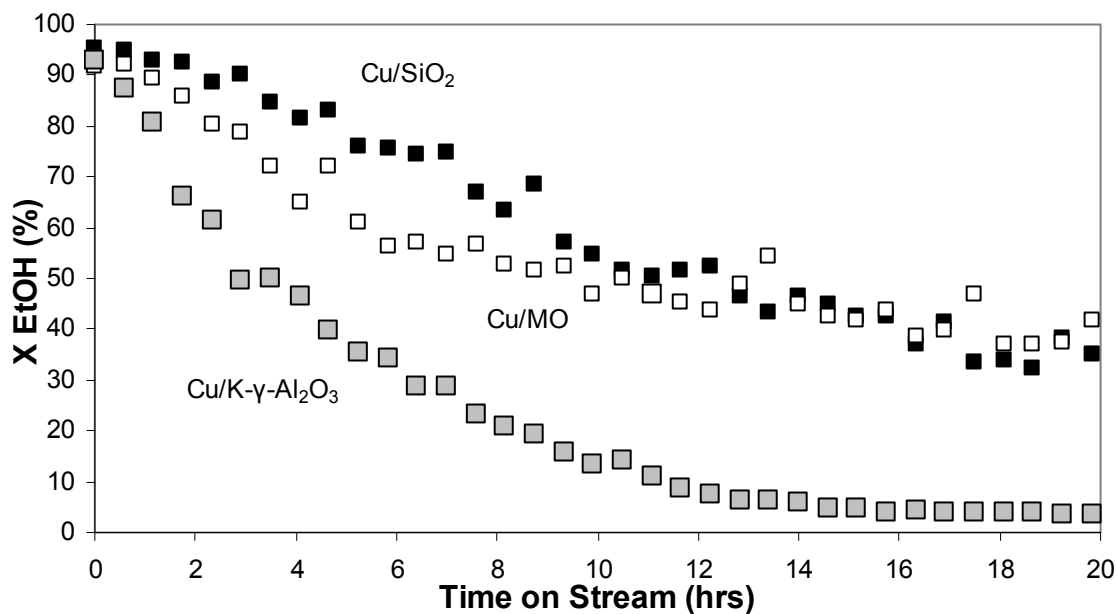
Figure 7.7 Ethanol conversion as a function of time on stream at 350°C, 0.1 MPa and EtOH:H_2O 1:1.

Since

- the reaction temperature is close to the Tamman temperature, the point above which copper particles become mobile on the surface (for Cu = 405°C),

- there is a decrease in copper surface area as seen from Tables 7.4 and 7.5,

- and since no coke formation was detected on any of these catalysts,

it is very likely that the main cause of deactivation is sintering, which usually follows concentration independent second-order kinetics (Fogler, 1999).

Thus, the deactivation law is modeled as $\dfrac{(1-a)}{a} = k_d t$ where a is a normalized activity, i.e., the reaction rate at time t divided by reaction rate at $t=0$, and k_d is a deactivation rate constant. In Fig. 7.8, the linear model is fitted to the data. The deactivation rate constants obtained from the slopes of the curves: k_d (Cu/SiO$_2$) =0.05 h^{-1}, k_d (Cu/ K-γ-Al$_2$O$_3$) = 0.27 h^{-1}, and k_d (Cu/MO) = 0.09 h^{-1} are in a good agreement with published values (Tu and Chen, 2001) and demonstrate that SiO$_2$ provides better stability for dispersed copper than MO, which in turn is more stable than the K-γ-Al$_2$O$_3$-supported catalyst. Stability can be related to the surface area of the support: with higher surface area, the mobilized particles have a lesser chance of encountering another copper cluster, thus decreasing the rate of aggregation. Also the rapid loss of activity observed on the K-γ-Al$_2$O$_3$ could be related to an adverse effect of mobile K, which can block copper sites (Juan-Juan et al., 2006; Snoeck and Froment, 2002).
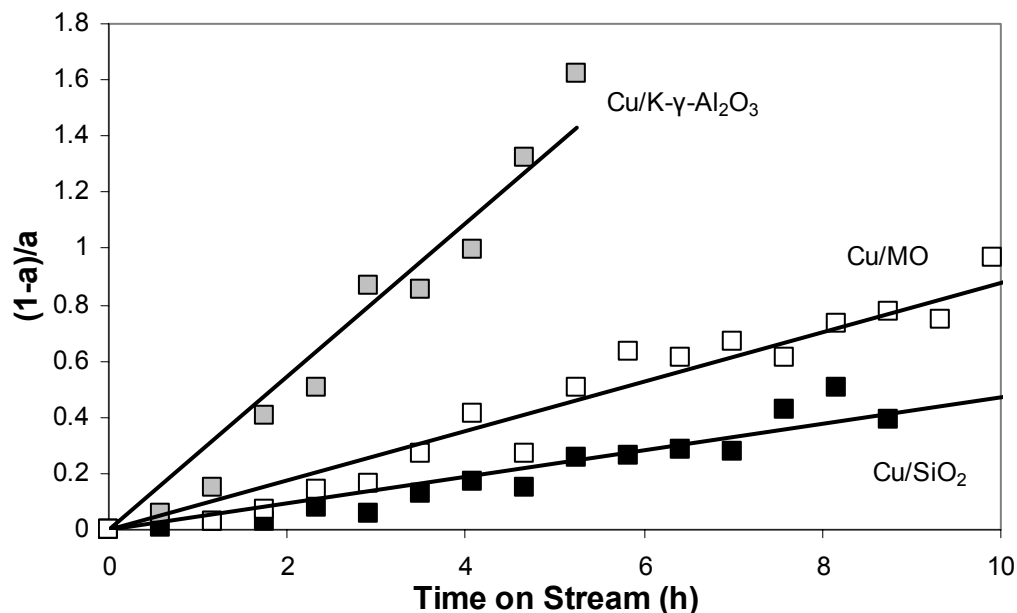
Figure 7.8 Determination of deactivation rate constants at 350°C, 0.1 MPa and EtOH:H$_2$O = 1:1.

Residence time

The effect of residence time was studied by using three different catalyst loadings: 0.1, 0.522 and 1 g at a constant temperature (275°C), pressure (0.1 MPa) and liquid feed flow rate (0.2 mL min^{-1}) of 1:1 EtOH:H$_2$O molar ratio mixed upon evaporation with 15 mL min^{-1} of N$_2$. Under these conditions, catalyst loadings correspond to GHSVs (STP) of 85 796, 16 436 and 8 580 mL h^{-1} g$_{cat}^{-1}$ respectively. From the results listed in Table 7.7, the general observations common to all catalysts are: as the catalyst loading increases, the ethanol conversion increases asymptotically approaching equilibrium. However this activity increase is offset by a decline in acetaldehyde selectivity. This decrease occurs because acetaldehyde again participated in subsequent reactions, mainly in the transformation to ethyl acetate. SiO$_2$, once more, proved to be the best support, followed by MO and K-γ-Al$_2$O$_3$.

Table 7.7 Effect of residence time, T = 275°C, P = 0.1 MPa, EtOH:H_2O = 1:1.

Catalyst	GHSV (STP) (ml h^{-1} g$_{cat}^{-1}$)	X EtOH* (%)	S AcAD (%)	S EtAc (%)	Y H_2	Deactivation (%X hr^{-1})
	85796	38	97	2	1.0	-0.1
15%Cu SiO$_2$	16436	64	91	7	1.1	-0.1
	8580	70	88	10	1.1	-0.2
	85796	16	97	3	0.8	-0.1
15%Cu K-γ-Al$_2$O$_3$	16436	33	95	2	1.0	-0.1
	8580	44	86	13	1.0	-0.2
	85796	28	97	3	1.0	-0.1
15%Cu MO	16436	42	94	6	1.1	-0.3
	8580	55	90	8	1.1	0.2

*X EtOH Equilibrium at 275°C =52%

Feed composition

The objective of this work is to study ethanol dehydrogenation as a part of a separation cycle, where the ethanol feed is expected to be recycled from the acetaldehyde hydrogenation step and, therefore, may contain unconverted acetaldehyde. Furthermore, the initial ethanol feedstock delivered into the dehydrogenation step can come from various sources and will likely contain some amount of water. Therefore, it is important to clarify the effect of acetaldehyde and water on the outcome of ethanol dehydrogenation.

H_2O co-feed

The liquid feed composition was varied using six different molar EtOH:H_2O ratios: 1:10, 1:5, 1:1, 5:1, 10:1 and pure ethanol. The temperature (275°C), pressure (0.1 MPa), catalyst weight (0.522 g) and liquid feed flow rate (0.2 mL min^{-1}) were kept constant over the duration of the experiments (20 h). The results are summarized in Table 7.8. Maintaining a constant liquid feed flow rate while varying the ethanol content leads to an interesting effect: with decreasing ethanol content the overall residence time decreases, because of a higher number of moles being fed into the system, but the residence time for ethanol molecules increases as illustrated in Fig. 7.9.
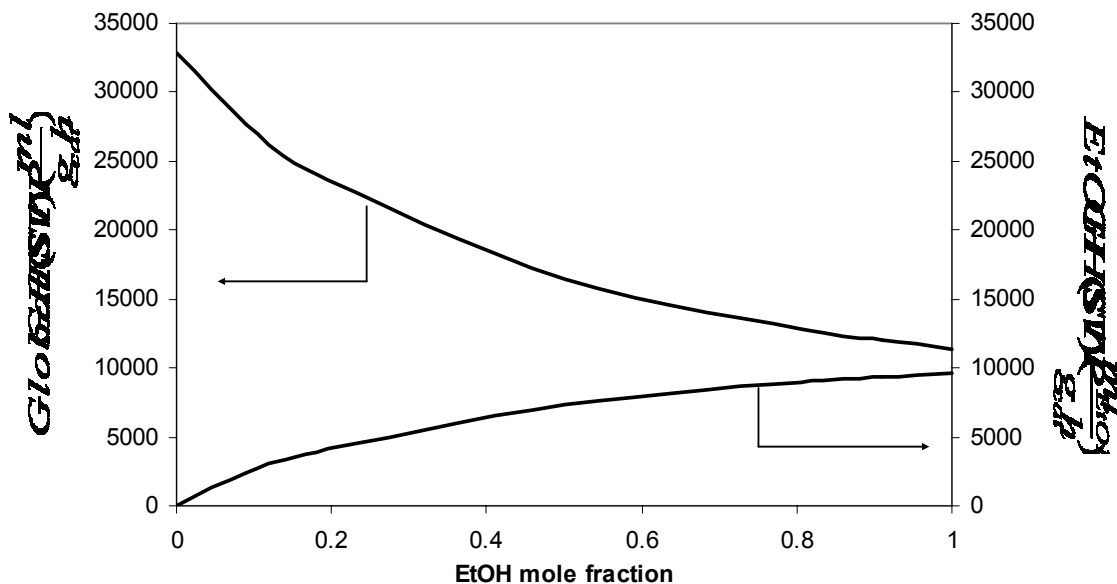
Figure 7.9 Effect of feed composition on global and ethanol GHSV.

These two opposing effects may be responsible for ethanol conversion being virtually independent of liquid feed composition. Another explanation may lie in the diluent effect of water, which lowers the partial pressure of ethanol. Lower pressures should, according to Le Chatelier's principle, favour the dehydrogenation as 2 moles of products are produced per mole of ethanol. However, the higher water content has a detrimental effect on TOF values as shown in Fig. 7.10. The addition of ethanol increases the TOF until presumably the surface is covered almost exclusively by ethanol and the effectiveness of each site is maximized. As expected, the increase in ethanol flow rate also results in increased hydrogen productivity, because even though the conversion is unaffected by the water content in the feed, the absolute number of ethanol moles converted increases. The large number of ethanol molecules on the surface then leads to a decrease in acetaldehyde selectivity as acetaldehyde has a greater chance to be converted into products of subsequent reactions.

107

Table 7.8 Effect of water in the feed on ethanol dehydrogenation, T = 275°C, P = 0.1 MPa.

Catalyst	EtOH/H$_2$O ratio (molar)	X EtOH (%)	S AcAD (%)	S EtAc/AA (%)	Y H$_2$	P$_{H2}$ (ml min^{-1} g$_{cat}^{-1}$)	TOF (s^{-1})	Deactivation (%X hr^{-1})
Cu/SiO$_2$	∞	64	85	13.4/0	1.1	113	0.20	-0.6
	10	60	89	7.0/0.0	1.1	91	0.19	-0.2
	5	62	91	6.0/0.0	1.1	93	0.20	-0.2
	1	64	91	6.7/0.0	1.1	78	0.17	-0.1
	0.2	54	94	0.3/5.6	0.9	31	0.07	-0.5
	0.1	66	95	0.0/5.1	1.0	25	0.06	-0.4
Cu/K-γ-Al$_2$O$_3$	∞	39	97	1.7/0.0	1.1	71	0.12	-0.9
	10	39	93	2.6/0.0	1.1	58	0.11	-0.1
	5	39	94	2.6/0.0	1.1	57	0.11	-0.2
	1	33	95	2.4/0.0	1.0	39	0.08	-0.1
	0.2	35	94	0.2/5.1	1.0	21	0.04	-0.1
	0.1	39	96	0.0/3.9	0.9	14	0.03	-0.4
Cu/MO	∞	51	89	7.4/0.0	1.1	93	0.10	-0.4
	10	45	98	1.2/0.0	1.1	71	0.10	0.1
	5	47	94	4.5/0.0	1.1	68	0.10	-0.2
	1	42	94	5.5/0.0	1.1	53	0.07	-0.3
	0.2	45	93	0.0/6.7	1.1	30	0.04	-0.2
	0.1	49	93	0.0/6.7	1.1	21	0.03	-0.2

Small additions of water helped to improve the stability of all three catalysts and, in the case of MO- and SiO$_2$-supported catalysts, also improved the selectivity to acetaldehyde. The stability improvements are ascribed in the literature (Herman et al., 1979) to stabilization of a balance between metallic copper and CuO through the addition of extra oxygen by water to the system. Both phases are presumably required for ethanol dehydrogenation, because of the stabilization of reactive oxygenate intermediates on the surface (Herman et al., 1979). Excess water, at EtOH:H$_2$O molar ratios lower than 1, had detrimental effect on catalyst stability and also caused a transition in selectivity of major by-products from ethyl acetate to acetic acid. This switch is in good agreement with the reaction pathway shown in Fig. 7.6 where ethyl acetate reacts with water to form acetic acid.
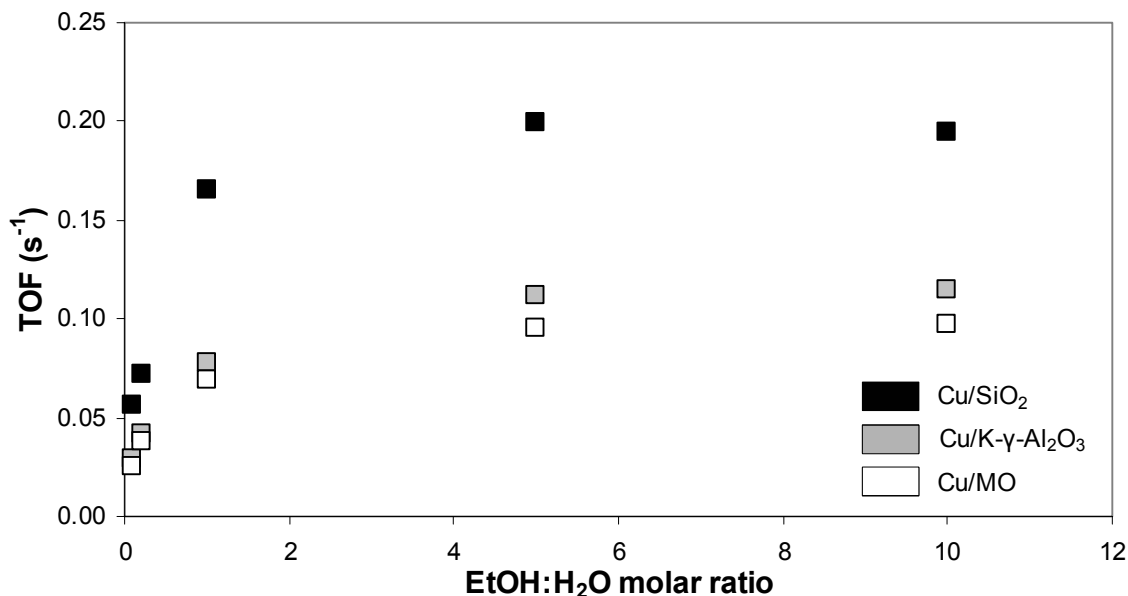
Figure 7.10 Effect of water in the feed on TOF at 275°C and 0.1 MPa.

It can be concluded that once again SiO_2 proved to be a superior support, providing the highest hydrogen productivity and TOFs in ethanol-rich environments. Overall, the data indicate, in agreement with literature (Armstrong and Hilditch, 1920), that the presence of water, in small quantities, improves the reaction selectivity to acetaldehyde, but can damage catalyst stability if used in excess.

Acetaldehyde co-feed

At this stage of the study, a 275°C test temperature, where negligible deactivation was expected, and a catalyst weight of 0.522 g were used to study the effect of acetaldehyde content on the ethanol dehydrogenation reaction at 0.1 MPa. Since in the previous section the beneficial effect of small amounts of water on catalyst stability had been established, the liquid feed consisted of a ternary mixture of $EtOH:H_2O:AcAd$ in ratios: 1:1:1, 1:1:0.5 and 1:1:0.1. In order to avoid the variation in residence time, which was observed with the addition of water to ethanol, the liquid flow rate was adjusted over the range of 0.2-0.23 mL min^{-1} to maintain a constant GHSV of 16 436 mL h^{-1} g$_{cat}^{-1}$. Furthermore, in order to properly reflect the effect of acetaldehyde on product distribution, in was necessary to modify the equation for calculation of AcAd selectivity to:

109

$$S_i = \frac{b_i \dot{n}_i - 2\dot{n}^0_{AcAd}}{\displaystyle\sum_{\substack{i \\ carbonaceous\ species}} b_i \dot{n}_i - 2\dot{n}^0_{AcAd}}$$

where $\dot{n}^0_{AcAd}$ is the inlet flow of acetaldehyde.

The results of acetaldehyde co-feed are presented in Table 7.9. It is apparent that the presence of acetaldehyde in the feed has a negative impact on both ethanol conversion and acetaldehyde selectivity. This is to be expected, as acetaldehyde is one of the products from ethanol dehydrogenation and therefore its presence will affect the reaction equilibrium. From a kinetic standpoint, acetaldehyde molecules compete for active sites with ethanol on the catalyst surface, thus lowering the TOF as can be seen from Fig. 7.11. Furthermore, acetaldehyde is a precursor of secondary reactions, and especially at the highest ratio studied (1:1:1 molar), it promotes formation of ethyl acetate and, to a lesser degree, of butyr- and croton-aldehydes, which are not shown in the table.

Table 7.9 Effect of acetaldehyde in the feed on ethanol dehydrogenation, T = 275°C, P = 0.1 MPa.

Catalyst	EtOH/H$_2$O/AcAd 1 : 1 : X (molar)	X EtOH (%)	S AcAD (%)	S EtAc (%)	Y H$_2$	P$_{H2}$ (ml min^{-1} g$_{cat}^{-1}$)	TOF (s^{-1})
Cu/SiO$_2$	0	64	91	7	1.1	78	0.17
	0.1	57	97	3	1.2	77	0.14
	0.5	50	92	7	1.2	59	0.10
	1	45	81	18	1.0	40	0.04
Cu/K-γ-Al$_2$O$_3$	0	33	95	2	1.0	39	0.08
	0.1	31	98	1	1.1	40	0.07
	0.5	19	93	2	1.2	23	0.04
	1	9	78	9	1.7	13	0.01
Cu/MO	0	42	94	6	1.1	53	0.07
	0.1	42	95	5	1.2	59	0.06
	0.5	30	87	10	1.3	40	0.04
	1	22	76	19	1.5	28	0.02

However, it can also be seen, that small amounts of acetaldehyde do not have critical effect and only negligibly lower the amount of hydrogen produced.
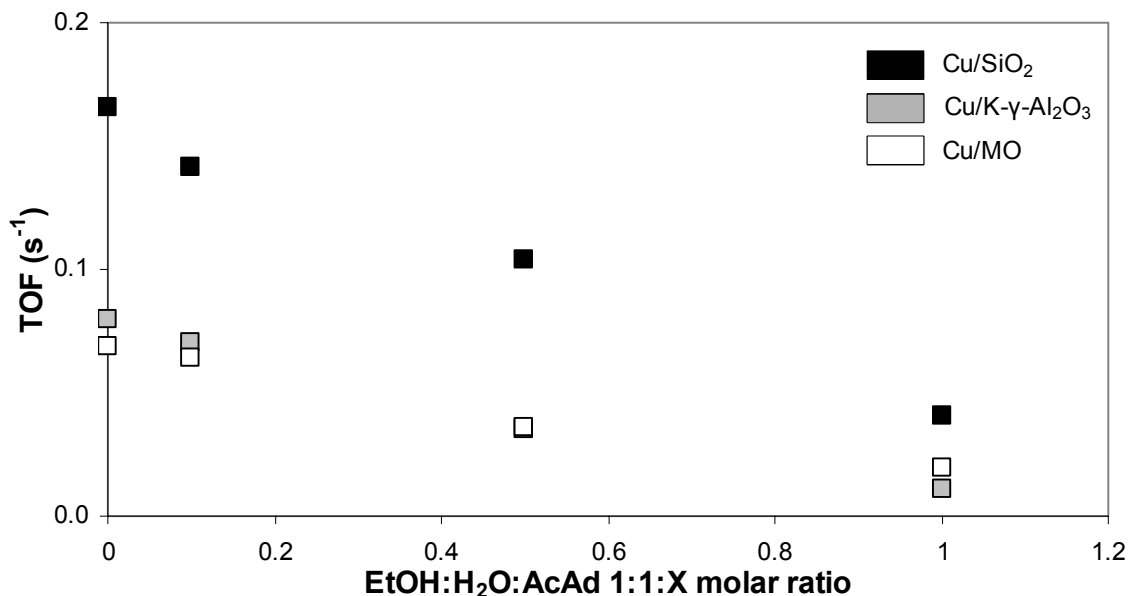
Figure 7.11 Effect of acetaldehyde in the feed on TOF at 275°C and 0.1 MPa.

.

Therefore, it can be concluded that ethanol feedstock coming from the other part of the cycle – acetaldehyde hydrogenation - will have to be purified to remove most of the unconverted acetaldehyde. However, the purification does not have to be absolute, because small amount of acetaldehyde will not critically hinder the dehydrogenation.

Pressure

Significant energy savings can be achieved by pressurizing the ethanol feedstock and carrying out the dehydrogenation under elevated pressure. Comparison of the energy required for pressurization of gaseous atmospheric pressure hydrogen and the hydrogen leaving a dehydrogenation reactor at pressure is depicted in Fig. 7.12. The calculations were carried out in Aspen Plus process simulation software using an isoentropic compressor model schematically depicted in Fig. 7.13.
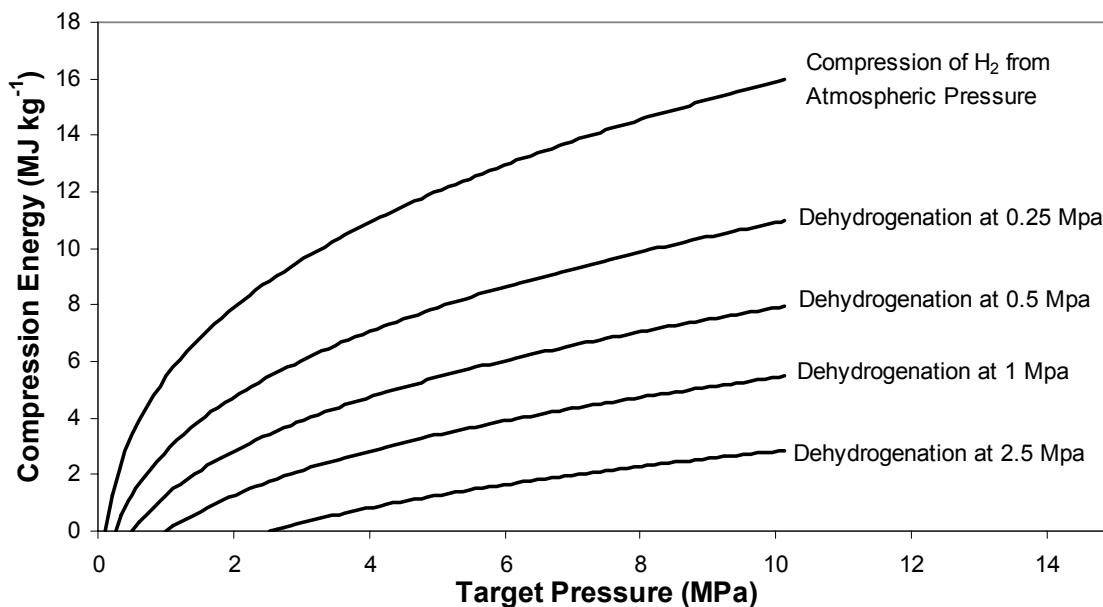
Figure 7.12 Comparison of energy requirements for compression of atmospheric hydrogen and pressurized hydrogen leaving the dehydrogenation vessel.

It is apparent that H_2 compression is initially very energy intensive, but levels off at higher pressures. Overall, significant energy savings can be obtained even at low operating pressures; for example, carrying the dehydrogenation at 0.5 MPa would cut in half the energy for compressing atmospheric H_2 to 10 MPa.
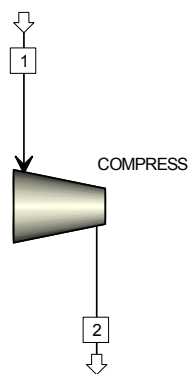
Figure 7.13 Schematic of an isoentropic compressor model.

As mentioned in the Catalyst Characterization section, the pressure experiments were studied with a lower catalyst loading, 0.1 g, in order to maintain the catalyst bed in the isothermal zone of the furnace. Liquid feed consisting of 1:1 EtOH:H_2O was delivered at a constant flow rate of 0.2 mL min^{-1} and mixed with 15 mL min^{-1} of N_2 tracer. The reaction was studied at 275°C, while system pressure was gradually increased from atmospheric pressure to 0.5 MPa. As can be seen from Fig. 7.14, with increasing pressure the activity of K-γ-Al_2O_3 and MO-supported catalyst remained virtually unchanged, while the activity of SiO_2-supported catalyst dropped slightly. After being returned to atmospheric pressure, the SiO_2-supported catalyst did not regain its initial activity, therefore, it can be assumed that the SiO_2-supported catalyst slowly deactivates at higher pressures. However, despite this deactivation, Cu/SiO_2 remained the most active catalyst. The negligible effect on TOF, seen in Fig. 7.14, is in direct conflict with thermodynamic expectations. It can therefore be assumed that dehydrogenation is limited by kinetics rather than by thermodynamics. The catalyst surface quickly becomes saturated with reactant and dehydrogenation itself becomes independent of the pressure in the system.
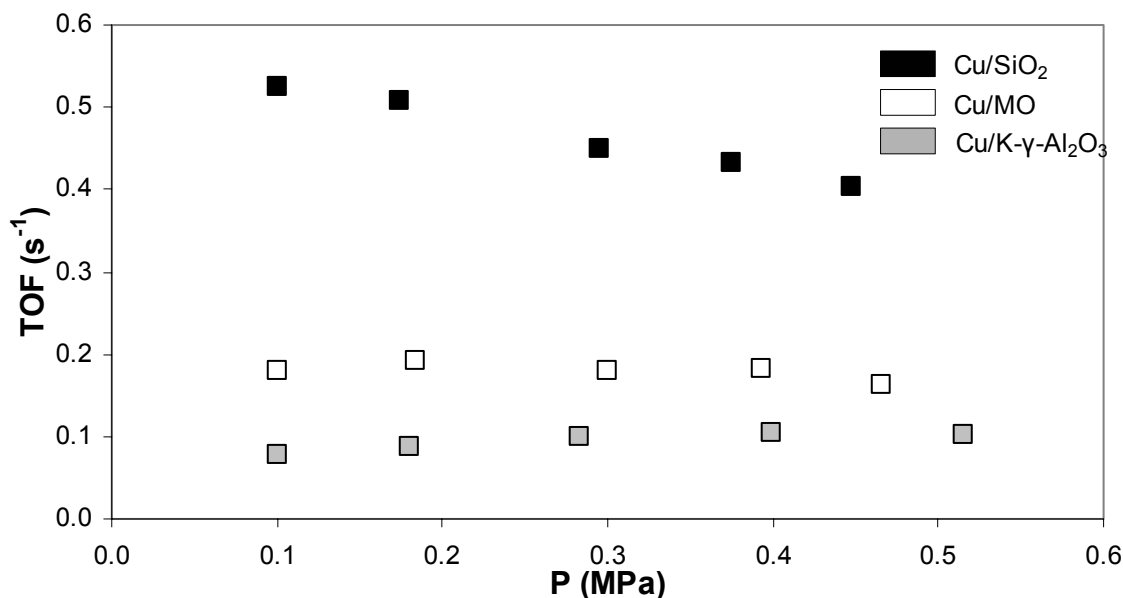
Figure 7.14 Effect of pressure on catalyst activity at 275°C and, EtOH:H_2O = 1:1.

.

Unlike activity, acetaldehyde selectivity, as seen in Fig. 7.15, decreases for all three catalysts as the pressure increases. This change is strongly correlated with an increase in ethyl acetate production. Ethyl acetate formation, producing 2 moles of products per 2 moles of reactants is expected to be independent of pressure, unlike ethanol dehydrogenation, in which one ethanol molecule decomposes into two product molecules. Therefore, it follows that ethyl acetate formation is favoured over ethanol dehydrogenation at higher pressures. It can be expected that further increase in pressure will result in more ethyl acetate, which though not affecting the amount of hydrogen produced, will reduce the acetaldehyde content of the exit stream. Nevertheless, as shown in Fig. 7.12, the most significant savings are achieved at low pressures and further increasing of the reaction pressure is not necessary for the viability of the cycle.
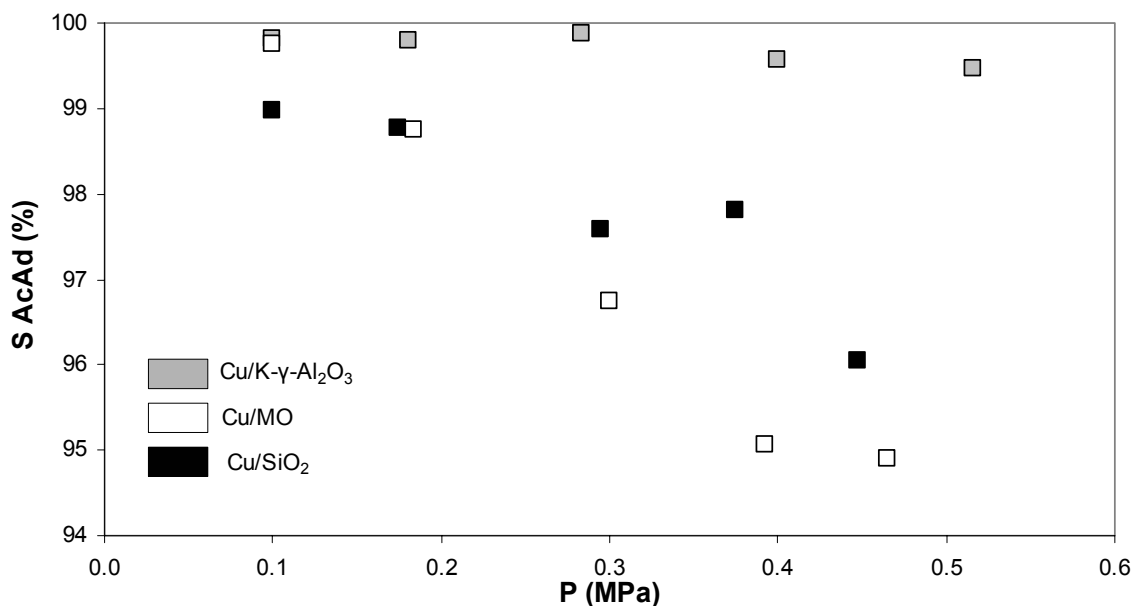
Figure 7.15 Effect of pressure on AcAd selectivity at 275°C and EtOH:H$_2$O = 1:1.

To conclude this section, hydrogen pressurized up to 0.5 MPa can be produced by ethanol dehydrogenation at the cost of a slight decrease in selectivity from acetaldehyde to ethyl acetate.

Dehydrogenation kinetics

Ethanol dehydrogenation kinetics were studied by observing the effect of residence time, which was varied at three levels by changing the loading of the catalyst

114

(0.1, 0.25 and 0.5 g), and the effect of temperature (five levels: from 200 to 300°C at 25°C increments) on the ethanol conversion. By combining data from temperature and residence time experiments, it was possible to calculate and compare frequency factors and activation energies of ethanol dehydrogenation for all three catalysts and determine the order of the reaction. Since the reaction conversion was higher than 10%, an integral tubular reactor model was used:

$$\frac{W}{\dot{V}} = \int_{Ca_0}^{Ca} \frac{dCa}{-r}$$

where, $\dot{V}$ is a total inlet gas flow rate and $-r$ is a rate of disappearance of ethanol per unit mass of catalyst. Assuming a first order reaction:

$$-r = kCa$$

where k is the reaction rate constant, with isothermal and isobaric conditions in the catalyst bed, the following substitution is made:

$$Ca = Ca_0 \left(\frac{1-X}{1+\varepsilon X}\right)$$

where ε takes into account the expansion of the gas mixture due to an increase in the number of moles (Fogler, 1999). The final equation can be obtained by integration:

$$-\ln\left(\frac{1-X}{1+\varepsilon X}\right) = k\frac{W}{\dot{V}}.$$

The experimental data are plotted in Fig. 7.16.
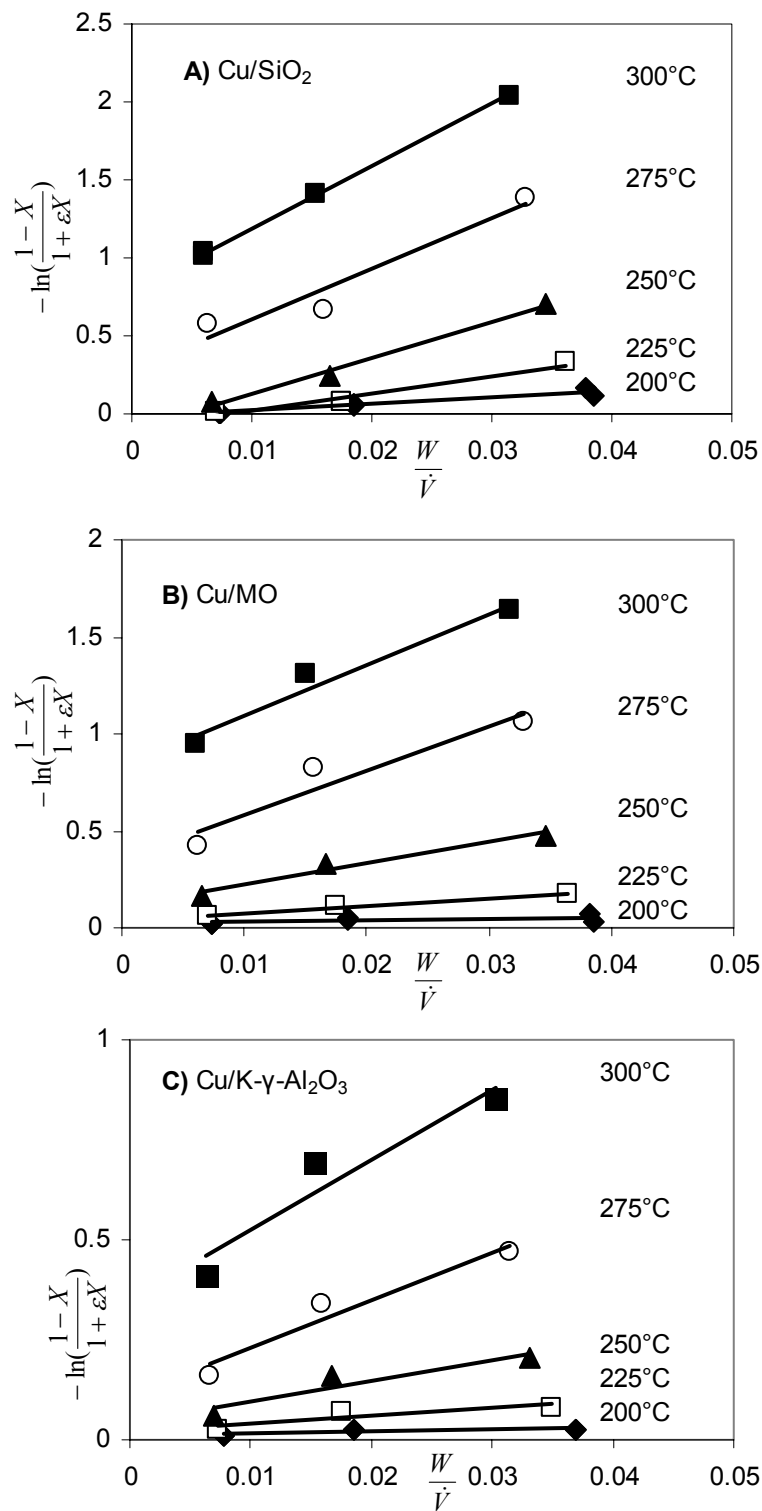
Figure 7.16 Test for the first order kinetics of a) Cu/SiO_2, b) Cu/ K-γ-Al_2O_3 and c) Cu/MO at 0.1 MPa and EtOH:H_2O = 1:1.

The linear relationship observed at lower temperatures confirms the first order reaction assumption in the temperature range of 200-250°C. As the conversion increases with increasing temperature, so does increase the extent of secondary reactions and the model loses its fit. The reaction rate constants were calculated from the slopes of the best lines of fit and the values from the temperature range 200-275°C were used to obtain activation energies and frequency factors according to the Arrhenius equation:

$$k_T = A \exp^{\frac{-E_a}{RT}}$$

The equation was linearized and from the plot of ln(k) against $\frac{1}{RT}$, depicted in Fig. 7.17, activation energies and frequency factors were obtained as slopes and intercepts respectively. Their values are listed together with reaction rate constants in Table 7.10.
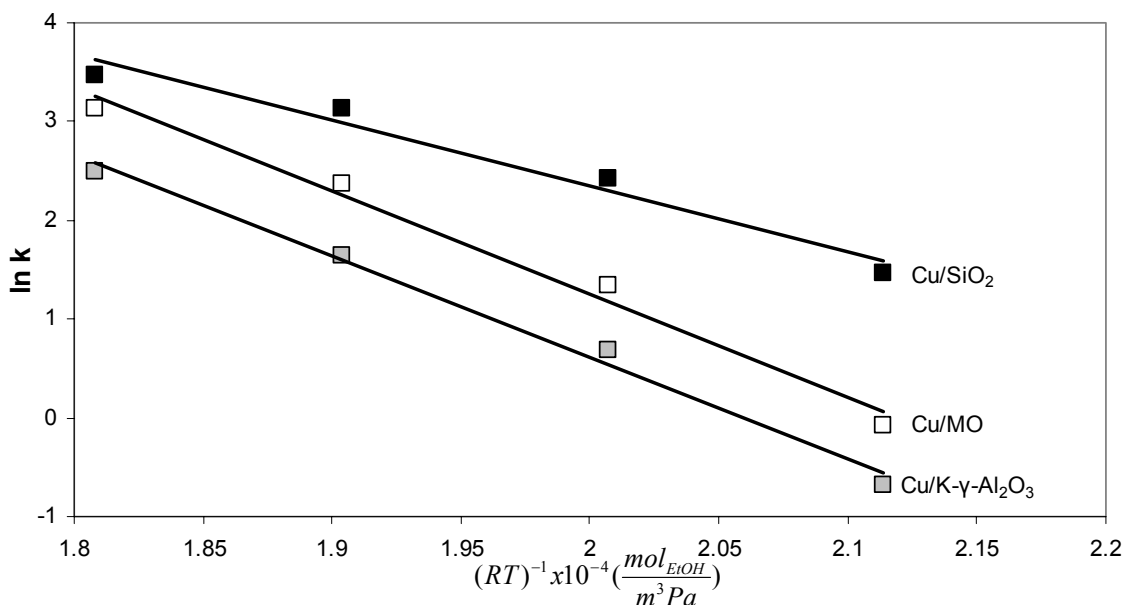
Figure 7.17 Temperature dependence of reaction rate constants at 0.1 MPa and EtOH:H_2O = 1:1.

Table 7.10 Dehydrogenation rate constants, frequency factors and activation energies.

Catalyst	Temperature (°C)	k (L h^{-1} g$_{cat}^{-1}$)	A (L h^{-1} g$_{cat}^{-1}$)	Ea (kJ mol^{-1})
Cu/SiO$_2$	200	4		
	225	11		
	250	23	6.0E+06	55
	275	32		
	300	40		
Cu/K-γ-Al$_2$O$_3$	200	1		
	225	2		
	250	5	1.5E+09	85
	275	12		
	300	18		
Cu/MO	200	1		
	225	4		
	250	11	4.2E+09	87
	275	23		
	300	26		

The values of activation energies shown in Table 7.10 once again confirm the superiority of Cu/SiO$_2$ catalyst. Despite the lower frequency factor, indicating the number of successful collisions leading to the product formation, activation energy, which represents the amount of energy required to overcome the energy barrier leading from reactants to products, is significantly lower than the values for the other two catalysts. On the other hand, the MO- and K-γ-Al$_2$O$_3$-supported samples have very similar activation energies and frequency factors, suggesting the reaction proceeds through the same mechanism. This view is consistent with the TPD characterization results, which showed a great similarity between the two supports. As mentioned before, the inertness of SiO$_2$ and its large surface area can be key reasons for its superiority by facilitating the adsorption of ethanol and desorption of acetaldehyde.

7.4 Conclusions

Out of three copper catalysts used in ethanol dehydrogenation, Cu/SiO$_2$ was found to provide superior conversion and hydrogen productivity under all conditions. This superiority can be most likely related the inertness and high surface area of the support. The selectivity to acetaldehyde – the other major dehydrogenation product – is affected

by conversion and residence time as it is converted in subsequent reactions, mainly to ethyl acetate. It was found that conversion steadily increases with increasing temperature and also with increasing residence time until equilibrium is achieved. Negligible signs of deactivation were observed for all catalysts at temperatures below 300°C. Above this temperature copper was subject to sintering and quickly lost its activity. Co-feeding water improved stability and selectivity to acetaldehyde at low EtOH:H_2O ratios but had a negative impact on stability if used in excess. On the other hand, co-feeding acetaldehyde always had a detrimental effect on both the activity and selectivity of any catalyst. The effect was not critical at low EtOH:AcAd ratios (below 1:0.1 molar) but became serious at higher AcAd contents. The catalysts' activities were found to be virtually insensitive to pressure. However, selectivity was influenced as the increased pressure resulted in more acetaldehyde being converted to ethyl acetate. The kinetic analysis provided evidence that ethanol dehydrogenation follows first-order reaction kinetics at low temperatures and confirmed differences between the catalysts.

The results prove that first part of this novel reactive separation process is a viable option for production of elevated-pressure, high-purity hydrogen from ethanol by dehydrogenation.

Chapter 8: Acetaldehyde hydrogenation

In this chapter, various supported and unsupported copper-based catalysts are characterized and their performance evaluated in acetaldehyde hydrogenation by syngas.

8.1 Introduction

Early in the 20th century, ethanol was commercially produced in Switzerland by hydrogenation of acetaldehyde by hydrogen over a Ni catalyst (Armstrong and Hilditch, 1920). This process was rendered economically obsolete by the availability of cheap petroleum, a widespread use of ethylene pyrolysis and ethylene's sequential hydration to ethanol. The interest in acetaldehyde hydrogenation was renewed with the investigation of syngas as an alternative resource base for production of various hydrocarbons. Acetaldehyde was considered an intermediate in the production of ethanol from syngas (Burch and Petch, 1992a; Trunschke et al., 1991; Arimitu et al., 1989). Promising results were obtained with Rh-(Burch and Petch, 1992a; Trunschke et al., 1991) and Cu-(Arimitu et al., 1989; Agarwal et al., 1988) based catalysts, which are commonly used in methanol synthesis from syngas.

Copper is of special interest because of its low cost and ability to preserve the C-C bond, the degradation of which would lead to undesirable secondary products, such as CH_4 and CO. Additionally, various promoting metals were added to Cu or Rh to improve the activity and selectivity in acetaldehyde hydrogenation. Thus Fe added to Rh, was reported by Burch and Petch (1992a) to selectively convert acetaldehyde to ethanol in the presence of hydrogen. Similarly a Cu-Zn mixed catalyst was identified by Arimitu et al. (1989) as an excellent post–treatment catalyst in the process of ethanol formation from syngas, transforming both acetaldehyde and acetic acid, formed from syngas in the previous step, into ethanol. Plausible explanations of the positive influence of promoter are:

- stabilization of a positive charge on the active metal component, which consequently stabilizes reactive intermediates on the surface (Herman et al., 1979; Ponec, 1992b; Hindermann et al., 1993),

- selective blocking of larger active metal clusters required for methanation (Burch and Hayes, 1997),

- formation of a new active phase on the interface of the active metal and the promoter (Burch and Hayes, 1997), and

- creation of a hydrogen pool providing extra hydrogen for the hydrogenation (Burch and Petch, 1992a).

On the other hand, Kenvin and White (1992) reported that acetaldehyde hydrogenation probably occurs by the addition of hydrogen that is chemisorbed on the same Cu site as the oxygenate and therefore, it is unlikely that hydrogen adsorbed on adjacent Cu or promoter sites could have any direct effect.

In this Chapter, the performances of unpromoted copper catalysts were compared to catalysts containing Fe and Zn metal promoters to determine the effect of the promoting metals. Furthermore, the performance of unsupported catalysts was evaluated against those supported on SiO_2. The best candidate from each group was selected and the effect of temperature, feed composition, residence time, and pressure on the acetaldehyde conversion and ethanol selectivity was established. Finally, a kinetic study was conducted to obtain basic kinetic parameters and gain insight into the mechanism of the acetaldehyde hydrogenation reaction.

8.2 Experimental section

8.2.1 Catalyst preparation

The copper-based catalysts used to study acetaldehyde hydrogenation can be divided into two groups: unsupported catalysts prepared by precipitation and SiO_2-supported catalysts prepared by incipient wetness impregnation.

Precipitation

Pure Cu, Zn and Fe oxides and binary mixtures (30, 50 and 70 mol. % on an elemental basis) of Cu-Zn and Cu-Fe were prepared by precipitation and subsequent calcination of the precipitates. The amounts of $Cu(NO_3)_2.3H_2O$ (Alfa Aesar, #12523, ACS 98-102% purity), $Fe(NO_3)_3.9H_2O$ (Alfa Aesar, #33315, ACS 98-101% purity) and $Zn(NO_3)_2.6H_2O$ (Aldrich, #228737, 98% purity) required to produce 40 g of catalyst

were dissolved in distilled water (approx. 0.7 L). The solution was fed dropwise into a 2-L, 3-neck, round-bottom flask filled with 750 mL solution of Na_2CO_3 (EMD, #SX0395-1, ACS) at the concentration required to convert the metal nitrates to their respective carbonates. The contents of the flask were vigorously stirred and pH continuously monitored by a pH meter. Due to possible formation of amphoteric $Zn(OH)_2$, which precipitates at a pH around 10.1, and upon further decrease in pH re-solubilizes, the pH was allowed, in the case of binary Cu-Zn mixtures, to drop from an initial value of ~11.8 to 10.1 and then held constant at 10.1 by dropwise addition of 8-M NaOH (Bioshop, #SHY 700, ACS). For pure Cu or Cu-Fe mixtures the final pH was 8.1, i.e., the pH where $Cu(OH)_2$ precipitates. Again, the pH was maintained at this value by dropwise addition of 8-M solution of NaOH. The resulting precipitates were brought to 65°C and left to age overnight at this temperature. The suspension was then filtered and re-suspended three times in distilled water in order to remove Na^+ and NO_3^- ions. The residue was dried overnight at 80°C, crushed to powder and calcined for 6 h at 550°C in a muffle furnace. The resulting oxide form of the catalyst was pressed, crushed and sieved to produce a desired mesh size of 35-45 mesh.

Incipient wetness impregnation

The Cu/SiO_2 catalysts were prepared by depositing 15 wt. % Cu with or without 0.5 or 5 wt. % of Fe or Zn on the SiO_2 support (Aldrich, grade 646, 35-45 mesh) by incipient wetness impregnation. The accessible pore volume of SiO_2 was experimentally determined to be 0.9 mL g^{-1}. The desired amounts of $Cu(NO_3)_2.2.5H_2O$ (Aldrich, #31288, 99.99% purity), $Fe(NO_3)_3.9H_2O$ and $Zn(NO_3)_2.6H_2O$ were dissolved in a proper volume of distilled water and the resulting solution was added dropwise to dry SiO_2. After each drop, the vial containing SiO_2 was vigorously shaken. After impregnation, this material was dried overnight at 80°C and calcined for 6 h at 550°C in a muffle furnace.

Prior to each reaction experiment, both unsupported and supported catalysts were reduced *in-situ* in 30:150 mL min^{-1} H_2 (Praxair, 4.5 PP):N_2 (Praxair, 4.8 PP) by carefully ramping the temperature at 5°C/min from room temperature to 300°C and dwelling at this temperature for 1 h.

8.2.2 Catalyst characterization

Thermogravimetric Analysis (TGA)

Thermogravimetric analysis was conducted utilizing a TA Instruments SDT 2960. The weight change of catalyst sample during oxidation in air was recorded as a function of temperature which was ramped at $10°C$ min^{-1} from room temperature to $900°C$. The results were used to determine the calcination temperature necessary for complete decomposition of metal hydroxides/carbonates in case of unsupported catalysts, and metal nitrates in case of SiO_2-supported catalysts, to their corresponding oxides.

BET, Copper content & Copper surface area

BET surface area was determined by a Micromeritics Gemini^{TM} V-Series surface analyzer. The samples were pretreated in N_2 at $300°C$ for 1 h in order to remove any moisture adsorbed on the catalyst surface.

Copper contents of both supported and unsupported catalysts were determined by temperature programmed reduction (TPR). A sufficient amount of catalyst, ranging from 0.03 g of CuO to 0.2 g for 15 wt. % Cu/SiO_2, was placed into a quartz fixed-bed down-flow microreactor (i.d. 4 mm, length 40 cm) and pretreated in air (approx. 470 mL min^{-1}) at $450°C$ for 3 h to ensure that all copper was oxidized to CuO. The reactor was then cooled to $30°C$ in N_2. TPR was carried out by ramping the temperature from $30°C$ to $300°C$ at $5°C/min$ in 30 mL min^{-1} of 4.97% H_2/N_2 stream. The amount of hydrogen consumed was detected by thermal conductivity detector (TCD) and used to estimate the wt. % of copper contained in each catalyst (Cu_{tot}).

In addition, the copper dispersion and copper surface areas of the supported catalysts were determined by H_2-N_2O titration following the method of Bond and Namijo (1989). Upon completion of the first TPR experiment, the reactor was cooled in O_2-free N_2 to $60°C$ and purged for an additional 30 min. The surface copper atoms were then selectively oxidized to Cu_2O by passing 80 mL min^{-1} of N_2O stream over the catalyst for 1 h. Following the N_2O treatment, the reactor was cooled to $30°C$ and purged with O_2-free N_2 to remove all traces of N_2O. A second TPR was carried out from 30 to $300°C$ at a rate of $5°C/min$ with 30 mL min^{-1} of 4.97% H_2/N_2. After the second TPR, the number of surface atoms (Cu_s) was calculated assuming an $O/Cu_s = 0.5$. The dispersion, defined as

Cu_s/Cu_{tot}, was computed using the Cu content determined from the first TPR. Assuming the equal presence of (100), (110) and (111) Miller index planes, the surface-atom density was 1.47×10^{19} atoms/m^2 (Bond and Namijo, 1989) and copper surface area could then be calculated. The average diameters of copper particles were calculated based on the assumption of spherical size of aggregates from the copper content, copper surface area and copper density of 8920 kg m^{-3} (Baram, 1989).

Catalytic activity

A standard down-flow, fixed-bed reactor consisting of a quartz tube (i.d. 10 mm, length 48 cm) with a quartz frit located 19 cm from the top rim of the tube (corresponding to the location of furnace's isothermal zone), was used for all atmospheric pressure experiments. The desired amount of catalyst was mixed with SiC (Kramer Industries, 36 grit) serving as a flow and temperature distributor. The mixture, with a combined weight ($w_{cat} + w_{SiC}$) always of 2.5 g, was then loaded onto the frit. In the case of higher pressure experiments, a thick-wall quartz reactor (i.d. 6 mm, length 45 cm) was utilized, which permitted limited loading of only 0.1 g of catalyst mixed with 1 g of SiC. The reactor was placed into a tubular convection furnace and the thermocouple, which controlled the reaction temperature, was inserted into the catalyst bed.

The gaseous stream consisting of H_2 and CO or N_2 was passed through a glass (atmospheric pressure) or stainless steel (elevated pressure) double-stage saturator filled with acetaldehyde and immersed in a temperature-adjustable fluid bath. It was verified, by passing the stream through the empty reactor and analyzing the outlet by GC, that the stream exiting the saturator was saturated with acetaldehyde. When H_2O or ethanol were co-fed, these liquids were delivered by an Eldex A-60-S stainless steel HP metering pump at the desired flow rate to an evaporator where the liquid stream was gasified and combined with the gaseous stream saturated with acetaldehyde. The ensuing gaseous feed was then passed over the catalyst bed. The resulting product stream was directed into an online Varian GC 3800 gas chromatograph. A novel gas chromatograph separation method previously developed (Chladek et al., 2007a, see Appendix A) allowed for simultaneous analysis of both gaseous and condensable components once every 32 min.

The reaction was studied in a pressure range of 0.1-0.5 MPa and temperatures ranging from 150 to 300°C.

8.3 Results and discussion

8.3.1 Catalyst characterization
TGA

Each of the SiO$_2$-supported catalysts yielded a similar TGA pattern (see Fig. 8.1) with one major Cu(NO$_3$)$_2$ decomposition peak occurring between 235°C and 250°C and tailing up to 430°C, which is in good agreement with literature data for decomposition of copper nitrate: 247-260°C (Lvov and Novichikin, 1995). As expected, the weight loss associated with the decomposition of the precursor containing lower amount of nitrates, i.e., precursors with 0.5% of Fe or Zn, was lower than that of precursors with 5% Fe or Zn.
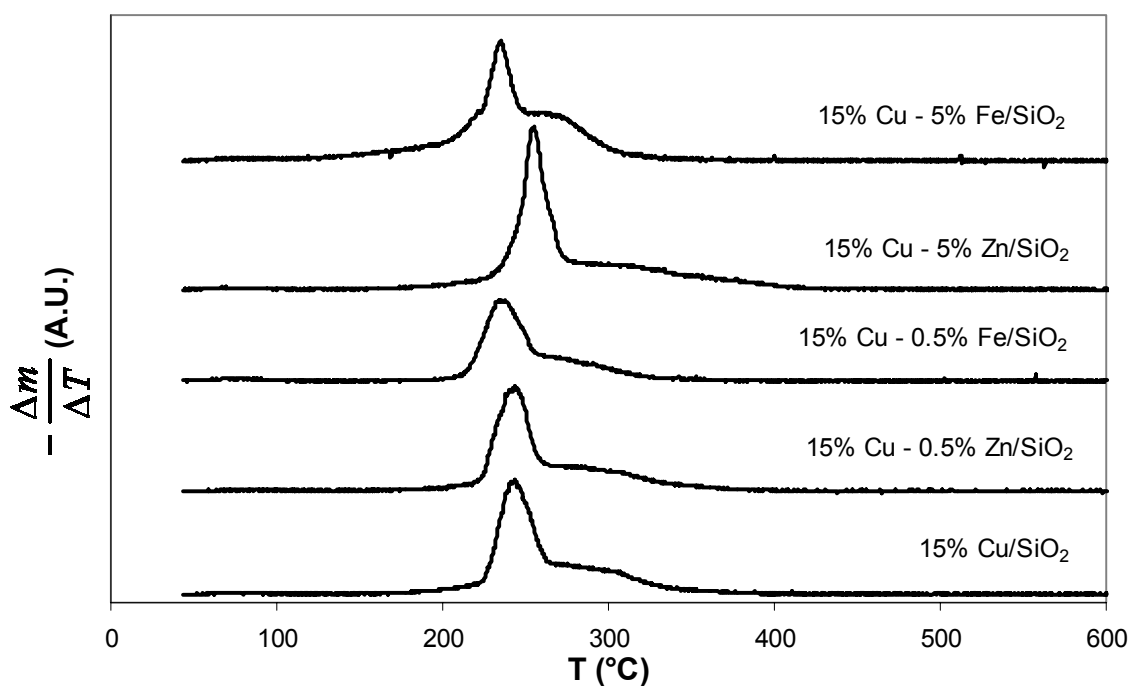
Figure 8.1 TGA profiles of SiO$_2$-supported catalysts in air.

The Cu and Fe precipitates did not show any significant change in weight suggesting a precipitation in their oxide form as CuO and Fe_2O_3 respectively. When co-precipitated, one decomposition peak appears at 340°C (see Fig. 8.2). The weight loss decreased with decreasing copper content and correlated well with the dehydration of $Cu_2(OH)_2CO_3$ (malachite) to CuO and was in good agreement with the decomposition temperature of 350°C reported in the literature (Kiseleva et al., 1992).
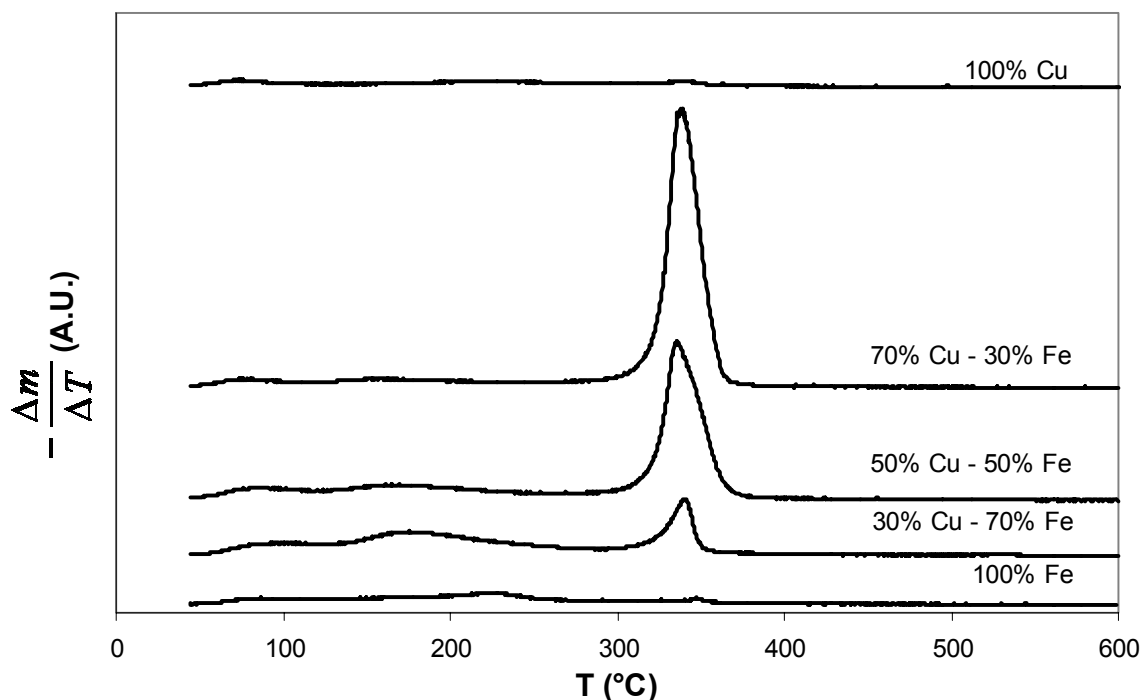
Figure 8.2 TGA profiles of unsupported Cu-Fe catalysts in air.

Zn precipitates from the solution in the form of $ZnCO_3$, which dehydrates to ZnO at 240°C as is indicated by the decomposition profile shown in Fig. 8.3 and close to the data reported in literature:205-258°C (Mu and Perlmutter, 1981). The addition of copper results in the appearance of a peak at 340°C, probably associated with dehydration of $Cu_2(OH)_2CO_3$, but also in the emergence of the peak having a maximum in the temperature range of 445-485°C. This high temperature decomposition is not observed in either of the pure oxides and therefore can only be related to a compound containing both Zn and Cu cations, most probably in a form of mixed carbonate-hydroxide.
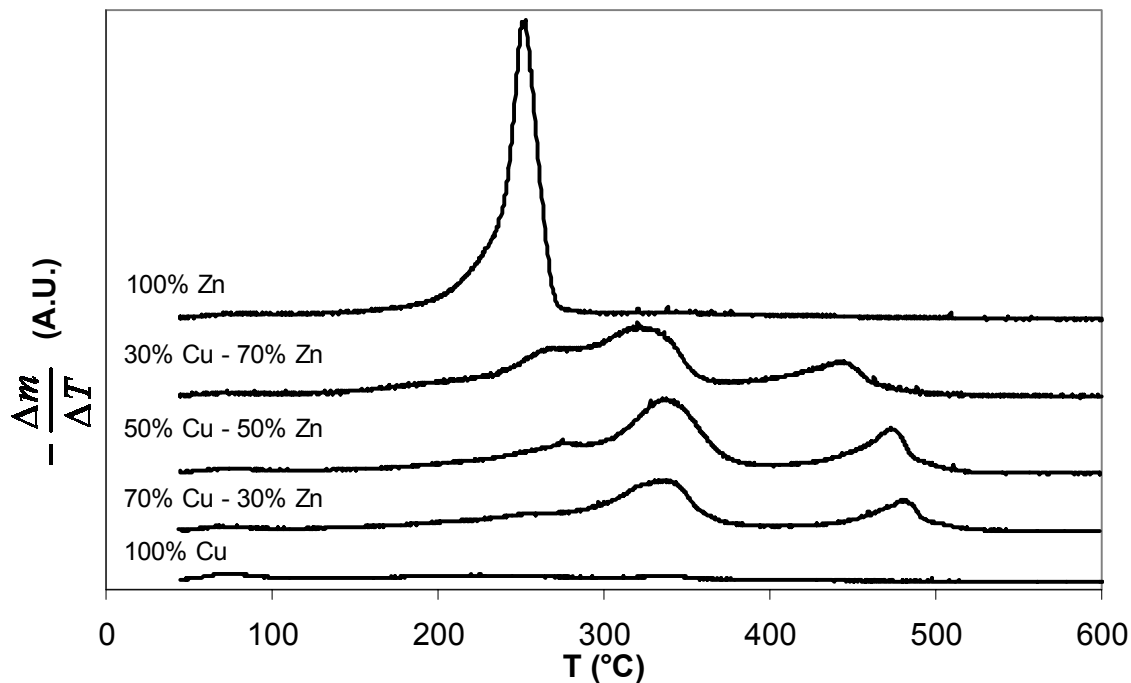
Figure 8.3 TGA profiles of unsupported Cu-Zn catalysts in air.

Based on these results, a temperature of 550°C was chosen as a safe temperature for catalyst calcination, ensuring that all metal containing compounds are converted to their corresponding oxides.

BET & Copper surface area

The copper contents of all catalysts and the copper dispersions, copper surface areas and copper particle sizes of the supported catalysts as measured by TPR and N_2O titration, together with total surface areas measured by BET are presented in Table 8.1. Even though SiO_2 provides a high BET surface area to the supported catalysts, the copper surface area calculated per g of catalyst is in the range of 10-15 m^2 g_{cat}^{-1} for both supported and unsupported catalysts, represented by unsupported Cu and assumed to be similar to BET surface areas in case of remaining unsupported catalysts, and therefore their performance can be compared without the exact knowledge of the actual number of the active sites.

Table 8.1 BET & copper surface area, copper content, dispersion & particle size.

Catalyst		Cu Content (TPR) (wt.%)	BET Surface Area (m^2/g_{cat})	Cu Surface Area (m^2_{cu}/g_{cat})	Cu Dispersion (%)	Cu Particle Diameter (nm)
Unsupported	Cu	100	11	11	-	-
Unsupported	Zn	0	15	-	-	-
Unsupported	Fe	0	21	-	-	-
Unsupported	7Cu3Fe	64	15	-	-	-
Unsupported	7Cu3Zn	62	15	-	-	-
Unsupported	5Cu5Fe	52	16	-	-	-
Unsupported	5Cu5Zn	49	17	-	-	-
Unsupported	3Cu7Fe	24	18	-	-	-
Unsupported	3Cu7Zn	29	14	-	-	-
SiO_2	15Cu	18	229	11	10	11
SiO_2	15Cu5Fe	16	214	11	10	10
SiO_2	15Cu5Zn	15	210	14	15	7
SiO_2	15Cu05Fe	19	236	15	13	8
SiO_2	15Cu05Zn	18	229	10	9	12

The TPR measurements (see Appendix B) proved that only CuO was reduced at temperatures below 300°C and both Fe and Zn remained in their oxide forms. All catalysts were, therefore, reduced at 300°C prior to the reaction.

8.3.2 Catalyst screening

Prior to the catalyst screening, the inertness of the reactor and SiC catalyst diluent was verified. Also, during all experiments, a carbon balance was performed on the exiting stream and always added up to 100±2%. Each data point in the catalyst screening is taken as an average of 3 or more injections with standard deviation in the range of 0.5-1.5%. The purpose of the catalyst screening was to investigate the effect of the Zn and Fe promoters on the hydrogenation reaction compared to unpromoted catalysts, unsupported Cu and Cu/SiO$_2$, and to identify the best candidates for further investigation. The catalyst performance was evaluated based on two primary criteria:

1) Acetaldehyde conversion:

$$X_{AcAd} = \frac{\dot{n}^0_{AcAd} - \dot{n}_{AcAd}}{\dot{n}^0_{AcAd}} = \frac{\sum\limits_{carbonaceous\ products}^{i} a_i \dot{n}_i}{\sum\limits_{carbonaceous\ products}^{i} a_i \dot{n}_i + \dot{n}_{AcAd}}$$

where

$\dot{n}^0_{AcAD}$ is the entering molar flow of acetaldehyde; $\dot{n}_{AcAD}$ is the exiting molar flow of acetaldehyde; a_i is the number of carbon atoms in any product species divided by the

number of carbon atoms contained in an acetaldehyde molecule; and $\dot{n}_i$ is the exiting molar flow of any carbonaceous product.

2) Main products selectivities:

$$S_i = \frac{b_i \dot{n}_i}{\displaystyle\sum_{\substack{i \\ carbonaceous\ species}} b_i \dot{n}_i}$$

where

b_i is a number of carbon atoms in a particular main product and $\dot{n}_i$ is molar flow of this product.

Acetaldehyde hydrogenation was studied with catalyst loadings of 0.522 g diluted with 2 g of SiC and AcAd:H_2:CO or AcAd:H_2:N_2 molar ratios of 1:1:0.33, where H_2 and CO or N_2 were delivered at constant flow rates of 56 mL min^{-1} and 18.7 mL min^{-1}, respectively, to the acetaldehyde saturator, which was maintained at constant temperature of -0.29°C. These conditions resulted in a constant gas hourly space velocity (GHSV STP) of 16 163 mL h^{-1} g$_{cat}^{-1}$, thus allowing comparison with the results obtained from the ethanol dehydrogenation study. The substitution of N_2 for CO allowed determination of the effect of CO on the reaction outcome. Furthermore, by feeding the syngas mixture directly to the reactor, by-passing the saturator, the extent of Fischer-Tropsch synthesis reactions was determined. The reactions were studied at atmospheric pressure and at two different temperature levels: 150 and 250°C. The main products selected for selectivity comparison were ethanol (EtOH) and products of secondary condensation reactions: ethyl acetate (EtAc), butyraldehyde (BA), crotonaldehyde (CA) and 1-butanol (BOH). To simplify the comparison, the catalysts were divided into two groups: supported and unsupported catalysts. Within each group, effects of temperature and CO presence were evaluated.

SiO$_2$-supported catalysts

The results for acetaldehyde hydrogenation carried out at 150°C in the presence of both CO and N_2 are presented in Figs. 8.4 and 8.5 and also in Table 8.2. The acetaldehyde conversion is <5% for all catalysts, which is much lower than the thermodynamic expectation of 93%, it can therefore be concluded that, at this

temperature, the reaction is limited by the kinetics. There is a slight promotional effect of Fe and Zn addition on conversion, and it can be noted, that this is the only case where promoters actually play a positive role. However, both metals have a detrimental effect on acetaldehyde selectivity. Furthermore, Fe has more negative influence on the selectivity than Zn. The selectivity is shifted from acetaldehyde to higher condensation species as seen from Table 8.2.

Figure 8.4 Acetaldehyde conversion as a function of Fe/Zn content on SiO_2 – supported catalyst at 150°C, 0.1 MPa and 1:1:0.33 AcAd:H_2:CO/N_2.

From the comparison between N_2- and CO-containing feeds, it can be seen that CO has no, or a negligible, effect on the outcome of the reaction and therefore acts as an inert. This observation is further confirmed by directly feeding the syngas mixture, by by-passing the saturator, into the reactor and detecting no products in the exit stream.

Figure 8.5 Ethanol selectivity as a function of Fe/Zn content on SiO_2 – supported catalyst at 150°C, 0.1 MPa and 1:1:0.33 AcAd:H_2:CO/N_2.

Table 8.2 Supported catalyst screening at 150°C, 0.1 MPa and 1:1:0.33 AcAd:H_2:CO/N_2.

Catalyst	X AcAd (%)		S ETOH (%)		S EtAC (%)		S BA (%)		S CA (%)		S BOH (%)	
	CO	N2	CO	N2	CO	N2	CO	N2	CO	N2	CO	N2
CuSi	3	2	86	84	8	7	3	3	0	0	1	2
Cu0.5%FeSi	3	3	67	68	19	16	8	8	0	0	5	4
Cu0.5%ZnSi	3	3	70	71	16	13	9	10	0	0	3	2
Cu5%FeSi	4	4	33	35	15	12	15	20	3	1	33	30
Cu5%ZnSi	4	3	56	57	21	9	20	27	0	0	3	4

More satisfying results, with regard to conversion, were obtained at 250°C and are presented in Figs. 8.6 and 8.7 and also in Table 8.3. Contrary to the experiments conducted at 150°C, the addition of Zn and Fe had negative effects on both acetaldehyde conversion and ethanol selectivity. Perhaps surprisingly, conversion-wise, this effect was more pronounced at the lower metal loading of 0.5 wt.%, while with regard to selectivity, the amount of secondary by-products increased steadily with increasing Fe/Zn content. Kenvin and White (1992) reported that acetaldehyde hydrogenation occurs solely on the copper particles where both H_2 and adsorbed acetaldehyde are present. Therefore, even if Fe and Zn provided extra hydrogen storage on the surface, as suggested by Takenaka et al. (2002) and Burch and Petch (1992a), this hydrogen may not be supplied to the active copper centres, thus effectively reducing the hydrogen concentration on the surface. The

effect of hydrogen insufficiency would be expected to be more significant if the metal clusters are isolated, as in the case of low metal loading, than if the extra hydrogen storage capacity is in direct contact with copper phase, which might be the case with 5% loading. The negative effect of promoters on selectivity may be related to formation of larger metal clusters, which are required for the formation of secondary products such as ethyl acetate (Kenvin and White, 1992; Gole and White, 2001)

It can therefore be concluded, that even though Zn has a less detrimental effect on the reaction outcome than the addition of Fe, the best catalyst is unpromoted Cu on SiO_2, providing a conversion of 42%, i.e., 16% lower than the equilibrium expectation of 58%, and a selectivity to ethanol of 93%.
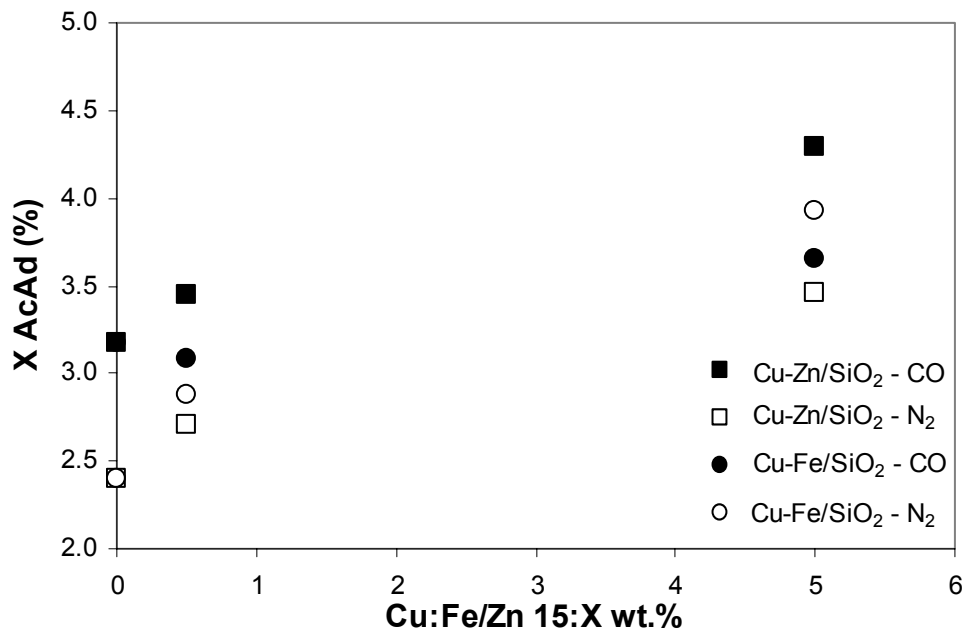

Figure 8.6 Acetaldehyde conversion as a function of Fe/Zn content on SiO_2 – supported catalyst at 250°C, 0.1 MPa and 1:1:0.33 AcAd:H_2:CO/N_2.

Once again, the presence of CO had only a negligible impact on the reaction outcome compared to N_2. When only the syngas mixture was fed, the CO conversion, defined in the same manner as acetaldehyde conversion, was less than 0.5%.
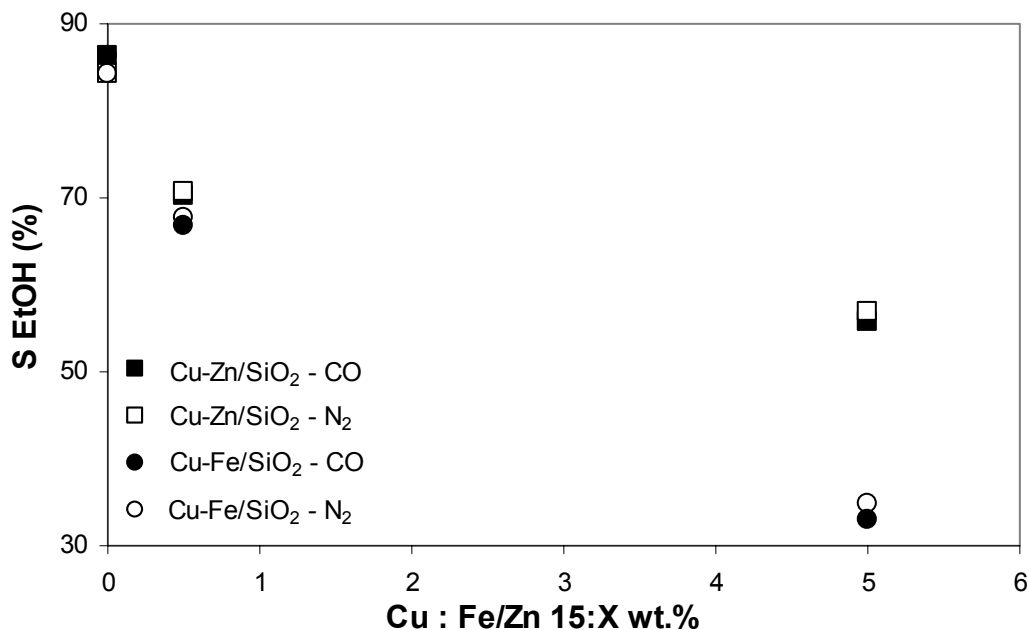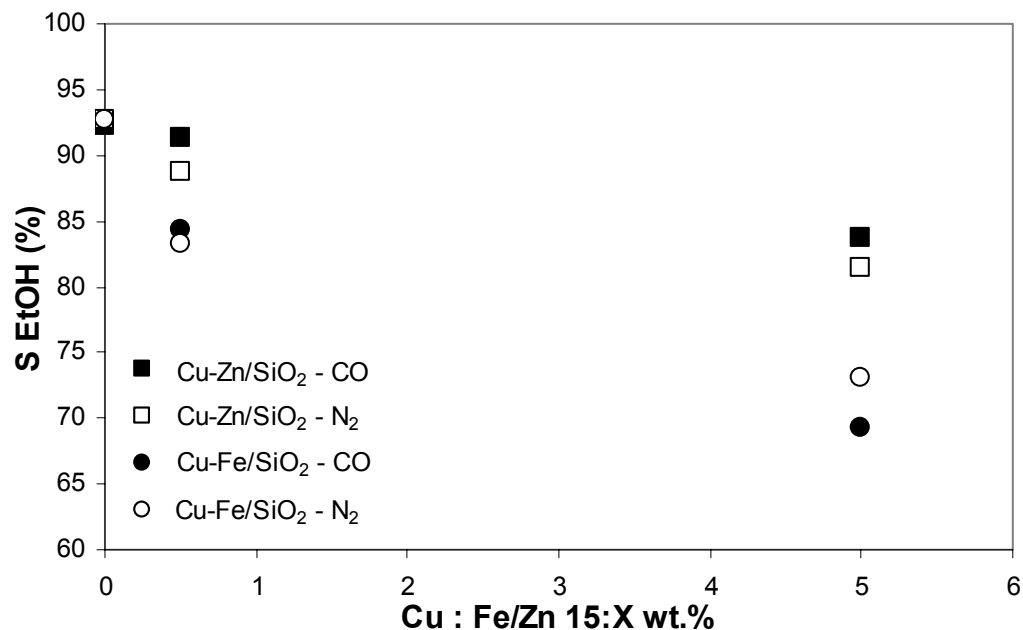
Figure 8.7 Ethanol selectivity as a function of Fe/Zn content on SiO_2 – supported catalyst at 250°C, 0.1 MPa and 1:1:0.33 AcAd:H_2:CO/N_2.

Based on these results, the unpromoted Cu/SiO_2 catalyst was selected as the best candidate among the supported catalysts for further investigation.

Table 8.3 Supported catalyst screening at 250°C, 0.1 MPa and 1:1:0.33 AcAd:H_2:CO/N_2.

Catalyst	X AcAd (%)		S ETOH (%)		S EtAC (%)		S BA (%)		S CA (%)		S BOH (%)	
	CO	N2	CO	N2	CO	N2	CO	N2	CO	N2	CO	N2
CuSi	42	43	92	93	6	5	1	1	0	0	0	0
Cu0.5%FeSi	29	28	84	83	9	9	5	5	0	0	0	0
Cu0.5%ZnSi	33	32	91	89	7	8	1	1	0	0	0	0
Cu5%FeSi	30	28	69	73	10	9	15	13	3	2	2	2
Cu5%ZnSi	40	40	84	81	10	8	4	4	0	2	1	3

Unsupported catalysts

The screening of unsupported catalysts was carried out in the same way as that of the supported ones, except that the effect of Zn/Fe addition was studied over the range of 0-100% content for 5 levels: 0, 30, 50, 70 and 100%. The results of the 150°C test are presented in Figs. 8.8 and 8.9 and summarized in Table 8.4. Once again, this temperature proved to be insufficient to provide significant acetaldehyde conversion. However, even at these low conversions, the addition of any amount of Zn or Fe had a negative impact

on conversion, with pure ZnO and Fe_2O_3 providing virtually no conversion. Furthermore, the pure Zn and Fe samples had such a low selectivity to EtOH that they were omitted from Fig. 8.9. This demoting effect can be related to the presumable location of hydrogenation – the copper particles – and Fe or Zn blocking these active sites.
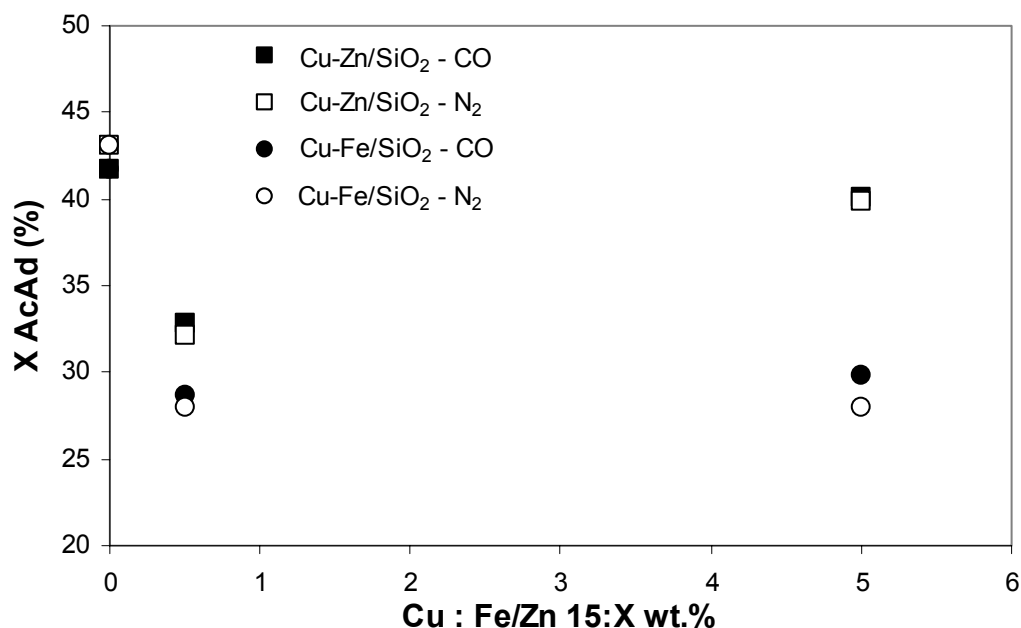

Figure 8.8 Acetaldehyde conversion as a function of Cu content in unsupported catalysts at 150°C, 0.1 MPa and 1:1:0.33 AcAd:H_2:CO/N_2.

The selectivity to ethanol varied from 61% to 94%. The highest value was achieved, together with highest conversion, on pure Cu in a CO-rich environment.
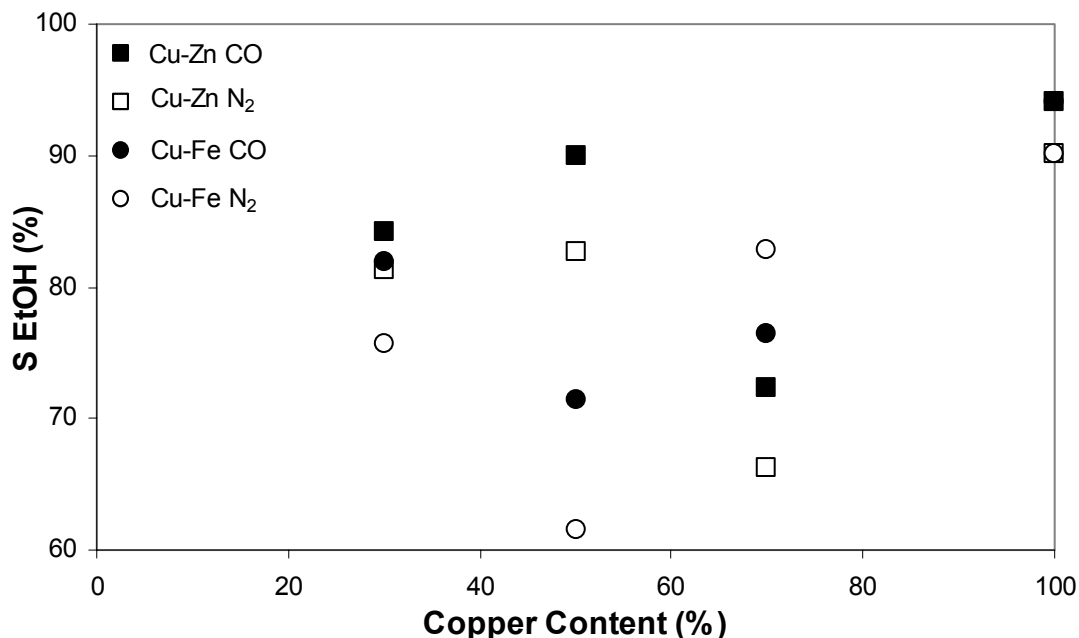
Figure 8.9 Ethanol selectivity as a function of Cu content in unsupported catalysts at 150°C, 0.1 MPa and 1:1:0.33 AcAd:H_2:CO/N_2.

With CO in the feed, a slightly improved conversion was observed in general, but CO presence did not have a clear effect on selectivity. However, the important fact for the implementation of the loop separation process is, that the presence of CO had no negative effect on the performance. The feed, consisting solely of hydrogen and CO resulted in no conversion of the syngas on any of the catalysts. Therefore, no parallel reactions involving H_2 and CO occur on those catalysts, at least for temperatures below 150°C.

Table 8.4 Unsupported catalyst screening at 150°C, 0.1 MPa and 1:1:0.33: AcAd:H_2:CO/N_2.

Catalyst	X AcAd (%)		S ETOH (%)		S EtAC (%)		S BA (%)		S CA (%)		S BOH (%)	
	CO	N2	CO	N2	CO	N2	CO	N2	CO	N2	CO	N2
100% Cu	3	2	94	90	3	0	0	0	1	5	1	1
70% Cu 30% Zn	3	1	72	66	4	5	10	14	11	4	0	3
50% Cu 50% Zn	3	2	90	83	0	5	3	5	6	6	0	2
30% Cu 70% Zn	2	1	84	81	0	0	3	7	10	7	0	0
100% Zn	0	0	0	56	13	9	0	0	0	0	68	16
70% Cu 30% Fe	2	1	76	83	0	0	4	8	18	5	0	0
50% Cu 50% Fe	2	1	71	62	0	5	5	8	18	14	1	4
30% Cu 70% Fe	2	2	82	76	0	6	4	0	1	4	10	11
100% Fe	1	0	0	21	4	4	0	0	0	0	92	69

Increasing the temperature to 250°C significantly improved the conversion and also had a positive effect on ethanol selectivity as seen from Figs. 8.10 and 8.11 and Table 8.5. At Zn/Fe contents ≤ 50%, Zn outperformed Fe; however, once again the co-precipitated catalysts did not match the performance of pure Cu, which gave a conversion of 53%. Similar to the data obtained at 150°C, ZnO and Fe_2O_3 proved to be inactive in acetaldehyde hydrogenation.
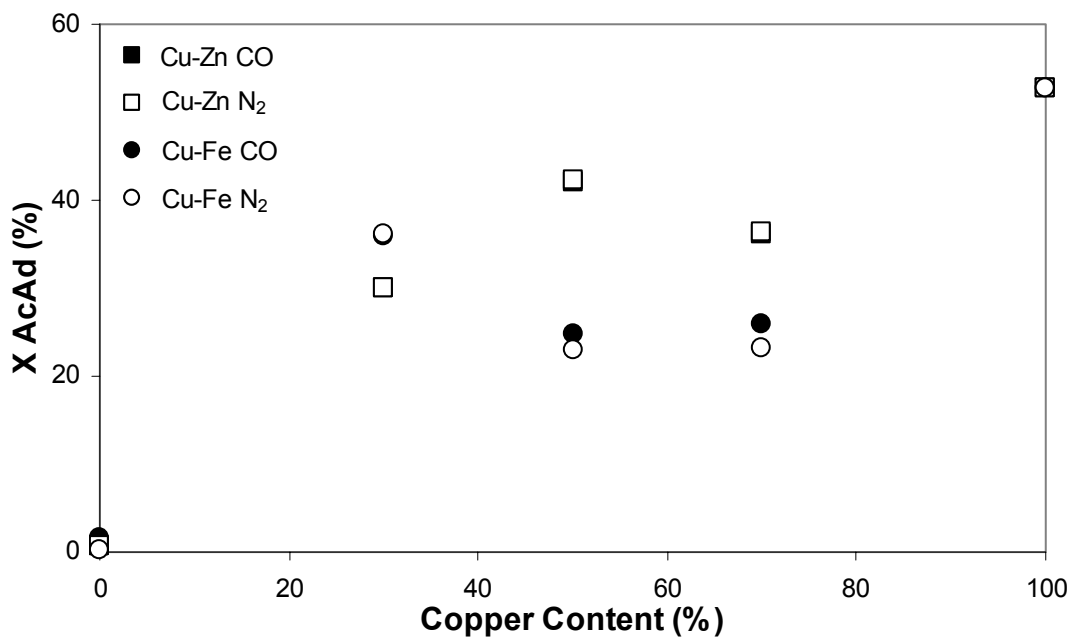
Figure 8.10 Acetaldehyde conversion as a function of Cu content in unsupported catalysts at 250°C, 0.1 MPa and 1:1:0.33 AcAd:H_2:CO/N_2.

All copper containing catalysts were >90% selective to ethanol, with no clearly discernible negative or positive effect of metal addition.

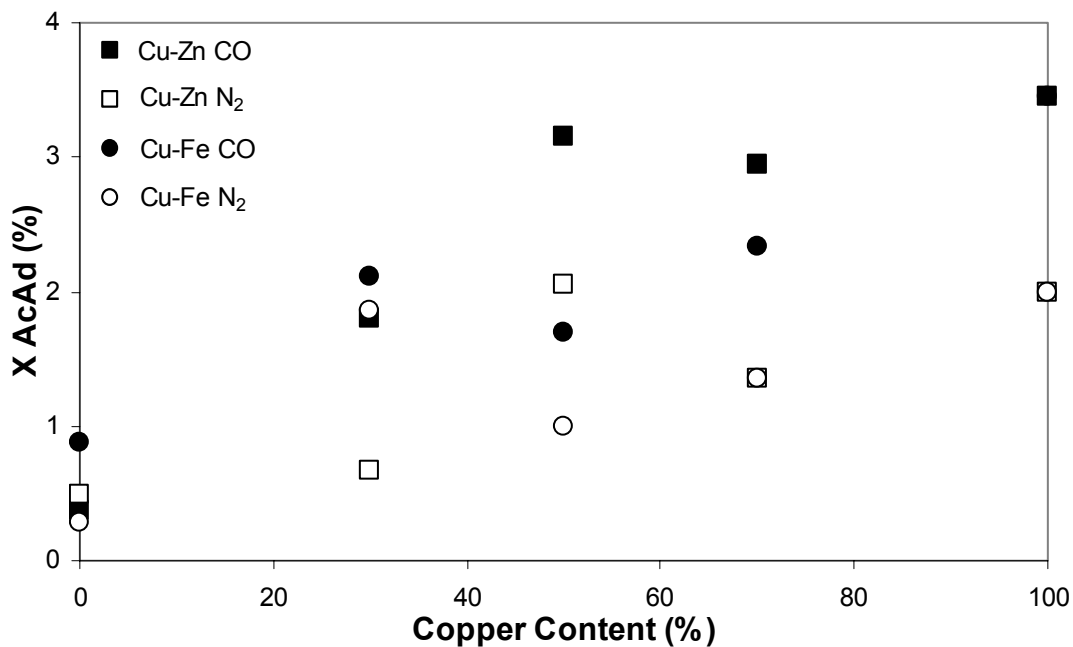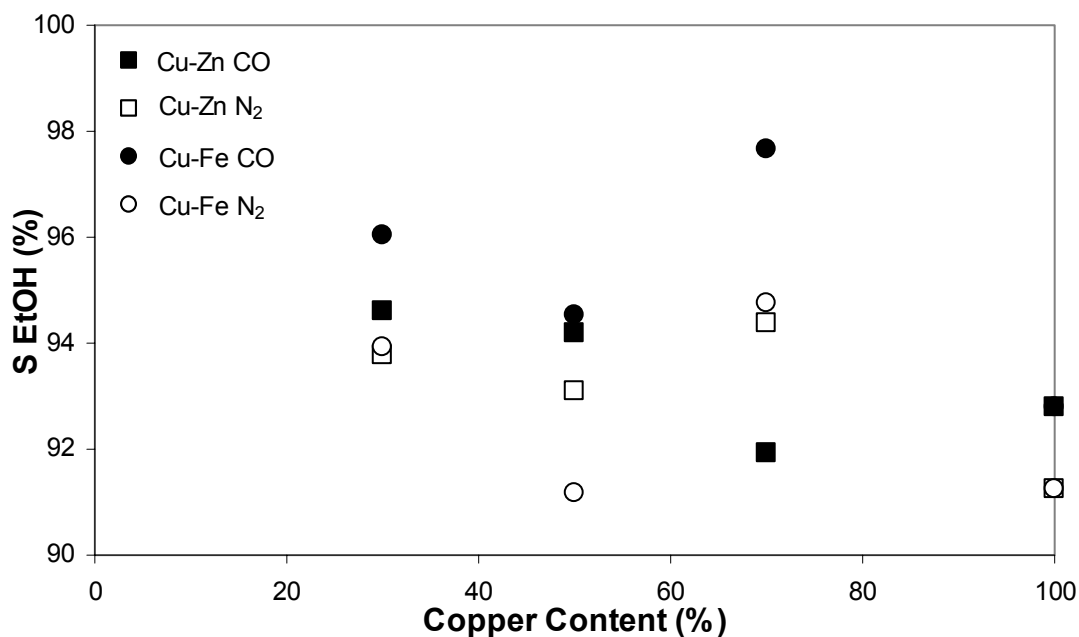**Figure 8.11** Ethanol selectivity as a function of Cu content in unsupported catalysts at 250°C, 0.1 MPa and 1:1:0.33 AcAd:H_2:CO/N_2.

Acetaldehyde conversion did not change with the switch between CO and N_2 in the feed. This suggests that both gases behave in the same manner and do not interfere or interfere to the same limited extent with ethanol formation. Furthermore, CO inclusion improved the selectivity to ethanol, which indicates that at least some of the secondary reactions are occurring on sites different from those for acetaldehyde hydrogenation. CO must then have a higher affinity to these sites than N_2.

Table 8.5 Unsupported catalyst screening at 250°C, 0.1 MPa and 1:1:0.33 AcAd:H_2:CO/N_2.

Catalyst	X AcAd (%)		S ETOH (%)		S EtAC (%)		S BA (%)		S CA (%)		S BOH (%)	
	CO	N2	CO	N2	CO	N2	CO	N2	CO	N2	CO	N2
100% Cu	53	53	93	91	6	7	0	0	0	0	0	0
70% Cu 30% Zn	36	36	92	94	7	5	0	0	0	0	0	0
50% Cu 50% Zn	42	42	94	93	6	6	0	0	0	0	0	0
30% Cu 70% Zn	30	30	95	94	4	4	0	0	0	0	0	0
100% Zn	1	1	0	39	7	10	0	0	0	0	82	12
70% Cu 30% Fe	26	23	98	95	1	1	0	0	0	0	0	0
50% Cu 50% Fe	25	23	95	91	3	3	1	1	0	0	0	0
30% Cu 70% Fe	36	36	96	94	2	0	0	0	0	2	0	0
100% Fe	1	0	0	28	3	7	0	0	0	0	92	45

When only syngas was passed over the catalysts, the pure oxides as well as the Cu-Zn mixed catalysts exhibited conversions lower than 0.5%. On the other hand, increasing the Fe content in Cu-Fe catalysts led to an increase in CO conversion from 1% to 3% with major products being CO_2 (34%), CH_4 (20%) and propylene (15%).

Based on these screening results, pure Cu was selected as the best candidate for further investigation providing acetaldehyde conversion of 53% and ethanol selectivity of 93%.

Consequently, Cu and Cu/SiO_2 were used in the investigations of the effect of temperature, feed composition, residence time, and pressure on the hydrogenation reaction. Since the presence of CO did not have a negative influence on the conversion or selectivity, and since syngas is a principal hydrogenating agent in the proposed loop, a 1:0.33 H_2:CO mixture was used as a hydrogenation mixture in all subsequent experiments, unless stated otherwise.

8.3.3 Acetaldehyde hydrogenation – Cu and Cu/SiO_2

Temperature

The effect of temperature was investigated in a temperature-programmed ramp experiment. A 1:1:0.33 mixture of AcAd:H_2:CO was passed over 0.522 g of reduced catalyst at a GHSV (STP) = 16 163 mL h^{-1} g$_{cat}$$^{-1}$, while the reaction temperature was ramped from 200°C to 300°C at a rate of 0.17°C min^{-1}. Such a slow temperature ramp had to be used in order to gather sufficient number of data points, with an analytical system, described in detail in Appendix A, permitting collection every 32 min. From the

temperature-dependent conversion profile presented in Fig. 8.12, it can be concluded that Cu is more active than Cu/SiO$_2$. This observation can be related to a large surface of the support, which may act as an inert storage for acetaldehyde, which has to desorb and re-adsorb on the active copper site, while in case of Cu, the whole surface is reactive. It is also possible that, despite slightly lower copper surface area, unsupported copper has a greater number of sites active for hydrogenation. On both catalysts, the conversion of acetaldehyde initially increased with increasing temperature, but, as the system approached thermodynamic equilibrium, conversion went through a maximum and then declined. It is tempting to attribute the profile solely to thermodynamic limitations, but the selectivity pattern, which displays an abrupt step change around 250°C for both catalysts, indicates the possibility of catalyst surface reconstruction.

Figure 8.12 Temperature ramp experiment at 0.1 MPa and 1:1:0.33 AcAd:H$_2$:CO on Cu and Cu/SiO$_2$ catalysts.

The deactivation of catalyst, which would lead to destruction of the active sites required for acetaldehyde hydrogenation and/or creation of sites needed for secondary reactions is one explanation, as the two major by-products' selectivities, those of diethyl ether (DEE) and ethyl acetate (EtAc), are strongly correlated with ethanol selectivity, as can be seen from Fig. 8.13.

Figure 8.13 Correlation between DEE & EtAc selectivities and EtOH selectivity at 200-300°C, 0.1 MPa and 1:1:0.33 AcAd:H$_2$:CO.

In order to investigate this deactivation hypothesis, stability experiments examining the effect of time-on-stream on acetaldehyde conversion and ethanol selectivity were carried out at three temperature levels: 225°C, 250°C, and 280°C. The GHSV (STP) was increased to 84 375 mL h^{-1} g$_{cat}^{-1}$ by loading 0.1 g of catalyst to accelerate the observation of any deactivation. The results of the stability experiments are depicted in Fig. 8.14. At temperatures higher than 250°C, a significant decrease in activity with time on stream was observed, while both catalysts exhibited fairly stable operation at 225°C. At 250°C, Cu proved to be more stable, experiencing deactivation of -0.22% h^{-1} compared to -0.38% h^{-1} with Cu/SiO$_2$. Increasing temperature to 280°C resulted in a quick deactivation for both catalysts.

The ethanol selectivity was unaffected by either temperature or loss of activity, remaining constant at 97% (Cu) and 93% (Cu/SiO$_2$) over 20 h-on-stream.

Figure 8.14 AcAd conversion as a function of time on stream at three temperature levels, 0.1 MPa and 1:1:0.33 AcAd:H_2:CO.

That Cu-based catalysts would have limited temperature operation range was to be expected, as Cu is prone to sintering. However, with regard to the results from ethanol dehydrogenation, where a similar Cu/SiO$_2$ catalyst (but with a lower copper loading) delivered stable operation up to 300°C, it is rather surprising to see the temperature span of stable acetaldehyde hydrogenation being limited to 250°C. By comparing the experimental conditions of acetaldehyde hydrogenation and ethanol dehydrogenation, presented in Chapter 7, three differences can be identified and connected to different mechanisms of deactivation:

1) The presence of CO: although no negative effect of CO was observed during catalyst screening, it might be possible that at higher temperatures (e.g., 280°C), CO irreversibly poisons active copper sites.

2) The presence of H$_2$O: ethanol dehydrogenation was carried out with a mixed EtOH:H$_2$O feedstock, while pure acetaldehyde was used in the data presented above for acetaldehyde hydrogenation. Some literature sources suggest that both Cu and CuO phases are required for successful ethanol dehydrogenation and that H$_2$O helps to maintain this balance (Herman et al., 1979).

141

3) Unlike ethanol dehydrogenation, acetaldehyde hydrogenation is an exothermic reaction and even though the temperature of the catalyst bed is 280°C, as a result of limitations in heat transfer through catalyst particles, the active sites may experience higher temperatures which can consequently lead to deactivation by sintering.

The contribution of the first two points listed above can be clarified by conducting co-feed experiments, where CO is once again substituted by an inert gas, such as N_2, or H_2O is co-fed together with acetaldehyde. The third point can be tested by BET (decrease in the surface area of unsupported copper) or TPR-N_2O.

Feed composition

N_2 co-feed

CO was replaced with N_2 and the resulting mixture of H_2:N_2 (56:18.7 mL min^{-1}) was bubbled through the acetaldehyde saturator maintained at -0.29°C in order to generate a 1:1:0.33 AcAd:H_2:N_2 stream, which was then passed over 0.1 g of catalyst mixed with 2.4 g of SiC. A GHSV (STP) of 84 375 mL h^{-1} g$_{cat}$$^{-1}$ and reaction temperature of 280°C – the temperature where deactivation was most significant – made the experiments directly comparable to the stability studies discussed in the previous section. The results plotted in Fig. 8.15 suggest that substitution of N_2 for CO had no effect on catalyst stability, as acetaldehyde conversion on both catalysts declined at the same rate. There is, however, an offset in conversion observed solely on Cu/SiO$_2$ catalyst for N_2-rich feed, suggesting that on supported catalyst only, CO may be blocking some hydrogenation sites. The same result, though not so pronounced, was obtained in the supported catalyst screening study conducted at 250°C and depicted in Fig. 8.6. This blockage has no effect on the rate of catalyst deactivation and it can therefore be concluded that CO is not responsible for deactivation.
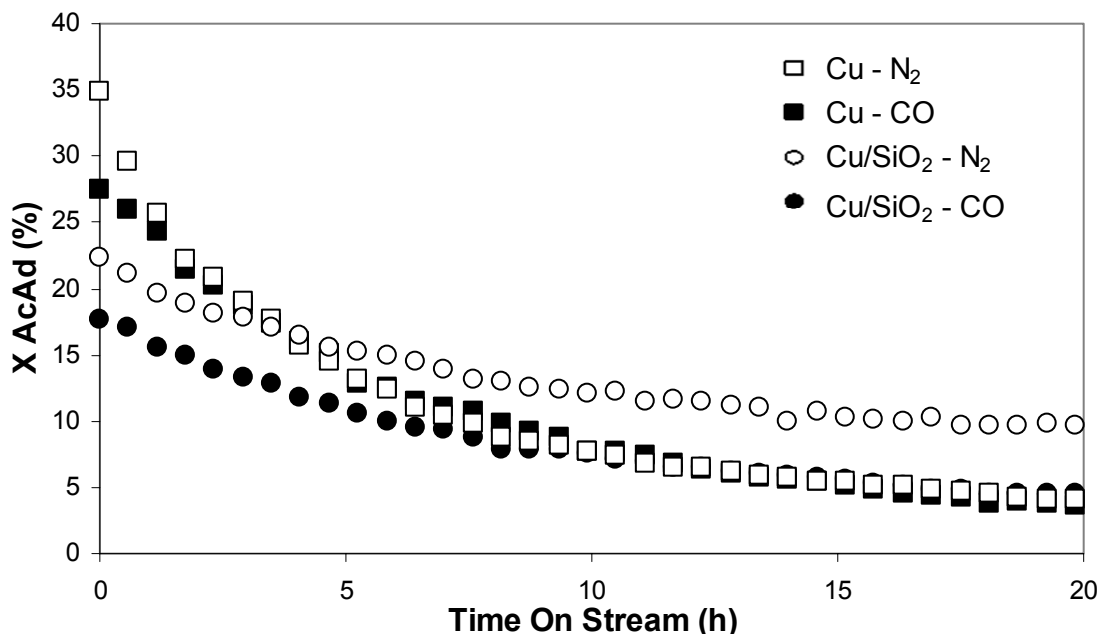
Figure 8.15 Comparison of the effects of N_2- and CO- rich feeds on AcAd conversion at 280°C, 0.1 MPa and 1:1:0.33 AcAd:H_2:CO/N_2.

H_2O co-feed

Water was delivered by an Eldex A-60-S piston pump at constant flow rate of 0.03 mL min^{-1} to a vaporizer where it was mixed with the outlet stream from saturator. The resulting mixture at molar ratio 1:1:1:0.33 of AcAd:H_2O:H_2:CO was passed over 0.1 g of catalyst at constant GHSV (STP) of 84 375 mL h^{-1} g$_{cat}^{-1}$. The reaction was studied once again at 280°C (the temperature where deactivation was most significant) and atmospheric pressure. The results depicted in Fig. 8.16 imply that water has a negative impact on initial conversion of both catalysts, which can be explained by the competition between water and acetaldehyde for active sites. However, similar to the ethanol dehydrogenation study presented in Chapter 7, water improves the stability of unsupported Cu and probably also of Cu/SiO$_2$, though the evidence is not as conclusive because of the lower initial conversion. Nonetheless, the deactivation is not completely suppressed and therefore the loss of activity cannot be attributed solely to the loss of Cu$^+$ ions on the surface. Furthermore, the decrease in acetaldehyde conversion will result in less heat being evolved during the reaction, therefore slowing the signs of any thermal related deactivation, such as sintering.
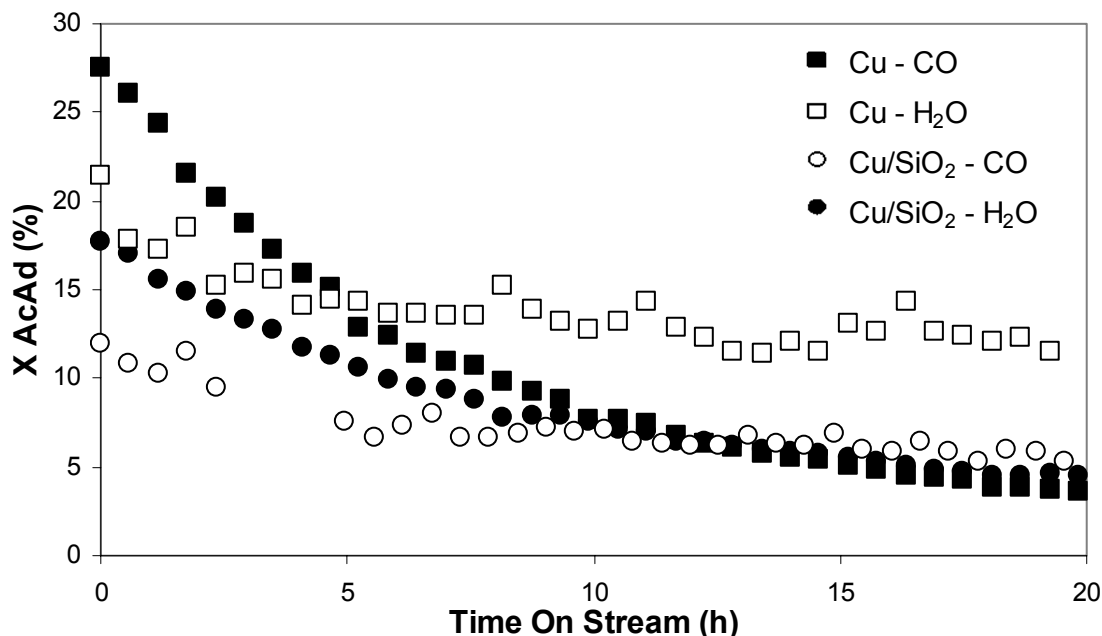
Figure 8.16 Effect of H_2O on catalyst stability at 280°C, 0.1 MPa and 1:1:1:0.33 AcAd:H_2:H_2O:CO compared to 1:1:0.33 AcAd:H_2:CO.

It can be therefore concluded that the most probable mechanism of deactivation is surface reconstruction, which is further supported by BET surface area measurement conducted on spent unsupported Cu catalyst (280°C), which resulted in a value of 6.6 m^2 g$^{-1}_{cat}$, compared to a value of 10.5 m^2 g$^{-1}_{cat}$ for the fresh catalyst. Loss of activity by sintering can be possibly assisted by the loss of Cu^0/Cu$^+$ equilibrium as suggested by H_2O co-feed experiments.

In order to avoid the deactivation, the reaction should be executed at temperatures not exceeding 250°C, which will result in slower kinetics. However, it might be possible to offset the lower conversion thus attained by increasing the amount of catalyst loading. Before this possibility is discussed, the investigation on the effect of ethanol in the feed will be presented.

EtOH co-feed

Since acetaldehyde hydrogenation is investigated as a part of a separation loop and since the ethanol dehydrogenation discussed previously in Chapter 7 resulted in

incomplete conversion of ethanol, the effect of residual ethanol on the outcome of the reaction was determined by co-feeding ethanol together with acetaldehyde.

In order to determine the effect of traces of ethanol in the acetaldehyde stream on activity and selectivity, three different AcAd:EtOH:H_2:CO feed compositions were prepared. Ethanol was mixed with acetaldehyde to form the liquid feed of desired concentration and was delivered to the vaporizer by a piston pump at a constant flow-rate of 0.1 mL min^{-1}, where it was mixed with an acetaldehyde-saturated H_2:CO stream. The resulting mixture was passed over 0.1 g of catalyst at 250°C. Since it was necessary for comparison purposes to maintain a constant GHSV of 84 375 mL h^{-1} g$_{cat}^{-1}$, the temperature of the saturator bath and flow rates of H_2 and CO had to be adjusted as well as the content of AcAd in the EtOH feed. The feed delivery conditions are summarized in Table 8.6.

Table 8.6 AcAd:EtOH:H_2:CO feed conditions.

Target Molar Ratio				Gas Flow Rate (ml/min)		T Sat (°C)	Liquid Feed Molar Ratio	
AcAd	EtOH	H_2	CO	H_2	CO		AcAd	EtOH
1	0	1	0.33	56.0	18.7	-0.29	-	-
1	0.25	1	0.33	48.7	16.2	-10.96	2.09	1
1	0.5	1	0.33	45.2	15.1	-6.10	0.68	1
1	1	1	0.33	39.3	13.1	-0.28	-	1

Results depicted in Fig. 8.17 indicate that ethanol addition had a detrimental effect on acetaldehyde conversion. Feed containing just 10 mol. % of EtOH caused a 30 and 50% loss of conversion on the Cu/SiO$_2$ and Cu catalysts respectively. Further increasing the ethanol content to 18 mol. % did not have such a dramatic effect. However, an increase to 30 mol. % revealed a difference in catalytic properties of the catalysts: while acetaldehyde conversion smoothly declined with increasing ethanol content on Cu/SiO$_2$, using unsupported copper resulted in the formation of acetaldehyde by ethanol dehydrogenation, instead of its consumption. The different behaviour of the two catalysts can possibly be explained by their total surface areas. Cu/SiO$_2$ has a large surface area owing to the support, where both ethanol and acetaldehyde can adsorb, rather than compete with H_2 for copper sites. On the other hand, on Cu, which has a 20- to 30-fold smaller total surface area, competition is greater and therefore the probability of an active site having both components required for hydrogenation (i.e., acetyl and hydrogen) is smaller. In contrast, ethanol does not require any additional reactant in order

to be dehydrogenated and, once the activation energy requirements are met, it can proceed to produce acetaldehyde and hydrogen. The selectivity to ethanol remained unaffected by the addition of ethanol and the product stream consisted of 99% (Cu/SiO_2) and 96% (Cu) ethanol.
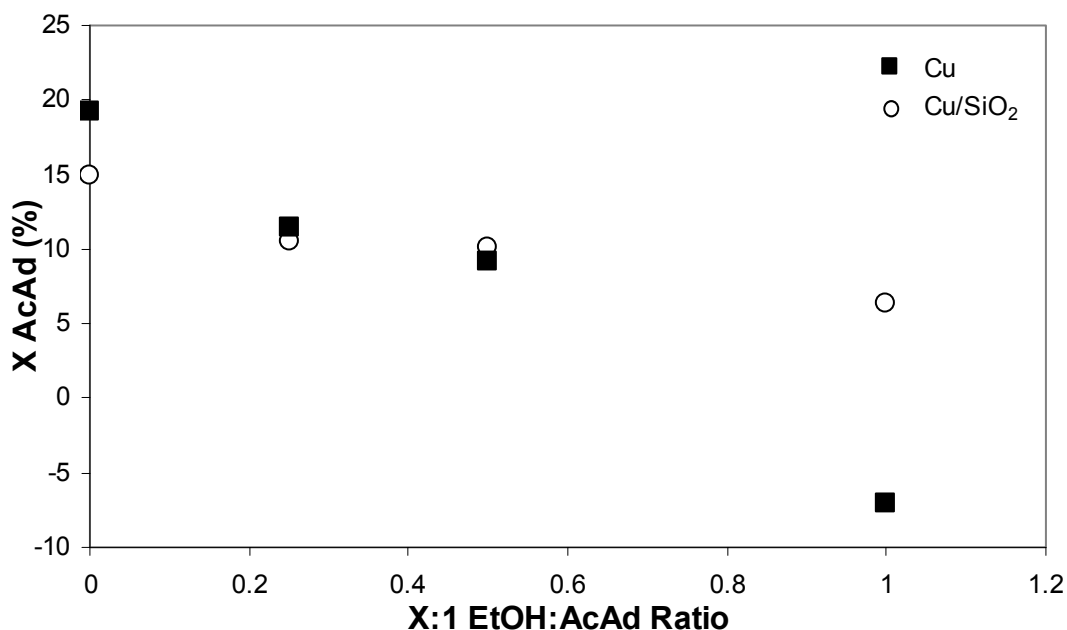
Figure 8.17 Effect of ethanol content on AcAd conversion on Cu and Cu/SiO_2 catalysts at 250°C, 0.1 MPa and 1:1:0.33:X $AcAd:H_2:CO:EtOH$ feeds.

Based on these results, it can be concluded that it is necessary to implement a separation step into the cycle between the dehydrogenation and hydrogenation steps in order to remove, or at least reduce, any ethanol impurities in the incoming acetaldehyde stream. Even though small quantities of ethanol will not render the catalysts completely inactive, they will seriously affect acetaldehyde conversion.

Residence time

The effect of residence time on acetaldehyde conversion was also investigated. The residence time was varied by using four levels of catalyst loading (0.1 g, 0.25 g, 0.5 g and 0.75 g). The reaction temperature was maintained constant at 244±1°C. A mixture of $AcAd:H_2:CO$ with a molar ratio 1:1:0.33 was used as a feed at a constant molar flow rate of $5.8 \cdot 10^{-3}$ mol min^{-1}. From the results displayed in Fig. 8.18, it is apparent that

acetaldehyde conversion can be improved by increasing the time reactants spend in the reactor, but this improvement is somewhat diminished by a decrease in ethanol selectivity. Similar to results obtained with ethanol dehydrogenation (see Chapter 7), acetaldehyde in the presence of ethanol takes part in subsequent reactions resulting mainly in ethyl acetate and to a lesser degree in C_4 – aldehydes. Kenvin and White (1992) attributed the extent of formation of these larger species solely to the size of copper particles, but since no particle size increase can be expected by simply adding more catalyst, it can be concluded that the prominence of secondary reactions is also a function of residence time. These conclusions are in good agreement with the results obtained in ethanol dehydrogenation and also with the literature (Franckaerts and Froment, 1964; Fujita et al., 2001; Iwasa and Takezawa, 1991; Raich and Foley, 1998).
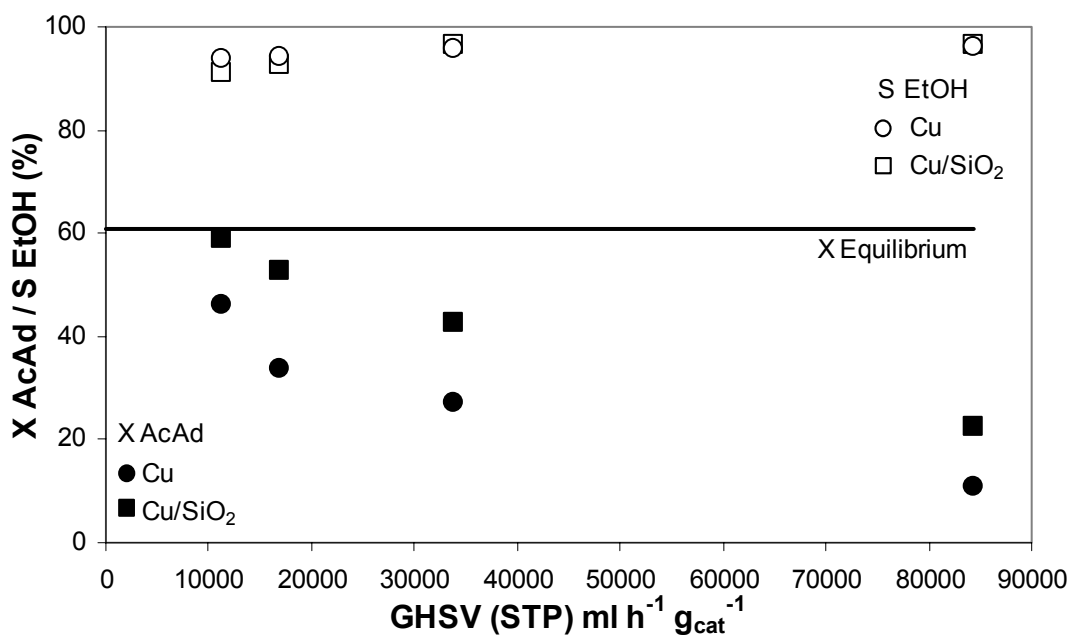
Figure 8.18 Effect of residence time represented by GHSV on AcAd hydrogenation at 244°C, 0.1 MPa and 1:1:0.33 AcAd:H_2:CO.

Pressure

The effect of pressure on activity and selectivity, which, according to thermodynamic calculations (see Chapter 5: Thermodynamics), is expected to be positive, was also investigated. Hydrogenation at elevated pressure would facilitate separation of gaseous and liquid products by condensation by increasing the condensation

points of individual species. Furthermore, a pressurized CO stream could also be water-gas shifted to produce a pressurized mixture of CO_2 and H_2.

The pressure experiments were conducted in a thick-wall quartz reactor in which 0.1 g of catalysts mixed with a reduced loading - in order to maintain the catalyst bed in the isothermal zone - of 1 g of SiC was placed. Hydrogenation was studied at 250°C, a pressure range of 0.1-0.5 MPa and with a constant molar flow of $2.51 \cdot 10^{-3}$ mol min^{-1} H_2 and $8.35 \cdot 10^{-4}$ mol min^{-1} CO being delivered to the stainless steel dual-stage acetaldehyde saturator, which was maintained at -0.29°C. Such a feed arrangement unfortunately does not allow for a clear determination of the pressure effect, because the acetaldehyde partial pressure is independent of total pressure and therefore, with increasing total system pressure, the amount of acetaldehyde transferred into the gas stream decreases. Consequently, the effect of increased pressure is coupled with the influence of increased residence time, as the lower number of moles of AcAd is transferred into the gas phase, as well as with the impact of excess hydrogen, which can favour the hydrogenation reaction and result in higher-than-expected conversions. For greater clarity, the effects of the different variables are summarized in Table 8.7.

Table 8.7 Pressure-related variations in residence time and feed composition.

W Catalyst (g)	T Sat (°C)	Pressure (MPa)	H_2 Flow (ml/min)	H_2 Flow (mol/min)	CO Flow (ml/min)	CO Flow (mol/min)	AcAd flow (ml/min)	AcAd flow (mol/min)	Feed Composition (mol %) H_2	Feed Composition (mol %) CO	Feed Composition (mol %) AcAd	GHSV (ml/(h g$_{cat}$))
0.1	-0.29	0.1	56.1	2.51E-03	18.7	8.35E-04	56.1	2.51E-03	43	14	43	78568
0.1	-0.29	0.2	28.1	2.51E-03	9.4	8.35E-04	10.2	9.11E-04	59	20	21	28577
0.1	-0.29	0.3	18.7	2.51E-03	6.2	8.35E-04	4.2	5.57E-04	64	21	14	17465
0.1	-0.29	0.4	14.0	2.51E-03	4.7	8.35E-04	2.2	4.01E-04	67	22	11	12575
0.1	-0.29	0.5	11.2	2.51E-03	3.7	8.35E-04	1.4	3.13E-04	69	23	9	9825

In the ensuing presentation of the results, the effect on the pressure will be discussed and an attempt to deconvolute the aforementioned parallel effects will be made by using data from thermodynamic Gibbs free energy modeling and also results discussed in the Residence Time section.

It can be seen from Fig. 8.19 and 8.20 that a combination of the three effects, i.e., increased pressure, increased residence time and an excess of H_2, had a large positive effect on both acetaldehyde conversion and ethanol selectivity. On both Cu and Cu/SiO$_2$ catalysts, conversion initially increased linearly with increasing pressure until 0.25 and 0.38 MPa respectively at which point conversion exceeded 90% and then rose only negligibly with increasing pressure. The following explanation is suggested:

1) Since the conversion is so close to unity, it is probable that system is at its thermodynamic equilibrium.

2) The surface of the catalyst may be fully saturated by adsorbed reactants and the reaction thus becomes independent of the system pressure.
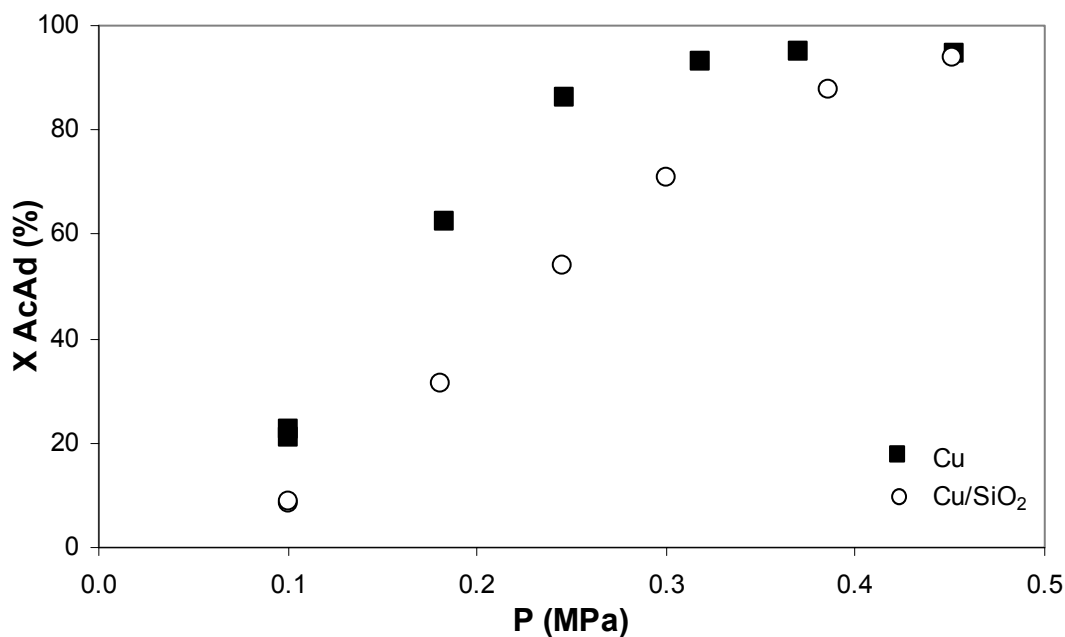
Figure 8.19 Effect of pressure on AcAd conversion on Cu and Cu/SiO_2 catalysts at 250°C and 1:1:0.33 $AcAd:H_2:CO$.

As seen in Fig. 8.20, the selectivity to ethanol initially increased with increasing pressure and then reached a plateau (Cu/SiO_2) or even went through a maximum (Cu). An initial increase is expected for the following reasons:

1) Thermodynamically, acetaldehyde hydrogenation is favourably affected by pressure as 2 moles of reactants are consumed to produce 1 mole, unlike ethyl acetate formation where reaction of 2 moles results in production of 2 moles.

2) Hydrogen, being in excess, shifts the hydrogenation equilibrium towards ethanol. On the other hand, being a by-product of ethyl acetate and butyraldehyde formation, it inhibits these reactions (see Fig. 5.1)

3) Excessive hydrogen and CO adsorb on the surface, thus competing for the active sites required for subsequent reactions and also diluting the concentration of

adsorbed ethyl and acetyl species, precursors of ethyl acetate formation, thus lowering the probability of their successful collision.

Reaching a plateau or going through maximum in Fig. 8.20 can be correlated with a diminishing effect of pressure on acetaldehyde conversion at pressures approaching 0.5 MPa and also promotion of secondary reactions at high acetaldehyde conversions.
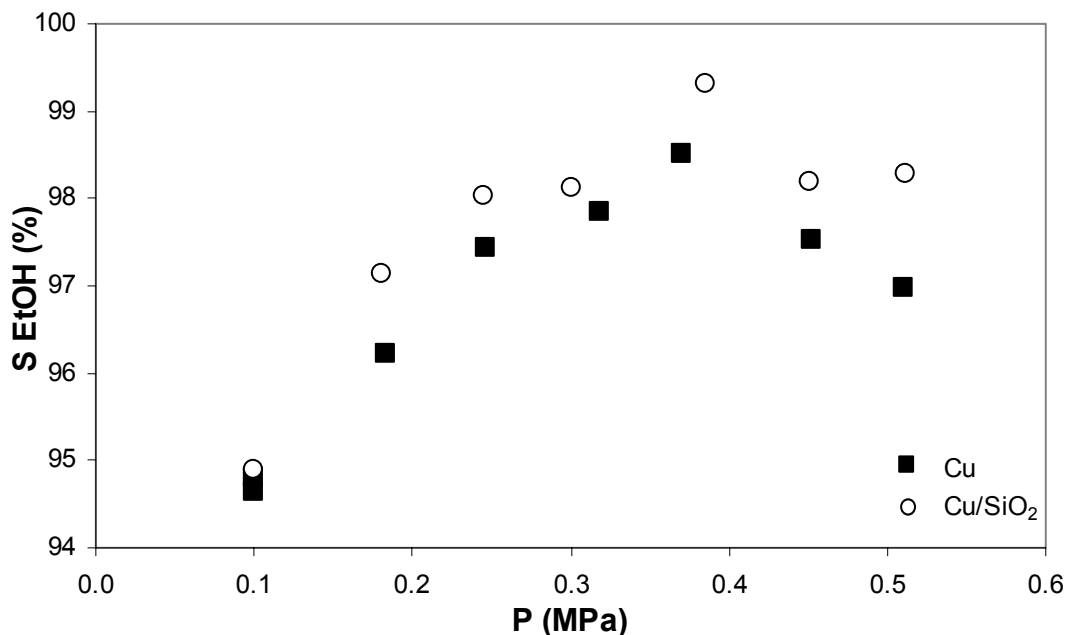
Figure 8.20 Effect of pressure on EtOH selectivity on Cu and Cu/SiO$_2$ catalysts at 250°C and 1:1:0.33 AcAd:H$_2$:CO.

After the pressure had been returned to atmospheric at the end of the experiment, no signs of deactivation were observed on either of the catalysts.

The deconvolution of the three effects is depicted in Fig. 8.21. The effect of residence time was estimated from Fig. 8.18, by fitting the data in the appropriate GHSV region with a linear model. The resulting equation was then used to estimate the expected conversion increase caused by the increase of the GHSV as a result of pressure increase. The impact of feed dilution by H$_2$ and CO was simulated in Aspen Plus process simulation software by using a Gibbs free energy minimization model of atmospheric reactor and changing the inlet flow composition. The same model, but with a constant 1:1:0.33 AcAd:H$_2$:CO feed and pressure varying from 0.1-0.5 MPa, was used for the estimation of the influence of pressure. Finally, the combined effect of feed composition

and pressure change was also simulated by the Gibbs free energy minimization model in Aspen Plus process simulation software. Each individual effect has a different potential for affecting the hydrogenation. The most significant is the residence time increase, which is expected to increase conversion by a maximum of 31% over the pressure range of 0.1-0.5 MPa. Both pressure increase and excess hydrogen can individually increase conversion by 20%; however, their combined effect results in a 36% increase at 0.5 MPa over the initial equilibrium acetaldehyde conversion obtained at 0.1 MPa. The experimental data plotted in the Fig. 8.21 suggest that the hydrogenation is not initially thermodynamically limited, but, with increasing pressure, quickly reaches equilibrium which then controls the reaction. Provided the feed composition could be maintained constantly stoichiometric, the data suggest that the reaction would still be controlled by thermodynamics at higher pressures, though the final conversion instead of being 90+% would stabilize at 80%.
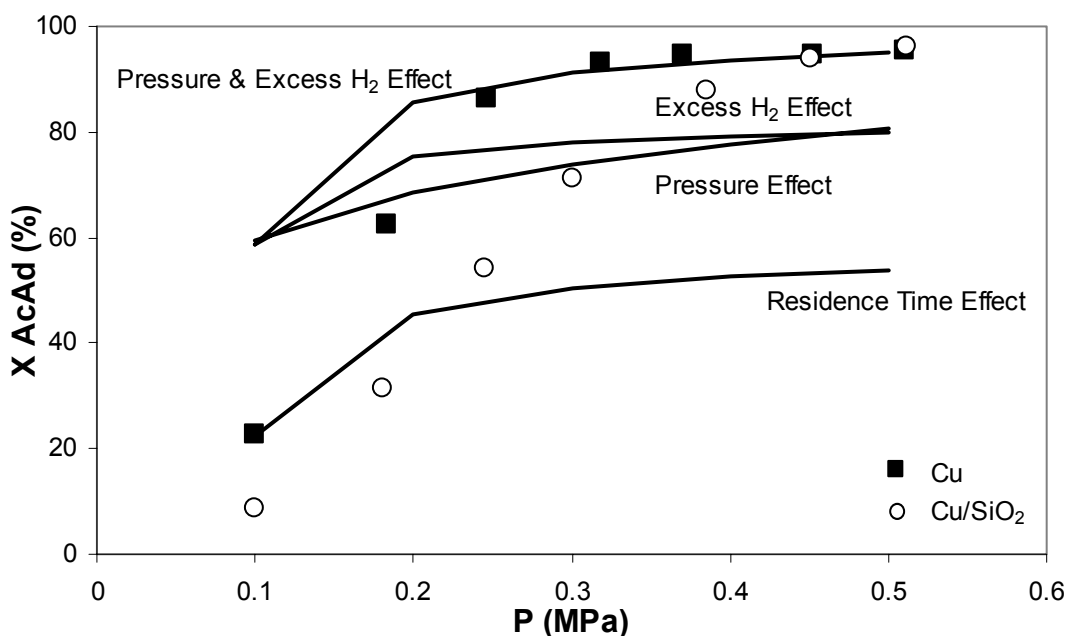
Figure 8.21 Deconvolution of the pressure, residence time and hydrogen concentration increase effects on AcAd conversion at 250°C and 1:1:0.33 AcAd:H_2:CO.

These data suggest that pressure has a significantly positive effect on the acetaldehyde conversion and possibly also on ethanol selectivity. With increasing pressure, the reaction quickly becomes thermodynamically controlled which limits

attainable conversion with stoichiometric feed to 80% at 0.5 MPa. Higher conversions, 93%+ can be achieved by increasing both hydrogen content and residence time.

Hydrogenation kinetics

Kinetic experiments were carried out in order to gain further insight into the reaction mechanism by determination of the reaction order and calculation of frequency factors and activation energies for both catalysts. Acetaldehyde hydrogenation kinetics were studied by accounting for the effects of residence time, which was varied at four levels by changing the loading of the catalyst (0.1, 0.25, 0.5, and 0.75 g), and the effect of temperature (4 levels: 200, 222, 243, and 265°C). An $AcAd:H_2:CO$ mixture at a molar ratio 1:1:0.33 and a constant flow rate of $5.846 \cdot 10^{-3}$ mol min^{-1} was used as a feed. Since the acetaldehyde conversion was higher than 10%, an integral tubular reactor model was used, which was modeled as:

$$\frac{W}{\dot{V}} = \int_{Ca_0}^{Ca} \frac{dCa}{-r}$$

where, $\dot{V}$ is a total inlet gas flow rate and $-r$ is a rate of disappearance of acetaldehyde per unit mass of catalyst. Assuming

1) a second order reaction with stoichiometric amount of reactants:

$$-r = kC_{AcAd}C_{H_2} = kC_{AcAd}^2 = kCa^2$$

where, k is the reaction rate constant, and

2) isothermal and isobaric conditions in the catalyst bed and substituting:

$$Ca = Ca_0 \left(\frac{1-X}{1+\varepsilon X} \right)$$

where ε takes into account the contraction of the gas mixture due to a decrease in the number of moles (Fogler, 1999), the final equation can be obtained by integration as:

$$\frac{1+\varepsilon X}{1-X} - 1 = kCa_0 \frac{W}{\dot{V}} .$$

By plotting $\dfrac{1+\varepsilon X}{1-X}-1$ against $Ca_0 \dfrac{W}{\dot{V}}$ the reaction rate constant, k, can be obtained from the slopes of the linear lines of best fit. The results, shown in Fig. 8.22, suggest that the 2nd order reaction assumption is valid over the whole temperature range studied. However, the model lost some of its goodness of fit at the highest temperature studied when combined with the high residence time, because the secondary and reverse reactions became more dominant.
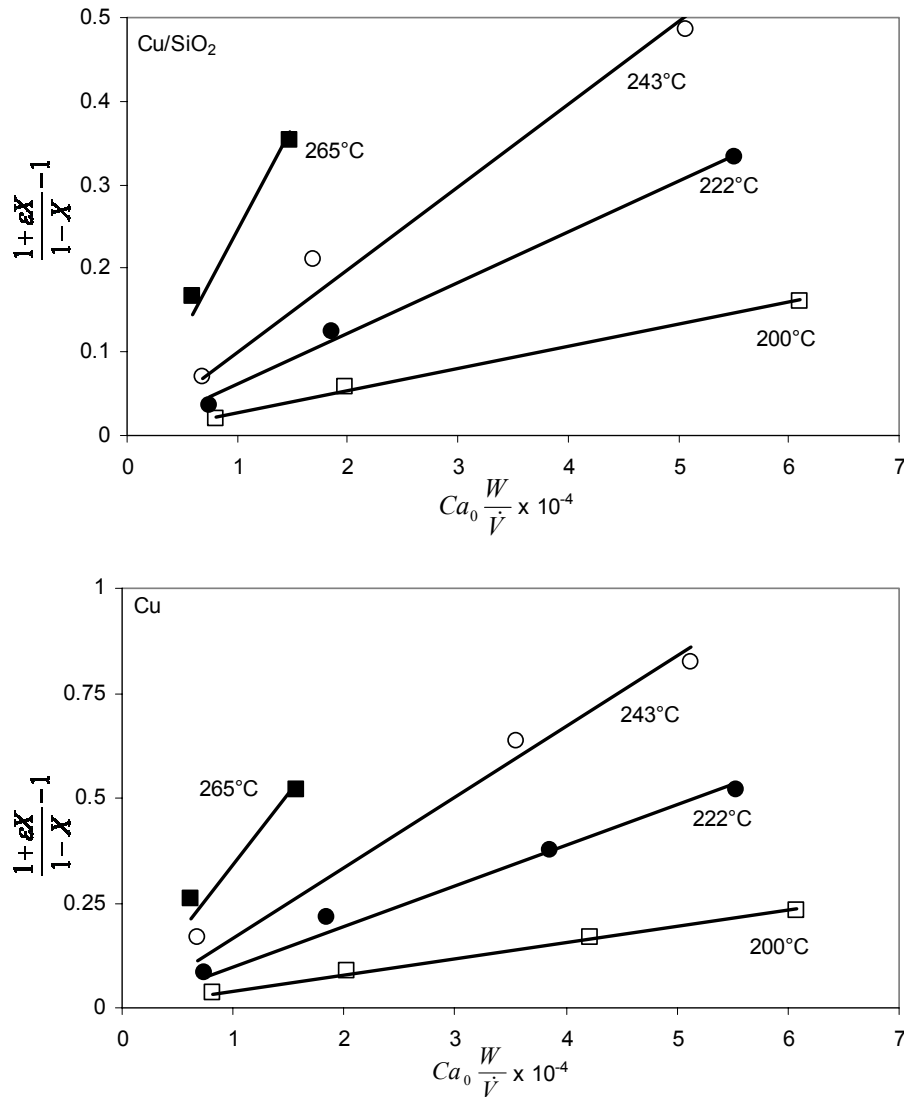
Figure 8.22 Determination of hydrogenation rate constants at 0.1 MPa and 1:1:0.33 AcAd:H_2:CO.

153

The reaction rate constants were calculated from the slopes of the lines of best fit and the values from the complete temperature range 200-265°C were used to obtain activation energies and frequency factors according to the Arrhenius equation:

$$k_T = A \exp^{\frac{-E_a}{RT}}$$

The equation was linearized and from the plot of *ln(k)* against $\dfrac{1}{RT}$, depicted in Fig. 8.23, the activation energies and frequency factors were obtained as slopes and intercepts respectively. Their values are listed together with the reaction rate constants in Table 8.8.
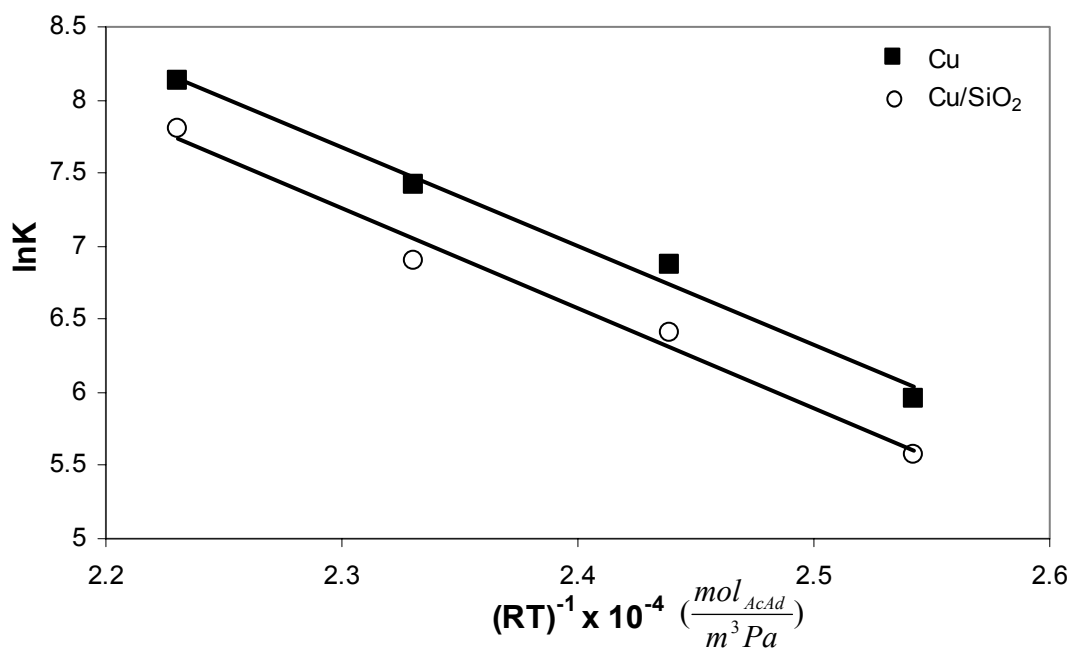
Figure 8.23 Determination of frequency factors and activation energies at 0.1 MPa and 1:1:0.33 AcAd:H_2:CO.

Table 8.8 Acetaldehyde hydrogenation rate constants, frequency factors and activation energies.

Catalyst	Temperature (°C)	k $(L^2 mol_{AcAd}^{-1} g_{cat}^{-1} h^{-1})$	A	Ea $(kJ\ mol^{-1})$
Cu/SiO$_2$	200	265	9.9E+09	68.5
	222	609		
	243	989		
	265	2447		
Cu	200	388	1.8E+10	69.4
	222	969		
	243	1674		
	265	3409		

The reaction rate constants in Table 8.8, confirm that Cu is a more active catalyst than Cu/SiO$_2$. However, hydrogenation on both catalysts has virtually identical activation energy and differs only slightly in frequency factor. This suggests that acetaldehyde hydrogenation is occurring selectively on copper sites, of which unsupported copper has apparently a larger exposed quantity, and is independent of the support or promoter. The kinetic studies thus support the rejection of promoters as was done during the catalyst screening study: since reaction is occurring exclusively on copper sites, promoters are at best superfluous and at worst can have a detrimental effect by blocking these sites.

8.4 Conclusions

Acetaldehyde hydrogenation has been studied over various copper-containing catalysts.Fe and Zn were tested as promoters of both unsupported Cu catalysts and SiO$_2$-supported catalysts. All catalyst were characterized by TGA, BET and TPR and found to have rather similar copper surface areas, in the range of 10-20 m^2 g$_{cat}^{-1}$.

The screening study, which investigated the effect of Fe and Zn addition on acetaldehyde conversion and ethanol selectivity on both catalyst types (unsupported and SiO$_2$-supported), found no beneficial effects of the promoters. Therefore unpromoted Cu and Cu/SiO$_2$ were selected as the best candidates from each group. The negative or negligible impact of the promoters was explained by kinetic experiments which resulted in very similar values of activation energies and frequency factors for both non-promoted catalysts, indicating that hydrogenation is taking place exclusively on the copper sites.

Consequently, the inert support, such as SiO_2, also does not affect a major reaction, but can lower the cost of the catalyst by using $1/5^{th}$ of the amount of copper needed to achieve the same results as unsupported copper. Furthermore, the large surface area of the support can, in some cases, serve as extra adsorption storage capacity for reactants.

Acetaldehyde hydrogenation was positively affected by temperature; however both copper catalysts showed significant deactivation at temperatures higher than 250°C. The limiting temperature affects the maximum attainable conversion. This hindrance can be partially overcome by increasing the residence time. The increase in conversion thus achieved was nevertheless offset by a decrease in ethanol selectivity, because secondary subsequent reactions, such as ethyl acetate and C_4-aldehydes formation, become more dominant. Acetaldehyde conversion can be better improved by increasing the operating pressure, which also positively affects the ethanol selectivity. At elevated pressures, the hydrogenation reaction may become limited by thermodynamics, allowing for 80% conversion at 250°C and 5 MPa. A further increase would then only be possible by shifting the thermodynamic equilibrium, e.g., by feeding H_2 in excess.

While CO acted as an inert, as confirmed by its substitution for N_2, on the unsupported Cu, it blocked some active sites on Cu/SiO_2, thus lowering the attainable conversion. This blockage was observed both in a screening study conducted at 250°C and in a stability experiment carried out at 280°C. CO nevertheless did not affect the stability of the catalyst. H_2O, on the other hand, improved stability of both catalysts possibly by maintaining the equilibrium of Cu^0/Cu^+ ions on the surface. The higher stability was unfortunately offset by lower conversion, caused by competition of H_2O molecules for active sites. Co-feeding ethanol, even at a low concentration of 10 mol. %, caused 30 and 50% losses of conversion on Cu/SiO_2 and Cu catalysts respectively. Since the hydrogenation reaction is a part of a separation loop process, these findings necessitate the implementation of purification of the AcAd stream leaving the ethanol dehydrogenation reactor.

Overall, the results prove that acetaldehyde hydrogenation can viably complement ethanol dehydrogenation as a part of the proposed novel catalytic separation process for the production of elevated-pressure, high-purity hydrogen from syngas.

Chapter 9: Conclusions and recommendations

A novel catalytic process for separation of pure hydrogen from synthesis gas was proposed and investigated and the following conclusions were drawn:

9.1 Conclusions

1) A loop process consisting of two complementary reactions, ethanol dehydrogenation and acetaldehyde hydrogenation by syngas, is a technologically viable option for production of high-purity elevated-pressure hydrogen.

2) Copper was identified as a promising active metal component of catalyst systems for both reactions.

3) Neither dehydrogenation nor hydrogenation achieved 100% conversion under the reaction conditions investigated. Furthermore, although the selectivity to the major product, acetaldehyde and ethanol respectively, reached 90%+, undesired by-products, of which ethyl acetate was the predominant, were produced. It will therefore be necessary to incorporate separation processes, such as fractionation, between the steps.

Specifically, for ethanol dehydrogenation:

4) Unsupported copper foam performed poorly because of its low surface area.

5) Out of three selected supported catalysts, Cu/SiO_2 provided the highest conversion and highest hydrogen productivity and was therefore identified as the best catalyst of this set. Its superiority can be related to the inertness and high surface area of SiO_2.

6) The effect of reaction conditions can be summarized as:

- The reaction temperature is limited to below 300°C because of copper sintering.

- Ethanol conversion is independent of pressure (Cu/MO, Cu/K-Al$_2$O$_3$) or slightly decreases with increasing pressure (Cu/SiO$_2$) in the range 0.1-0.5 MPa but selectivity to acetaldehyde decreases with increasing pressure in favour of ethyl acetate.

- Increasing the residence time results in increased conversion, but also in decreased acetaldehyde selectivity in favour of ethyl acetate.

- The small addition of water (EtOH/H$_2$O < 1) improves catalyst stability and acetaldehyde selectivity. The presence of acetaldehyde in the feed lowers ethanol conversion.

7) In the temperature range 200-250°C dehydrogenation follows first order kinetics with an activation energy of 55 kJ mol^{-1} for Cu/SiO$_2$.

For acetaldehyde hydrogenation:

8) Unsupported copper prepared by precipitation was identified as the best catalyst, followed by Cu/SiO$_2$. Addition of Zn or Fe as promoters was superfluous or detrimental to the reaction outcome.

9) The effect of reaction conditions can be summarized as:
   - The reaction temperature is limited to 250°C because of catalyst deactivation.
   - Acetaldehyde conversion and ethanol selectivity are enhanced by increasing pressure.
   - Increasing the residence time increased acetaldehyde conversion, but decreased ethanol selectivity in favour of ethyl acetate.
   - CO acts as an inert on unsupported Cu, but lowers the attainable conversion on Cu/SiO$_2$. The addition of water (AcAd/H$_2$O>1) improves catalyst stability, but decreases acetaldehyde conversion. The presence of even small amounts of ethanol in the feed significantly lowers acetaldehyde conversions.

10) Acetaldehyde hydrogenation follows overall second order reaction kinetics in the temperature range 200-265°C. The activation energy of 69 kJ mol^{-1} is virtually identical for both supported and unsupported catalysts, indicating the occurrence of hydrogenation solely on copper sites.

9.2 Recommendations

For successful implementation of this catalytic separation process on an industrial scale, the following issues will need to be addressed in future work:

1) Separation of main and secondary products in each step and the recycle of unconverted reactants.

2) Improving thermal stability of copper catalysts, by its incorporation into the support lattice, in order to increase attainable conversion and therefore reduce separation requirements.

3) Optimization of heat management for the whole process; most importantly the design of the reactor, which would allow direct recuperation of heat from the exothermic portion of the cycle to the endothermic one.

4) Determination of the effect of impurities present in syngas, such as sulfur oxides or metal carbonyls, on catalyst performance.

5) Study of the catalyst performance under pressures higher than 0.5 MPa.

6) Examining the possibility of catalyst reactivation by oxidation, as seen in copper foam experiments.

7) Global optimization and cost analysis of the complete cycle from economic point of view.

Nomenclature

Roman letters

a	normalized activity (dimensionless)
a_i	number of carbon atoms in any product species divided by the number of carbon atoms contained in an AcAd/EtOH molecule (dimensionless)
A	frequency factor (units depending on order of reaction)
A_x	cross sectional area (m^2)
bi	number of carbon atoms in a particular product (dimensionless)
C	molar concentration (mol m^{-3})
Cp	heat capacity (J kg^{-1} K^{-1})
d	pore diameter (m)
d_p	particle diameter (m)
D_{AB}	bulk diffusivity (m^2 s^{-1})
D_e	effective diffusivity (m^2 s^{-1})
D_K	Knudsen diffusivity (m^2 s^{-1})
E_a	activation energy (J mol^{-1})
FM	flow meter
g_c	conversion factor (1 kg m N^{-1} s^{-2})
G	mass velocity (kg s^{-1})
$GHSV$	gas hourly space velocity (mL h^{-1} g_{cat}^{-1})
h	heat transfer coefficient (W m^{-2} K^{-1})
ΔH	heat of reaction (J mol^{-1})
j_D	mass transfer factor (dimensionless)
j_H	heat transfer factor (dimensionless)
k	reaction rate constant (units depending on order of reaction)
k_c	external mass transfer coefficient (m s^{-1})
K_B	Boltzmann constant (J K^{-1})
Δm	change in weight (g)
M	molecular mass (g mol^{-1})
MFC	mass flow controller
$\dot{n}$	molar flow rate (mol min^{-1})
P	pressure (Pa)
P_{H2}	hydrogen productivity (mol h^{-1} g_{cat}^{-1})
PI	pressure indicator
PT	pressure transducer
r	reaction rate (mol m^{-3} s^{-1})
r_{AB}	molecular radius (m)
R	ideal gas law constant (8.314 Pa m^3 mol^{-1} K^{-1})
S	selectivity (% or dimensionless)
t	time (s)
T	temperature (°K or °C)
TIC	temperature indicator and control
TOF	turnover frequency (s^{-1})
TT	temperature transducer

v	gas velocity (m s^{-1})
$\dot{V}$	volumetric flow rate (m^3 min^{-1})
W	catalyst weight (g)
X	conversion (% or dimensionless)
y	molar fraction
Y	yield (dimensionless)

Greek letters

ε	correction factor for expansion/contraction of the gas mixture due to a change in the number of moles during reaction (dimensionless)
ε_{AB}	energy of molecular attraction (J)
λ	heat conductivity (W m^{-1} K^{-1})
μ_i	dynamic viscosity (Pa s)
υ	kinematic viscosity (m$^2 \cdot$s^{-1})
ρ	density (kg m^{-3})
Φ_P	pellet porosity (dimensionless)
σ	constriction factor (dimensionless)
$\tilde{\tau}$	tortuosity (dimensionless)

General indexes

i	pertaining to species i
0	initial

List of references

Aberuagba,F., Kumar,M., Gupta,J.K., Muralidhar,G. & Sharma,L.D. Preparation and characterization of MgO/Al$_2$O$_3$ mixed oxides support for hydrotreating catalysts. *Reaction Kinetics and Catalysis Letters* **75**, 245-250 (2002).

Abu-Zied,B.M. & El Awad,A.M. The synergism of cadmium on the catalytic activity of Cd–Cr–O system. *Journal of Molecular Catalysis A: Chemical* **176**, 227-246 (2001).

Agarwal,A.K., Wainwright,M.S., Trimm,D.L. & Cant,N.W. Acetaldehyde hydrogenation over a Cu/SiO$_2$ catalyst. *Journal of Molecular Catalysis* **45**, 247-254 (1988).

Alcala,R., Shabaker,J.W., Huber,G.W., Sanchez-Castillo,M.A. & Dumesic,J.A. Experimental and DFT studies of the conversion of ethanol and acetic acid on PtSn-based catalysts. *Journal of Physical Chemistry B* **109**, 2074-2085 (2005).

Alejandre,A., Medina,F., Salagre,P., Correig,X. & Sueiras,J.E. Preparation and study of Cu-Al mixed oxides via hydrotalcite-like precursors. *Chemistry of Materials.* **11**, 939-948 (1999).

Alexander,C.S. & Pritchard,J. Chemisorption of hydrogen on evaporated copper films. *Journal of the Chemical Society, Faraday Transactions 1: Physical Chemistry in Condensed Phases* **68**, 202-215 (1972).

Anderson,J.B. A criterion for isothermal behaviour of a catalyst pellet. *Chemical Engineering Science* **18**, 147-148 (1963).

Arimitu,S., Tanaka,K. & Saito,T. Progress in C1 Chemistry in Japan. Yoneda,Y. (ed.), pp. 143-201 (Kodanscha Ltd., Elsevier, Tokyo,1989).

Armstrong,E.F. & Hilditch,T.P. A study of catalytic action at solid surfaces. III. the hydrogenation of acetaldehyde and the dehydrogenation of ethyl alcohol in presence of finely-divided metals. *Proceedings of the Royal Society of London.Series A, Containing Papers of a Methematical and Physical Character* **97,** 259-264 (1920).

Baram,J. Heat transfer characteristics in centrifuge melt-spinning. *Journal of Materials Science* **23**, 3656-3659 (1988).

Benitez,J.J., Carrizosa,I. & Odriozola,J.A. Diffuse reflectance FT-IR characterization of active sites under reaction conditions: the production of oxygenates in the CO/H2 reaction . *Applied Spectroscopy* **48**, 1208-1212 (1994).

Bond,G.C. Catalysis by Metals., pp. 407-436 (Academic Press Inc. (London) Ltd., London,1962).

Bond,G.C. & Namijo,S.N. An improved procedure for estimating the metal surface area of supported copper catalysts. *Journal of Catalysis* **118**, 507-510 (1989).

Burch,R. & Petch,M.I. Investigation of the reactions of acetaldehyde on promoted rhodium catalysts. *Applied Catalysis A: General* **88**, 61-76 (1992a).

Burch,R. & Petch,M.I. Investigation of the synthesis of oxygenates from carbon monoxide/hydrogen mixtures on supported rhodium catalysts. *Applied Catalysis A: General* **88**, 39-60 (1992b).

Burch,R. & Hayes,M.J. The preparation and characterisation of Fe-Promoted Al$_2$O$_3$-Supported Rh catalysts for the selective production of ethanol from syngas. *Journal of Catalysis* **165**, 249-261 (1997).

Carlos-Cuellar,S., Li,P., Christensen,A.P., Krueger,B.J., Burrichter,C.& Grassian,V.H. Heterogeneous uptake kinetics of volatile organic compounds on oxide surfaces using a Knudsen cell reactor: Adsorption of acetic acid, formaldehyde, and methanol on Fe_2O_3, Al_2O_3 and SiO_2. *Journal of Physical Chemistry A* **107**, 4250-4261 (2003).

Chang,F.W., Kuo,W.Y. & Lee,K.C. Dehydrogenation of ethanol over copper catalysts on rice husk ash prepared by incipient wetness impregnation. *Applied Catalysis A: General* **246**, 253-264 (2003).

Chang,F.W., Yang,H.C., Roselin,L.S. & Kuo,W.Y. Ethanol dehydrogenation over copper catalysts on rice husk ash prepared by ion exchange. *Applied Catalysis A: General* **304**, 30-39 (2006).

Chen,S.P. & Voter,A.F. Reconstruction of the (310), (210) and (110) surfaces in fcc metals. *Surface Science* **244**, L107-L112 (1991).

Chin,P., Sun,X., Roberts,G.W. & Spivey,J.J. Preferential oxidation of carbon monoxide with iron-promoted platinum catalysts supported on metal foams. *Applied Catalysis A: General* **302**, 22-31 (2006).

Chladek,P., Coleman,L.J.I., Croiset,E. & Hudgins,R.R. Gas chromatography method for the characterization of ethanol steam reforming products. *Journal of Chromatographic Science* **45**, 153-157 (2007a).

Chladek,P., Croiset,E., Epling,W. & Hudgins,R.R. Characterization of copper foam as catalytic material in ethanol dehydrogenation. *Canadian Journal of Chemical Engineering* (2007b). *In Press.*

Chuang,S.S.C., Pien,S., Ghosal,K., Soong,Y., Noceti,R.P. & Schehl,R.R. Carbon monoxide hydrogenation over Na-Mn-Ni catalysts: Effects of catalyst preparation methods on the C2+ oxygenate selectivity. *Applied Catalysis* **70**, 101-114 (1991).

Chung,M.J., Han,S.H., Park,K.Y. & Ihm,S.K. Differing characteristics of Cu and ZnO in dehydrogenation of ethanol: A deuterium exchange study. *Journal of Molecular Catalysis* **79**, 335-345 (1993).

Church,J.M. & Joshi,H.K. Acetaldehyde by dehydrogenation of ethyl alcohol. *Industrial and Engineering Chemistry* **43**, 1804-1811 (1951).

Colley,S.W., Tabatabaei,J., Waugh,K.C. & Wood,M.A. The detailed kinetics and mechanism of ethyl ethanoate synthesis over a Cu/Cr_2O_3 catalyst. *Journal of Catalysis* **236**, 21-33 (2005).

Davidson,J.M., McGregor,C.M. & Doraiswamy,L.K. Kinetics of the palladium-catalyzed vapor-phase thermal decomposition of ethanol . *Industrial and Engineering Chemistry Research* **40** , 101-107 (2001a).

Davidson,J.M., McGregor,C.M. & Doraiswamy,L.K. Mechanism of palladium-catalyzed decomposition of ethanol-a comparison of chemical kinetic and surface science studies. *Industrial and Engineering Chemistry Research* **40**, 108-113 (2001b).

Davy,H. Some new experiments and observations on the combustion of gaseous mixtures, with an account of a method of preserving a continued light in mixtures of inflammable gases and air without flame. *Philosophical Transactions of the Royal Society of London (1776-1886)* **107**, 77-85. (1817).

Deng,J., Cao,Z. & Zhou,B. Catalytic dehydrogenation of ethanol in a metal-modified alumina membrane reactor. *Applied Catalysis A: General* **132**, 9-20 (1995).

Deng,J. & Wu,J. Formaldehyde production by catalytic dehydrogenation of methanol in inorganic membrane reactors. *Applied Catalysis A: General* **109**, 63-76 (1994).

Di Cosimo,J.I., Díez,V.K., Xu,M., Iglesia,E. & Apesteguía,C.R. Structure and surface and catalytic properties of Mg-Al basic oxides. *Journal of Catalysis* **178**, 499-510 (1998).

Ehwald,H., Ewald,H., Gutschick,D., Hermann,M., Miessner,H., Ohlmann,G. & Schierhorn,E. A bicomponent catalyst for the selective formation of ethanol from synthesis gas. *Applied Catalysis* **76**, 153-169 (1991).

Fogler,H.S. Elements of Chemical Reaction Engineering. Prentice Hall, New Jersey (1999).

Franckaerts,J. & Froment,G.F. Kinetic study of the dehydrogenation of ethanol. *Chemical Engineering Science* **19**, 807-818 (1964).

Freni,S., Mondello,N., Cavallaro,S., Cacciola,G., Parmon,V.N. & Sobyanin,V.A. Hydrogen production by steam reforming of ethanol: A Two Step Process. *Reaction Kinetics and Catalysis Letters* **71**, 143-152 (2000).

Froment,G.F. & Bischoff,K.B. Chemical Reactor Analysis and Design. Wiley, New York (1979).

Fujita,S.I., Iwasa,N., Tani,H., Nomura,W., Arai,M. & Takezawa,N. Dehydrogenation of ethanol over Cu/ZnO catalysts prepared from various coprecipitated precursors. *Reaction Kinetics and Catalysis Letters* **73**, 367-372 (2001).

Giani,L., Cristiani,C., Groppi,G. & Tronconi,E. Washcoating method for Pd/γ-Al$_2$O$_3$ deposition on metallic foams. *Applied Catalysis B: Environmental* **62**, 121-131 (2006).

Gole,J.L. & White,M.G. Supported catalysts prepared from mononuclear copper complexes: Catalytic properties. *Journal of Catalysis* **135**, 81-91 (1992).

Guglielminotti,E., Giamello,E., Pinna,F., Strukul,G., Martinengo,S. & Zanderighi,L. Elementary steps in CO hydrogenation on Rh catalysts supported on ZrO$_2$ and Mo/ZrO$_2$. *Journal of Catalysis* **146**, 422-436 (1994).

Guglielminotti,E., Pinna,F., Rigoni,M., Strukul,G. & Zanderighi,L. The effect of iron on the activity and the selectivity of Rh/ZrO$_2$ catalysts in the CO hydrogenation. *Journal of Molecular Catalysis A: Chemical* **103**, 105-116 (1995).

Herman,R.G., Klier,K., Simmons,G.W., Finn,B.P., Bulko,J.B. & Kobylinski,T.P. Catalytic synthesis of methanol from CO/H2 I. Phase composition, electronic properties, and activities of the Cu/ZnO/M$_2$O$_3$ catalysts. *Journal of Catalysis* **56**, 407-429 (1979).

Hindermann,J.P., Hutchings,G.J. & Kiennemann,A. Mechanistic aspects of the formation of hydrocarbons and alcohols from CO hydrogenation. *Catalysis Reviews: Science and Engineering* **35**, 1-127 (1993).

Hudgins,R.R. A general criterion for the absence of diffusion control in an isothermal catalyst pellet. *Chemical Engineering Science* **23**, 93-94 (1968).

Hudgins,R.R. A general criterion for avoiding film diffusion control in heterogeneous catalytic reactions. *Canadian Journal of Chemical Engineering* **50**, 427-430 (1972).

Idriss,H., Diagne,C., Hindermann,J.P., Kiennemann,A. & Barteau,M.A. Effect of addition of Pd,Co and Pd-Co on CeO$_2$. Syngas conversion and acetaldehyde reaction. 2119-2122. 1992. Elsevier Science. New Frontiers in Catalysis. Guczi, L. 19-6-1992.

Idriss,H., Diagne,C., Hindermann,J.P., Kiennemann,A. & Barteau,M.A. Reactions of acetaldehyde on CeO_2 and CeO_2-supported catalysts. *Journal of Catalysis* **155**, 219-237 (1995).

Inui,K., Kurabayashi,T. & Sato,S. Direct synthesis of ethyl acetate from ethanol over Cu-Zn-Zr-Al-O catalyst. *Applied Catalysis A: General* **237**, 53-61 (2002).

Inui,K., Kurabayashi,T., Sato,S. & Ichikawa,N. Effective formation of ethyl acetate from ethanol over Cu-Zn-Zr-Al-O catalyst. *Journal of Molecular Catalysis A: Chemical* **216**, 147-156 (2004).

Iwasa,N. & Takezawa,N. Reforming of ethanol - dehydrogenation to ethyl acetate and steam reforming to acetic acid over copper-based catalysts -. *Bulletin of the Chemical Society of Japan* **64**, 2619-2623 (1991).

Juan-Juan,J., Roman-Martinez,M.C. & Illan-Gomez,M.J. Effect of potassium content in the activity of K-promoted Ni/Al_2O_3 catalysts for the dry reforming of methane. *Applied Catalysis A: General* **301**, 9-15 (2006).

Kanoun,N., Astier,M.P. & Pajonk,G.M. New vanadium-copper-zinc catalysts, their characterization and use in the catalytic dehydrogenation of ethanol. *Applied Catalysis* **70**, 225-236 (1991a).

Kanoun,N., Astier,M.P. & Pajonk,G.M. Selective dehydrogenation of ethanol over Cu catalysts containing Zr or V and Zr . *Reaction Kinetics and Catalysis Letters* **44**, 51-56 (1991b).

Kanoun,N., Astier,M.P. & Pajonk,G.M. Dehydrogenation of ethanol and CO_2-H_2 conversion on new coprecitated Cu/Cr-Al catalysts. *Journal of Molecular Catalysis* **79**, 217-228 (1993).

Kazanskii,V.B. Spectroscopic study of the state of the surface ions of transition metals in deposited oxide catalysts and formation of surface complexes with chemisorption. *Kinetika i Kataliz* **11**, 455-466 (1970).

Kenvin,J.C. & White,M.G. Supported catalysts prepared from mononuclear copper complexes: Catalytic properties. *Journal of Catalysis* **135**, 81-91 (1992).

Kiseleva,L.A, Ogorodova,L.P., Melchakova,L.V., Bisengalieva,M.R. & Becturbanov,N.S. Thermodynamic properties of copper carbonates – malachite $Cu_2(OH)_2CO_3$ and azurite $Cu_3(OH)_2(CO_3)_2$. *Physics and Chemistry of Materials* **19**, 322-333 (1992).

Lee,G. & Ponec,V. On some problems of selectivity in syngas reactions on the group VIII metals. *Catalysis Reviews: Science and Engineering* **29**, 183-218 (1987).

Lin,W.H. & Chang,H.F. A study of ethanol dehydrogenation reaction in a palladium membrane reactor. *Catalysis Today* **97**, 181-188 (2004).

Liu,B., Cao,Y. & Deng,J. Catalytic dehydrogenation of ethanol in Ru-modified alumina membrane reactor . *Separation Science and Technology* **32**, 1683-1697 (1997).

Lvov,B.V. & Novichikhin,A.V. Mechanism of thermal decomposition of hydrated copper nitrate in vacuo. *Spectrochimica Acta B* **50**, 1459-1468 (1995).

Marino,F., Boveri,M., Baronetti,G. & Laborde,M. Hydrogen production via catalytic gasification of ethanol. A mechanism proposal over copper-nickel catalysts. *International Journal of Hydrogen Energy* **29**, 67-71 (2004).

Mears,D.E. Diagnostic criteria for heat transport limitations in fixed bed reactors. *Journal of Catalysis* **20**, 127 (1971).

Morgenstern,D.A. & Fornango,J.P. Low-temperature reforming of ethanol over copper-plated raney nickel: A new route to sustainable hydrogen for transportation. *Energy and Fuels* **19**, 1708-1716 (2005).

Mu,J. & Perlmutter,D.D. Thermal decomposition of carbonates, carboxylates, oxalates, acetates, formats, and hydroxides. *Thermochimica Acta* **49,** 207-218 (1981).

Nishiguchi,T., Matsumoto,T., Kanai,H., Utani,K., Matsumura,Y., Shen,W.J. & Imamura,S. Catalytic steam reforming of ethanol to produce hydrogen and acetone. *Applied Catalysis A: General* **279**, 273-277 (2005).

Ojeda,M., Granados,M.L., Rojas,S., Terreros,P., García-García,F.J.& Fierro,J.L. Manganese-promoted Rh/Al$_2$O$_3$ for C2-oxygenates synthesis from syngas. *Applied Catalysis A: General* **261**, 47-55 (2004).

Peloso,A., Moresi,M., Mustachi,C. & Soracco,B. Kinetics of the dehydrogenation of ethanol to acetaldehyde on unsupported catalysts . *Canadian Journal of Chemical Engineering* **57**, 159-164 (1979).

Pestryakov,A.N., Fyodorov,A.A. & Shurov,V.A. Foam metal catalysts with intermediate support for deep oxidation of hydrocarbons. *Reaction Kinetics and Catalysis Letters* **53**, 347-352 (1994).

Pestryakov,A.N., Fyodorov,A.A., Gaisinovich,M.S., Shurov,V.P., Fyodorova,I.V.& Gubaydulina,T.A. Metal-form catalysts with supported active phase for deep oxidation of hydrocarbons. *Reaction Kinetics and Catalysis Letters* **54**, 167-172 (1995).

Pestryakov,A.N., Yurchenko,E.N. & Feofilov,A.E. Foam-metal catalysts for purification of waste gases and neutralization of automotive emissions. *Catalysis Today* **29**, 67-70 (1996).

Pestryakov,A.N., Lunin,V.V., Devochkin,A.N., Petrov,L.A., Bogdanchikova,N.E.& Petranovskii,V.P. Selective oxidation of alcohols over foam-metal catalysts. *Applied Catalysis A: General* **227**, 125-130 (2002).

Pestryakov,A.N., Lunin,V.V., Bogdanchikova,N.E., Petranovskii,V.P. & Knop-Gericke,A. Supported foam-silver catalysts for alcohol partial oxidation. *Catalysis Communications* **4**, 327-331 (2003).

Ponec,V. Cu and Pd, two catalysts for CH$_3$OH synthesis: the similarities and the differences. *Surface Science* **272**, 111-117 (1992a).

Ponec,V. Active centres for synthesis gas reactions. *Catalysis Today* **12**, 227-254 (1992b).

Raich,B.A. & Foley,H.C. Ethanol dehydrogenation with a palladium membrane reactor: An alternative to Wacker chemistry. *Industrial and Engineering Chemistry Research* **37**, 3888-3895 (1998).

Rasko,J. & Kiss,J. Adsorption and surface reactions of acetaldehyde on TiO$_2$, CeO$_2$ and Al$_2$O$_3$. *Applied Catalysis A: General* **287**, 252-260 (2005a).

Rasko,J. & Kiss,J. Adsorption and surface reactions of acetaldehyde on alumina-supported noble metal catalysts. *Catalysis Letters* **101**, 71-77 (2005b).

Rieder,K.H. & Stocker,W. Hydrogen-induced subsurface reconstruction of Cu(110). *Physical Review Letters* **57**, 2548 (1986).

Shamsi,A. & Spivey,J.J. Partial oxidation of methane on Ni-MgO catalysts supported on metal foams. *Industrial and Engineering Chemistry Research* **44**, 7298-7305 (2005).

Shen,J., Cortright,R.D., Chen,Y. & Dumesic,J.A. Microcalorimetric and infrared spectroscopic studies of γ-Al$_2$O$_3$ modified by basic metal oxides. *Journal of Physical Chemistry* **98**, 8067-8073 (1994).

Sheng,P.Y., Bowmaker,G.A. & Idriss,H. The reactions of ethanol over Au/CeO₂. *Applied Catalysis A: General* **261**, 171-181 (2004).

Shiau,C.-Y. & Chen,T.-W. Kinetics of catalytic dehydrogenation of ethanol over copper-chromia catalyst . *Journal of the Chinese Institute of Chemical Engineers* **32**, 141-147 (1991).

Sirijaruphan,A., Goodwin,Jr, Rice,R.W., Wei,D., Butcher,K.R., Roberts,G.W. & Spivey,J.J. Metal foam supported Pt catalysts for the selective oxidation of CO in hydrogen. *Applied Catalysis A: General* **281**, 1-9 (2005a).

Sirijaruphan,A., Goodwin,Jr, Rice,R.W., Wei,D., Butcher,K.R., Roberts,G.W. & Spivey,J.J. Effect of metal foam supports on the selective oxidation of CO on Fe-promoted Pt/γ-Al₂O₃. *Applied Catalysis A: General* **281**, 11-18 (2005b).

Snoeck,J.W., Froment,G.F. & Fowles,M. Steam/CO₂ reforming of methane. carbon formation and gasification on catalysts with various potassium contents. *Industrial and Engineering Chemistry Research* **41**, 3548-3556 (2002).

Sodesawa,T. Dynamic change in surface area of Cu in dehydrogenation of methanol over Cu-SiO₂ catalyst prepared by ion exchange method. *Reaction Kinetics and Catalysis Letters* **24**, 259-266 (1984).

Spitzl,R., Niehus,H. & Comsa,G. Structure investigation of the nitrogen induced Cu(110)-(2 x 3) phase with 180° low energy impact collision ion scattering spectroscopy. *Surface Science* **250**, L355-L362 (1991).

Szymanski,G.S., Rychlicki,G. & Terzyk,A.P. Catalytic conversion of ethanol on carbon catalysts. *Carbon* **32**, 265-271 (1994).

Takenaka,S., Yamada,C., Kaburagi,T. & Otsuka,K. Storage and supply of hydrogen mediated by iron oxide: modification of iron oxides. Gaigneux, E., De Vos, D. E., Grange, P., Jacobs, P. A., Martens, J. A., Ruiz, P., and Poncelet, G. 143(1), 795-802. 2002. Amsterdam, The Netherlands, Elsevier. Studies in Surface Science and Catalysis.

Treybal,R.E. Mass Transfer Operations. McGraw-Hill, New York (1980).

Trunschke,A., Böttcher,H.-C., Fukuoka,A., Ichikawa,M. & Miessner,H. Olefin hydroformylation and selective hydrogenation of acetaldehyde on Mo-promoted Rh/SiO₂ catalysts derived from metal salt and heteronuclear cluster precursors. *Catalysis Letters* **8**, 221-228 (1991).

Tu,Y.-J., Li,C. & Chen,Y.-W. Effects of chromium promoter on copper catalysts in ethanol dehydrogenation. *Journal of Chemical Technology and Biotechnology* **59** , 141-147 (1994b).

Tu,Y.-J. & Chen,Y.-W. Effects of alkaline-earth oxide additives on silica-supported copper catalysts in ethanol dehydrogenation. *Industrial and Engineering Chemistry Research* **37**, 2618-2622 (1998).

Tu,Y.-J. & Chen,Y.-W. Effects of alkali metal oxide additives on Cu/SiO₂ catalyst in the dehydrogenation of ethanol. *Industrial and Engineering Chemistry Research* **40**, 5889-5893 (2001).

Tu,Y.J., Chen,Y.W. & Li,C. Characterization of unsupported copper--chromium catalysts for ethanol dehydrogenation. *Journal of Molecular Catalysis* **89**, 179-189 (1994a).

Wang,Y. & Li,J. Probing study of Rh catalysts on different supports in CO hydrogenation. *Reaction Kinetics and Catalysis Letters* **76**, 141-150 (2002).

Yin,H., Ding,Y., Luo,H., Zhu,H., He,D., Xiong,J. & Lin,L. Influence of iron promoter on catalytic properties of Rh-Mn-Li/SiO$_2$ for CO hydrogenation. *Applied Catalysis A: General* **243**, 155-164 (2003).

Zhang,R., Sun,Y. & Peng,S. In situ FTIR studies of methanol adsorption and dehydrogenation over Cu/SiO$_2$ catalyst. *Fuel* **81**, 1619-1624 (2002).

Zhao,H., Kim,J. & Koel,B.E. Adsorption and reaction of acetaldehyde on Pt(1 1 1) and Sn/Pt(1 1 1) surface alloys. *Surface Science* **538**, 147-159 (2003).

168

Appendix A

## Gas Chromatography Method for the Characterization of Ethanol Steam Reforming Products

Petr Chladek, Luke J.I. Coleman, Eric Croiset, and Robert R. Hudgins
Department of Chemical Engineering, University of Waterloo, Waterloo, ON, N2L 3G1,

Canada

Abstract

Ethanol steam reforming is a promising reaction for producing fuel cell hydrogen. Depending on catalyst and reaction conditions, mixtures of condensable hydrocarbons and organic and inorganic gases are produced. This paper proposes an economic and effective solution for separating and detecting these compounds employing a GC equipped with two columns, two 6-way valves and two detectors.

Introduction

The production of hydrogen from bio-ethanol has received much research attention in the last few years. Ethanol derived from cellulosic materials is considered an eco-friendly hydrogen source because it is renewable, non-toxic, and could significantly reduce greenhouse gas emissions, making it a good candidate for hydrogen production. Ethanol steam reforming is the most commonly studied ethanol conversion process because of its high hydrogen and potentially low carbon monoxide yields. For hydrogen production, the overall ethanol steam reforming reaction is given in equation 1.

$$CH_3CH_2OH_{(g)} + 3H_2O_{(g)} \xleftrightarrow{\text{Catalyst}} 6H_{2(g)} + 2CO_{2(g)} \tag{1}$$
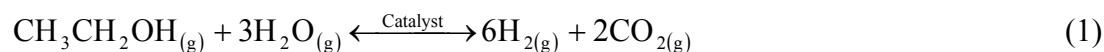
The ethanol steam reforming reaction, given in equation 1, is an endothermic equilibrium limited reaction that is not favoured in the forward direction for reaction temperatures below 330°C.

169

The overall ethanol steam reforming reaction above is an idealized reaction. In real applications, depending on the catalyst and the operating conditions, a wide variety of reaction products could be expected such as H_2, H_2O, CO, CO_2, methane, ethylene, ethane, propylene, acetaldehyde, ethanol, acetone, acetic acid, diethyl ether, ethyl acetate, crotonaldehyde, butanol, and deposited amorphous carbon. In general, ethanol steam reforming is conducted in continuous fixed-bed reactors at temperatures ranging from 300 to 850°C on a variety of catalysts. The analysis of such a wide range of species by conventional gas chromatography is not trivial, especially on-line.

Throughout the ethanol steam reforming literature, the product gas streams have been analyzed by several techniques. A commonly used approach requires the partitioning of the sample by condensation, in which the incondensable species are detected and quantified in an on-line manner, and the liquid sample periodically collected and analyzed [1-4]. This analytical approach generally requires multiple GCs, which can be prohibitively expensive; however, method development and column selection are relatively easy tasks. A major drawback of this analytical approach is the determination of the species and overall material balances because of inaccurate measurement of the liquid flow rate, which is generally quite low. In addition, unlike the discrete gas sampling, the collected liquid sample represents a time-averaged sample, which leads to inaccurate determination of species distribution and does not allow for accurate determination of kinetics, especially when the studied system is inherently dynamic. Finally, the volatility of species in the collected liquid sample can be a problem and must be considered.

Another common analytical approach employs a single or multiple GC(s) with multiple columns, multiple detectors, and multiple sample injections [5-14]. This approach requires the entire product sample to remain in the gas phase and the sample is separated into multiple injections and each injection is analyzed for specific species. This requires more thorough method development and column selection. The columns are usually selected such that the sample is divided into separable and inseparable fractions on each

column/detector arrangement and all separable species are quantified. This technique has been successful in accurately determining the composition of the detectable species in the product stream, but the quantification of the amount of the undetectable species, especially water, is difficult because there are numerous undetectable species for each column/detector arrangement. The result is a lack of confidence for the quantity of water in the product stream, which is a major concern because water typically accounts for up to 50 volume % of the total injected sample, and consequently a lack of confidence in the species and overall material balances.

The single GC, multi-column, multi-detector, single injection approach described here was developed to overcome the limitations mentioned above. On the one hand the product stream is analyzed in its entirety without necessitating any phase separation. On the other hand in this method all species are detected in one injection (no undetectable species) and the concentration of water can be determined with confidence by subtraction. This approach exploits differences in column selectivity and species affinity in addition to temperature programming and column order switching to separate and detect the entire injected sample.

Separation and Quantification Strategy

Figure 1 presents a schematic diagram of the GC's column, valve, and detector arrangement. The product stream exiting the reactor is continuously fed to the sample injection valve that is maintained at the same temperature as the product stream.
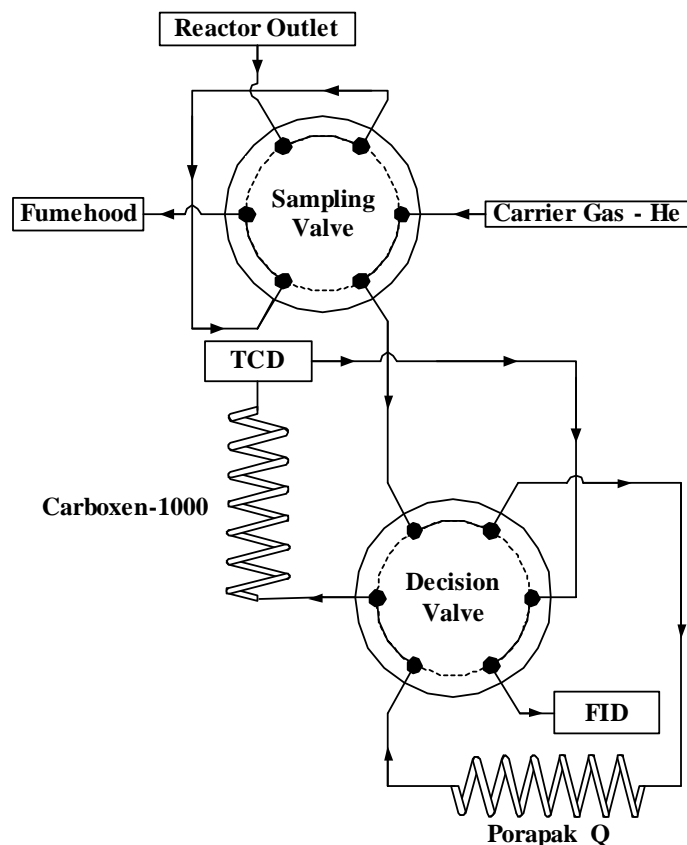
Figure 1: Block diagram of the multi-column, multi-detector, single injection GC.

A block diagram of the initial column/detector arrangement is given in Figure 2a. The entire sample is injected and the sample enters the first column, which is capable of separating condensable (heavy fraction) species. The initial GC oven temperature is selected such that the condensable species adsorb in the heavy fraction column, and the non-condensable (light fraction) species continue to a second, light fraction, column. Once the light fraction species elute from the heavy fraction column, the decision valve, shown in Figure 1, switches to position 2. As shown in Figure 2b, the column/detector arrangement changes, so that the carrier gas is fed directly to the light fraction column. The carrier gas enters the light fraction column, passes through a flow-through, preferably non-destructive, detector [e.g. thermal conductivity detector (TCD)], and continues to the heavy fraction column.

A
Carrier Gas
and Sample

Porapak Q

Carboxen-1000

| TCD | | FID |

Heavy Fraction   Light Fraction

B
Carrier
Gas

Carboxen-1000

| TCD |

Porapak Q

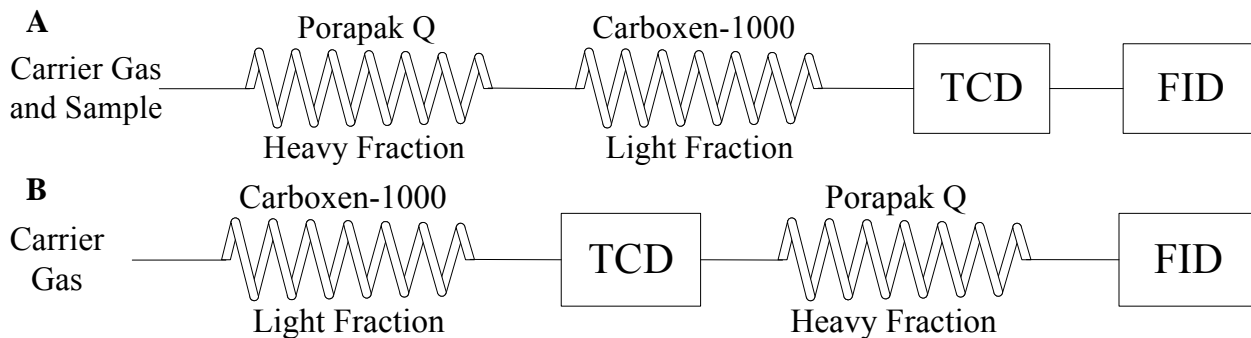| FID |

Light Fraction   Heavy Fraction

Figure 2: Block diagram of the column and detector arrangement for A) decision valve position #1 and B) decision valve position #2.

A temperature program is applied and species elute from their respective columns. The first detector (e.g. TCD) whose effluent becomes the carrier gas for the column separating the heavy fraction detects the light fraction species initially. The heavy fraction column effluent, which contains the heavy and light fraction species, is sent to a second detector [e.g. flame ionization detector (FID)] for analysis. This arrangement allows for double detection of the combustible light fraction components, such as methane. The temperature program must be developed such that the light fraction species do not adsorb on the heavy fraction column, but are retained by the light fraction column and the species eluting from the light fraction column do not interfere, or co-elute, with the species from the heavy fraction column.

Experimental
Instrument
The gas chromatograph (GC) used in this study was a Varian CP-3800 (Varian Inc., Palo Alto, CA) equipped with a 1041 splitless on-column injector, TCD, FID, two 6-way valves (VICI, Houston, TX) enclosed in a dual valve heating oven, and electronic flow controllers (EFCs) controlling all gas flow rates. The GC was controlled and automated by the Star GC Workstation (ver. 5.50) software package (Varian Inc.).

Ultra-high purity helium, 99.999%, (Praxair Inc., Danbury, CT), which was further purified by passing through a helium purifier (Supelco, Inc., Bellefonte, PA), was used as the carrier and TCD reference gas. Hydrogen, 99.995%, (Praxair Inc.) and in-house

produced zero-gas air were used to generate the FID flame. A 15' x 1/8" stainless steel column containing 60/80 mesh Carboxen-1000 (Supelco Inc.) was used for separation of the light fraction species. For separation of the heavy fraction species, a 6' x 1/8" stainless steel column containing 50/80 mesh Porapak Q was used. The carrier gas flow rate was set at 55 mL min^{-1}. The valve heating oven, injector, and detectors were set at 250°C. The sample loop volume was 500 μL.

Chemicals

For species identification and calibration, two custom certified calibration gas mixtures (Praxair Inc.) whose compositions are given in Table I, were used in addition to pure H_2, N_2, CH_4, C_2H_4, propylene, acetaldehyde, acetone, diethyl ether, ethyl acetate, crotonaldehyde, 1-butanol, and anhydrous ethanol (Commercial Alcohols Inc., Toronto, ON). All gases were minimum 99.995% grade and supplied by Praxair Inc. and all liquids were ACS grade and supplied by Sigma-Aldrich Co., unless otherwise stated.

Table I: Composition of custom certified calibration gases

Calibration Gas #1		Calibration Gas #2	
Species	Concentration (vol%)	Species	Concentration (vol%)
H_2	30.03	C_2H_2	0.499
O_2	3.0	C_2H_4	3.09
Ar	9.0	C_2H_6	3.00
CO	30.0	N_2	93.0
CH_4	7.97	Trace Hydrocarbon	Balance
CO_2	20.0	Mixture	

Results and Discussion

The first step of method development was the characterization of the light and heavy fractions and identification of suitable light and heavy fraction columns. The Carboxen-1000 column was identified from literature [15] as a good candidate for separating the light fraction, permanent gases and light (C1-C2) hydrocarbons. The heavy fraction column was identified on a trial-and-error basis, because the constraints for selection of this column were more stringent. The heavy fraction column must adequately separate the heavy fraction species, have no activity for the separation of the light fraction species, and its integrity cannot be hindered by any of the species in the injected sample. Porapak

Q, a high surface area, cross-linked polymer packing without a stationary phase coating, typically used for separating small chain, slightly polar species, was selected as the heavy fraction column.

The next step was the identification of the light fraction, and determination of its retention time in the heavy fraction column. This was achieved by connecting the Porapak Q (heavy fraction) column directly to the TCD and injecting a prepared mixture of the two certified calibration gases with the column oven at 35°C. The permanent gases (H_2, N_2, CO, CH_4, and CO_2) co-eluded in less than 4 minutes while the C2-species from calibration gas #2 were adequately separated and eluded after 4 minutes. The 4-minute mark was selected as the time to actuate the decision valve to position 2.

The column, detector, and valve arrangement given in Figure 1 was then implemented. The temperature program suggested by Supelco Application Note 112 [15] for separation of permanent gases and C2 hydrocarbons using the Carboxen-1000 column was selected as the starting point for temperature program development. The proposed temperature program consisted of a temperature hold at 35°C for 4 minutes and an aggressive temperature ramp rate of 20°C min^{-1} to 225°C. Mixtures containing the two custom calibration gases and condensable species (e.g. water, ethanol, acetaldehyde, etc.) were used to "tailor" the temperature program. Analysis of the simulated product stream resulted in good separation and quantification of the permanent gas species, C2 hydrocarbons (acetylene, ethylene, and ethane), but resulted in co-elution, or peak shouldering of acetaldehyde and methane from the heavy fraction column and poor separation of the remaining hydrocarbons. The temperature ramp rate was reduced to 5°C min^{-1} from 155°C to 225°C to allow for better separation of these species. The resulting temperature program is given in Table II.

Table II: GC oven temperature program

Temperature(°C)	Rate (°C min^{-1})	Hold (min)	Total Time (min)
35	0.0	5.0	5.0
155	20.0	0.0	11.0
225	5.0	0.0	25.0

The separation strategy can be described with the aid of the schematic diagram (Figure 1), the column/detector arrangements (Figures 2a and 2b), and the resulting TCD and FID chromatograms given in Figures 3 and 4, respectively. The product gas stream exiting the reactor was injected into the GC. The sample passed through the decision valve and entered the Porapak Q column that was held at 35ºC. The heavy condensable species adsorbed on to the column while the light gaseous species continued, unresolved, to the Carboxen-1000 column. Hydrogen, being the least retained species, was detected by the TCD (Figure 3) at minute 2 and was subsequently burned by the FID (no detection).
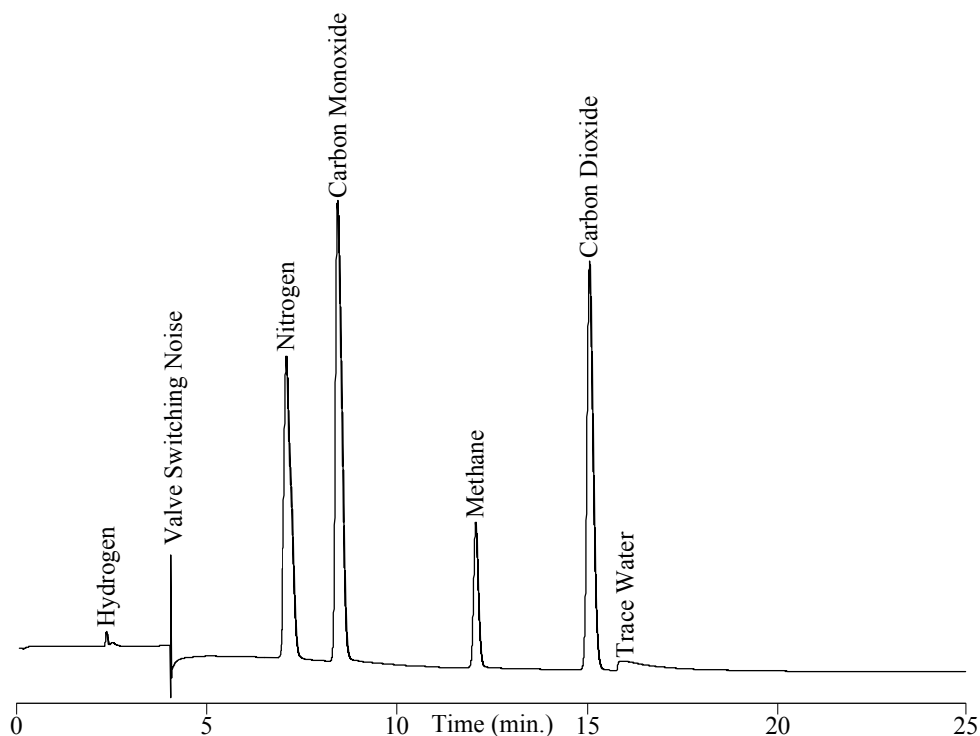

Figure 3: TCD Plot – Light fraction (Carboxen-1000) column separation.

After 4 minutes, the decision valve was switched to position 2 and at minute 5 the column oven temperature was ramped at a rate of 20°C min^{-1} to 155°C. During this temperature ramp ethylene, acetylene, ethane, and propylene eluted from the Porapak Q column and were detected by the FID (Figure 4). In addition, nitrogen and carbon monoxide eluted from the light fraction column, were detected by the TCD, and then fed to the heavy fraction, Porapak Q column, as a pseudo-carrier gas. These species were not detected by the FID and did not interfere with the quantification of species eluting from

the Porapak Q column. The temperature oven was then increased to 225°C at a reduced ramp rate of 5°C min^{-1} to give better separation of the more strongly adsorbed species. At minute 10.5, the FID sensitivity was reduced from attenuation level 12 to 11, because the concentrations of acetaldehyde, methane, and ethanol were expected to be high, and would therefore create very large, potentially detector saturated peaks. Acetaldehyde was the next species to desorb from the heavy fraction column, while shortly afterwards, methane eluted from the light fraction column. Methane was detected by the TCD and then eluted from the heavy fraction column and was detected by the FID. Ethanol desorbs from the heavy fraction column at minute 12.75 followed by CO_2 from the light fraction column. Again, when CO_2 eluted from the light fraction column it passed through the TCD, where it was detected, then passed through the heavy fraction column and the FID, but being non-combustible was not detected by the FID. The elution of acetone and diethyl ether from the heavy fraction column occurred at minutes 15.6 and 16.0, respectively. At minute 18, the FID sensitivity was increased from attenuation 11 to 12 to allow for detection of trace amounts of the remaining species. The remaining hydrocarbon species, ethyl acetate, crotonaldehyde, and butanol eluted from the heavy fraction column and were detected by the FID. The method ended at minute 25 at which point the decision valve was returned to position 1 and the column oven cooled to its initial temperature.
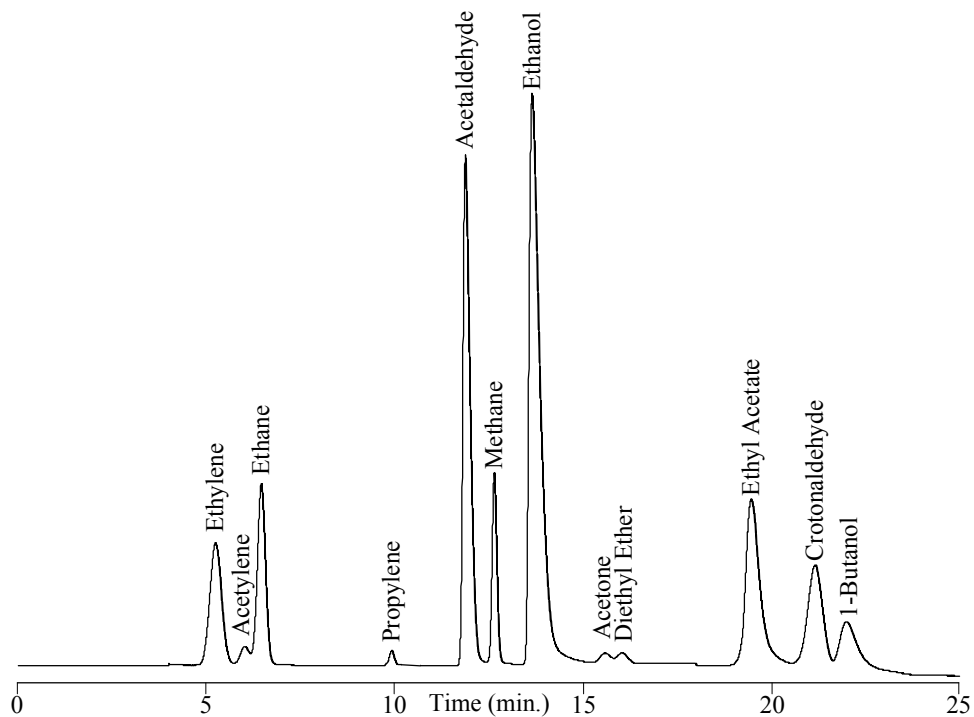
Figure 4: FID plot – Heavy fraction (Porapak Q) column separation.

Once the separation method was developed a calibration of each species was obtained using combinations of the two custom calibration gases, pure gases (H_2, N_2, CH_4, and C_2H_4), water and liquid organics. The results of the calibration are given in Table III. The calibrated range for hydrogen is quite broad (3.0-99.0%), but the flow rate of the carrier gas, helium, was very large, resulting in a hydrogen concentration seen by the detector below 5%. The polarity of the hydrogen peak was positive for the entire range (no peak inversion), however, the relationship between hydrogen concentration and peak area was quadratic, not linear. The resulting concave-upward quadratic model accounts for the nonlinearity in the thermal conductivity of mixture of hydrogen and helium [16].

Table III: GC calibration results

Species	Range (%mol)	Detector	Model	R^2	# of data points*
Hydrogen	3.0 - 99.0	TCD	Quadratic	0.9996	17
Nitrogen	1.0 - 99.3	TCD	Linear	0.9991	33
Carbon Monoxide	3.0 - 30.0	TCD	Linear	0.9991	6
Methane	0.8 - 20.0	TCD	Linear	0.9991	10
		FID	Linear	0.9990	10
Carbon Dioxide	2.0 - 20.0	TCD	Linear	0.9995	6
Acetylene	0.05 - 0.499	FID	Linear	0.9977	6
Ethylene	0.031 - 30.0	FID	Linear	0.9951	14
Ethane	0.30 - 3.0	FID	Linear	0.9973	6
Propylene	0.01 - 0.1	FID	Linear	0.9989	6
Acetaldehyde	0.44 – 18.0	FID	Linear	0.9987	7
Ethanol	0.30 – 84.0	FID	Linear	0.9991	12
Acetone	0.01 - 0.17	FID	Linear	0.9999	3
Diethyl Ether	0.01 - 0.1	FID	Linear	0.9975	3
Ethyl Acetate	0.01 - 0.16	FID	Linear	0.9996	3
Crotonaldehyde	0.01 - 0.1	FID	Linear	0.9829	3
1-Butanol	0.01 - 0.09	FID	Linear	0.897	3

* Each data point represents an average of a minimum of five replicate injections.

Conclusions

The composition of the stream resulting from ethanol steam reforming varies with the catalyst employed, reaction conditions [temperature, reactant feed concentration, feed gas flow rate, and time on-stream (catalyst deactivation)]. The analysis of such a complex and varying gas composition is no trivial task. The described analytical method provides a versatile and inexpensive tool for separating and detecting samples containing both gaseous and condensable species. By adjusting the time of the decision valve actuation, temperature program and detector sensitivity, the method can be fitted to obtain a desirable degree of separation and detection for different species produced in various reactions all in one GC. The authors believe that by simply employing appropriate column selections, temperature programming, and detector type and sensitivity, a broader range of applications can be achieved.

Acknowledgements

References

1. F. Auprêtre, C. Descorme, and D. Duprez. Bio-ethanol catalytic steam reforming over supported metal catalysts. Catal. Comm. 3: 263-267 (2002).
2. A.J. Akande, R.O. Idem, and A.K. Dalai. Synthesis, characterization and performance evaluation of Ni/Al2O3 catalysts for reforming of crude ethanol for hydrogen production. Appl. Catal. A: Gen. 287: 159-175 (2005).
3. A. Aboudheir, A. Akande, R. Idem, and A. Dalai. Experimental studies and comprehensive reactor modeling of hydrogen production by the catalytic reforming of crude ethanol in a packed bed tubular reactor over a Ni/Al2O3 catalyst. Int. J. Hydrogen Energy 31: 752-761 (2006).
4. H.S. Roh, Y. Wang, D.L. King, A. Platon, and Y.H. Chin. Low temperature and H2 selective catalysts for ethanol steam reforming. Catal. Lett. 108(1–2): 15-19 (2006).
5. M.S. Batista, R.K.S. Santos, E.M. Assaf, J.M. Assaf, and E.A. Ticianelli. Characterization of the activity and stability of supported cobalt catalysts for the steam reforming of ethanol. J. Power Sources 124: 99-103 (2003).
6. S. Cavallaro, V. Chiodo, A. Vita, and S. Freni. Hydrogen production by auto-thermal reforming of ethanol on Rh/Al_2O_3 catalyst. J. Power Sources 123: 10-16 (2003).
7. C. Diagne, H. Idriss, and A. Kiennemann. Hydrogen production by ethanol reforming over $Rh/CeO_2–ZrO_2$ catalysts. Catal. Comm. 3: 565-571 (2002).
8. A.N. Fatsikostas, D. Kondarides, and X.E. Verykios. Production of hydrogen for fuel cells by reformation of biomass-derived ethanol. Catal.Today 75: 145-155 (2002).
9. S. Freni. Rh based catalysts for indirect internal reforming ethanol applications in molten carbonate fuel cells. J .Power Sources 94: 14-19 (2001).
10. V.V Galvita, G.L. Semin, V.D. Belyaev, V.A. Semikolenov, P. Tsiakaras, and V.A. Sobyanin. Synthesis gas production by steam reforming of ethanol. Appl Catal A: Gen 220: 123-127 (2001).
11. V. Klouz, V. Fierro, P. Denton, H. Katz, J.P. Lisse, S. Bouvot-Mauduit, and C. Mirodatos. Ethanol reforming for hydrogen production in a hybrid electric vehicle: process optimisation. J.Power Sources 105: 26-34 (2002).
12. D.K. Liguras, D.I. Kondarides, and X,E, Verykios. Production of hydrogen for fuel cells by steam reforming of ethanol over supported noble metal catalysts. Appl Catal B: Enviro 43: 345-354 (2003).
13. J. Llorca, P.R. de la Piscina, J.A. Dalmon, J. Sales, and N. Homs. CO-free hydrogen from steam-reforming of bioethanol over ZnO-supported cobalt catalysts. Appl Catal B: Enviro 43: 355-369 (2003).
14. S. Velu, N. Satoh, C.S. Gopinath, and K. Suzuki. Oxidative reforming of bioethanol over CuNiZnAl mixed oxide catalysts for hydrogen production. Catal. Lett. 82: 145-152 (2002).
15. Application Note 112 "Analysis of Permanent Gases, Light Hydrocarbons, and Light Polar Compounds, Using Packed Column GC". Supelco, Inc. (1996).
16. B.J. Gudzinowicz. The Practice of Gas Chromatography. L.S. Ettre and A. Zlatkis, Eds. John Wiley and Sons, New York, NY, 1967, p. 246.

Appendix B

The TPR profiles of supported and unsupported Cu-based catalysts used in acetaldehyde hydrogenation are presented in this Appendix.
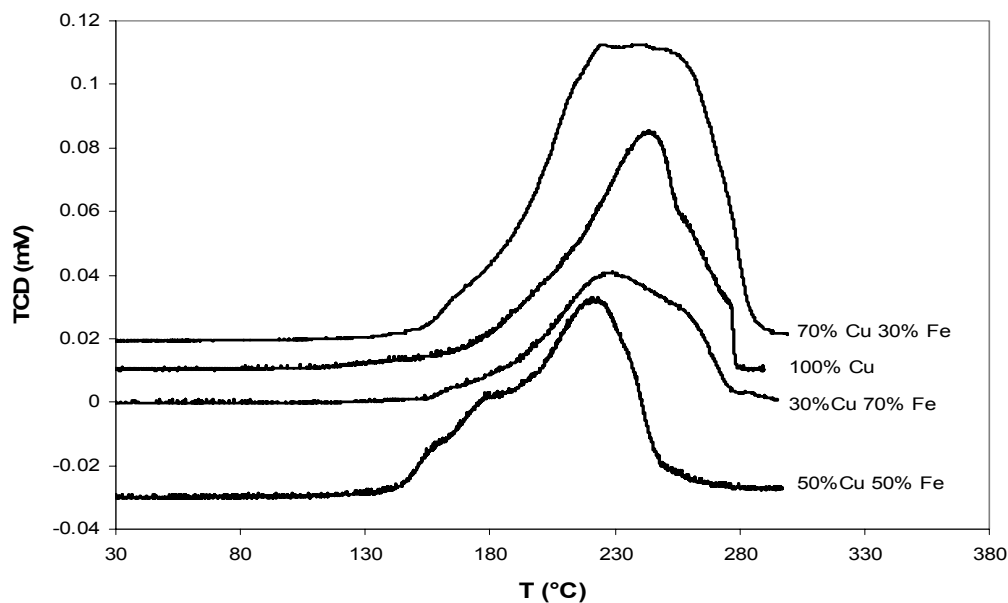

Fig B1. TPR profiles of precipitated Cu-Fe catalysts in $5\%H_2/N_2$ at $5°C/min$.
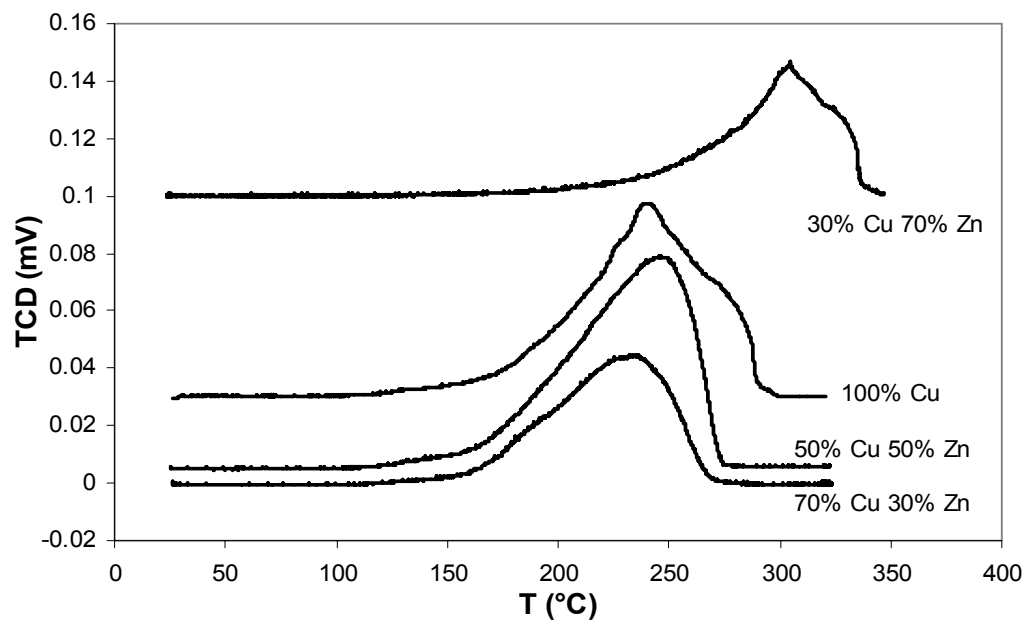

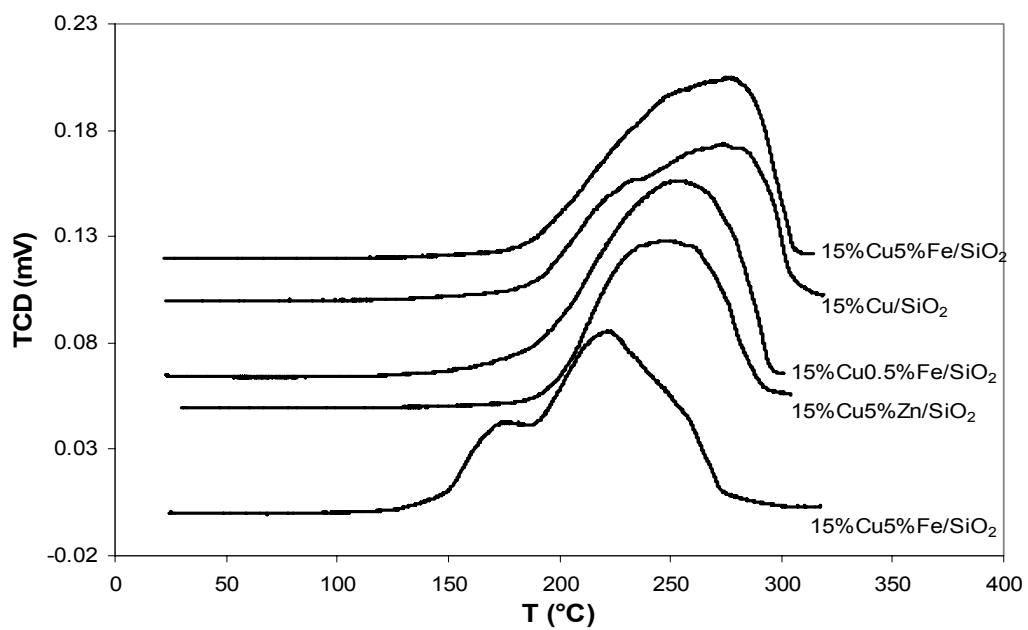**Fig B2.** TPR profiles of precipitated Cu-Fe catalysts in $5\%H_2/N_2$ at $5°C/min$.

Fig B3. TPR profiles of impregnated Cu-Fe/Zn/SiO$_2$ catalysts in 5%H$_2$/N$_2$ at 5°C/min.